Journal of the
OPTICAL SOCIETY
of AMERICA

VOLUME 40, NUMBER 4 APRIL, 1950

Recommendations of the International Commission on Illumination (I.C.I.), Eleventh Session (1948)

EDITORIAL COMMENT

AS a result of the publication of a recent paper by K. S. Weaver in this Journal,[1] the author has been criticized by J. Terrien of Paris in a Letter to the Editor[2] to which Dr. Weaver has replied.[3] Dr. Terrien felt that Dr. Weaver had apparently "ignored" the "almost unanimous" acceptance of certain recommendations in optical terminology. On the other hand, Dr. Weaver has pointed out, and many American workers will confirm this statement, that the recommendations of the International Commission on Illumination at their meeting in June, 1948,* have not been published in a form available to the American workers for their consideration or information.

The mechanism of operation of I.C.I., from the viewpoint of dissemination of proposed action and the collection of opinion, is not too satisfactory for American scientists as compared with the European scientists, where the larger number of smaller European subdivisions of the Commission are able to contact scientists and discuss proposals in a shorter time. It should not be considered that American acceptance has been obtained when adequate dissemination or discussion opportunity has not been provided to American workers in the field.

The essential actions of the I.C.I. at their 1948 session are reproduced below and it must be remembered that these are not binding agreements but rather recommendations. Only those sections have been reproduced which involve specific recommendations for other than further study. Comments on the acceptability or lack of acceptability by workers in the fields concerned should be transmitted to L. E. Barbrow, Secretary of the U. S. National Committee of I.C.I. (National Bureau of Standards, Washington 25, D.C.) so that the American representatives may have suitable information upon which to base their actions as to changes in these recommendations. The next meeting of I.C.I. is scheduled to be held in Stockholm June, 1951, but committee consideration would require a reasonable time in advance of this date for discussion of suggestions which may be submitted.

[1] K. S. Weaver, J. Opt. Soc. Am. 39, 278 (1949).
[2] J. Terrien, J. Opt. Soc. Am. 39, 88 (1949).
[3] K. S. Weaver, J. Opt. Soc. Am. 40, 60 (1950).
* The complete proceedings will probably be published by I.C.I. during the present year.

OFFICIAL RECOMMENDATIONS OF THE INTERNATIONAL COMMISSION ON ILLUMINATION

1b. Definitions and Symbols

1. It is recommended that the new unit for luminous intensity (which is such that the luminance or photometric brightness of a blackbody at the temperature of freezing platinum equals 60 units of intensity per square centimeter) shall be called in all countries by the Latin name "candela," with the symbol "*cd*."

2. It is resolved that the colorimetric terms, definitions, and symbols indicated in Recommendation 9 of the Colorimetry Committee (7) be adopted by the present Committee.

3.† It is recommended that the symbol L be no longer used to denote a quantity of light (product of a luminous flux by a time). It shall henceforth be reserved, equally with the symbol B, to denote a luminance (photometric brightness).

4. It is recommended that, to avoid inconsistencies within the I.C.I., propositions relating to definitions and symbols put forward by other Technical Committees (for example, Committees on Light and Vision, Colorimetry, Diffusing Materials) should invariably be submitted to Committee 1b for consideration. This should be done as early as possible, and in any case before the recommendations are submitted to the Plenary Session. Joint meetings of these various committees with Committee 1b should be arranged if necessary.

4. Light and Vision

1. It is recommended that the possibility be studied of determining and adopting a spectral sensitivity curve for the dark-adapted eye, on the following lines: the curve should be based on recent investigations by Wald and Crawford as well as on earlier or later work that is relevant, the object being to determine a curve that corresponds as nearly as possible to the response of the so-called "rod mechanism" in the extrafoveal retina (not nearer than 5° from the center of the fovea) of the average young subject (less than about 30 years of age). The possibility of fixing a correction to allow for the change of the curve with increasing age should also be examined.

2. It is recommended that, when for special purposes the luminous effects of radiant energies of various spectral compositions are evaluated by methods that do not rest on the standard luminosity function adopted by the I.C.I. in 1924, the unit of the quantity corresponding to luminance (photometric brightness) should always be chosen so that this quantity has the numerical value 60 (c.g.s. system) for a blackbody at the temperature of freezing platinum.

† Not accepted by the Netherlands.

7. Colorimetry‡

1. *Proposed Standard Illuminant E.*—

(a) It is recommended strongly that the use of the standard illuminants *A*, *B*, and *C*, recommended by the I.C.I. in 1931, be continued for all appropriate types of work; further, that the proposed standard illuminant "*E*" be not adopted, either for the colorimetry of non-self-luminous objects or as a standard of artificial daylight.

(b) It is recommended that the achromatic point ($x_w=y_w=z_w=\frac{1}{3}$), representing the equi-energy source, be used for the determination of dominant wave-lengths and purity in the colorimetry of light sources.

2. *Excitation and Colorimetric Purity.*—It is recommended that Excitation Purity be represented by the symbol p_e, and calculated by the one of the formulas $p_e=(y-y_w)/(y_d-y_w)$, or $p_e=(x-x_w)/(x_d-x_w)$, for which the numerator has the greater arithmetic value.

It is recommended that Colorimetric Purity be represented by the symbol p_c, and be calculated by the formula: $p_c=p_e\cdot y_d/y$.

In these expressions (x, y, z) are the chromaticity coordinates (trichromatic coordinates) of the light in question, referred to the 1931 I.C.I. system.

(x_w, y_w, z_w) are the chromaticity coordinates (trichromatic coordinates) of the achromatic reference point, which is conventionally taken to have zero purity. For self-luminous (primary) sources, these are the coordinates of the equi-energy point ($\frac{1}{3}$, $\frac{1}{3}$, $\frac{1}{3}$). For light reflected from or transmitted by a body (secondary source) (x_w, y_w, z_w) are the coordinates of the light used to illuminate the body. This illuminant must always be appropriately specified.

(x_d, y_d, z_d) are the chromaticity coordinates (trichromatic coordinates) of the point on the spectrum locus, or on the straight line joining its extremes, representing the light required to be mixed with light of chromaticity coordinates (x_w, y_w, z_w) to match the light considered.

3. *Standard Observer.*—It is recommended that the National Committees encourage researches on the practical value of the luminosity factors adopted by the I.C.I. in 1931, with special reference to the extremes of the visible spectrum.

4. *Ultraviolet Content of Standard Illuminants.*—

(a) It is recommended that the offer made through the United States Committee by Messrs. Davis and Gibson to determine the relative energy distributions of illuminants *B* and *C* below 370 mμ, including the spectral transmission factor of the cells, be accepted.

(b) It is recommended that National Committees study the question of a standard illuminant having relatively more ultraviolet energy than illuminants *A*, *B* and *C*, for the colorimetry of fluorescent materials.

5. *Purple Colors.*—It is agreed that some scale for the specification of colors represented by points lying on the straight line joining the ends of the spectrum locus on the chromaticity diagram is desirable. It is recommended that the National Committees study the respective merits of various scales.

The following suggestions for the identification of such colors have been put forward:

(1) By the coordinate x or y.

(2) By the ratio $(u-v)/(u+v)$, where u and v are the distances of the point from the ends of the spectrum locus, on the chromaticity diagram.

(3) By the ratio $(x-x_{380})/(x_{700}-x_{380})$.

(4) By the angle around the equi-energy point of the line joining the equi-energy point and the point representing the color under consideration, taking the angle for the line to the point $x=0$, $y=1$ as 180°, the angle increasing with increase in dominant wave-length.

(5) By the angle around the equi-energy point taking the direction of the x axis as 0°, the angles decreasing with increase in dominant wave-length.

‡ A questionnaire on this section was published in this Journal in 1948, see K. S. Gibson, J. Opt. Soc. Am. 38, 67 (1948).

6. *Metric Purity.*—It is recommended that National Committees study the possible merits of the concept "metric purity," which may be defined as follows: The chromaticity interval, on any assumed uniform chromaticity scale or chart, between the points representing the adopted achromatic stimulus and the stimulus considered.

7. *Color and Color Rendering Properties of Illuminants.*—It is recommended:

(a) that the color and color rendering properties of illuminants should be measured and expressed in terms of:

(i) chromaticity coordinates on the standard I.C.I. System;

(ii) luminance in agreed spectral bands;

(b) that in view of established practice the spectral bands used in (a) above should provisionally be as follows:

Spectral Band No.	Wave-length limits
1	380 to 420 mμ
2	420 to 440 mμ
3	440 to 460 mμ
4	460 to 510 mμ
5	510 to 560 mμ
6	560 to 610 mμ
7	610 to 660 mμ
8	660 to 760 mμ

(c) that methods of appraising color rendering properties, including confirmation of the best spectral band intervals, should be further explored by National Committees.

8. *Subjective Appearance of Colors.*—It is recommended that systematic studies be continued on the correspondence between colors as actually perceived and the specification of these colors in the standard I.C.I. System.

9. *Colorimetric Terminology.*—It is recommended that the following terms, definitions and symbols be adopted:

Luminance. This term is recommended for use as equivalent to, and by preference in place of, the expression "photometric brightness" defined in 1924 by the I.C.I. (Symbol *L* or *B*).

Luminance factor of a non-luminous body, under specified conditions of illumination and observation. The ratio of the luminance of the body considered, illuminated, and observed under these conditions, to the luminance of a non-absorbing perfect-diffuser receiving the same illumination. (Symbol β.)

Dominant wave-length of a colored light, not purple. The wave-length of the spectral radiation which, when combined in suitable proportions with the specified achromatic light, yields a match with the light considered (for the standard eye). (Symbol λ_d.)

Complementary wave-length of a light. The wave-length of the spectral radiation which, when combined in suitable proportions with the light considered, yields a match (for the standard eye) with the specified achromatic light. (Symbol λ_c.)

Excitation purity, colorimetric purity. See Recommendation 2.

Chromaticity of a stimulus. The color-quality definable by the trichromatic coordinates, or by the dominant (or complementary) wave-length and purity taken together.

Tristimulus values of a light. The amounts of the three reference or matching stimuli required to give a match with the light considered, in a given trichromatic system. In the standard I.C.I. (1931) colorimetric system the symbols *X*, *Y*, *Z* are recommended for the tristimulus values.

Chromaticity coordinates. The ratio of each of the tristimulus values of a light to their sum. In the standard I.C.I. (1931) colorimetric system the symbols x, y, z are recommended for the chromaticity coordinates.

Brightness or Luminosity. (No agreement was reached on the term.) The attribute of visual perception in accordance with which a surface appears to us to emit more or less light.

"Lightness." The attribute of visual perception in accordance with which a body seems to transmit or diffuse a greater or lesser fraction of the incident light. Note: This attribute is the psychosensorial analog of the photometric quantity "luminance factor."

"Hue." The attribute of visual perception denoted by: blue, green, yellow, red, purple, etc. Note: This attribute is approximately the psychosensorial analog of the colorimetric quantity "dominant wave-length."

JOURNAL OF THE OPTICAL SOCIETY OF AMERICA VOLUME 40, NUMBER 4 APRIL, 1950

Extrapolation from the Michelson-Morley Experiment

HERBERT E. IVES
Upper Montclair, New Jersey
(Received January 11, 1950)

The invariance with motion of the measurement of two-way light signals in the Michelson-Morley experiment is extrapolated to one-way measurements. The time of arrival of signals at a distant point is accepted as indeterminate, in accordance with the before-and-after characterization of Robb; but it is shown that, in spite of this indeterminancy, definite expressions can be obtained for the operations involved in measuring one-way signals. Extension of the same reasoning leads to Lorentz-type transformations expressed in terms of observable rod and clock readings, which include the self-observed velocities of moved clocks used to set the epochs of distant clocks.

I. INTRODUCTION: RADIATION AND NEWTONIAN RELATIVITY

THE problem to be treated here is the unique relation of radiation to matter considered with respect to Newtonian relativity. According to Newton,[1] "The motions of bodies included in a given space are the same among themselves, whether that space is at rest or moving uniformly forward in a right line, without any circular motion." Both in Newton's statement and in the explanation he gives, "bodies" entering the "space" from without do not partake of this relativity. Thus all the motions in the "ship" he cites are not the same if we include among these a projectile originating from a point outside the ship. Not conforming to this exception however is the famous example given by the Michelson-Morley experiment, that electromagnetic radiation, entering from a source outside a "space" henceforth behaves, as judged by its transit from its point of entry to a mirror (the two confines of the space) and back, as though it were a body included in the given space. In the case of the projectile Newtonian relativity is preserved by extending the bounds of the space considered to include the projector; we no longer consider the ship as the space, but the moving earth on which both ship and projector are carried. In the case of radiation and only radiation, it is not necessary to investigate the source or to include it in the "space;" indeed, the motions of the sources of radiation (be they the primary sources or the mirrors reflecting radiation) do not affect the assumption by the radiation entering the Michelson-Morley apparatus, of the character of a body originating its motion in the given space.

What is true of the out-and-back transit of radiation in the Michelson-Morley experiment may or may not be true of radiation proceeding in one direction out or back in a physically bounded space. Measurements of the one-way transit of light signals present, as we shall see, peculiar problems, and no precision laboratory experiments of this sort figure in the history of optics. What we shall consider here primarily is the *extrapolation* of that invariance with motion shown by two-way light signals, to apply also to one-way signals, arriving.thereby at certain relations between matter, which forms the boundaries of our experimental "space," and radiation, which is independent of these boundaries.

In its objectives this study is similar to the current expositions of the Special Theory of Relativity, but these start with the paradox that the velocity of light is at the same time independent of the velocity of the source and isotropic with respect to it. In order to conform to this paradox a restricted ritual of measurement is imposed, in which clocks are narrowly limited in their permissible roles (set as to epoch by light signals *ascribed* the velocity c, and to be moved only "infinitely slowly"). The present treatment leads to observable relations and performable operations free from these restrictions.

The basic difference between the development below and the current developments of the Special Theory of Relativity lies in the treatment of the question of *simultaneity*. In the Special Theory of Relativity the time of arrival of a light signal at a distant point is *defined* as half the time of its out-and-back journey. Here, this time, following the contention of Robb,[2] is accepted as indeterminate, to the extent that it is after the signal's emission and before its return. This indeterminancy, as will appear, does not actually have to be resolved or evaded by arbitrary definition in order to derive perfectly definite relations among the operations which must be performed in making one-way light signal measurements.

II. RADIATION FUNDAMENTALS

Consider a group of light sources and mirrors all in relative motion with respect to each other. Let the radiation from these fall upon a shutter which opens and closes to transmit a brief pulse, which proceeds to a distant radiation detecting instrument, shutter and radiometer being in any state of uniform motion with respect to each other and the light sources and mirrors. The result to be expected from this hypothetical experiment, by consideration of a variety of physical and astronomical observations, is that the radiations from the several sources and mirrors will arrive at exactly the

[1] I. Newton, *Mathematical Principles*, translated by F. Cajori (University of California Press, Berkeley, 1946), Corollary V, p. 20.

[2] A. A. Robb, *A Theory of Space and Time* (Cambridge University Press, London, 1914).

same instant at the radiometer. The indicated result warrants the statement that the velocity of light is independent of the velocity of its physical source, and of the velocity of a mirror from which it is reflected, irrespective of what method or convention of measurement (involving behaviors of rods and clocks) we may employ in the further step of arriving at quantitative values for the velocities involved.

Consider next the determination of the actual measured value of the velocity of light. In the ordinary precision laboratory measurement this is made by sending a light signal from a point of entry at which is a clock, to a distant mirror, at the end of a fixed path, and back to the clock. Our *certain* information is that the to-and-fro transit takes a finite time, by the clock at the origin, and that the signal does in the interval arrive at and leave the mirror. As to the time of arrival at the mirror, we can only say with assurance that it is some time *after* its leaving the clock at the origin and *before* its return. In default of a clock at the mirror, set as to epoch by some unimpeachable procedure, we have no means of definitely determining this time, but we can be sure that *some* instant recorded by the clock at the origin corresponds with (is synchronous with) the distant event. This time *exists* as surely as the distant event *occurs*.* In terms of this real but indeterminate time the allotment of the total transit time into *out*-and-*back* intervals cannot be made definite, we must expect the intervals on any randomly chosen platform to be in general *unequal*. Put in another way, which is more convenient for mathematical treatment, we say that the velocity of the signal out, in terms of the length of the path and the time by the clock at the origin, may be expected to be in general different from the velocity back. We shall carry through our discussion on the basis of accepting this real but undetermined inequality of velocity.

III. THE "DEFINITION" USED AS THE BASIS FOR THE SPECIAL THEORY OF RELATIVITY

Our starting point that the time of transit of out-and-back signals on any randomly chosen platform must be accepted to be in general different, is in direct disagreement with that used in current treatments of the Special Theory of Relativity, which start with the *definition* that these times are always *equal* on *all* platforms.

The grounds for making this definition demand critical scrutiny. It is *not* true, as ordinarily stated,[3] that it is required by "the principle of relativity," and the "firm basis of experiment" that "the velocity of light always measures as c." The experiment in question is the out-and-back measurement of the velocity of light,—no experiments on the one-way transit of light signals exist of comparable precision. This experiment requires that

$$t_0+t_b=2D/c. \tag{1}$$

A general solution of this is

$$t_0=(D/c)-F, \tag{2}$$

$$t_b=(D/c)+F, \tag{3}$$

that is, the out-and-back transit times are unequal, in agreement with the contention of the last section. Introduction of the principle of relativity, or the more specific thesis of this paper, namely, the extrapolation of the invariance of two-way measurement to one-way measurement, demands that F shall be a function solely of measurable quantities on the platform of measurement. It does not require that F shall be zero.

The use of different transit times for out-and-back signals, from which the present discussion starts, together with the extrapolation which is to be explored, thus crystalizes into discovering the exact value of the function F of relations (2) and (3), which take the place of the limited and untenable "definition" of the Special Theory of Relativity.

IV. THE MEASURED TIME OF TRANSIT OF OUT-AND-BACK LIGHT SIGNALS

We consider first the procedure used in the customary method of measuring the velocity of light, that is, by sending a light signal along a fixed path to a mirror at the far end and back to the origin, where a clock measures the elapsed time. Let d be the length of the fixed path, at one end of which is a clock C, at the other a mirror R. Adjacent to the clock is the point of entry of the light signal into the system. This may be imagined to be a shutter, which opens and closes to allow an instantaneous pulse of light to pass into the system from a physical source, whose position or velocity with respect to the shutter need not concern us.

Designate by c_0 the undetermined velocity of the light proceeding from C to R, and by t_0 the time, likewise undeterminable, by the clock C, for the signal to reach R. We have

$$t_0=d/c_0, \tag{4}$$

and similarly

$$t_b=d/c_b, \tag{5}$$

for the return signal. For the total time, out and back, we have

$$t_0+t_b=d[(c_0+c_b)/c_0c_b]. \tag{6}$$

Now from the experimental invariance of this total time, which is always $2d/c$, we have

$$d[(c_0+c_b)/c_0c_b]=2d/c$$

or

$$(c_0+c_b)/c_0c_b=2/c. \tag{7}$$

We shall find that, armed with this relation, we do not need to know the individual values of c_0 and c_b, or commit ourselves (as by a definition) to relative values of t_0

* That there is a limitation, clearly recognized and accurately defined, to the *exactness* with which simultaneity between distant events can be determined, does not warrant the extreme position of some philosophers, that simultaneity is thereby rendered *non-existent*.

[3] A. Einstein, Ann. d. Physik 4, 891 (1905).

and t_b, in order to describe light signal relations in terms of performable operations and observable quantities.

Consider next, in Fig. 1, a platform $C'-R'$ of length D, moving with respect to our initial platform or coordinate system with a velocity W (in terms of divisions on the initial platform, and time by the clock C). Let the moving platform be furnished with a clock C' at one end, which is coincident with C when the light signal enters the system, and let there be a mirror at the far end which reflects the signal back to the clock C'. Then, all times being measured by the clock C, we have for the out signal

$$D+Wt_0=c_0t_0 \tag{8}$$

and for the back signal

$$D-Wt_b=c_bt_b. \tag{9}$$

The total transit time of the signal, out and back on $C'-R'$ is then

$$t=t_0+t_b=D[(c_0+c_b)/c_0c_b]/[1-(W/c_0)][1+(W/c_b)]. \tag{10}$$

By experiment however, if the time is measured by the clock C', at the origin on the *moving* platform, we always get the same result no matter what the velocity of the platform, that is, W *disappears*.

We have at our disposal as factors to account for this disappearance *only* the clock on the moving platform and the length of that platform. *We are forced to conclude* that these must be altered by their motion with respect to the initial platform. We accordingly make the following substitutions:

$$D_i'=D'f_D(W) \tag{11}$$

$$t_i'=(t_0+t_b)_i'=(t_0+t_b)'/f_T(W)=t'/f_T(W) \tag{12}$$

then

$$t'=D'[(c_0+c_b)/c_0c_b]f_D(W)f_T(W)/[1-(W/c_0)][1+(W/c_b)]. \tag{13}$$

If then

$$f_D(W)f_T(W)=\left(1-\frac{W}{c_0}\right)\left(1+\frac{W}{c_b}\right), \tag{14}$$

we get

$$t'=(t_0+t_b)'=D'[(c_0+c_b)/c_0c_b]=2D'/c, \tag{15}$$

which is invariant with motion, W having disappeared.

The meaning of these relations is as follows: D' is the length of the moving platform as measured by standard measuring rods laid end to end on it; D_i' is its length in terms of the standard measuring rods laid end to end on the initial platform. Similarly, t' is the time of the out and back light signal transit as measured by the clock on the moving platform, t_i' is the time as measured by the clock on the initial platform. The moving platform and the measuring rods on it are altered in the ratio $f_D(W):1$, the frequency of the clock on the moving platform is altered in the ratio $f_D(W):1$, by comparison with the rods and clock on the initial platform. We can add to the relation (14), from consideration of the meaning of $f_D(W)$ and $f_T(W)$ just discussed, the information that these functions take the value unity when $W=0$. The exact values of $f_D(W)$ and $f_D(W)$ individually cannot be obtained from the consideration of out-and-back signals, but as will appear, we do not need them in order to solve the immediate problem of determining F.

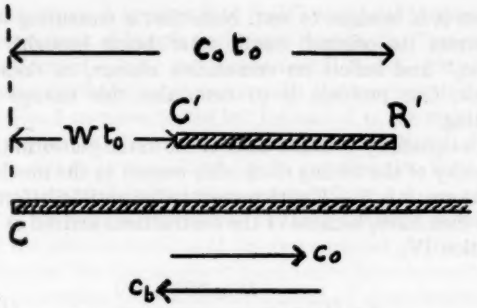

FIG. 1. Light-signal and clock-at-origin relations on initial and relatively moving platforms.

V. THE MEASURED TIME OF TRANSIT OF ONE-WAY LIGHT SIGNALS

We now proceed to apply the relations just found to account for the invariance of two-way light signals, to the measurement of signals sent in one direction, imposing the requirement that these also shall be invariant with the motion of the platform.

For the measurement of signal transit times in one direction it is necessary to know the time of entry of the signal at one point, and the time of its reception at another. This means that we can no longer use *one* clock, we must have *two*, and the second must be made to run at the same rate as the first (which can be insured by sending a train of signals at a given rate from the first), and also must be set in some known relation to the first, to be established by performable operations confined to the moving platform. The use of light signals to perform this setting operation is barred, for we do not know the definite values of c_0 or W, since both involve arrival times at distant points expressed in terms of times by the clock at the origin. Seeking for some performable operation, we choose that of moving an auxiliary clock from coincidence with the clock C' to coincidence with the mirror R' and setting a clock at R' to agree in epoch with the moved setting clock. The moved setting clock is carried along the path $C'-R'$ at a uniform velocity, as measured by the observed path length on the moving platform, divided by the elapsed time, *as measured by the moving clock itself*. This is a definite performable operation, which we shall now investigate.

The setting clock is set to agree in epoch with the clock C' when they are in coincidence. It is then moved to the far end of the platform at a self-observed velocity. It will have its rate changed during its motion, as found in Section IV, and this will cause a change of setting

when it is brought to rest. Note that a measuring rod assumes its original length after being brought to "rest," and suffers no cumulative change, as does a clock. Our problem is to determine this change of setting.

Designate by Y in the units of the initial platform the velocity of the setting clock with respect to the moving platform; it is $W+Y$ with respect to the initial platform. We then have, because of the contractions arrived at in Section IV,

$$Y=D_i'/\tau_i'=\frac{D'f_D(W)f_T(W)}{\tau'}, \tag{16}$$

where τ_i' is the time by a clock stationary on the initial platform, and τ' is the time as indicated by the moved clock. Designating D'/τ', the self-observed velocity of the clock, by q, we have

$$Y=D_i'/\tau_i'=qf_D(W)f_T(W+Y). \tag{17}$$

Consider now the difference of setting or epoch of the two clocks in their final "rest" positions at the two ends of the moving platform. The clock left standing at the origin on the moving platform measures the time τ_i' as $\tau_i'f_T(W)$, the moved clock measures it as τ'. The difference in indication of the two clocks, Δ, is

$$\Delta=\tau_i'f_T(W)-\tau'. \tag{18}$$

From the relations

$$\begin{aligned} D_i'/\tau_i'&=Y\\ D_i'&=D'f_D(W)\\ D'/\tau'&=q, \end{aligned} \tag{19}$$

we have

$$\Delta=\frac{D'f_D(W)f_T(W)}{Y}-\frac{D'}{q}. \tag{20}$$

We now direct our attention to the observed time of transit t' of the one-way light signal in terms of the time t_i', as indicated by the clock on the initial platform; it is

$$t'=t_i'f_T(W)-\Delta. \tag{21}$$

For the light signal considered in Fig. 1, proceeding *out* from C' to R' with a velocity c_0-W, this gives

$$\begin{aligned} t_0'&=\frac{D'f_D(W)f_T(W)}{c_0-W}-\frac{D'f_D(W)f_T(W)}{Y}+\frac{D'}{q}\\ &=\frac{D'}{c_0}+\frac{D'W}{c_0c_b}-\frac{D'f_D(W)f_T(W)}{Y}+\frac{D'}{q}. \end{aligned} \tag{22}$$

In this expression the second and third terms on the right are functions of W [Y is a function of W by (17)], and must for the postulated invariance with motion of the platform be replaced by quantities referred to the moving platform alone. Designating by K some function which shall be independent of W, we put

$$K=\frac{D'W}{c_0c_b}-\frac{D'f_D(W)f_T(W)}{Y}. \tag{23}$$

From this expression we obtain for Y

$$Y=\frac{D'f_D(W)f_T(W)}{(D'W/c_0c_b)-K}. \tag{24}$$

Now we also have for Y the expression (17). Putting (23) in (17) we get

$$\begin{aligned} \frac{D'}{(D'W/c_0c_b)-K}&=\frac{qf_T(W+Y)}{f_T(W)}\\ &=\frac{qf_D(W+Y)f_T(W+Y)}{f_T(W)f_D(W+Y)}\\ &=\frac{q\{[1-(W+Y/c_0)]\}\{[1+(W+Y)/c_b]\}}{f_T(W)f_D(W+Y)}. \end{aligned} \tag{25}$$

By expansion and substitution from (24) and (17), we finally obtain

$$\frac{D'^2}{q^2}=\frac{f_D(W)f_T(W+Y)}{f_T(W)f_D(W+Y)}\left(K+\frac{D'}{c_0}\right)\left(K-\frac{D'}{c_b}\right). \tag{26}$$

Directing attention to the first factor on the right, involving the functions f_D and f_T, in view of the fact that this must be constant for all values of W and Y, we find its value by putting $Y=0$, which yields an identity; this factor is therefore *unity*. We therefore can obtain K by solving the equation

$$\frac{D'^2}{q^2}=\left(K+\frac{D'}{c_0}\right)\left(K-\frac{D'}{c_b}\right). \tag{27}$$

The solution, after substituting $(2c_0c_b)/(c_0+c_b)=c$ from (7), is

$$K=-\frac{D'}{c}+\frac{D'}{c_b}\pm\frac{D'}{q}\left(1+\frac{q^2}{c^2}\right)^{\frac{1}{2}}. \tag{28}$$

Reverting now to (22) which in terms of K is

$$t_0'=(D'/c_0)+K+(D'/q), \tag{29}$$

we get

$$t_0'=\frac{D'}{c}\pm\frac{D'}{q}\left(1+\frac{q^2}{c^2}\right)^{\frac{1}{2}}+\frac{D'}{q}. \tag{30}$$

We choose the minus sign from the experimental fact that a slowly transported chronometer ($q\cong 0$) shows a time closely approximating D'/c, and not the value approaching infinity which the plus sign would demand,

getting finally

$$t_0' = \frac{D'}{c} - \frac{D'}{q}\left[\left(1+\frac{q^2}{c^2}\right)^{\frac{1}{2}} - 1\right]. \quad (31)$$

For t_b', adhering to the same clock setting, we have

$$t_b' = (t_0+t_b)' - t_0'$$

$$= \frac{2D'}{c} - \frac{D'}{c} + \frac{D'}{q}\left[\left(1+\frac{q^2}{c^2}\right)^{\frac{1}{2}} - 1\right]$$

$$= \frac{D'}{c} + \frac{D'}{q}\left[\left(1+\frac{q^2}{c^2}\right)^{\frac{1}{2}} - 1\right]. \quad (32)$$

To recapitulate what we have done: we have started with the individually unidentifiable times of out-and-back transits of light signals, in terms of *one* clock at the origin, and have arrived at definite expressions for these individual out-and-back transit times, as the difference of indication of *two* clocks, one at each end of the path, set in their respective epochs by a quantitatively definite operation.

Referring back to Section III we see that we have obtained the function F as

$$F = D'\left[\left(1+\frac{q^2}{c^2}\right)^{\frac{1}{2}} - 1\right]\Big/ q, \quad (33)$$

which, as required by our postulated extrapolation of the invariance of two-way signals to one-way signals, involves only observed quantities and is independent of the motion of the platform.

It has not been necessary in obtaining F, to know the individual values of c_0 and c_b, or of $f_D(W)$ and $f_T(W)$, but the values of the latter functions can be obtained immediately from the preceding work.

Referring to Eq. (26) we recall that we have found the factor

$$\frac{f_D(W)f_T(W+Y)}{f_T(W)f_D(W+Y)}$$

to have the value unity for all values of W and Y. Remembering from Section IV that $f_D(W)$ and $f_T(W)$ must equal unity when $W=0$, we make this substitution and get

$$[f_T(Y)/f_D(Y)] = 1,$$

that is, f_D and f_T must be identical. From (14) it follows that

$$f_D(W) = f_T(W) = \left[\left(1-\frac{W}{c_0}\right)\left(1+\frac{W}{c_b}\right)\right]^{\frac{1}{2}}. \quad (34)$$

The interpretation of this factor is made clearer by expanding the term on the right, giving

$$f_D(W) = f_T(W) = \left(1 - \frac{W}{c_0} + \frac{W}{c_b} - \frac{W^2}{c_0 c_b}\right)^{\frac{1}{2}}.$$

from which it appears that $f_D(W)$ and $f_T(W)$ represent *contractions* of length and clock rate on the "moving" platform if $c_b > c_0$, and *expansions* if $c_b < c_0$. Also it is easily checked that if we consider the moving platform in Fig. 1 to move to the left instead of to the right, for given values of c_0 and c_b, the changes of length and clock rate will be in opposite sense. In one direction they will be contracted, in the other expanded.

A physical interpretation of these relations, in terms of the relative motions of the two material platforms, is obscure. We can however bring order into the problem by changing to a different system of coordinates, as described in Section VI.

VI. THE COORDINATE SYSTEM FOR RADIATION

Acceptance of the idea that the velocity of light (independent of the velocity of source or mirror) is in general different in different directions from any randomly chosen material clock, in terms of divisions on a scale to which the clock is attached, and times as measured by the clock, carries with it the corollary that *another* coordinate system of clock-at-origin and scale can be postulated, which is in motion with respect to the first at such a velocity that in it the velocity of light is *equal* in all directions.

The essential content of this isotropic coordinate system is the same as that with which we have worked; it is in fact an alternative way of expressing our original contention. The difference between this unique coordinate system and our initial system is that the latter is a randomly chosen material one, whereas the new one, while it could, by accident of choice, be a material one, is not experimentally identifiable. Since however it has developed that velocities with respect to the initial one disappear in the final expressions, our situation is not significantly different when we shift to the new system. (The philosophical issue here is that we are not violating operational principles by using conceivable although experimentally unidentifiable operations in our theoretical attack, provided our final equations represent only performable operations and measurements.) As appears at once, we gain considerable simplification in the mathematical work, by adopting a Radiation Coordinate System.

Using this selected unique coordinate system we find, by exactly parallel reasoning to that of Sections IV and V, that

$$f_D(W)f_T(W) = 1 - (W^2/c^2). \quad (35)$$

Using this in place of (14) in the study of light signals sent in one direction (Section V), we obtain different (simpler) values for Y and K, but identically the same final result (value of F), confirming the identical content of the two systems.

In this selected coordinate system the functions representing changes of length and clock frequency take the simple and more perspicuous form

$$f_D(W) = f_T(W) = [1 - (W^2/c^2)]^{\frac{1}{2}}, \quad (36)$$

that is, the alterations of length and clock rate are *contractions*, in terms of motion with respect to the coordinate system in which the radiation is isotropic.† The contractions are of the second order in W/c, so that they are independent of the direction of motion, and thus do not present the problem of physical interpretation that is met with in the factors of expansion and contraction, depending on direction, appearing in the development based on a randomly chosen material coordinate system.

(The isotropic character of radiation in this uniquely selected system is to be distinguished from the isotropy of radiation in the Special Theory of Relativity where it is *manufactured* for *all* coordinate systems by the ritual of setting distant clocks by light signals *ascribed* the value c. In terms of the findings of this study this means imposing the condition that the q of (31) must be negligibly small.)

The coordinate system in which the velocity of light is the same in all directions in terms of a clock at the origin has been used in an earlier paper[4] to derive relations between events of all sorts on relatively moving platforms. These are the relations appropriate to Newtonian relativity, with added terms containing c, the velocity of light, reflecting the unique character of radiation as a moving "body" discussed in Section I. The relations are Lorentz-type transformations between observable and measurable quantities, with terms involving the self-observed velocities of moved setting clocks.‡ They constitute the relations between matter and radiation adumbrated in the Introduction. The relations for one-way light signals given by Eqs. (31) and (32) there appear as special cases of the transformations. The contraction factors, in terms of observable velocities, which are contained in the Lorentz-type transformations, mimic in from those of the isotropic coordinate system (36), again with the addition of terms containing the self-observed setting clock velocities.

In the paper referred to, the contraction factors, which comprise the necessary and sufficient physical properties of matter on which to build the complete discussion, were taken over from a previous study[5] where they emerged as a consequence of requiring the phenomena of radiation pressure to conform to the principles of conservation of energy and momentum. The W in the expression $[1-(W^2/c^2)]^{\frac{1}{2}}$ was there the velocity with respect to the medium. According to the findings of the present paper the same contraction factors can be obtained by extrapolating from the Michelson-Morley experiment, without invoking any principles of presumed universal application or any physical properties of radiation beyond the experimentally established transmission characteristics presented in Section II. The Lorentz-type transformations quoted could, it appears, have been derived, as we have derived the invariant relations for light signals, by carrying through the development with different values for c_0 and c_b, although at the price of more intricate mathematical work. The "medium" is identical, so far as its use in this problem is concerned, with the coordinate system indicated as mathematically the most simple and convenient to express the "before and after" indeterminancy of distant times. This coordinate system is at the same time the one in which the alterations of length and clock rate are capable of intelligible physical interpretation.

VII. DISCUSSION

The development given here is not presented as preferable to that which postulates a light transmitting medium in which the interactions of radiation and matter conform to the conservation principles,[5] and in which the phenomena of aberration and rotational motion find a ready explanation.§ It pretends only to show the bare minimum of accepted facts and assumptions necessary for the rigorous derivation of Lorentz-type transformations in terms of observable operations and measurements, without the use of arbitrary definitions or the imposition of restricted rituals of measurement. This bare minimum appears to consist (starting with the accepted facts of radiation transmission) of: (1) the invariance of two-way light signal measurement exhibited in the Michelson-Morley experiment; (2) the attribution of times for distant events within a range set by "before and after" relations; (3) the extrapolation of the invariance exhibited in the Michelson-Morely experiment to one-way light signals.

The last of these, the extrapolation of the *invariance* of the Michelson-Morley experiment to one-way light signals, is not the same thing as adopting the *same* value c, for both two-way and one-way signals, which is done

† The contraction factor for length at right angles to the direction of motion is unity (no contraction) since the increased length of the out-and-back path is exactly balanced by the shorter time indicated by the moving clock. The derivation of the contraction factors by the consideration of light signals alone, here given, is to be compared with that of H. A. Lorentz, who invoked the variation of mass of the electron with motion to fix the individual values. See H. E. Ives, J. Opt. Soc. Am. **37**, 810 (1947).

[4] H. E. Ives, J. Opt. Soc. Am. **39**, 757 (1949).

‡ These transformations become the original Lorentz transformations if the self-observed velocities of the moved setting clocks are made zero. This does not correspond to a performable operation since infinite time would be required for a measurement. An alternative procedure for eliminating the additional terms, not open to this objection, is to use as "times" not the indications of the clocks moved to distant points, but these indications advanced by the amount $r'[(1+q^2/c^2)^{\frac{1}{2}}-1]/q$. Adoption of these "times" yields the familiar form of the Lorentz transformations and the "interval," but the "times" are operationally defined.

[5] H. E. Ives, Phil. Mag. **36**, 392 (1945).

§ The to-and-fro excursion of stellar images by which the phenomenon of aberration is made manifest does not fall within the scope of Newtonian relativity, since the motion is not uniform "in the same right line." The idea sometimes met with that aberration, like the phenomena here considered, may be described in terms of the relative motions of the bodies concerned, is immediately refuted by the existence of spectroscopic binaries with velocities comparable with that of the earth in its obit. These exhibit aberrations no different from other stars. In all cases the aberration is caused by the earth's to-and-fro motion with respect to the wave pattern set up by external sources of radiation.

in the Special Theory of Relativity. Here the measured value of the velocity of light for two-way signals is $(2D'/t')=c$, while for one-way signals the measured value is

$$\frac{D'}{t'}=\frac{c}{1\pm(c/q)\{[1+(q^2/c^2)]^{\frac{1}{2}}-1\}}.$$

As stated in the Introduction, the goal of this paper is the same as that of the Special Theory, but by the use of "before and after" relations, in place of a commitment by "definition" to identical values for out and back velocities on all platforms, with its attendant paradox,‖ and by the addition of relations consequent on the free use of clocks, we achieve the goal without the restrictions on permissible measuring operations characteristic of the Special Theory.

‖ The "logical contradiction" in the Special Theory of Relativity which has bothered philosophers, summarized by the objection that "light cannot proceed with objectively equal velocity with reference to an observer A, and with reference to an independently moving observer B" (see discussion by A. Wenzl, in the recently published "Albert Einstein, Philosopher-Scientist," Northwestern University, Evanston, Illinois, p. 587), does not arise in the present exposition. Defining velocity as the ratio of the distance traveled in one direction on a body, to the time by a clock *at the origin* on the body, the velocity of light is *not* equal on bodies in relative motion with respect to each other, but differs by substantially the amount of this relative motion. The "logical" difficulty arises from the loose use of the term "velocity" to cover several different "rod-clock-quotients."

VIII. EXPERIMENTAL CONFIRMATION OF THE EXTRAPOLATION

No precision laboratory measurements on one-way light signal transit times, to which recourse could be made to test the findings of this paper, have thus far been performed. It is not, however, necessary to make such measurements, involving fixing the epoch of distant clocks by moved setting clocks (the experimental difficulties are formidable), in order to test the validity of the extrapolation of the Michelson-Morley experiment here studied. Direct and decisive confirmation is furnished by the experimental observation of the predicted change of clock rate with motion in the Ives-Stilwell experiment on high speed canal rays.[6]

[6] H. E. Ives and G. R. Stilwell, I and II, J. Opt. Soc. Am. **28**, 215 (1938); **31**, 369 (1941). In these experiments the conditions of test correspond to the use of setting clocks moved at negligible velocities, since the velocities of the canal rays were obtained from their Doppler effects, using tke value c for the velocity of light.

Group for the Advancement of Spectrographic Methods

THE 13th meeting of the Group for the Advancement of Spectrographic Methods will be held June 21, 22, and 23, 1950, at the Central Armament Laboratory, 1 St. Thomas Aquinas Place, Paris. Authors who plan to present papers should send two copies of the typewritten text and the figures to the Secretary of the Group for the Advancement of Spectrographic Methods, 1 St. Thomas Aquinas Place, Paris 7, France.

Loyd A. Jones Recognized in PSA Journal

THE February number of the PSA Journal, the official publication of the Photographic Society of America (Vol. 16, p. 67, 1950), presents an interesting word and photograph picture of Loyd A. Jones, past president of the Optical Society of America (1929–1931) and recipient in 1943 of the Ives Medal of the Optical Society of America.

Local Section News Letter

THE Local Section News Letter (No. 5) of February, 1950, which is edited by the Secretary for Local Sections of the Optical Society (Stanley S. Ballard), has initiated a history of local sections of the Optical Society. The first article of the series is a History of the Rochester Section from 1915 to 1924. This article has been contributed by Leon V. Foster.

The Use of Briquetted Samples in the Spectrochemical Analysis of Carbon and Alloy Steels and Other Metals

J. F. WOODRUFF
Research Laboratories, Armco Steel Corporation, Middletown, Ohio

(Received December 1, 1949)

At the Armco Steel Corporation, over a period of several years, a number of spectrochemical methods have been developed which utilize briquetted powders, drillings, millings, nibblings, and grindings. The paper describes briquetted sample techniques for the routine analysis of steel, zinc, and zinc base alloys. Low and plain carbon steels are analyzed quantitatively for such elements as tin, lead, manganese, nickel, chromium, molybdenum, cobalt, titanium, aluminum, zinc, and boron. Zinc and zinc base alloys are analyzed quantitatively for cadmium, iron, lead, tin, antimony, and aluminum. Operational details, such as sample holders, spectrum lines utilized, source-units and source-unit constants employed, and precision and accuracy data over a five-year period are discussed.

DURING the past ten years, the steel industry has been utilizing the spectrograph for supplementing wet chemical analysis in the solution of many metallurgical problems. In the past, metallurgists were sometimes handicapped in the solution of their problems due to the lack of analytical manpower, or due to the inability of obtaining the necessary data by the usual analytical techniques. However, with the advent of the spectrograph as a versatile and rapid analytical tool, the metallurgist has been able to explore and investigate more thoroughly certain phenomena in steel making.

It is interesting to note, however, that most spectrochemical laboratories are using solid specimens in the analysis of steel or other metals. Yet in some laboratories, samples received for analyses are not readily adapted to solid specimen techniques. Dietert[1] reported that steel grindings could be compressed into briquettes and these briquettes sparked or arced in a manner similar to that used for solid specimens. Other workers in the field have also described in the literature[2–6] quantitative methods which used briquetted samples. Even though these investigators have shown that satisfactory precision can be obtained with this mode of sampling, it has not been universally accepted by other laboratories.

Since 1943 the spectrochemical section of the Armco Research Laboratories has successfully analyzed steel and other materials by arcing or sparking briquettes formed from powders, cuttings, drillings, millings, or grindings. Since laboratories do not always receive material in a form which can be conveniently adapted to solid electrode methods, a description of some of the briquetted-sample techniques used in this laboratory may be of interest.

TABLE I. Elements and ranges determined using briquetted techniques.

Element	Matrix	Concentration range percent
Tin	High alloy steels	0.002 –0.040
Tin	Low alloy steels	0.001 –0.090
Tin	Plain carbon steels	0.005 –0.050
Tin	Zinc and zinc base alloys	0.001 –0.030
Lead	Low alloy steels	0.0005–0.030
Lead	Plain carbon steels	0.0001–0.005
Lead	Zinc and zinc base alloys	0.001 –2.00
Manganese	Plain carbon steels	0.001 –0.80
Nickel	Low alloy steels	0.50 –1.50
Nickel	Plain carbon steels	0.001 –0.36
Chromium	Low alloy steels	0.010 –0.15
Chromium	Plain carbon steels	0.001 –0.15
Molybdenum	Low alloy steels	0.015 –0.15
Molybdenum	Plain carbon steels	0.001 –0.050
Cobalt	Plain carbon steels	0.001 –0.010
Copper	Plain carbon steels	0.03 –0.50
Titanium	Low alloy steels	0.010 –0.080
Aluminum	Low alloy steels	0.020 –0.050
Aluminum	Plain carbon steels	0.001 –0.10
Aluminum	Zinc or zinc base alloys	0.010 –5.00
Cadmium	Zinc and zinc base alloys	0.010 –1.00
Iron	Zinc and zinc base alloys	0.010 –0.60
Antimony	Zinc and zinc base alloys	0.010 –0.20

SCOPE

Briquetted techniques have been developed and used for routine analysis of steel, zinc, and zinc base alloys. Low alloy and plain carbon steels are analyzed quantitatively for such elements as tin, lead, manganese, nickel, chromium, molybdenum, cobalt, titanium, and aluminum. Zinc and zinc base alloys are analyzed quantitatively for cadmium, iron, lead, tin, antimony, and aluminum. All the methods to be described use briquettes of samples as received. Table I shows the elements and concentration ranges of these elements in the various matrices which are determined from briquetted shavings, millings, drillings, or nibblings.

Other methods which use briquetted techniques have been developed for determining columbium, zinc, boron, and zirconium in steels. At the present time, however, insufficient data have been collected on pre-

[1] H. W. Dietert, J. Opt. Soc. Am. 31, 693 (1941).

[2] Nausbaum, Hackett, and Fry, J. Opt. Soc. Am. 34, 33 (1944).
[3] C. J. Neuhaus, J. Opt. Soc. Am. 33, 167 (1943).
[4] J. R. Churchill and R. G. Russell, Ind. Eng. Chem. Anal. Ed. 17, 24 (1945).
[5] W. J. Peohlman, Welding J., Research Supplement, New York, 24, 564s (1945).
[6] B. F. Scribner, J. Research Nat. Bur. Stand. 28, 165 (1942).

TABLE II. Operating conditions for the analysis of ingot iron and plain carbon steels.

Method No.	A-1	A-2	A-3	A-4	A-5	A-6
Source unit	Baird	Baird	Baird	Baird	Baird	A.R.L. multisource
Source	a.c. arc	a.c. arc	a.c. arc	a.c. arc	a.c. spark	Arc-like
Voltage	2200 v	2200 v	2200 v	2200 v	30 v (primary)	940 v
Current	3 amp.	3 amp.	3 amp.	3 amp.	2.5 amp. (primary)	15 amp. (primary)
Capacitance	—	—	—	—	0.0025 μf	60 μf
Inductance	—	—	—	—	Residual	480 mh
Resistance	—	—	—	—	—	25 ohms
Source gap	2 mm	2 mm	2 mm	2 mm	2 mm	2 mm
Electrode (upper)	Two briquettes of steel millings, drillings or nibblings—the flat ends are held 45° from the horizontal (see Fig. 1)					(+) briquette tilted (see Fig. 2A)
Electrode (lower)						(−) ¼-in. diameter carbon with a 120° cone tip
Sector wheel setting	None	None	None	Full/½*	None	None
Preburn/exp (time in sec.)	0/30	10/30	0/120	0/60	0/30	60/30
Line pairs	Table III	Table III	Table III	Table III	Table III	Table IV

Methods:
A-1 Cr, Ni, Mo, Sn, and Mn in plain carbon steels.
A-2 Total Al in plain carbon steels.
A-3 Zn in plain carbon steels.
A-4 B in plain carbon steels.
A-5 Cu in plain carbon steels.
A-6 Ni, Cr, Mo, Sn, Pb, Mn, Co, Cu, and Si in ingot iron.

* Rotating sector wheel used to filter one-half of the radiant power reaching the slit.

cision in terms of wet chemical values for these elements and, therefore, these methods will not be discussed.

APPARATUS

Grating Spectrograph and Accessories

The spectrograph is a three-meter grating spectrograph which has an aluminum-coated concave grating ruled 15,000 lines per in. Three orders of spectra are used for analysis. However, only the second order with a dispersion of 2.6A per mm is used for quantitative steel analysis. Further discussion of this type of spectrograph can be obtained in the literature.[7,8]

The spectrograph is supplied with four fixed slits, namely: 25, 50, 75, and 100μ. For all quantitative work, the 50μ slit is used. This slit provides ample resolution and at the same time gives a line that can be easily and accurately photo-metered.

A Universal arc-spark stand is positioned on the optical bench so that the distance from the electrodes to the slit is 93 cm. A quartz lens of 25 cm focal length is located 68.5 cm from the slit. In addition, a rotating variable sector disk is placed between the lens and the slit at the stigmatic focal point of the spectrograph. This rotating aperture prevents overexposure of some of the spectral lines used in the briquetted-sample techniques and can be adjusted from one-half to $\frac{1}{64}$ of the full exposure for one-half of the light reaching the slit.

Special holders are used to hold the briquettes when exciting the sample. These holders permit the briquettes to be held one above the other with their flat ends held 45° from the horizontal (see Fig. 1). This method of holding the briquettes provides a steady, smooth burning arc. Wandering of the arc is kept at a minimum and is confined to a plane parallel to the optical axis of the system. When one briquette is used

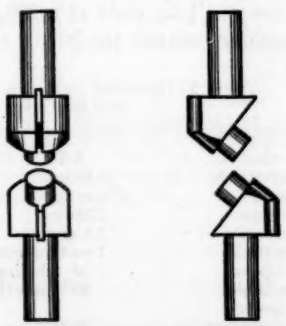

FIG. 1. Mounting of electrodes for arcing or sparking two briquettes.

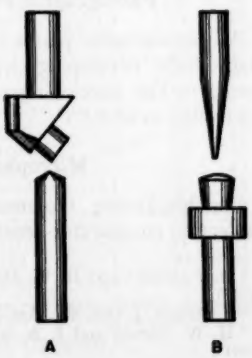

FIG. 2. Mounting of electrodes for arcing or sparking one briquette with counter carbon electrode.

[7] W. R. Brode, *Chemical Spectroscopy* (John Wiley and Sons, Inc., New York, 1943), second edition, pp. 41, 59, 121, 364, 365.
[8] W. S. Baird, *Proceedings of the Sixth Summer Conference on Spectroscopy and its Applications* (John Wiley and Sons, Inc., New York, 1939), p. 80.

TABLE III. Element and internal standard iron lines used in the analysis of plain carbon steels.

Element line	Iron line	Concentration range percent
3101.88 Ni	3173.69 Fe	0.001–0.360
3014.76 Cr	3173.69 Fe	0.015–0.150
3578.69 Cr	3567.04 Fe	0.001–0.020
3208.83 Mo	3173.69 Fe	0.010–0.050
3170.35 Mo	3173.69 Fe	0.001–0.010
3330.59 Sn	3173.69 Fe	0.015–0.100
3175.02 Sn	3173.69 Fe	0.001–0.015
3273.96 Cu	3265.62 Fe	0.030–0.500
3577.88 Mn	3543.67 Fe	0.100–0.800
3082.16 Al	3165.01 Fe	0.010–0.100
3302.59 Zn	3329.53 Fe	0.010–0.100
2496.78 B*	2391.47 Fe	0.001–0.050

* Tentative methods.

with a counter carbon electrode, the briquette is either tilted as shown in Fig. 2A or held flat as is shown in Fig. 2B. The latter technique is used in the analysis of zinc or zinc base alloys. The briquette of this material is tapered and has a smooth-rounded top surface. The tilted briquette with a counter carbon electrode is used in some cases for steel analysis.

Excitation

The various types of excitation used in this laboratory are provided by two source units, namely: The Baird Associates' power panel and the A.R.L. Dietert multisource unit.[7,9]

In general, briquetted samples of steel are excited with a 2200-v a.c. arc from the Baird Associates' power panel with either 2½ amp. or 3 amp. current in the primary. The briquetted zinc and zinc base alloys are excited by arc-like and spark-like discharges produced by the A.R.L. Dietert multisource unit.

In one method, samples of steel are excited with an a.c. spark from the Baird Associates' power panel (prewar model with a 500-w transformer). The original circuit has been modified to include an auxiliary gap and additional condensers to give an added capacitance of 0.0025 μf. The control voltage at the transformer primary is 30 v. The current at the primary is 2.5 amp.

Photographic Plate Processing

All photographic plates are processed with commercially built developing, washing, and drying equipment.[7,10] The developing machine is thermostatically controlled to 68±1°C.

Microphotometer

Line-blackening measurements are made with a projection comparator-densitometer.[7,11]

[9] M. F. Hasler and H. W. Dietert, J. Opt. Soc. Am. 33, 218 (1943).
[10] J. Schuch, J. Opt. Soc. Am. 32, 116 (1942).
[11] H. W. Dietert and J. A. Schuch, J. Opt. Soc. Am. 31, 54 (1941).

TABLE IV. Element and internal standard iron lines used in the analysis of ingot iron.

Element line	Iron line	Concentration range percent
3101.88 Ni	3171.66 Fe	0.010 –0.050
3170.35 Mo	3171.66 Fe	0.001 –0.010
3175.02 Sn	3171.66 Fe	0.001 –0.020
2833.07 Pb	3171.66 Fe	0.0001–0.010
2801.06 Mn	3171.66 Fe	0.001 –0.020
3412.34 Co	3171.66 Fe	0.001 –0.010
2843.25 Cr	3171.66 Fe	0.001 –0.010
2824.37 Cu	3171.66 Fe	0.030 –0.10
2881.58 Si	3171.66 Fe	0.0001–0.010

STANDARDS

All spectrochemical quantitative analyses are based on standard samples. These standard samples, numbering over 200, were carefully standardized chemically for one or more elements by at least two analysts. The National Bureau of Standards samples and standard samples from other steel companies are also used whenever their chemical and metallurgical properties permit.

In many cases, laboratory heats were especially made for spectrochemical standards. Only those heats on which the analyses show homogeneity are used for standards. In addition, sheet and bar samples are obtained from the Armco Operating Divisions for spectrochemical standards, especially from degraded heats which show an unusual amount of some impurity.

These laboratory-prepared standards and the National Bureau of Standard samples are used to check the analytical working curves whenever a method is used for the analysis of the miscellaneous samples received in the laboratory.

SAMPLE PREPARATION

The A.R.L. Dietert briquetting press is used to compress the metal millings, drillings, nibblings, etc., into a form preparatory to arcing or sparking.

Briquettes of steel are made by compressing the chips in a ¼-in. mold at a 200,000 lb./sq. in. A rough weighing controls the length of the briquetted chips.

TABLE V. Operating conditions for the analysis of low and high alloy steels.

Method No.	A-7	A-8	A-9
Source unit	Baird	Baird	Baird
Source	a.c. arc	a.c. arc	a.c. arc
Voltage	2200 v	2200 v	2200 v
Current	2.5 amp.	3 amp.	2.5 amp.
Electrode (upper)	Two briquettes of steel millings, drillings, or nibblings—the flat ends are held 45° from the horizontal (see Fig. 1)		
Electrode (lower)			
Preburn/exp. (time in sec.)	10/10	0/30	0/30
Line pairs	Table VI	Table VI	Table VI

Methods:
A-7 Sn in high alloy steels.
A-8 Ti, Mn, Al, Ni, Cr, Sn, Pb, and Mo in low alloy steels.
A-9 Al in low alloy steels.

TABLE VI. Element and internal standard iron lines used in the analysis of low and high alloy steels.

Element line	Iron line	Concentration range percent
2833.07 Pb	3173.69 Fe	0.001–0.030
3330.59 Sn	3173.69 Fe	0.010–0.100
3175.02 Sn	3173.69 Fe	0.001–0.020
3186.45 Ti	3173.69 Fe	0.200–0.800
3070.27 Mn	3173.69 Fe	0.020–0.080
3082.16 Al	3173.69 Fe	0.500–1.500
3114.12 Ni	3173.69 Fe	0.100–0.150
3053.88 Cr	3173.69 Fe	0.015–0.150
2816.15 Mo	2886.32 Fe	0.015–0.150
3175.02 Sn*	3175.45 Fe	0.001–0.050
3961.51 Al	3963.11 Fe	0.001–0.030

* Used for high alloy steel.

The size of the chips is not critical as long as they can be transferred to the $\frac{1}{4}$-in. diameter mold.

For softer metals, such as zinc, a $\frac{1}{4}$-in. diameter tapered mold is used because of the tendency of the metal to adhere to the mold. The pressure used on soft metals is approximately 40,000 lb./sq. in. or less and depends on the physical nature of the metal being briquetted.

SAMPLE PROCEDURES

The operating conditions for the various methods which use briquetted samples can best be shown in Tables II–VIII.

The transmittancies of the analytical line pairs shown in Tables II–VIII are measured with a projection comparator-densitometer and the wave-lengths of these spectral lines are those given in the M.I.T. wave-length tables.[12]

In general, photographic plates used with these methods are calibrated using a mercury lamp and a

TABLE VII. Operating conditions for the analysis of zinc and zinc base alloys.

Method	A-10	A-11
Source unit	A.R.L. multisource	A.R.L. multisource
Source	Arc-like	Arc-like
Voltage	940 v	940 v
Current	15 amp. (primary)	15 amp. (primary)
Capacitance	60 μf	60 μf
Inductance	480 mh	480 mh
Resistance	25 ohms	25 ohms
Electrode (upper)	(+) $\frac{1}{4}$-in. diameter carbon pointed with pencil sharpener and the end ground flat (1 mm)	
Electrode (lower)	(−) dome-shaped tapered briquette held vertically (see Fig. 2B).	
Electrode gap	2 mm	2 mm
Sector wheel setting*	Full/$\frac{1}{3}$	Full/$\frac{1}{12}$
Preburn/exp. (time in sec.)	0/10	0/40
Line pairs	Table VIII	Table VIII
Methods:		
A-10 Al, Pb, Cd, and Fe in zinc and zinc base alloys.		
A-11 Sn, Sb, and residual Al in zinc and zinc base alloys.		

* Rotating sector wheel used to filter one-half of the radiant power reaching the slit.

[12] G. H. Harrison, *M.I.T. Wave-Length Tables* (John Wiley and Sons, Inc., New York, 1939).

TABLE VIII. Element and internal standard lines used in the analysis of zinc and zinc base alloys.

Element line	Zinc line*	Concentration range percent
3261.06 Cd	3018.35 Zn	0.03 –0.30
3261.06 Cd*	3018.35 Zn	0.20 –0.80
3021.07 Fe	3018.35 Zn	0.03 –0.60
2833.07 Pb	3018.35 Zn	0.001–0.03
2833.07 Pb*	3018.35 Zn	0.30 –2.00
3082.16 Al	3018.35 Zn	0.03 –0.30
3082.16 Al*	3018.35 Zn	0.20 –5.00
2877.92 Sb	3018.35 Zn	0.02 –0.20
3175.02 Sn	3018.35 Zn	0.001–0.03

* Sectored step photo-metered.

rotating step sector. The log$T$/log$I$ curve for plates of the same emulsion is plotted on a calculating board designed by King.[13] Only the first two or three plates of a batch of plates with the same emulsion are calibrated. There are exceptions to this rule. A check calibration is made when investigating variables which are out of control.

Using the calibration curve, the galvanometer readings of the analytical lines and the internal standard lines are converted to log intensity ratios. These log intensity ratios are then converted to percent concentration by using analytical curves which have previously been established from standard samples. The average of duplicate determinations are reported.

REPRODUCIBILITY

In order to determine the reproducibility of values by a standard analytical procedure, data were collected over a period of several months. These data were obtained from standards used in routine analyses to check the analytical working curves. Thus, the precision as determined for any one element would include all the factors which influenced the spectrochemical analyses.

TABLE IX. Typical reproducibility tests of standard samples.

Standard sample	Element determined	Arithmetic mean concentration (%)	Percent standard deviation	No. of observations	No. of plates used
Low alloy steel	Al	0.0066	13.0	183	76
Plain carbon steel	Al	0.077	3.1	76	38
High alloy steel	Sn	0.038	4.5	50	25
Plain carbon steel	Cr	0.050	2.4	64	32
Plain carbon steel	Mo	0.007	7.1	60	30
Plain carbon steel	Ni	0.036	4.7	60	30
Plain carbon steel	Sn	0.027	6.7	54	27
Low alloy steel	Pb	0.010	8.0	75	38
Plain carbon steel	Cu	0.107	1.3	24	12
Low alloy steel	Pb	0.010	8.0	75	38
Plain carbon steel	Cu	0.107	1.3	24	12
Plain carbon steel	Mn	0.58	2.1	36	18
Zinc alloy	Pb	1.05	2.9	30	12
Zinc alloy	Cd	0.20	2.1	28	12
Zinc alloy	Fe	0.10	5.0	24	12
Zinc alloy	Al	3.92	1.1	20	10
Zinc alloy	Al	0.08	1.4	24	12

[13] C. King, J. Opt. Soc. Am. 32, 112 (1942).

TABLE X. Comparison of typical results of determinations made by spectrographic and by chemical methods.

No. of samples	Element	Matrix	Concentration range percent	Average concentration %	Average deviation from chemical %
76	Al	Steel (Type A)	0.006 –0.026	0.010	0.001
38	Al	Steel (Type B)	0.018 –0.078	0.031	0.001
82	Al	Steel (Type C)	0.006 –0.053	0.028	0.001
43	Al	Zinc (alloy)	0.08 –4.03	0.68	0.03
70	Sn	Steel (Type D)	0.006 –0.038	0.012	0.001
90	Sn	Steel (Type B)	0.001 –0.099	0.021	0.001
61	Sn	Steel (Type A)	0.008 –0.049	0.017	0.001
28	Sn	Steel (Type E)	0.020 –0.071	0.032	0.003
34	Sn	Zinc (alloy)	0.010 –0.021	0.012	0.001
43	Pb	Zinc (alloy)	0.18 –1.18	0.63	0.04
79	Pb	Steel (Type A)	0.0005–0.028	0.0034	0.0005
21	Pb	Steel (Type E)	0.0009–0.012	0.0048	0.0003
150	Ni	Steel (Type B)	0.004 –0.36	0.064	0.003
98	Ni	Steel (Type A)	0.67 –1.36	0.82	0.05
111	Mo	Steel (Type B)	0.002 –0.050	0.012	0.001
53	Mo	Steel (Type A)	0.014 –0.135	0.079	0.005
119	Cr	Steel (Type B)	0.002 –0.133	0.040	0.002
45	Cr	Steel (Type A)	0.021 –0.091	0.043	0.004
320	Mn	Steel (Type B)	0.15 –0.60	0.36	0.01
99	Mn	Steel (Type A)	0.42 –0.89	0.56	0.03
70	Ti	Steel (Type A)	0.014 –0.064	0.048	0.004
36	Cu	Steel (Type B)	0.033 –0.31	0.110	0.006
34	Sb	Zinc (alloy)	0.004 –0.12	0.064	0.007
32	Fe	Zinc (alloy)	0.03 –0.42	0.096	0.01
70	Cd	Zinc (alloy)	0.04 –0.56	0.16	0.02

Table IX shows the typical reproducibility tests made for a few elements in different matrices. The percent standard deviation varied from 1.1 percent for an element concentration of 4.0 to 13.0 percent for an element concentration of 0.005 percent. The percent standard deviation is found by dividing the standard deviation obtained for a series of determinations by the arithmetic mean concentration of the element in question and multiplying by 100.

ACCURACY

In any laboratory the accuracy of any test method is usually determined by comparison with an accepted alternate method. Therefore, when a spectrochemical method is developed in our laboratory, a measure of the accuracy of results obtained by this method is determined by comparison of the results with those obtained by wet chemical methods. Also, after a spectrochemical method has been accepted for routine control, frequent check analyses are made by the wet chemical laboratory.

Comparison of analyses by both the wet chemical and spectrochemical methods are shown in Table X. These comparisons were made over a considerable period of time and include all data obtained. Table X shows the number of samples from which the comparisons were made, the elements determined in different matrices, the concentration range of each element, the average concentration of each element, and the average deviation of the spectrographic values from those obtained chemically.

These data were not obtained under idealized conditions, but include errors from all variables encountered, such as wet chemical errors, excitation errors, segregation errors, photographic errors, etc. Such errors cannot be eliminated entirely when analyses are made from day to day, on a routine basis, in a laboratory that receives all types of material for analysis.

For the most part, however, the average deviations observed between the spectrographic and chemical determinations are sufficiently small to permit the spectrochemical methods to be used for routine control. In some cases, spectrographic determinations are superior in accuracy to routine chemical determinations.

SUMMARY

Outlines of the techniques using briquetted samples have been discussed for the analysis of steels, and other metals. These techniques were developed to meet specific needs for rapid analysis on problems encountered by the Armco Research Laboratories. In most cases, only drillings, millings, etc., of the samples to be analyzed were available; therefore, it was necessary to develop methods using briquetted samples.

These techniques have been used with success by our laboratory for several years. For the most part, the accuracy obtained by spectrochemical methods compare favorably with that obtained by routine wet chemical methods.

ACKNOWLEDGMENTS

The author expresses his appreciation to The Armco Steel Corporation for permitting presentation of these studies; to Mrs. L. J. Canody for preparation of samples and spectrochemical analyses, and to Mr. A. H. Thomas and Mr. C. S. Mills for their assistance and suggestions.

JOURNAL OF THE OPTICAL SOCIETY OF AMERICA VOLUME 40, NUMBER 4 APRIL, 1950

Low Intensity Reciprocity-Law Failure in Photographic Exposure
II. Multiplet-Quantum Hits in a Critical Time Period*†

J. H. WEBB
Kodak Research Laboratories, Eastman Kodak Company, Rochester, New York
(Received January 19, 1950)

In a previous paper, the author analyzed the low intensity reciprocity-failure curve by means of probability formulas applied to the exposure conditions required to establish the stable sublatent-image speck. Experiments have shown that low intensity reciprocity failure results from instability of the latent image in its initial stages of formation due to thermal motion. The theory given is based on the postulate that a stable subspeck can be formed in a grain only when that grain receives a multiplet hit of size 2, 3, or, in general, s quanta within a small critical time period τ. By application of the probability theory, it is possible to calculate what fraction of grains will acquire a stable subspeck when a large number of identical grains are subjected to an exposure of total duration, t, in which the average number of effective quanta per grain in the whole exposure is y. By varying the time and intensity factors of exposure reciprocally, the reciprocity failure can be calculated and compared with experiment. If it is assumed that the critical τ-period is a constant invariable quantity for all grains, it can be shown that the reciprocity-failure curve has a slope at low intensities that is characteristic of the number of quanta required to establish the stable subspeck, the slope being zero for one quantum, -1 for two quanta, -2 for three quanta, etc. In the present paper, the theory is extended to the case of variable τ-period among the grains, and it is found that the same simple conclusions as to slope of the reciprocity-failure curve hold in this case as were found in the constant τ-period case.

INTRODUCTION

IN a former paper[1] on this same subject, hereafter referred to as (I), the reciprocity-law failure at low intensities was treated by probability formulas applied to the exposure conditions required to establish the just-stable sublatent image.†† In this work, it was assumed that low intensity reciprocity-law failure is due to instability of the latent-image speck when it starts to form due to thermal motion. It was assumed that the latent-image photo-product is built up in a series of discrete steps individually initiated by the successive absorption of discrete quanta of light. Experiments[2–7] have shown that after a certain number of these discrete steps, the photo-product speck attains a critical size that is stable but not yet developable. Below this critical size, the speck tends to disintegrate under thermal motion. Accordingly, the building of the stable subspeck under low light illumination is inefficient, because there is more time for the speck to disintegrate while it is being built up to its critical size. This inefficiency of latent-image formation in its initial stages accounts for the reciprocity-law failure at low exposing intensities.

In (I) it was shown to be possible to formulate the problem of latent-image formation at low intensities according to the postulate that at least 2, 3, or, in general, s discrete processes must occur during a critical time period, τ, in order to produce a just-stable subspeck. Thus, during a total exposure time, t, in which the total effective exposure of a single grain (all grains assumed to be identical in size and inherent sensitivity) is y quanta, it would be required that 2, 3, or, in general, s quanta would have to be absorbed by one grain in a critical time period, τ. Of course, to build the stable subspeck to developable size would require additional quanta (e.g., 6 to 8) but those quanta received after the stable subspeck is formed would be utilized with 100 percent efficiency and thus would not contribute to the reciprocity-law failure.

Two formulas were used in the previous paper (I) to derive the theoretical H and D curves‡ for the two and three quantum-hit cases. The first formula, which was developed earlier by L. Silberstein[8] specifically to treat reciprocity-law failure, gives the probability, P, that in an exposure of duration, t, in which one grain receives on the average a total of y effective quanta, at least two of these quanta will strike the grain within a critical time period, τ, thus,

$$P=1-\epsilon^{-y}\sum_{j=0}^{m+1}\frac{y^j}{j!}\left[1-(j-1)\frac{\tau}{t}\right]^j, \qquad (1)$$

in which $m=(t/\tau)-1$. The number of photographic grains, k, per unit area attaining a just-stable speck will be given by PN, where N is the total number of grains per square centimeter. Thus, we can write, for the fraction of grains acquiring a stable speck:

$$k/N=P. \qquad (2)$$

The second formula, treating the general case of the

* Communication No. 1309 from the Kodak Research Laboratories.
† Presented at the New York Meeting of the Optical Society of America, March, 1950.
[1] J. H. Webb, J. Opt. Soc. Am. **40**, 3 (1950).
†† For a similar treatment of this problem of reciprocity-law failure at low intensity, the reader is referred to the recent paper by E. Katz, J. Chem. Phys. **17**, 1132 (1949).
[2] C. E. Weinland, J. Opt. Soc. Am. **15**, 337 (1927); **16**, 295 (1928).
[3] J. H. Webb and C. H. Evans, J. Opt. Soc. Am. **28**, 431 (1938).
[4] P. C. Burton and W. F. Berg, Phot. J. **86B**, 2 (1946).
[5] P. C. Burton, Phot. J. **86B**, 62 (1946).
[6] P. C. Burton, Phot. J. **88B**, 13 (1948).
[7] W. F. Berg and P. C. Burton, Phot. J. **88B**, 84 (1948).
‡ The term, "H and D curve," used throughout this paper refers to the relationship, k/N *versus* log exposure to produce the stable sublatent image.
[8] L. Silberstein, J. Opt. Soc. Am. **29**, 432 (1939).

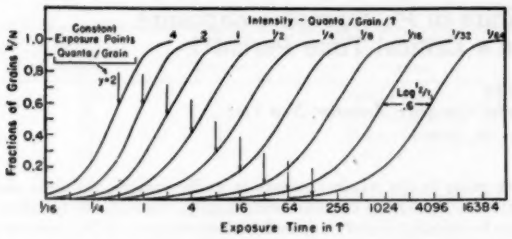

FIG. 1. Theoretical time-scale exposure curves calculated for varying exposure intensities from the double-hit formula, (1).

absorption of 2, 3, or, in general, s quanta by a grain within a critical time period, τ, is an approximation formula that was first worked out by L. Silberstein[9] in a purely mathematical connection. Silberstein treated the problem of a random distribution of n points along a line of unit length and calculated the expected (average) number of occurrences of s points falling within a given small fractional element, λ, of this line. By identifying λ with our τ/t, and n with our exposure value per grain, y, then Silberstein's formula, adapted to our case, becomes:

$$Q_s(y)=s\left(\frac{\tau}{t}\right)^{s-1}\frac{y!}{(y-s)!s!}\times\left\{1-\frac{4+K}{s+1}\frac{\tau}{t}(y-s)-\frac{s-1}{s}\frac{\tau}{t}\right\}, \quad (3)$$

in which $K=s-1(\frac{1}{2}+\frac{1}{3}+\cdots+1/s)$. The formula, (3), is a good approximation under the conditions: $\tau/t\ll 1$ and $y\tau/t<\frac{1}{2}$. $Q_s(y)$ is the average number of occurrences of multiplet absorption of size, s, in a critical time, τ, when there are y total quantum hits on a grain in the period of exposure, t. If $Q_s(y)$ is the average number of s-multiplets, then the probability of one or more s-multiplet hits in the total exposure time, t, will be

$$P=1-e^{-Q_s(y)}. \quad (4)$$

As was done in the case of Eq. (2) above, this probability, P, can be identified with the fractional number of photographic grains acquiring a just-stable speck, thus,

$$k/N=1-e^{-Q_s(y)}, \quad (5)$$

in which $Q_s(y)$ has the value given by (3).

For exposures at extremely low intensities and long exposure times, the quantities, y/t and τ/t, become very small indeed. Under these circumstances, as shown in (I), the expression, (3), reduces to the simplified form,

$$Q_s(y)=\frac{[y(\tau/t)]^{s-1}y}{(s-1)!}. \quad (6)$$

Since y/t is the intensity factor, I, of the exposure expressed in effective quanta per grain per unit of time, (6) can be written in the form,

$$\frac{Q_s(y)}{t}=\frac{(I\tau)^{s-1}I}{(s-1)!}=F_s, \quad (7)$$

which defines the frequency, F_s, of multiplet hits of size, s, per unit of time. The reduced equation for the fraction of grains having one or more multiplet hits of size, s, in the exposure time, t, can then be written,

$$k/N=1-e^{-F_s t}. \quad (8)$$

Series of H and D curves can be calculated from the Eqs. (1) and (4) for doublet and triplet cases, respectively, for a series of descending values of intensity, I, as was done in the earlier paper. The intensity values, $I=y/t$, can be specified in terms of effective quanta per grain per unit of time, τ. In Fig. 1 is shown a series of theoretical curves obtained from Eq. (1) for the doublet case. These are time-scale curves plotted as a function of exposure time expressed in units of the critical time period, τ. By projecting a horizontal line across the H and D curves of Fig. 1 for the constant ordinate value, $k/N=0.5$, exposure values, $y(=It)$, required to produce this constant effect at different intensities can be obtained. Exposure values obtained in this way from Fig. 1 are shown in Fig. 2 by the curve labeled "$s=2$." In addition, reciprocity-failure curves are also shown in Fig. 2 for the two other cases of $s=3$ and $s=1$. The $s=3$ curve was obtained from H and D curves plotted according to Eq. (4), corresponding to triplet hits in the critical time, τ. The curves marked "$s=1$" were derived from H and D curves plotted according to the simple Poisson equation (see Paper I),

$$k/N=1-e^{-y}\sum_{j=0}^{r-1}\frac{y^j}{j!}, \quad (9)$$

for r values of 2 and 3, respectively. This equation is a

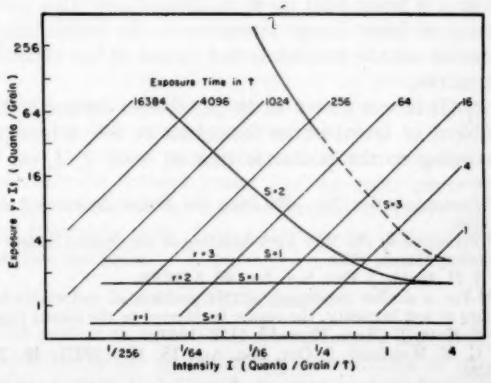

FIG. 2. Theoretical reciprocity-failure curves for sub-image: (a) from the exposure curves of Fig. 1 for the double-hit ($s=2$) case; (b) from exposure curves from formula (4) for the triple-hit ($s=3$) case; and (c) from exposure curves from formula (9) for the single-hit ($s=1$) case.

[9] L. Silberstein, Phil. Mag. 36, 319 (1945).

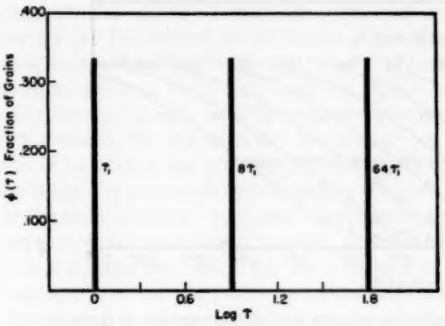

FIG. 3. Distribution of τ-periods among grains of mixture emulsion in which $\frac{1}{3}$ of grains have τ-period, τ_1; $\frac{1}{3}$ of grains have τ-period, $8\tau_1$; $\frac{1}{3}$ of grains have τ-period, $64\tau_1$.

function of the exposure factors, I and t, only through their product, y, and thus cannot account for reciprocity-law failure. It merely gives the number of grains that receive at least r quanta when the average grain receives a total of y quanta. Of course, formula (9) corresponds to the simple case of $s=1$, since the absorption of any single quantum would always occur within a single τ-period, no matter how short.

EXTENSION OF ANALYSIS TO VARIABLE τ-PERIOD

In the paper (I) and in the analysis given above, it has been assumed that the critical τ-period is a constant, invariable quantity, the same for each grain. With this restriction, it has been found that the reciprocity-failure curves (Fig. 2) approach constant limiting slope values at low intensity that are characteristic of the number of quanta required to establish the stable subspeck.

It is natural to inquire whether this simple conclusion, arrived at for a constant τ-period for all grains, would still hold for the case in which τ has a wide distribution of values for the different grains of the emulsion. As will be seen subsequently, it is possible to show that the conclusion that the slope of the reciprocity-failure curve approaches the value, $-(s-1)$, for the case of s-size multiplet hits, is also valid for variable periods among the grains.

The simplest and most instructive way to show the effect of a variation of the τ-values is to work out an illustrative example in which τ covers a wide range of values among grains. For this purpose, we assume an emulsion made up of a mixture of three equal batches of grains for which the τ-periods have the discrete values, τ_1, $8\tau_1$, and $64\tau_1$, respectively, thus covering a range of 1 to 64. Such a distribution of τ-periods among the grains can normally be represented by a function, $\varphi(\tau)$, such that $\varphi(\tau)d\tau$ represents the fraction of all grains whose τ-periods lie between τ and $\tau+d\tau$. The function chosen here is shown by the discontinuous graph in Fig. 3. The function, $\varphi(\tau)$, must satisfy the normalizing condition,

$$\int_0^\infty \varphi(\tau)d\tau=1,$$

and this is achieved in the present case by dividing the grain into three equal fractions, with one-third having the τ-period, τ_1, one-third having the τ-period, $8\tau_1$, and one-third having the τ-period, $64\tau_1$.

By means of the curves of Fig. 1 derived from Eq. (1), it can be shown readily by a superposition process how the reciprocity-failure curve behaves for an emulsion composed of these three types of grains. The procedure is illustrated graphically in Fig. 4. A first set of H and D curves, corresponding to the first one-third fraction of the grains with τ-period equal to τ_1, would be identical with the curves of Fig. 1. These have been redrawn as the solid-line curves (1–9) in Section A of Fig. 4. This series of curves has been extended to lower intensity values as shown by the dashed curves (10–15). A second series of H and D curves, corresponding to the second one-third fraction of the grains with τ-period equal to $8\tau_1$ is shown in Section B of Fig. 4. These H and D curves, represented by the solid lines (4–12), are identical with the solid-line curves of Section A, except they have been shifted by a factor of eight along the exposure axis. It is immediately obvious that this is the correct position for these curves, because if the τ-period is increased by a factor of eight times, then the curves for the same intensity values, expressed in terms of quanta/grain/τ, will correspond to a lower absolute intensity level (quanta/sec.) by a factor of eight. Therefore, they must be translated by this amount along the exposure time axis. That the solid-line curves of Section B should have the same shapes as those of Section A is obvious, if it is considered that the τ-period for the curves of Section B has been increased eightfold, while the intensity (quanta/sec.) has been decreased by the same factor, so that the average number of quanta per grain per τ-period remains unchanged and is statistically identical

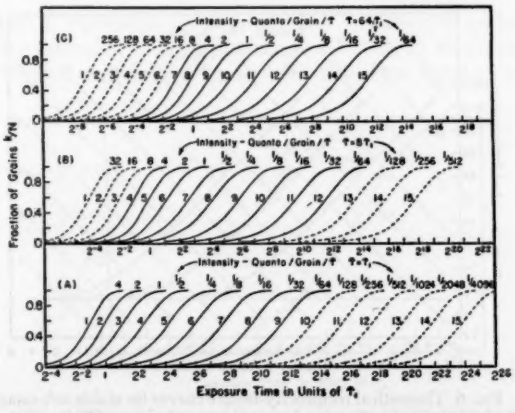

FIG. 4. Theoretical exposure curves for three emulsions with grains having τ-periods, τ_1, $8\tau_1$, and $64\tau_1$, respectively, for the doublet-hit case ($s=2$), for varying exposing intensity.

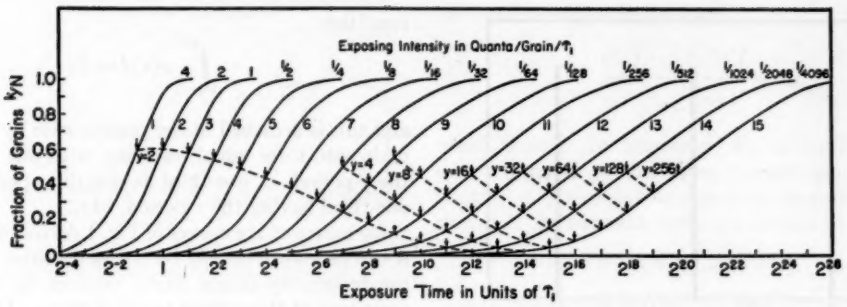

FIG. 5. Theoretical exposure curves with varying intensity for mixture emulsion comprised of three equal fractions of grains having widely differing τ-periods. Curves obtained by summing the three sets of curves in Fig. 4.

in the two cases. Here again the H and D curves have been extended to lower intensity values, as shown by the dashed curves (13–15), in order to have a one-to-one correspondence between H and D curves for the first and second fractions of grains. For the same reason, the H and D curves have been extended to higher intensity levels. These latter, shown by the dashed curves (1–3) in Section B, were obtained from the formula, (9), for the case, $r=2$. It was assumed that two quanta are required to establish the stable subspeck, but under these conditions of high intensity, there is no inefficiency due to reciprocity-law failure, since the average number of quanta per τ-period is greater than 2.

In Section C of Fig. 4 is shown a third series of H and D curves, where the solid-line curves (7–15) are again duplicates of those in Sections A and B but shifted by an additional factor of eight along the exposure axis. The dashed curves (1–6) represent H and D curves at the higher intensity values, i.e., more than two quanta per τ-period, and these show no reciprocity-law failure.

It is to be noted that there are 15 H and D curves in each of the sections, A, B, and C, of Fig. 4. To obtain the series of H and D curves for the emulsion composed of a mixture of three equal fractions of grains of the type

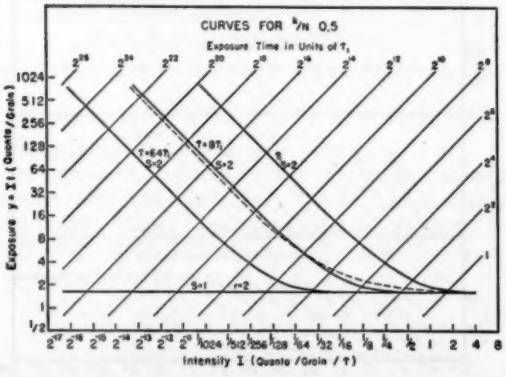
CURVES FOR k/N 0.5
Exposure Time in Units of τ_1
Exposure $y=\bar{\imath}\tau_1$ (Quanta/Grain)
Intensity $\bar{\imath}$ (Quanta/Grain/τ)

FIG. 6. Theoretical reciprocity-failure curves for stable sub-image for doublet-hit ($s=2$) case; (——) three separate emulsions having τ-periods, τ_1, $8\tau_1$, and $64\tau_1$, respectively; and (- - - -) for a mixture emulsion comprised of a mixture of the three types of grains.

discussed, it is only necessary to sum the ordinates of the curves of corresponding number in the three sections of Fig. 4, multiply the sum by the normalizing factor, $\frac{1}{3}$, and plot the resulting values of k/N as a function of exposure time. This has been done in Fig. 5, in which the exposure times and intensity factors are expressed in units of the shortest τ-period, i.e., τ_1. For convenient reference, dashed lines of constant exposure (y quanta per grain) have been drawn in to indicate the decrease in k/N, for constant exposure, with increased exposure time.

If a horizontal line is extended across the H and D curves of Fig. 5 at the height, $k/N=0.5$, the points of intersection with the successive H and D curves locate the exposure values required to produce the constant k/N value with decreasing intensity. Exposure values obtained in this manner are shown in Fig. 6 by the dashed curve, which thus represents the reciprocity-law failure for the mixture emulsion composed of grains with varying τ-values. The three solid-line curves of Fig. 6 represent the reciprocity-failure curves of three separate homogeneous emulsions composed of grains with τ-periods, τ_1, $8\tau_1$, and $64\tau_1$, respectively. It should be observed that the curve for the composite mixture emulsion is in close agreement with that of the intermediate emulsion having all grains of $8\tau_1$-type, thus falling at the approximate position of the geometrical mean between the curves of τ_1- and $64\tau_1$-periods. It is also to be noted that the curve for the mixture emulsion has closely the same shape as that of the curves for the three homogeneous emulsions, turning up with a slope of unity at low intensities. Thus, the wide distribution of τ-periods assumed in the mixture emulsion does not appear to affect the conclusion arrived at for the emulsion with grains having a single τ-period, as regards the ultimate slope approached by the reciprocity-failure curve at low intensity. The effect of variable τ-periods is to introduce a slight alteration in the shape of the reciprocity-failure characteristics in the region of intermediate intensities.

Though the graphical analysis carried out in Figs. 4 and 5 is somewhat crude, it makes possible an under-

standing of the effect of variable τ-periods on the reciprocity-law failure and on the shapes of the H and D curves that is not easily gained otherwise. For example, in the three sections, A, B, and C, of Fig. 4, the lowest intensity curves (14–15) have in each case reached the point for which the loss of speed is constant for each successive halving of the intensity level. Also, however, at this point the curves of corresponding number (e.g., 15) in the three sections, A, B, and C, are spread along the exposure axis by a factor of eight between curves which will remain constant at all lower intensities. This wide spread between the positions of the curves along the exposure axis, when the curves are summed, gives rise to the wide latitude exhibited by the H and D curves at low intensity as shown in Fig. 5. In fact, experimental H and D curves rarely show such a large change in their slope with intensity as indicated in Fig. 5, which indicates that the wide variation of τ-periods assumed here (64 times) is larger than occurs in ordinary emulsions.

To illustrate the change in slope of the H and D curve at low intensity due to an alternative distribution of τ-periods among the grains, another distribution of τ-periods, shown by the function, $\varphi(\tau)$, in Fig. 7, is employed in a second example. An emulsion is assumed to be made up of three types of grains: 65 percent having a τ-period, τ_1; 25 percent, $2\tau_1$; and 10 percent, $4\tau_1$. By making use of the three curves marked "15" in Fig. 4, adjusting their maximum heights in accordance with $\varphi(\tau)$, and placing them along the exposure axis with separations of powers of two, the curves can be summed to give the H and D curve in Fig. 8. It will be noticed that this H and D curve has a slope very different from that of the curve, 15, that was derived in Fig. 5. However, a series of H and D curves drawn in accordance with the distribution function, $\varphi(\tau)$, of Fig. 7 would yield a reciprocity-failure curve closely the same as that shown in Fig. 6. Accordingly, it may be concluded that the form of the distribution function for the τ-values among the grains has little effect on the general shape of the reciprocity characteristic but a marked effect on the shapes of the H and D curves for the stable subspeck produced at different intensity levels.

LIMITING SLOPE OF THE RECIPROCITY-FAILURE CURVE INDEPENDENT OF THE FUNCTION, $\varphi(\tau)$

From the analysis given in the preceding section, it appears that the form of the function, $\varphi(\tau)$, affects the reciprocity-failure curve slightly at intermediate intensity values, but has no effect on the ultimate slope approached by this curve at extremely low intensities. Indeed, it is readily possible to show by analytical means that this is a generally valid conclusion, the asymptotic slope approached by the reciprocity-failure curve at low intensities being dependent only upon the number of quanta required to establish the stable subspeck.

At extremely low intensities, the simplified equation, (8), accurately represents the H and D curve. The exponential term in Eq. (8),

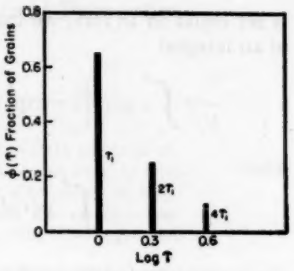

FIG. 7. Distribution of τ-periods among grains of mixture emulsion in which 65 percent of grains have τ-period, τ_1, 25 percent have τ-period, $2\tau_1$, and 10 percent have τ-period, $4\tau_1$.

$$F_s t=\frac{(I\tau)^{s-1}It}{(s-1)!}=\frac{I^s t}{(s-1)!}\tau^{s-1}, \tag{10}$$

determines, for any exposure value, It, the fraction of grains, k/N, acquiring a stable subspeck. Accordingly, the reciprocity-failure curve of the types shown in Figs. 2 and 6, constructed for a constant value of k/N, requires that $F_s t$ remain constant at all intensity levels, I. Therefore, the equation of the reciprocity-failure curve at low intensities, where (10) is valid, corresponds to the condition:

$$I^s t=\text{constant}, \tag{11}$$

since $\tau^{s-1}/(s-1)!$ is already a constant.

If now we assume an emulsion made up of a distribution of grains in which a fraction, a_1, of grains has a τ-period, τ_1, a fraction, a_2, a period, τ_2, a fraction, a_3, a period, τ_3, etc., we can write the equation of the composite exposure curve of all grains as

$$\frac{k}{N}=\sum_1^L a_i\left[1-\exp\left(-\frac{I^s t}{(s-1)!}\tau_i^{s-1}\right)\right], \tag{12}$$

in which

$$\sum_1^L a_i=1,$$

and L represents the total number of classes of grains. By extension to a continuous distribution in which the fraction of grains having a τ-period between τ and $\tau+d\tau$

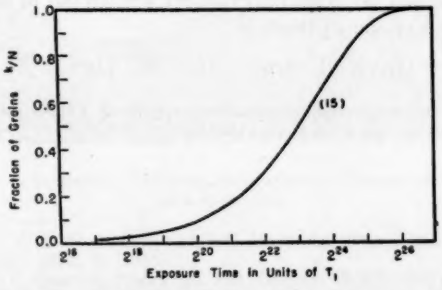

FIG. 8. Theoretical exposure curve calculated for extremely low exposing intensity for emulsion made of grains with τ-periods distributed as in Fig. 7.

is set equal to $\varphi(\tau)d\tau$, we can write (12) in the form of an integral

$$\frac{k}{N}=\int_0^A \varphi(\tau)\left\{1-\exp\left[-\frac{I^s t}{(s-1)!}\tau^{s-1}\right]\right\}d\tau, \quad (13)$$

where

$$\int_0^A \varphi(\tau)d\tau=1. \quad (14)$$

The reciprocity-failure curve represents the relationship between $\log It$ and $\log I$, for the condition k/N constant. In order to keep k/N constant, it may be seen from (13) and (14) that the equation

$$\int_0^A \varphi(\tau)\exp\left[-\frac{I^s t}{(s-1)!}\tau^{s-1}\right]d\tau=\text{constant}, \quad (15)$$

must be satisfied, and this must hold for all values of I. Since I is independent of τ, it is readily seen that (15) can be satisfied only provided

$$I^s t/(s-1)!=\text{constant}. \quad (16)$$

If (16) holds, then (15) will be satisfied regardless of the form of the function $\varphi(\tau)$ since the integral is merely a function of its limits and these are constants. Since s is a constant, the condition (16) can be written

$$It=C_1 I^{-(s-1)}, \quad (17)$$

where C_1 is a constant. Writing (17) in logarithmic form, we find

$$\log It=C_2-(s-1)\log I, \quad (18)$$

which is the equation of the reciprocity-failure curve. Accordingly, the equation of the reciprocity-failure curve at extremely low intensities becomes a straight line with slope $-(s-1)$, irrespective of the form of the function, $\varphi(\tau)$.

SHAPE OF THE *H* AND *D* CURVE DEPENDENT UPON $\varphi(\tau)$

The equation of the exposure curve of the stable subspeck (8) can also be treated analytically from the standpoint of variable τ in a straightforward manner.¶ Equation (8), with the exponent written out in full for grains of one τ-period, is

$$(k/N)_1=1-\exp\{-[(I\tau)^{s-1}It]/[(s-1)!]\}. \quad (8')$$

¶ This was brought to my attention by Dr. F. Urbach, to whom I wish to express my sincere thanks.

If it is desired to treat this equation for variable τ-period, it is only necessary to multiply the right side by the function, $\varphi(\tau)d\tau$, which gives the distribution of τ-periods among the grains, and integrate over the total range of τ-periods. Thus,

$$\frac{k}{N}=\int_0^A \varphi(\tau)\left\{1-\exp\left[-\frac{(I\tau)^{s-1}It}{(s-1)!}\right]\right\}d\tau, \quad (17)$$

where the normalizing condition must hold:

$$\int_0^A \varphi(\tau)d\tau=1.$$

In general, the equation of the exposure curve, (17), will depend upon the functional form of $\varphi(\tau)$, as indeed was shown in the graphical treatment given earlier. This is readily seen from Eq. (17), in which it is no longer possible to use the condition $I^s t=\text{constant}$, as was done in Eq. (13).

An interesting case can be treated by using an exponential distribution of τ-periods and applying the analysis to the doublet-hit case for which $s=2$. As pointed out to the author by F. Urbach, this is the type of distribution of τ-periods that would result from an exponential decay of the product of the first hit of the doublet. We take as the distribution function:

$$\varphi(\tau)=C\exp(-\tau/\bar{\tau}), \quad (18)$$

in which we assume $\tau=0\rightarrow\infty$, $\bar{\tau}$ is the average τ-period, and C is equal to $1/\bar{\tau}$.

Inserting (18) in (17) and setting $s=2$, we find

$$\frac{k}{N}=\frac{1}{\bar{\tau}}\int_0^\infty e^{-\tau/\bar{\tau}}[1-\exp(-I^2 t\tau)]d\tau. \quad (19)$$

Carrying out the integration, we obtain

$$\frac{k}{N}=\frac{I^2 t\bar{\tau}}{1+I^2 t\bar{\tau}}. \quad (20)$$

Equation (20) is thus seen to differ in form from Eq. (8),

$$k/N=1-\exp(-I^2 t\tau),$$

that would hold for an emulsion of grains with a single τ-period. It is therefore obvious that the shape of the H and D curve will depend upon the functional form of the distribution function, $\varphi(\tau)$.

JOURNAL OF THE OPTICAL SOCIETY OF AMERICA VOLUME 40, NUMBER 4 APRIL, 1950

The Structure of Evaporated Metal Films and Their Optical Properties

R. S. SENNETT* AND G. D. SCOTT
Department of Physics, University of Toronto, Toronto, Canada

(Received January 6, 1950)

The structure of evaporated films of eight different metals in thicknesses from 30 to 500A has been observed in the electron microscope and correlated with their optical properties. The stable form of films thinner than a characteristic thickness was found to be aggregated. For each film the absorptions for wavelengths in the visible were determined from the measured transmissions and reflections. The rate of formation is shown to affect the structure and the optical properties, slow rates in general giving more aggregated structure and increased light absorption.

The Garnett theory has been used to explain the peculiar variation with thickness of the optical properties of thin metallic films in terms of the observed structure of the films and the bulk properties of the metal. The presence or absence of absorption maxima and their change with wave-length can be predicted qualitatively on the basis of this theory for all the films studied.

INTRODUCTION

IT is well known that thin films of a number of metals show brilliant colors while those of other metals have only a metallic appearance. The similarity between the colors of gold films and colloids of that metal was first reported by Faraday[1] in 1857 and led him to suggest an aggregated structure for the thin films.

The optical constants, n the refractive index and k the extinction coefficient, have been determined for metallic films by a number of different methods. Pogany[2] found n and k for platinum, palladium, gold, and silver films from the change in polarization of light reflected from the films. However, most workers have measured the transmission and reflection of the films and employed graphical methods[3] to determine the values of n and k. In this way Murmann[4] found a maximum in the product nk for silver films at a thickness of approximately 100A. Krautkrömer has reported a similar variation in the case of gold films.[5]

The electromagnetic theory was applied to the optical properties of thin films by Drude[6] in 1894. This gave good agreement with experiment for films thicker than about 200A by assuming that the films were continuous. However to maintain the agreement in thinner films a marked change of the optical constants with thickness had to be postulated. In 1904 Garnett[7] showed that this change in the optical constants from those of the bulk metal could be explained by assuming that the thinner films were composed of numerous small aggregates.

In the early work the structure of films could be inferred only from studies of the various properties. Light microscope observations showed that in thick films of a number of metals aggregates appeared upon heating.[8] Though x-ray and electron diffraction studies[9] suggested that metal films in general are aggregated, this fact has been proved conclusively by electron microscope observations.[10,11] These latter results have shown that films of most metals thinner than a characteristic thickness are composed of separate aggregates with definite channels between them. However no detailed comparison has been reported between the structure observed in the electron microscope and the experimentally determined properties.

EXPERIMENTAL

The variation with thickness of the structure and of the optical properties was determined for films of the following metals: silver, gold, copper, aluminium, antimony, nickel, palladium, and chromium.

The films were formed by vacuum evaporation of the metal from a tungsten filament or a molybdenum boat. The techniques involved in such evaporations have been

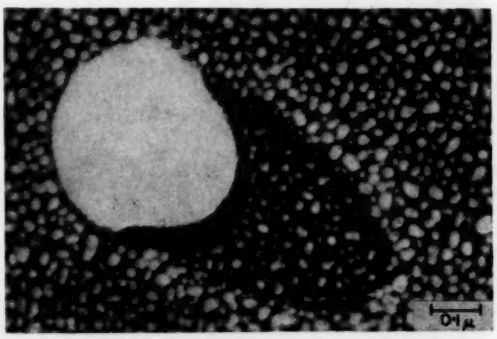

FIG. 1. Similarity of the structure of silver on Formvar and on silica substrates.

* Part of this research was carried out while one of the authors (R.S.S.) was a holder of a Studentship from the National Research Council of Canada.

[1] M. Faraday, Trans. Roy. Soc. (London) **147**, 145 (1857).
[2] B. Pogany, Ann. d. Physik **49**, 531 (1916).
[3] K. Försterling, Ann. d. Physik **30**, 745 (1937).
[4] H. Murmann, Zeits. f. Physik **80**, 161 (1933).
[5] J. Krautkrömer, Ann. d. Physik **32**, 537 (1938).
[6] P. Drude, Ann. d. Physik **51**, 77 (1894).
[7] J. C. M. Garnett, Trans. Roy. Soc. (London) **203A**, 385 (1904).
[8] E. N. da C. Andrade and J. G. Martindale, Trans. Roy. Soc. (London) **235A**, 69 (1935).
[9] A. G. Quarrell, Proc. Phys. Soc. (London) **49**, 279 (1937).
[10] R. G. Picard and C. S. Duffendack, J. App. Phys. **14**, 291 (1943).
[11] H. Levinstein, J. App. Phys. **20**, 306 (1949).

Structure and Optical Properties of Silver Films Rapidly Evaporated (2 Seconds)

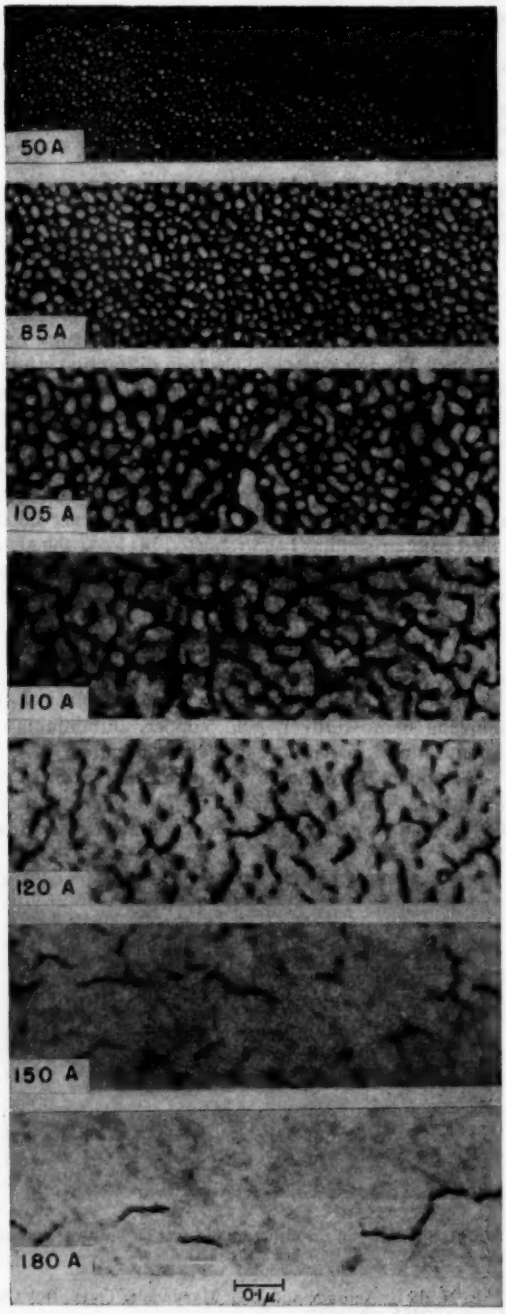

FIG. 2a. Electron micrographs of silver films showing the structure at the seven indicated thicknesses.

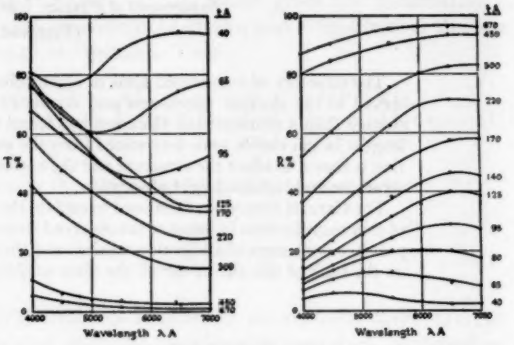

FIG. 2b. Wave-length variation of the transmission and reflection of silver films for different thicknesses.

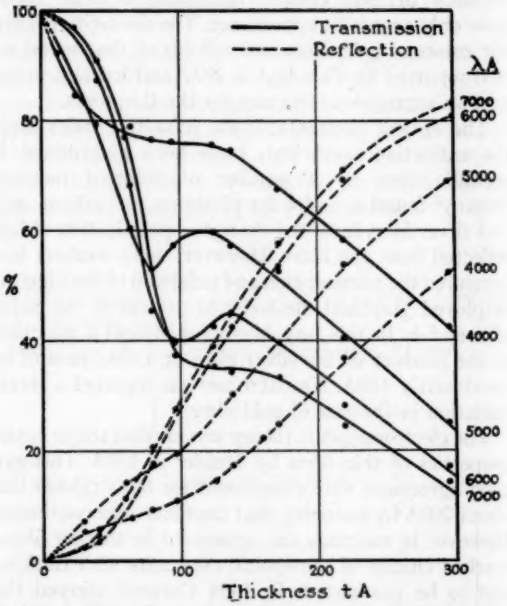

FIG. 2c. Variation of transmission and reflection with thickness.

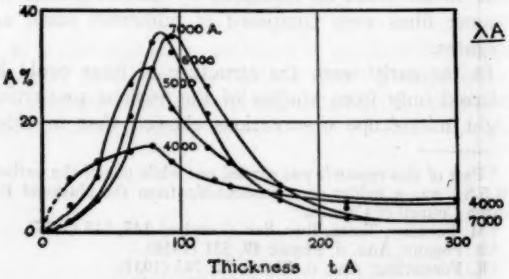

FIG. 2d. The absorption of silver films against thickness for different wave-lengths.

Structure and Optical Properties of Silver Films Evaporated Slowly

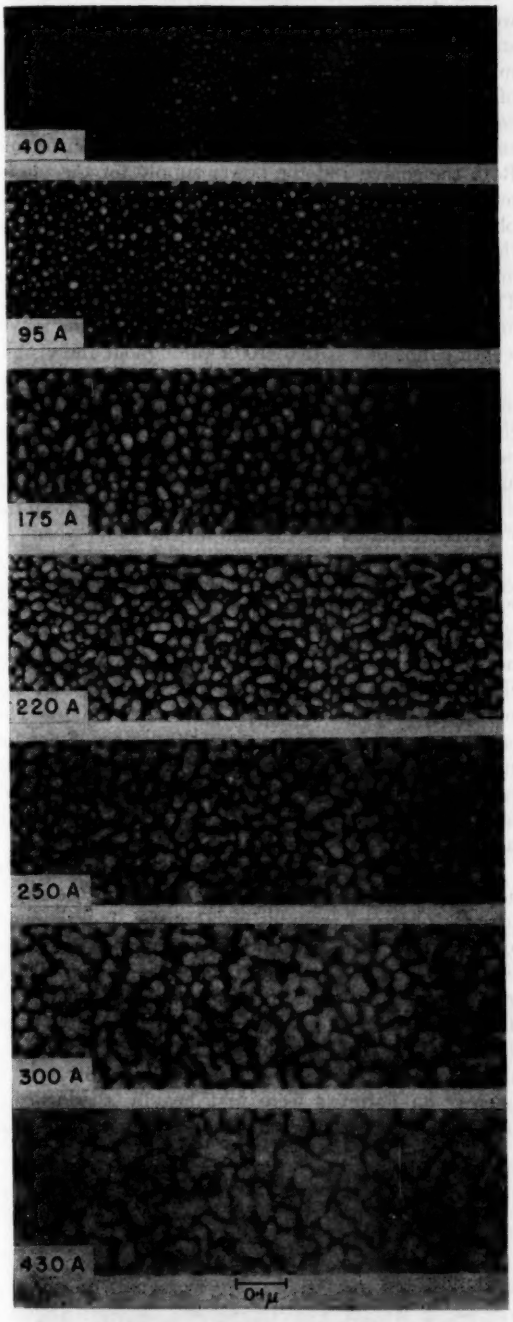

FIG. 3a. Electron micrographs of silver films deposited in 20 minutes.

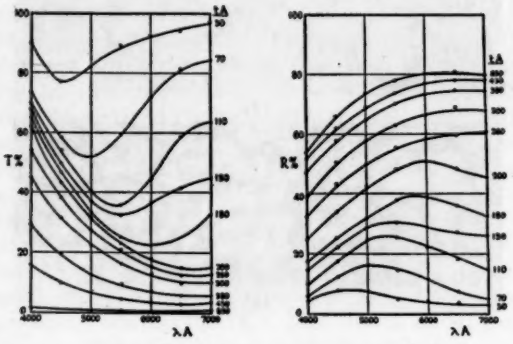

FIG. 3b. Transmission and reflection of silver films deposited in 20 minutes.

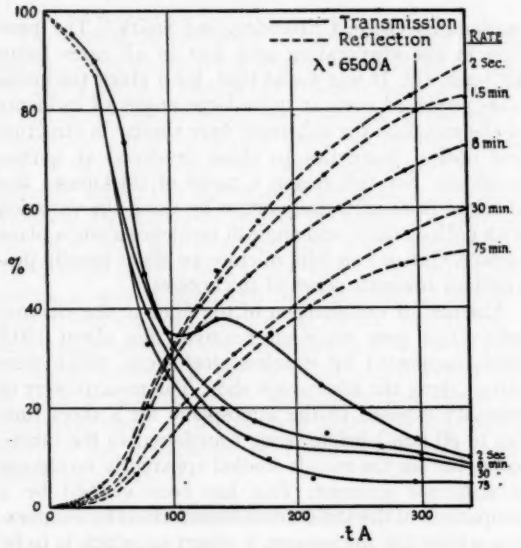

FIG. 3c. Variation of transmission and reflection with thickness for different times of evaporation (at 6500A).

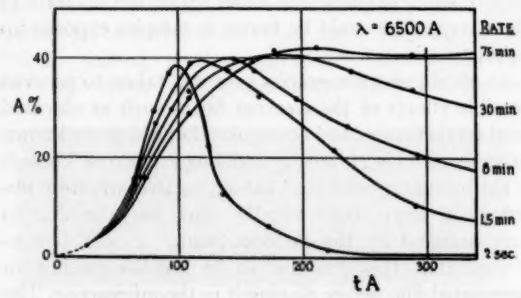

FIG. 3d. The absorption of silver films against thickness for different rates.

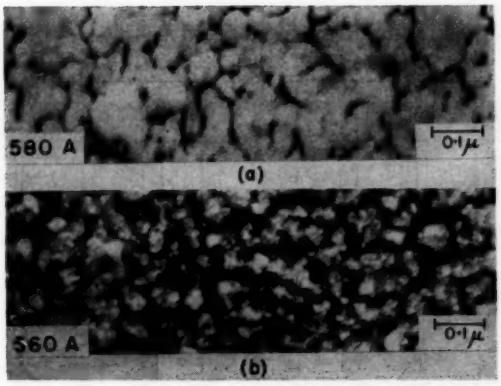

FIG. 4. Difference in structure of silver films of approximately the same thickness (a) deposited in 20 min. (b) deposited in 75 min.

outlined by Olsen, Crittenden, and Smith.[12] The pressure in the evaporating unit was in all cases below 10^{-4} mm Hg. It was found that, for a given thickness, films produced even at quite large angles of incidence of the metal on the substrate were similar in structure and optical properties to those produced at normal incidence. For this reason a range of thicknesses was obtained from each evaporation by using the variation with both distance and angle of incidence along a plane surface. One or two 3-in. microscope slides usually provided an adequate series of thicknesses.

Mounts for examination of the films in the electron microscope were made on Formvar film about 150A thick, supported by stainless steel mesh, which were placed along the microscope slide. The mounts were of necessity exposed to the atmosphere for a short time (up to 30 min.) before being transferred to the microscope, but for the metals studied apparently no change in structure occurred. This has been verified by a comparison of the structure of films formed by evaporation within the microscope, a report on which is to be presented elsewhere. Electron diffraction of silver films exposed to the air for several days indicated the presence of silver sulphide and silver oxide, but no trace of these impurities could be found in samples exposed up to thirty minutes.

In obtaining micrographs care was taken to prevent possible effects of the electron beam such as elevated local temperatures and contamination which are known to occur with high intensity and long exposures. Though it has been suggested that the aggregated structure observed in many thin metallic films may be due to bombardment by the electron beam,[13] it was demonstrated that this was not so by shadow-casting an aggregated film before placing it in the microscope. The image in this case showed each aggregate with its corresponding shadow proving that the aggregates were unchanged from those in the original film.

The optical transmissions and reflections of the films were determined using a constant deviation spectroscope fitted with a photo-multiplier 931A. The glass microscope slide with the film was mounted on the table of a goniometer which carried a white-light source, a condensing lens and a lens to project an image of a small area of the film onto the slit of the spectroscope. Both the source and the power supply for the photomultiplier were stabilized. With the output of the photomultiplier connected directly to a microammeter, the response of the system was linear with incident intensity for output currents up to 250 microamp. The transmissions and reflections of film areas 2×0.5 mm could be determined to ±2 percent for wavelength bands of less than 100A throughout the visible.

The transmission coefficient, T, of the film was determined by taking the light transmitted by the clear glass as reference intensity. For the reflection coefficient, R, the reflection from a previously measured silver surface was used as reference intensity. An approximate correction to R was made by subtracting T^2R_g from the observed reflection for the film on the slide, where R_g is the reflection of the glass slide itself. The absorption coefficient of the film, A, was found by assuming $T+R+A=100$ percent. It is clear that A includes the light scattered by the film. The scattered light was measured at different angles for a slowly evaporated silver film 150A thick and it was estimated that the total scattering was about 1.5 percent at 5500A. The value of A in this case was about 40 percent. Since for smaller absorptions it was found that the scattering was even a smaller fraction of A, it was considered that for the purposes of this paper the scattering could in all cases be neglected.

It is to be noted that the optical properties were measured for films deposited on glass whereas the structure was observed for films on Formvar. It was found however that films produced on Formvar coated glass slides had the same optical properties as films similarly produced on glass itself. Furthermore the structure of a film on Formvar was found to be the same as that of the film on silica. This is illustrated in Fig. 1, which is a micrograph of an aggregated silver film. Polystyrene spheres[14] on Formvar were first heavily shadow-cast with silica before evaporating the silver, so that in the

FIG. 5. Gold film 75A thick, deposited in 2 sec.

[12] Olsen, Crittenden, and Smith, J. App. Phys. 16, 425 (1945).
[13] D. A. Was, Physica 6, 382 (1939).
[14] R. C. Backus and R. C. Williams, J. App. Phys. 20, 224 (1949).

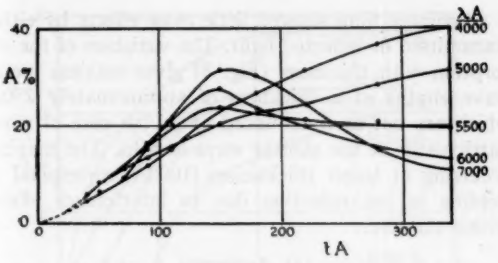

FIG. 6. The optical absorption of (2-sec.) gold films against thickness for different wave-lengths.

"shadow" the silver has a Formvar substrate whereas in the adjacent areas it has a silica substrate. It is evident that the aggregated structure is similar in the two areas.† Similar observations were made for Formvar and chromium as substrates for silver. For certain metals, e.g. zinc and cadmium (not among those considered here), the structure on chromium was found to be different from that on Formvar.

The thicknesses of the films could be estimated from the mass of metal evaporated. However measurements, which were accurate within 5 percent, were made by an extension of the multiple interference method discussed by Tolansky.[15] This yields an *average* value equivalent to that given by the mass per unit area for aggregated as well as continuous films. Details of the techniques employed here will be published separately.

RESULTS

(a) Silver

The major part of the experimental work was done with silver films which, with decreasing thickness, display blue and red colors. A series of micrographs indicating the change in structure with thickness for rapidly evaporated silver films is given in Fig. 2a. The micrographs indicate that as the film grows the aggregates initially formed increase in size but at first remain well separated. With increasing thickness the aggregates begin to join and then merge together leaving only a few "cracks" which in turn are finally obliterated.

The transmissions and reflections of these films are plotted against wave-length in Fig. 2b and against thickness in Fig. 2c. The absorptions have a maximum for all wave-lengths at thicknesses somewhat less than 100A (Fig. 2d). As can be seen from the micrographs this is just below the "critical" thickness—that for which the aggregates begin to merge and for which, as is well known, a rapid decrease in the electrical resistivity of the film occurs.

(b) Rate of Evaporation

The effect of the rate of evaporation was studied by forming films in different times, viz.: 1.5, 8, 20, 30, and 75 minutes and comparing their structure and properties which the "fast" films referred to in (a), which were formed in about 2 seconds. The more slowly evaporated silver films were in general more intensely colored. Micrographs showing the variation in structure with thickness for films formed in 20 minutes are given in Fig. 3a. It is clear that the "slow" films are generally more aggregated for thicknesses over 100A. A comparison of the structure and thickness of the slow films of Fig. 3a with the fast films of Fig. 2a shows that the aggregates of slowly formed films tend to grow more in height, i.e., become thicker before joining together than do the aggregates of rapidly formed films which tend to remain thin and grow out over the substrate. For example the 175A 20-min. film exhibits well-separated aggregates whereas the 180A 2-sec. film is almost continuous. This effect is further illustrated in Fig. 4, in which a 580A film formed in 20 minutes can be compared with a film of essentially the same thickness (560A) formed in 75 minutes.

The optical transmissions and reflections are shown, against wave-length for a 20-min. evaporation in Fig. 3b, and against thickness for different rates at 6500A in Fig. 3c. The effect of rate of evaporation on the optical properties is most strikingly indicated by the plot in Fig. 3d, of the absorption at 6500A against thickness for different times. For slower rates the peak in the curve broadens and moves to greater thickness. The absorption of a 300A film increases from about 2 percent at 2 sec. to 40 percent at 75 min. From work with other metals as well as silver this result appears to be quite general and suggests that for the optical metallic coatings usually required evaporations should be carried out as rapidly as possible. The practical importance of rate in such evaporations was apparently first noted by Crawford, Gray, Schawlow, and Kelly[16] of this laboratory, in the preparation of aluminium coated interferometer plates.

(c) Temperature of Substrate

Temperature can have a marked effect on the structure of evaporated films. In the foregoing experiments the temperature of the substrate remained in all cases less than 35°C. However it was found that silver films formed on substrates at higher temperatures (70° to 300°C) showed greater aggregation and more pronounced colors, the changes increasing with tempera-

FIG. 7. Copper film 120A thick (2-sec. evaporation).

† All micrographs shown are reversed in contrast, the metal appearing light on a dark background, and are at 75,000×.

[15] S. Tolansky, *Multiple-Beam Interferometry* (Clarendon Press, Oxford, 1948).

[16] Crawford, Gray, Schawlow, and Kelly, J. Opt. Soc. Am. 39, 888 (1949).

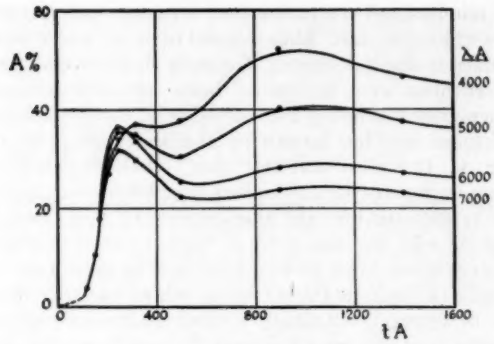

FIG. 8. The absorption of aluminum films against thickness.

ture. Heating normal "fast" films after formation produced films that were similar to those formed at the higher temperature.

(d) Other Metals

Rapidly evaporated (2-sec.) films of a number of other metals were studied to determine the dependence of optical characteristics on the properties of the metal.

(1) *Gold*

The structure resembled very closely that of the 2-sec. silver films. The thickness for which the aggregates began to merge was found to be approximately 180A which is slightly greater than in the case of silver. Thinner films consisted of well-defined aggregates (see Fig. 5) while thicker films had a mottled appearance even when the substrate was completely covered.

The thinner gold films appear green and blue by transmitted light, red by reflected light. The variation in the transmission and reflection with thickness is rather similar to that of silver. The variation of the absorption with thickness (Fig. 6) shows a maximum for wave-lengths greater than 5000A, but only a gradual increase with thickness for shorter wave-lengths.

(2) *Copper*

The structure was also aggregated in films thinner than 200A (Fig. 7), but the aggregates did not appear as regular or as well-defined as in gold or silver films.

The light transmitted by copper films 200A thick was of a green color which changed to blue at thicknesses below 50A. The variation of the absorption coefficient with thickness was similar to gold but the maxima occur at slightly greater thicknesses and only for wave-lengths above 5500A.

(3) *Aluminum*

Aluminum films had an aggregated structure at all thicknesses less than 300A. The aggregates appeared to have poorly defined boundaries, but to maintain their individuality even in quite thick films.

Aluminum films showed little color effects by either transmitted or reflected light. The variation of the absorption with thickness (Fig. 8) gives maxima for all wave-lengths at a thickness of approximately 250A, which are not as pronounced as in the case of silver particularly at the shorter wave-lengths. The maxima occurring at larger thicknesses (1000A) correspond to minima in the reflection due to interference effects within the film.

(4) *Antimony*

In antimony films thinner than 400A, well-defined regularly shaped aggregates were observed as shown in Fig. 9. The films appeared brown by transmitted light since the transmission was greater at all thicknesses for the longer wave-lengths. However, in contrast to the metals discussed above the absorption was found to increase continuously with increasing film thickness as shown in Fig. 10.

(5) *Nickel*

Films thinner than 300A had an aggregated structure. Very small aggregates were observed in the thinner films (Fig. 11). The light transmission at thicknesses greater than 100A was very nearly the same for all wave-lengths in the visible. With thinner films there was a slight maximum at 5000A giving a green color to the films. Figure 10 shows the gradual increase in the absorption with increasing thickness.

(6) *Palladium*

Thin films appeared to have a fine aggregated structure although in general they were much more continuous than the films described above. The films showed very little color either by transmitted or reflected light. The absorption was found to be slightly greater at shorter wave-lengths but increased continuously with thickness (Fig. 10).

(7) *Chromium*

With the resolution obtainable in the electron microscope, chromium films even as thin as 20A appeared continuous. The variation in the absorption with thickness showed only a gradual increase (Fig. 10) as in the case of antimony, nickel, and palladium films.

DISCUSSION

The migration of the metal after reaching the substrate is probably the most important factor in de-

FIG. 9. Antimony film 180A thick.

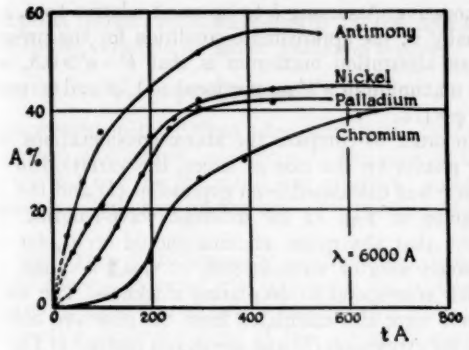

FIG. 10. Variation of the absorption of Sb, Ni, Pd, Cr, films with thickness (at 6000A).

termining the stable form of thin metallic films. Some of the features of the process of migration have been discussed by Lennard-Jones[17] and by Appleyard.[18] It is clear that the migration will depend on the metal, the nature of the substrate, and the substrate temperature. The results on rates given indicate that the migration is a function also of the intensity of the incident stream of atoms, i.e. the number of atoms incident on unit area per unit time. It should be noted that in the experiments described here the intensity is not independent of film thickness, though the thicknesses studies varied by only a factor of 10 whereas the evaporation times were changed by a factor of over 2000. The manner in which the structure of the film depends on the rate of arrival of atoms at the substrate and their migration time and distance after reaching the substrate is not immediately evident. The experimental results however suggest that in the rapidly evaporated films the migration of an atom is altered by the subsequent arrival of other atoms in the same vicinity and presumably during what would be the normal or independent time of migration.

The brilliant colors observed in thin films of silver, gold, and copper cannot be explained by any of the ordinary principles of interference and diffraction. However, as has been described, they do depend on (1) the structure of the film since marked changes were produced by altering the rate of formation or the temperature either during or after formation, and on (2) the properties of the metal since films of different metals but with similar structure have quite different optical properties. Such results can be explained qualitatively from the theory of solids[19] by considering the absorption to be due to the free and bound electrons with the free electrons being more important for the longer wave-lengths and the bound electrons for the shorter wave-lengths. The transition between the two effects occurs in the ultraviolet for silver and aluminum, in the visible for gold and copper, and in the infra-red for antimony, nickel, palladium, and chromium.

In the case of thick films the observed properties are very similar to those of the bulk metal. However marked differences occur in thinner films where the structure becomes aggregated. It may be assumed that for the aggregated films the absorption due to the free electrons will greatly increase. This was found in silver and aluminium films at all wave-lengths, and in gold and copper films for wave-lengths greater than 5500A. However the absorption due to the bound electrons should show only a gradual change as was found in gold and copper films for wave-lengths shorter than 5500A and in antimony, nickel, palladium, and chromium films for all radiations in the visible.

A classical theory developed by Garnett[7] can be used to explain some of the observed results in more detail. Using Rayleigh's calculation of the dipole induced in a metal sphere by a periodic electric field,[20] and Lorentz's result for the mutual influence of neighboring dipoles,[21] Garnett derived an expression for the effective refractive index n' and the effective extinction coefficient k' of a medium consisting of randomly distributed uniform metal spheres of radius much less than the wavelength of the exciting radiation. The calculation led to the following expressions for n' and k' in terms of n and k, the values for the bulk metal:

$$n'k'=\frac{3qb}{(1-qa)^2+4q^2b^2}, \tag{1}$$

$$k'^2-n'^2=2-\frac{3(1-qa)}{(1-qa)^2+4q^2b^2}, \tag{2}$$

where q is the volume of metal per unit volume of medium and necessarily $0<q<1$, and

$$a=\frac{(k^2-n^2+1)(k^2-n^2-2)+4n^2k^2}{(k^2-n^2-2)^2+4n^2k^2}, \tag{3}$$

$$b=\frac{3nk}{(k^2-n^2-2)^2+4n^2k^2}. \tag{4}$$

Garnett then extended this theory to thin films in which case q depends on the structure and thickness of the film.

The product $n'k'$ gives a measure of the absorption

FIG. 11. Nickel film 75A thick.

[17] J. E. Lennard-Jones, Trans. Faraday Soc. 28, 333 (1932).
[18] E. T. S. Appleyard, Proc. Phys. Soc. (London) 49, 118 (1937).
[19] N. F. Mott and H. Jones, *The Theory of the Properties of Metals and Alloys* (Oxford University Press, New York, 1936).
[20] Lord Rayleigh, Phil. Mag. 44, 28 (1897).
[21] H. A. Lorentz, Ann. d. Phys. und Chem. 9, 641 (1880).

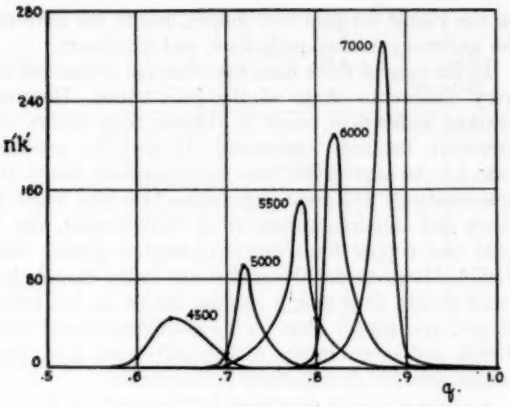

FIG. 12. The values of $n'k'$ for silver films calculated from Garnett's theory.

of the film, the relationship derived by Goos[22] being:

$$n'k' = (\lambda/4\pi t)n_2(A/T), \qquad (5)$$

where t is the thickness of the film, n_2 is the refractive index of the substrate, λ is the wave-length of light, T is the transmission of the film, and A its absorption. Differentiation of (1) shows that $n'k'$ and therefore the absorption will have a maximum if $q^2 > 1/(a^2+4b^2)$. Since q must be less than unity, $a^2+4b^2>1$. Substitution from (3) and (4) gives the condition that $K>0$, where

$$K = 2(k^2-n^2)^3 - 9(k^2-n^2)^2 + (12+8n^2k^2)(k^2-n^2) - 4 - 12n^2k^2. \qquad (6)$$

The values of K calculated from the bulk constants[23] are given in Table I for the metals which were studied. This shows that for the cases where absorption maxima were observed, *viz.*, silver, gold, copper, and aluminum, the value of K is positive whereas in the other cases K is negative. Assuming b to be small relative to a, as it usually is, the approximate condition for the presence of an absorption maximum is that $k^2-n^2>0.5$, with the maximum in $n'k'$ proportional to $1/qb$ and occurring for $q \doteqdot 1/a$.

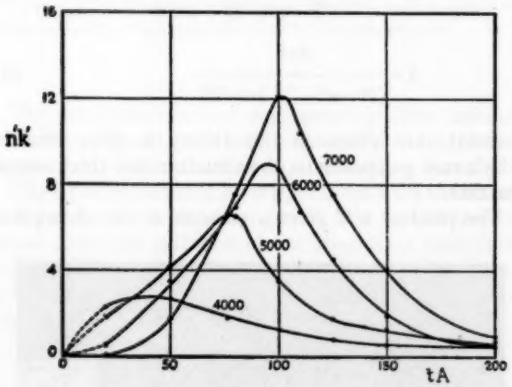

FIG. 13. The values of $n'k'$ for silver films determined from the observed optical properties of the films.

[22] F. Goos, Zeits. f. Physik **100**, 95 (1936).
[23] *International Critical Tables*, V, 248 (1929).

In order to compare the above considerations with our results for the case of silver, the variation in $n'k'$ with q was calculated from expression (1) and the plot is given in Fig. 12 for different wave-lengths. This shows that absorption maxima should occur, for successively shorter wave-lengths, at smaller values of q which correspond to decreasing thickness. The values of $n'k'$ were also calculated from the observed absorption by expression (5) and are shown plotted in Fig. 13, against thickness. It is seen that the absorption maxima for silver vary with wave-length in the manner predicted by Garnett's theory, however they are smaller in value and broader. This may be explained by the fact that the films are composed of particles considerably different from the uniform spheres assumed in developing the theory.

TABLE I. Criterion for presence of a maximum in the variation of light absorption with thickness in thin metallic films: $K>0$ for maximum.

Metal	λ	n	k	k^2-n^2	K
Silver	5890	0.18	20.6	425	1.5×10^3
Gold	4000	1.58	1.13	−1.22	−107
	5800	0.42	6.65	44.3	1.7×10^5
Copper	3950	1.17	1.50	0.88	−5.3
	6000	0.56	5.51	30.0	5.2×10^4
Aluminium	5890	1.28	3.66	11.8	2.0×10^3
Antimony	5890	3.04	1.63	−6.6	-2.6×10^3
Nickel	5890	1.79	1.86	0.25	−35
Palladium	6000	1.92	1.31	−1.9	−270
Chromium	6080	3.28	1.31	−9.7	-4.4×10^3

Similar calculations for gold films show that absorption maxima are predicted by the theory only for wave-lengths greater than 5000A, as indeed was found.

When the films were prepared at a slower rate or heated during or after formation, they were found to be more aggregated which corresponds to a decrease in the value of q. For such changes the theory predicts that the absorption maxima should occur at shorter wave-lengths for the same thickness, or at greater thicknesses for the same wave-lengths. The latter case is illustrated in Fig. 3d.

Garnett's theory can also be used to explain observations on metals other than those studied here; for example, the absorption maxima found by Wood[24] in films of sodium and potassium which had an aggregated structure visible in the light microscope. Fukuroi[25] reported similar maxima in mercury, cadmium, and zinc films prepared and studied at low temperatures. As can be predicted from Garnett's theory, for each of these three metals the magnitude of the maxima in the

[24] R. W. Wood, Phil. Mag. **38**, 98 (1919).
[25] T. Fukuroi, Inst. Phys. and Chem. Research Tokyo **32**, 172 (1937).

absorption varied with wave-length in the opposite sense to the variation for silver, gold, and copper.

CONCLUSIONS

Evaporated metallic films when sufficiently thin are in general aggregated in structure. The aggregation depends not only on the metal, the substrate, and the temperature, but also on the rate of deposition of the film.

In the region of thickness for which marked changes of light absorption occur, the aggregates are beginning to merge to form a more nearly continuous film.

Garnett's classical theory of the optical properties of thin metallic films which is expressed in terms of the structure of the films and the optical constants of the bulk metal predicts, in a qualitative way, all the observed results.

As rapid rates of formation reduce aggregation for a given thickness, and this in turn reduces the light absorption, one of the conditions for the production of high quality reflection coatings is a high rate of deposition of the metal.

ACKNOWLEDGMENTS

We wish to express thanks to Professor M. F. Crawford for stimulating the investigation of the evaporation rate, to Mr. T. A. McLauchlan for assistance in some of the experimental work, and to Mr. D. R. Welch for reproduction of the micrographs.

JOURNAL OF THE OPTICAL SOCIETY OF AMERICA VOLUME 40, NUMBER 4 APRIL, 1950

Dark Adaptation Level and Size of Testfield

ERNST WOLF AND MICHAEL J. ZIGLER
Psychological Laboratory and Visual Research Laboratory, Wellesley College, Wellesley, Massachusetts*
(Received December 14, 1949)

Data for dark adaptation curves were obtained for four square fields, subtending respectively 2.5, 5, 10, and 20 degrees at the eye, (a) when the subject indicated when light could just be perceived and (b) when parallel fine lines could just be detected. The levels attained in both the cone and in the rod segments of this function were found to vary when the area of the testfield exposed to the eye was changed, being higher for a smaller than for a larger testfield. This denotes that sensitivity is greater for a larger than for a smaller field of retinal stimulation. These findings indicate that the limit between so called photopic and scotopic vision is not to be regarded as fixed and definite but as functionally variable.

THE retinal cones are usually regarded as the receptive elements involved in photopic vision, and the rods basic to scotopic vision. The nature of the dynamic changes occasioned in each of the two kinds of retinal receptor during photic stimulation has recently been intensively investigated. First to be identified was a reversible cycle of changes occurring in the rods—rhodopsin⇌retinene⇌vitamin A, and later a similar cycle for the cones involving iodopsin has been detected.[1]

One approach to the study of the functional interrelationship existing between photopic and scotopic vision conceivably may be made in terms of a careful study of the dark adaptation function. This function is based on sensitivity measurements made at intervals during a stay in the dark. The nature of the general characteristics of the function has been under special study for some years.[2,3]

If the eye has been just previously exposed to a bright field, the dark adaptation function obtained is known to be duplex in form, i.e., made up of two segments; the first supposedly is based on cone vision, and the second on rod vision. During the first few minutes in the dark, sensitivity to light increases very rapidly, then more slowly until the function is asymptotic with respect to the abscissa. Sensitivity to light begins suddenly to increase again, rapidly at first, then progressively more and more slowly, gradually approaching a constant value. The total extent of the descent in the first (cone) segment of the dark adaptation function for specific experimental conditions has been estimated to represent an increase in sensitivity of about one hundred fold, while that of the second (rod) segment comprises a much greater increase in sensitivity, perhaps one hundred times that represented in the descent of the cone segment.[4,5]

Experiments have indicated that the dark adaptation function does not maintain the same level when the size of the testfield used in measuring sensitivity thresholds

---

* Sponsored by American Optical Company.

[1] G. Wald, *Vision: Photochemistry. Medical Physics* (Year Book Publishers, Chicago, 1944).

[2] A. Kohlrausch, *Handbuch d. normalen und pathologischen Physiol.* **12**, 1499 (1931).

[3] H. Piper, Zeits. f. Psych. und Physiol. d. Sinnesorgane. **31**, 161 (1903).

[4] S. Hecht, "Vision II," *Handbook Gen. Exp. Psychol.* (Clark University Press, Worcester, Mass., 1934).

[5] Hecht, Haig, and Wald, J. Gen. Physiol. **19**, 321 (1935).

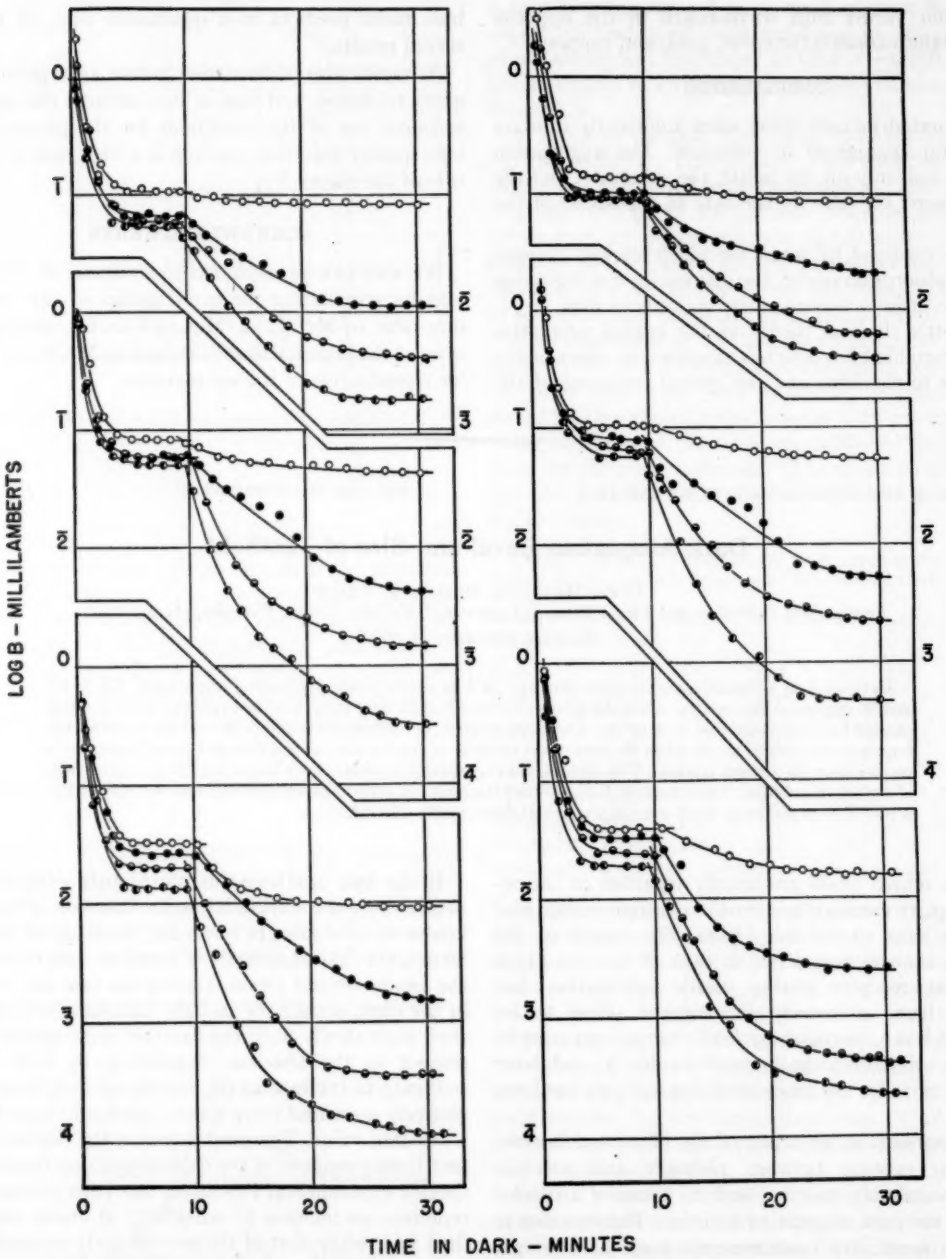

FIG. 1. Fovea. Dark adaptation functions, central stimulation, four sizes of testfield, 2.5, 5, 10, and 20 degrees obtained from two subjects. At the top, functions for detection of fine lines; in the middle, those for light detection under the same conditions; and at the bottom, those for light perception after the striped target was removed from the path of light.

during a stay in the dark is changed.[5] Therefore, the present study was made of the way in which the characteristics of the dark adaptation function behaved as the size of the testfield was systematically varied and data for dark adaptation functions were obtained both when test exposure was made in the fovea (central fixation) and in the parafovea.

LIGHT EXPOSURE

Just before measurements for a given dark adaptation function began, the eye to be tested was exposed

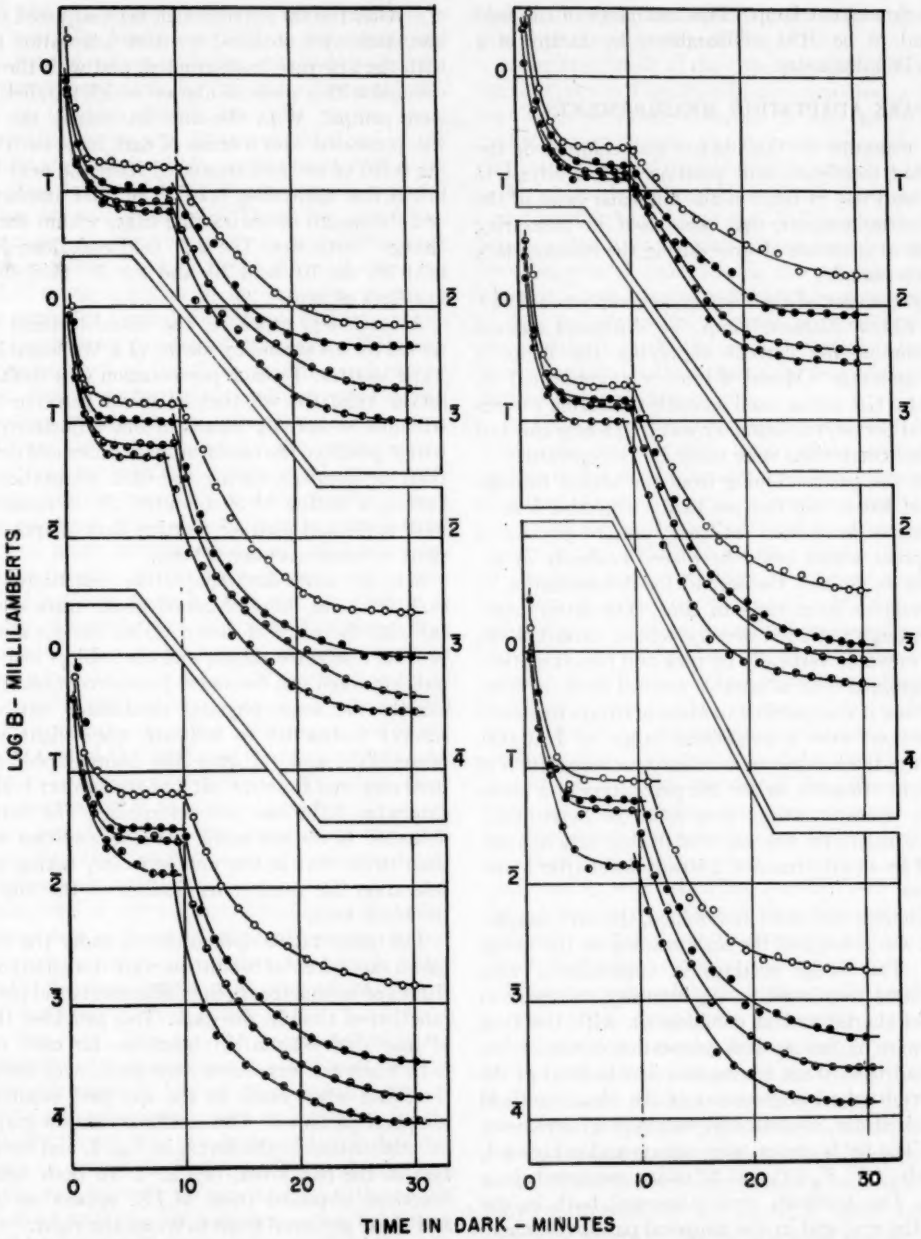

FIG. 2. Parafovea. Dark adaptation functions, parafoveal stimulation, four sizes of testfield, 2.5, 5, 10, and 20 degrees obtained from two subjects. At the top, functions for detection of fine lines; in the middle, those for light detection under the same conditions; and at the bottom, those for light perception after the striped target was removed from the path of light.

to radiant flux from a 20-watt fluorescent warmtone lamp for 10 minutes. The fluorescent tube, mounted horizontally in a frame at the level of the eye, was screened from the subject except for a circular aperture 1 inch in diameter. The head of the subject, held in position by a head rest, was so situated that the eye to be tested was directly in front of the aperture. A 20-diopter biconvex crown lens, focused on the coating of the fluorescent tube, served as condenser for the light reaching the eye. The fluorescent tube was also screened by a Corning 3389 (Noviol A) filter to avoid complications in dark adaptation produced by ultraviolet energy

from the fluorescent lamp.[6] The luminance of the field was found to be 2193 millilamberts by means of a Macbeth illuminometer.

DARK ADAPTATION MEASUREMENTS

When exposure to this source was completed, the subject had merely to shift position and to adjust to another head rest in front of the binocular head of the visual discriminometer that was used in measuring thresholds at intervals of time during the ensuing dark adaptation period.[7]

The light source of the discriminometer was a 5.5V–30A-flat ribbon filament lamp. To safeguard against fluctuations in the current supplying the lamp, a Weston ammeter (Model #155) was connected in series and a *GR* variac used as control. During the experimental period, the ammeter was frequently checked and needed corrections were made by the operator.

Two of the beams coming from the source through systems of lenses and mirrors to the objective lens of the binocular head were utilized: one to provide a fixation point which could be placed centrally or eccentrically as desired, the second for determination of light thresholds from time to time. The latter beam passed through a graded density wedge, ratio 1–1000, that was movable vertically by rack and pinion motion. When combined with a suitable neutral filter, or filter combination, it was possible to make accurate threshold determinations over a brightness range of 1:10,000. In this way, the luminance necessary for recognition of a mere light stimulus, or for the perception of a series of equally spaced vertical lines could be determined. Change in sensitivity was followed during dark adaptation until sensitivity reached a steady level after about 30 minutes.

For each light threshold determined, the dark adaptation time was noted and the scale reading on the wedge recorded. The wedge settings in combination with neutral filters were read in log intensity values from calibration charts, and in combination with the time readings were plotted as dark adaptation curves.

The quadrilateral slit mechanism just in front of the wedge permitted an adjustment of the visual testfield to any desired size, measured by means of a micrometer eyepiece. The fields chosen were square and subtended, respectively, 2.5°, 5°, 10°, and 20° of arc, measured along the edge. The testfields were presented both in the center of the eye, and in the temporal parafovea where the distance between fixation point and the adjacent edge of the testfield subtended an arc of 6°. Light thresholds were determined for two observers, E.W. and M.J.Z., both of whom have served regularly in experiments of this type for a number of years. All observations were made monocularly; E.W. used the left, M.J.Z. the right eye.

After the slit aperture had been adjusted to a given size, data were obtained for dark adaptation functions with the aperture unobstructed, and with the aperture covered with a piece of film on which parallel fine lines were printed. With the film interposed, the observer was presented with a series of dark bars, each subtending 0.26° of arc and separated from the next bar by a bright line subtending 0.26°. The total number of lines and the length of contrasting edges within the testfield changed with size. The 2.5° field contained 5, and 5° field 10, the 10° field 20, and the 20° field 40 vertical fine lines of light.

At each test exposure, the visual testfield was presented for 0.4 second by means of a Wollensack Alphax Type shutter. To each presentation of a flash, the observer indicated whether he could perceive the light stimulus or not. By means of fine adjustments of the wedge position, the operator made threshold determinations at intervals during the dark adaptation period. During a sitting of 30 minutes, 21–24 measurements were made and used for plotting dark-adaptation functions in the conventional form.

Sets of four dark-adaptation functions, one for each field size, were obtained under three conditions: (a) with the piece of film covering the slit aperture to provide a suitable target, and the subject instructed to indicate when fine lines were just perceptible, (b) under exactly the same physical conditions, but with the subject instructed to indicate when light was just perceptible, and (c) after the photographic film had been removed from the slit and the subject told to indicate when light was just perceptible. The radiant flux delivered to the eye under the last condition was more than twice that in the previous case, taking into consideration the total transmittance of the film bearing the black bars.

The quantitative data gathered under the three different experimental conditions were converted into logarithms of luminance, B, in millilamberts and plotted as a function of time in the dark. This provided three sets of four dark-adaptation functions for each observer, both when test exposures were made with central fixation, and when made in the specified locality in the temporal parafovea. The results are shown graphically; for stimulation in the fovea, in Fig. 1, and for stimulation in the parafovea, in Fig. 2. In both figures, the functions obtained from M.J.Z. appear on the left, and those gathered from E.W. on the right.

Inspection reveals that all dark-adaptation functions gathered with the four different sizes of testfield and under the three end-point conditions, both for stimulation in the fovea and for stimulation in the parafovea, subscribe to the general pattern of dark-adaptation functions. In every instance, the form of the function is duplex, but their variation in general shape and extent affords a number of significant comparisons.

The level of the dark adaptation curve varies in relation to change in size of testfield; as field size is

[6] E. Wolf, Trans. Am. Acad. Ophthalm. Otol., 1949, p. 400.
[7] W. J. Crozier and A. H. Holway, J. Gen. Physiol. 22, 341 (1939).

increased, the entire curve indicates lower luminances for both centrally located as well as for parafoveal testfields. For the rod segment, the vertical displacement is more pronounced than for the cone segment, particularly for central stimulation. The various final cone adaptation-levels are, however, displaced in the proper order and sufficiently in amount to be significant.

If the final levels of the rod segments for central stimulation be compared with those for parafoveal stimulation for a given observer, it becomes evident that the final rod level attained with the most restricted field of 2.5° is much higher in the functions obtained with the centrally located field than with the corresponding function for parafoveal stimulation. This may be observed in each of the three conditions of experimentation. For larger testfields the differences between corresponding functions are comparatively smaller. The fact that the rod segment for the centrally presented 2.5° field descends only little is chiefly responsible for the fact that the total extent of the vertical spread of the rod segments under any of the three experimental conditions is much greater for central than for parafoveal measurements. In the former case it varies from 1.17 to 2.13 log unit, while in the latter case from 0.77 to 1.17 only. The difference in extent of differentiation of the levels of the rod segments in the two cases is to be attributed to the fact that a 2.5° testfield centrally located includes the rod free fovea and only a small extrafoveal region containing relatively few rods, whereas an area of the same size in the parafovea contains a dense arrangement of rods and only a few cones. Other workers using a testfield subtending 2° of arc at the eye found that the rod segment of the dark adaptation function usually is barely indicated and sometimes entirely lacking.[5]

The final level of the rod segment of any given function corresponds to a lower luminance when test exposure is made in the parafovea than when made in the center under the same conditions. A comparison of corresponding functions in Figs. 1 and 2 shows that this is regularly the case. This may be correlated with the greater number of rods available in parafoveal fields as compared with centrally located fields of equal size.

A functional relationship also is indicated in the way that the "break" in the duplex function behaves in relation to change in field size. The sudden sharp drop of the rod segment appears earliest with the 20° testfield, and comes progressively later as testfield size is reduced. Also the rate of change in sensitivity during the initial descent of the rod segment after the break is most rapid for the 20° field, and becomes progressively slower as the size of the testfield becomes smaller.

Although change in sensitivity during the early descent of the cone segment in relation to testfield size is not so pronounced as for the rods, this does not necessarily mean that differences in velocity do not occur also in cone adaptation as field size is varied. It may merely mean that it is much more difficult to obtain threshold measurements in early cone adaptation with the same degree of accuracy.

If the final levels of the cone segments of corresponding functions in Figs. 1 and 2 are compared, a difference usually is indicated, although in this case it is by no means so pronounced, but it is always in the opposite direction. The final cone level of a given function shown in Fig. 1 tends to be slightly lower than that for the corresponding function in Fig. 2. This is consistent with the fact that a given central area contains more cones than an area of equal size in the parafoveal location. Thus, it is not unexpected that during the early phase of dark adaptation with cones predominantly active, the sensitivity at the center of the retina is found to be somewhat greater than that in an area of the same size located in the parafovea.

In Figs. 1 and 2, if comparisons are made vertically within one figure or the other, certain differences that pertain to the several conditions of experimentation are apparent. The corresponding functions depicted at the top in both figures are considerably higher than those shown in the middle of the two figures. With respect to the level finally attained by the rod segment, the function shown at the top usually is about or nearly half a log unit higher than the corresponding function shown at the middle in the figures. The separation between final levels of cone segments in corresponding functions shown at the top and in the middle, while much smaller in magnitude, nevertheless consistently indicates that the function in the middle is lower than that at the top. The meaning of the difference between levels of corresponding functions obtained under the two conditions seems to be that, at any given time in the dark-adaptation period, the light threshold is considerably lower than the threshold for the perception of fine vertical lines. Others have stated that the luminance required for the detection of a black cross is about three times as great as that for the light threshold.[8]

If corresponding functions shown in the middle and at the bottom in the two figures are compared, considerable differences may be observed. A function shown at the bottom is much lower than the corresponding one depicted in the middle. The chief reason for the difference here is that the beam of light transmitted to the eye was unobstructed when the data for the functions shown at the bottom were gathered; whereas, a striated pattern covered the slit aperture when data for the functions shown in the middle were accumulated. The threshold for light detection ought to be found lower when flux density is greater than when substantially reduced by the presence of the striped target. Actual luminance measurements with the striped film in place or removed give a ratio of 1:3.4, which should correspond to a shift of 0.53 log unit on our scale. This is of the right order of magnitude for the difference between

[8] Hecht, Haig, and Chase, J. Gen. Physiol. **20**, 831 (1937).

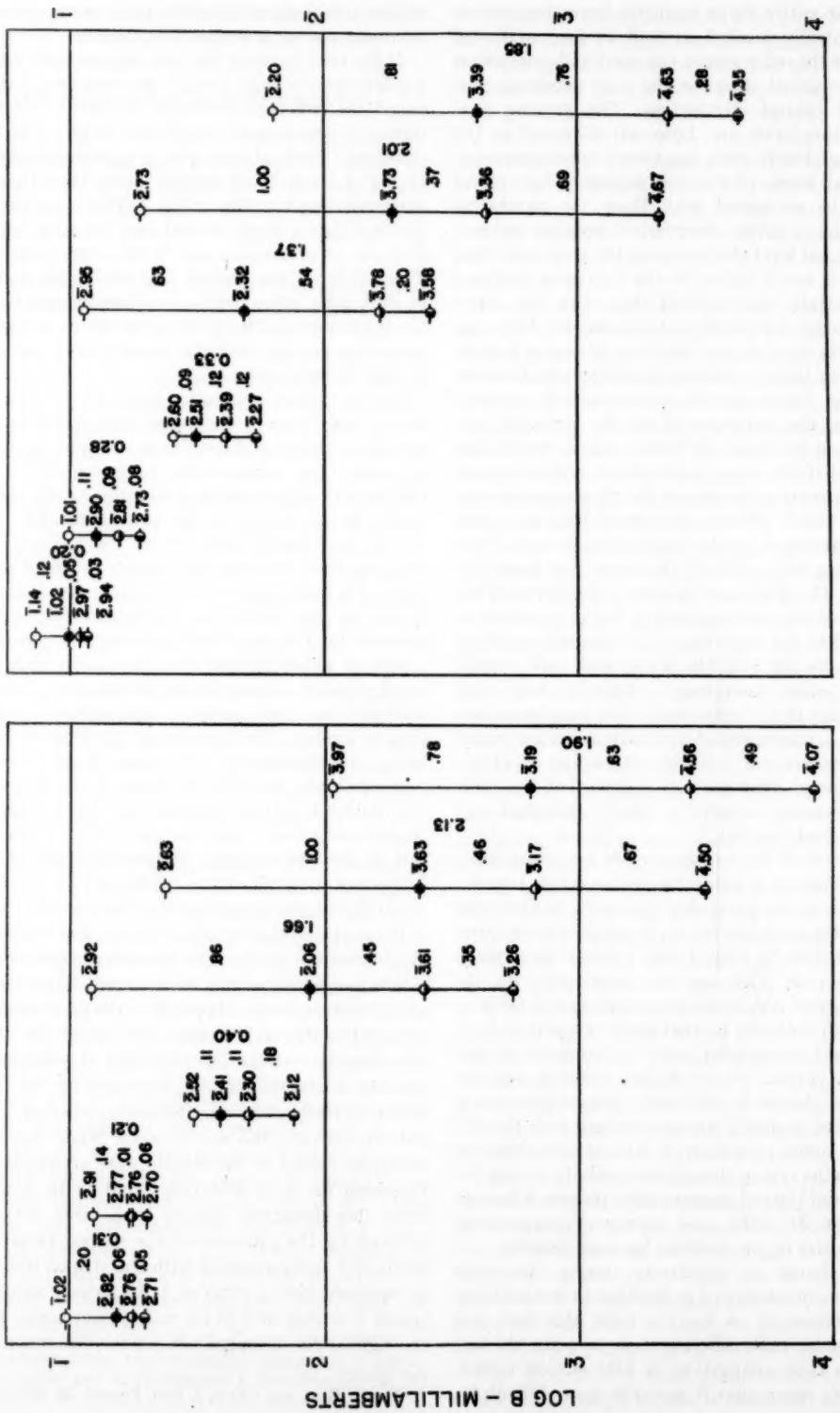

FIG. 3. Fovea. Diagram of final cone and rod levels for dark adaptation functions shown in Fig. 1. (See text.)

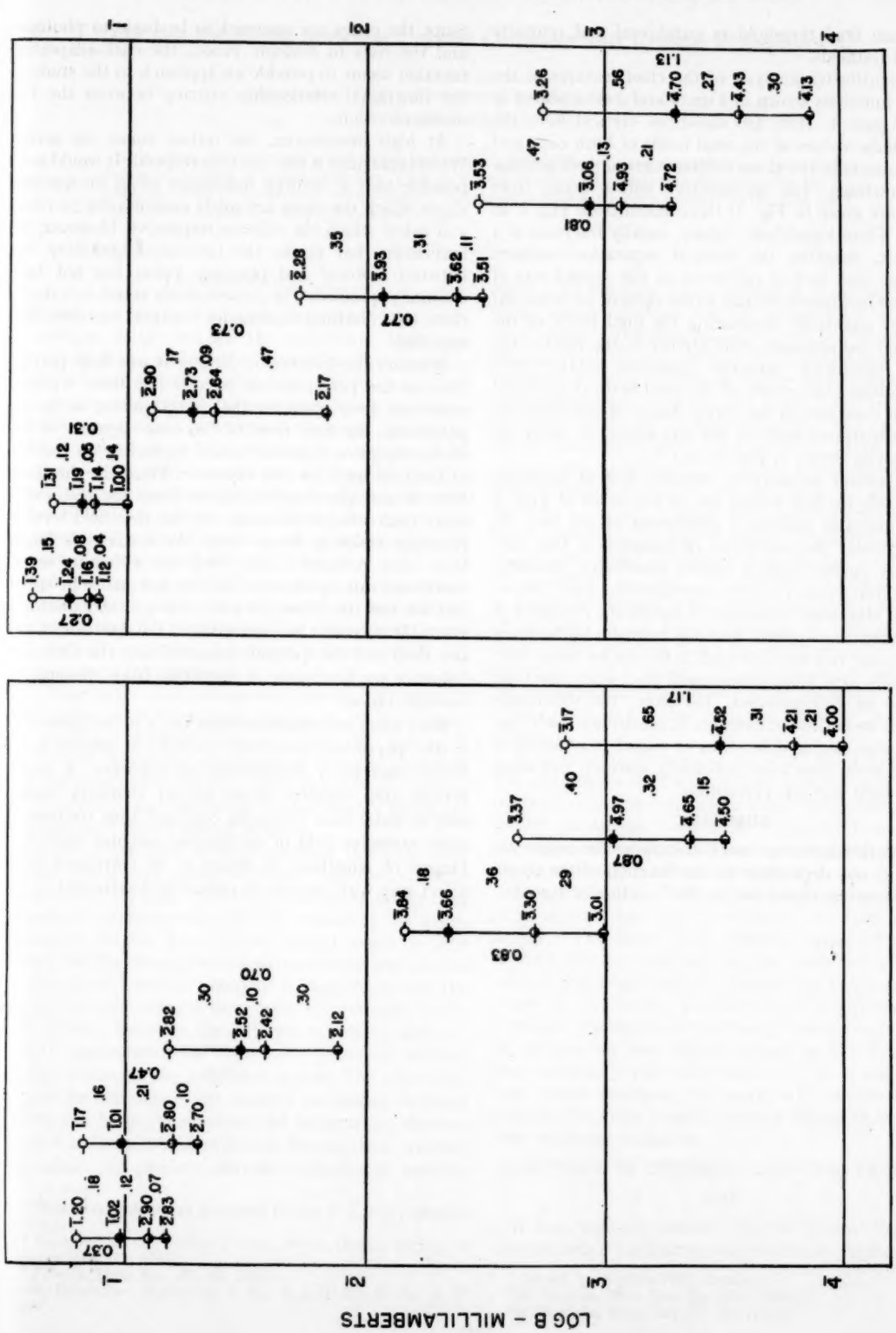

FIG. 4. Parafovea. Diagram of final cone and rod levels for dark adaptation functions shown in Fig. 2. (See text.)

the mean final threshold in parafoveal and centrally located testfields.

A quantitative analysis of the chief features of the sets of functions shown in Figs. 1 and 2 is exhibited in Figs. 3 and 4. Here are shown in vertical lines the logarithmic values of the final levels of both cone and rod segments in the three different sets of dark-adaptation functions. The quantitative values taken from Fig. 1 are given in Fig. 3; those taken from Fig. 2, in Fig. 4. Three logarithmic values, usually fractions of a log unit, denoting the vertical separation between adjacent cone and/or rod levels in the several sets of functions, are presented just to the right of (or between) the four quantities designating the final levels of the cone and rod segments. Still farther to the right is the single logarithmic quantity (numeral rotated 90°) that indicates the extent of the total vertical spread of the four cone and/or rod levels. Many of the quantitative comparisons made in the text above are based on the analysis shown in Figs. 3 and 4.

Comparison horizontally between sets of functions shown side by side within one or the other of Figs. 1 and 2 indicates individual differences of the two observers under like conditions of stimulation. One subject may possess slightly greater sensitivity, however, despite differences between corresponding functions of the two observers, a number of significant instances of close agreement appear. Also the individual differences between the two subjects tend to be smaller when light thresholds were being determined than when fine lines were to be distinguished. Therefore, the differences may not be entirely differences in sensitivity itself, but to a certain degree differences in regard to criterion of judging when lines were sufficiently distinct, and when a faint light was just perceptible.

SUMMARY

The dark-adaptation function includes two segments, an earlier one depending on the function of the cones, and a later one depending on the function of the rods. Since the cones are assumed to be basic to photopic, and the rods to scotopic vision, the dark-adaptation function seems to provide an approach to the study of the functional relationship existing between the two modes of vision.

At high luminances, the retinal cones are active. When luminance is low, the rods respond. It would seem possible that a limiting luminance could be specified above which the cones are solely contributing to vision and below which the rods are responsive. However, the luminance that marks the functional boundary line between scotopic and photopic vision has not been definitely specified. The present study seems to indicate that this limiting luminance cannot be definitely specified.

Whether the criterion of judgment was light perception, or the perception of parallel fine lines, whether exposures were made in the central retina or in the parafovea, the final level of the cone segment of the dark-adaptation function varied depending on the size of the field used for test exposure. Thus, the threshold level of scotopic vision is higher when the testfield is small than when it is larger, and the threshold level of photopic vision is lower when the testfield is larger than when reduced in size. Only for a definite set of conditions can a particular limiting luminance be specified for the transition between scotopic and photopic vision. It may also be assumed that the duration of the test flash and the spectral composition of the flash will influence the luminance of transition from photopic to scotopic vision.

Both when test exposures were made in the fovea and in the parafovea, sensitivity to light is greater for a larger than for a smaller field of exposure. A larger retinal area contains more retinal elements (cones and/or rods) than a smaller one, and thus contains a more extensive field of discharging receptor elements. Degree of sensitivity is shown to be correlated in a direct way with the size of retinal field activated.

On the Relations between Crystal Counters and Crystal Phosphors*†

RUDOLF FRERICHS
Department of Physics, Northwestern University, Evanston, Illinois
(Received January 3, 1950)

It is shown that all crystals which yield pulses under irradiation with nuclear particles or gamma-rays belong to the class of crystal phosphors. They show luminescence by irradiation in the absorption band, a power law of decay and primary and secondary photo-currents. This statement is proven for CdS, ZnS, AgCl, AgBr, TlCl, diamond of the Type 2 and solid argon.

INTRODUCTION

IN his paper on the mobility of electrons in pure polar crystals Seitz[1] reaches the conclusion that any crystal having sufficiently high electron mobility should be able to act as a counter. But he points out that another important factor enters in the problem. The cross section for capturing of electrons σ_t is of the order of magnitude of 10^{-15} cm^2 and the velocity of the electrons at the field strengths usually applied reaches about 10^7 cm/sec. Hence, in order to obtain traveling times of 10^{-7} sec., which are necessary to resolve fast sequences of counted pulses, the concentration of trapping centers should be $<10^{15}$/cm^3.

The results obtained with counting crystals up to 1949 have been thoroughly discussed by Hofstadter.[2] But he reaches the conclusion: "the more general question, what properties determine which crystal will count is not yet answered."

It is the purpose of this paper to show that all crystals which give pulses are crystal phosphors, at least under the condition of temperature at which they are used. They show the optical phenomena of a crystal phosphor and the pulses obtained by nuclear particles are related to the primary and secondary photo-currents which are characteristic for crystal phosphors.

On the other hand, phosphorescence is always connected with a large number of traps. Therefore, strongly luminescent crystals will produce pulses of rather long duration corresponding to low resolving in time. According to the band theory model which is best suited for the description of photoelectric phenomena in phosphors, a crystal phosphor is characterized by the general energy scheme developed by Johnson, Seitz, and others. Between the full valence band and the empty conduction band there are two sets of distinct energy states in the forbidden region. The activating impurities determine a set of states containing electrons which can be easily removed, for instance by electron impact or by suitable irradiation. Hence, the activating impurities can produce electron vacancies or positive holes. The electron traps determine a second set of states where electrons can be captured for a certain time interval. This interval depends on the temperature of the crystal. At low temperatures the electrons remain captured for long periods; at higher temperatures they are released into the conduction band. Filled traps thus represent stationary negative charges. The excitation of the phosphor is given by a direct or indirect lifting up of electrons from the activating impurities into the conduction band. The electron returns to the activating impurity in an act of recombination under emission of a light quantum. The recombination rate determines the decay curve, which has generally the form: $I=1/(a+bt)^2$ (I=intensity, t=time). The electron can be captured in traps and released from them by suitable irradiation, by heating, or by the application of high electrical fields. As the position of the activating impurities in the energy scheme is usually lower than that of the traps, the extinguishing irradiation will be generally of longer wave-length than the radiation emitted from the phosphor.

The excitation process is connected to an ionization. The electron leaves the activating impurity and travels freely through the conduction band. This distinguishes crystal phosphors from other types of luminescent materials, where the electron is only lifted up to a higher state of the activating impurity.[3]

The mechanism of the photo-conductivity in phosphor crystals has been investigated recently by the author.[4] The large photo-currents produced in CdS crystals can be explained by the combined action of positive and negative space charges due to the different states of the crystal. At this point it is not necessary to go into the details of this theory. However, it should be pointed out that crystal phosphors like CdS yield large secondary photo-currents. As CdS is one of the best crystal counters, it is worth while to investigate whether the other crystal counters belong to the same class of photo-conductors.

DISCUSSION OF DIFFERENT COUNTING CRYSTALS

CdS

It was originally assumed by the author[5] that CdS crystals which yield large photo-currents are not neces-

* This investigation was sponsored by the U. S. Navy, Bureau of Ships.
† Presented at the Buffalo meeting of the Optical Society of America (October, 1949).

[1] F. Seitz, Phys. Rev. 73, 549 (1947).
[2] R. Hofstadter, Nucleonics 4, No. 4, 2 (1949); 4, No. 5, 29 (1949).
[3] Cornell Symposium 1946, Report p. 9.
[4] R. Frerichs, Phys. Rev. 76, 1869 (1949).
[5] R. Frerichs, Phys. Rev. 72, 594 (1947).

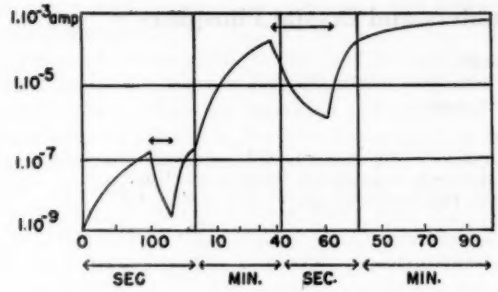

FIG. 1. Secondary photocurrents in AgCl at intermittent irradiation. Curves taken at −170°C. Dark period↔.

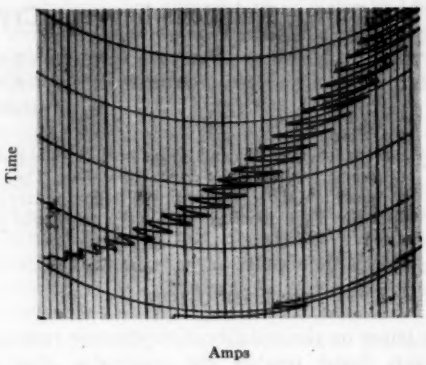

FIG. 2. Secondary photo-currents in CdS at intermittent irradiation with gamma-rays. Full scale=$2\cdot10^{-8}$ amp. One time interval=70 sec.

sarily luminescent("incomplete phosphors"). However, Kallmann and Warminsky[6] observed the largest pulses in brightly luminescent CdS crystals. Alpha-particles produce pulses up to 10 volts on an input resistor of 10^6 ohms. Crystals which show small luminescence yield much smaller pulses. In the first case, the size of the pulses is not proportional to the energy of the particle. This corresponds to the "Geiger region" of the gas counter. In the second case the energy of alpha-particles can be directly determined from the size of the pulse. This corresponds to a "proportional counter." Pulses obtained with beta-, gamma-, x-rays and neutrons are smaller in size. CdS crystals can be selected for good counting properties by the intensity of their luminescence.

In agreement with the ideas of Seitz[1] the small pulses of the CdS crystals which show small luminescence are of short duration ($<10^{-7}$ sec.). The large pulses obtained in strongly luminescent crystals, which have well-developed trapping states, have long duration ($\sim10^{-4}$ sec.).

ZnS

Natural ZnS crystals yield large secondary current. Lehfeldt[7] observed that the dependance of the secondary photo-currents from the number of excited centers parallels the total light emitted during the decay ("Lichtsumme"). Similar high secondary photo-currents have been observed in commercial crystals phosphors. Gudden and Pohl[8] have always emphasized the close relations between secondary currents and phosphorescence.

AgCl, AgBr, RlCl, TlJ

AgCl crystals grown by the methods of Kyropoulos or Bridgman show at room temperature ionic conductivity of about 10^7 ohm cm. Below −100°C the dark current becomes $<2\cdot10^{-9}$ amp. Lehfeldt found that AgCl crystals show at liquid air temperature a strong luminescence during irradiation with ultraviolet light. Randall and Farnell, Hallama, and Burton[9] have published photographs of the luminescence of pure AgCl taken at −189°C. The spectrum extends from 4300 to 6400 with a maximum at 5150A. Lehfeldt observed a slight phosphorescence after the irradiation. He points to the fact that the stored excitation energy in AgCl can be released by the application of strong electrical fields in the same way as the energy in crystal phosphors. AgCl shows large secondary photo-currents at low temperatures. They have a pronounced maximum at −200°C and decrease sharply at lower temperatures. Lehfeldt gives curves for this relation between 0 and −258°C. If the secondary currents play a deciding role in the production of pulses, the investigation of the AgCl counter at different temperatures should yield an optimum at −200°C.

At periodical irradiation the secondary currents in AgCl build up according to Fig. 1. A comparison with Fig. 2 obtained with CdS crystals shows the resemblance of the general shape. Long before the band theory of phosphors was developed, Lehfeldt pointed out that the different branches of the AgCl curve are due to centers of different lifetimes. These are identical with the traps of modern theory. AgBr and TlCl are likewise luminescent at low temperatures, and they show the same secondary photo-currents as other crystal phosphors. The maximum for AgBr is situated at −250°C, for TlCl at −70°C, for TlBr at −100°C. Data on the optimal counting temperature of AgBr were not available to the author.[10] Hofstadter points out that TlCl, TlJ crystals show good counting up to −115°C. He also emphasizes that Tl halogenides should be useful at still higher temperatures (−70°C). This would be in agreement with Lehfeldt's measurements of secondary currents.

[6] H. Kallmann and R. Warminsky, Ann. d Physik **6**, 69 (1948).
[7] W. Lehfeldt, Nachr. Ges. Wiss. Göttingen, p. 263 (1933); p. 29 (1935).
[8] B. Gudden and R. Pohl, Zeits. f. Physik **3**, 98 (1920); **4**, 206 (1921).
[9] J. T. Randall, Trans. Faraday Soc. **35**, 1 (1939), Fig. 6, Plate II; Farnell, Hallama, and Burton, Nature **164**, 146 (1949).
[10] K. A. Yamakawa, thesis, Princeton (1949).

Diamond

It is well known that counting diamonds are rare. According to Curtiss and Brown[11] only two in about a hundred industrial diamonds are useful as counters. Friedman, Birks, and Gauvin[12] pointed out that the best counting diamonds belong to Type 2 in the classification of Robertson, Fox, and Martin,[13] and they attempted to correlate the counting property with the transparency down to 2250A which is characteristic for Type 2 diamonds. Hofstadter[14] discusses the problem further. He points out that according to Raman and his school[15] Type 2 diamonds do not show luminescence under irradiation with ultraviolet light, and he considers the absence of this luminescence a rough criterion for a good counting crystal.

Gudden and Pohl[16] as well as Robertson, Fox, and Martin[13] have investigated the photo-conductivity of diamonds. The latter found that Type 2 diamonds are very different from Type 1, regarding the photoelectric properties. All diamonds show a certain amount of photo-conductivity. Type 2 diamonds, however, can be activated by radiation of 2300A. They acquire a condition in which certain longer wave-lengths can quench the photo-conductivity while others augment it. This is exactly what one expects from a crystal phosphor. Figures 3 and 4 show that the distribution of lattice absorption, photo-conductivity, quenching, and stimulating radiation is very similar in Type 2 diamonds and in CdS. There remains only the apparent contradiction of the presence of luminescence in non-counting diamonds of Type 1 and of the absence of luminescence in counting diamonds of Type 2. Generally luminescence is observed under irradiation with filtered ultraviolet of the wave-length 3650A. However, the luminescence which is related to the photo-conductivity in Type 2 diamonds should be excited by radiation which falls in the region of the lattice absorption (~2250A). The luminescence of diamonds of Type 1 is due to some accidental impurities which are not related to the photo-conductivity of the diamond lattice itself. Diamonds of Type 2 irradiated with ultraviolet of the wave-length 2260A show a bright blue luminescence,[17] and it is the presence of this luminescence which should be the criterion for good counting diamonds.

Solid Argon

Davidson and Larsh[18] obtained pulses due to polonium alpha-radiation in solid argon in polycrystalline condition. Hutchinson[19] irradiated solid argon with gamma-rays. He obtained pulses, and he observed polarization phenomena in which pulses continued after removal of the applied field. This indicates a connection between the pulses and some states of long duration. Less than one percent of oxygen dissolved in the argon quenched all pulses. Considerable amounts of nitrogen do not affect the counting properties.

According to numerous papers of Vegard[20] published during 1924 to 1935 and according to McLennan, Ireton, and Samson,[21] solid argon as well as solid nitrogen shows a strong and persistent luminescence under bombardment with fast electrons, if all traces of oxygen are absent. McLennan, Ireton, and Samson found that the spectra emitted from solid argon and from solid nitrogen are very similar. They attribute the luminescence to a small impurity, probably hydrogen, which is built into the argon or nitrogen lattice. Measurements of the photo-conductivity have not been made. But, according to extended measurements of the decay curves, this luminescence in solid nitrogen follows the law: $I=1/(a+bt)^2$, which is characteristic for a photo-conductive crystal phosphor. McLennan, Ireton, and

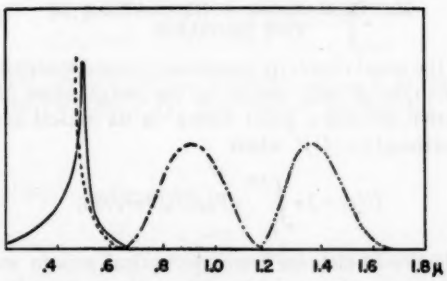

FIG. 3. Photoelectric properties of CdS in arbitrary scale. Photoelectric response to equal incident energy (——). Absorption curve (– – –). Quenching absorption (—·—). Stimulating absorption (—···—).

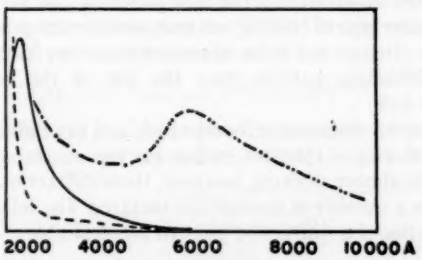

FIG. 4. Photoelectric properties of Type 2 diamond in arbitrary scale. Photoelectric response to equal incident energy (——). Absorption curve (– – –). Quenching absorption (—·—). Stimulating absorption (—···—).

[11] L. F. Curtiss and B. W. Brown, Phys. Rev. **72**, 643 (1947).
[12] Friedman, Birks, and Gauvin, Phys. Rev. **73**, 187 (1948).
[13] Robertson, Fox, and Martin, Phil. Trans. Roy. Soc. London **232A**, 463 (1934).
[14] R. Hofstadter, Phys. Rev. **73**, 630 (1948).
[15] C. V. Raman, Proc. Ind. Acad. Sci. **19A**, 189 (1944); **24A**, 1 (1946).
[16] B. Gudden and R. Pohl, Zeits. f. Physik **3**, 123 (1920). Physik. Zeits. **23**, 417 (1922). Zeits. f. tech. Physik **3**, 199 (1923).
[17] B. Gudden and R. Pohl, Zeits. f. tech. Phys. **3**, 199 (1922), footnote 2. This footnote wrongly attributed this luminescence to Type 1 diamond, whereas Type 2 yields this luminescence which these authors correctly pointed out in Physik. Zeits. **23**, 417 (1922).
[18] N. Davidson and A. E. Larsh, Jr., Phys. Rev. **74**, 220 (1948).
[19] A. W. Hutchinson, Nature **162**, 610 (1948).
[20] L. Vegard, Zeits. f. Physik (1924–1935).
[21] McLennan, Ireton, and Samson, Proc. Roy. Soc. London **120**, 303 (1928).

Samson also found that the decay curve, plotted in a diagram: $1/(I)^{\frac{1}{2}}$ as a function of time, consists of different straight parts. This indicates different sets of trap levels which discharge successively as time progresses. An investigation of the optical absorption and of the photo-conductivity to be expected is difficult, as the wave-lengths fall in the Schuman region. It is, however, quite safe to predict photo-conductivity in this region.

CONCLUSION

All crystals which yield good counting properties belong to the class of crystal phosphors. They show luminescence, a power law of decay, and photo-conductivity related to this luminescence.

A search for new and better counting crystals among the large number of natural and artificial crystal crystal phosphors might thus be promising.

JOURNAL OF THE OPTICAL SOCIETY OF AMERICA VOLUME 40, NUMBER 4 APRIL, 1950

The Resolving Power of a Coated Objective II

J. ERNEST WILKINS, JR.
American Optical Company, Instrument Division, Buffalo, New York
(Received January 19, 1950)

The diffraction pattern produced by an objective may be altered by applying coats to its exit pupil. If a coating is applied in such a manner as to reduce the diameter of the central bright disk, the central maximum intensity of the diffraction pattern is reduced. In this paper that diffraction pattern which has the highest central maximum intensity is shown for each fixed diameter of the central bright disk. The coating producing this diffraction pattern is such as to make a central zone of the exit pupil out of phase by one-half wave-length with the rest of the exit pupil, the size of the central zone being determined by the diameter of the central bright disk.

INTRODUCTION

IN his Brown University notes,[1] Luneberg has considered the problem of obtaining an increase in resolving power of an objective by altering the diffraction pattern produced by the objective. The diffraction pattern may be altered by applying thin coats of metal or dielectric material to the exit pupil.

In order to improve the resolving power the coating should be applied so that the resulting diffraction pattern has a narrower central disk than is the case for the uncoated objective. In the first paper of this series[2] a particular type of coating was proposed for this purpose, but no attempt was made to control any other feature of the diffraction pattern than the size of the central bright disk.

Many coatings can be found which lead to a diffraction pattern with a specified radius for the central bright disk. In almost all cases, however, these diffractions will possess a number of undesirable features. The following properties of a diffraction pattern are desirable:

1. A high central maximum intensity.
2. A large amount of energy in the central bright disk.
3. A large fraction of the transmitted energy lies in the central bright disk.
4. A high ratio of the central maximum intensity to the maximum intensity in the first diffraction ring.

A diffraction pattern may possess any one of these properties without possessing all of them.

We now propose the problem of finding a coating which produces a diffraction pattern with specified radius for its central bright disk and which is optimum with respect to one of the above listed properties (or any other desirable property which may occur to the reader). In this paper we shall exhibit the coating and diffraction pattern which is optimum with respect to property 1. A mathematical proof of the optimum character is reserved for the appendix.

MATHEMATICAL FORMULATION OF THE PROBLEM

In the usual circularly symmetric optical systems the distribution of light energy in the image plane of an objective viewing a point source on its optical axis is proportional to $|U|^2$, where

$$U(r)=2\pi\int_0^{\rho_m}\rho P(\rho)J_0(2\pi r\rho)d\rho, \qquad (1)$$

in which r is distance from the optical axis in wavelengths, ρ is the variable numerical aperture in the image space, ρ_m is the maximum numerical aperture, J_0 is the Bessel function of the first kind and zero order, and $P(\rho)$ is the pupil function describing the transmission properties of the coating and objective.[2] The pupil function $P(\rho)$ is the product of a coating function $c(\rho)$ which determines the amplitude and phase transmission of the exit pupil when an absorbing and refracting coating is applied, and a function $\Psi(\rho)$ which determines the amplitude and phase distribution over the exit pupil in the absence of a coating, i.e., when $c(\rho)=1$. The

[1] R. K. Luneberg, *Mathematical Theory of Optics* (Brown University Press, Providence, 1944), pp. 391–395.
[2] H. Osterberg and J. E. Wilkins, J. Opt. Soc. Am. **39**, 553 (1949).

function $\Psi(\rho)$ was analyzed in detail in a previous paper.[2] Here $\Psi(\rho)$ is regarded as known. By virtue of the definition of the coating function, $c(\rho)$ can never exceed unity in absolute value, and so

$$|P(\rho)| \leqq |\Psi(\rho)|. \tag{2}$$

The radius of the central bright disk is the smallest positive number r_0 for which

$$U(r_0)/2\pi = \int_0^{\rho_m} \rho P(\rho) J_0(2\pi r_0 \rho) d\rho = 0. \tag{3}$$

We are only interested in a radius r_0 which is less than that corresponding to the Airy limit in the image space, i.e.,

$$r_0 < 0.6098/\rho_m. \tag{4}$$

The central intensity is proportional to

$$|U(0)|^2 = 4\pi^2 \left| \int_0^{\rho_m} \rho P(\rho) d\rho \right|^2,$$

and so the determination of a coating and resulting diffraction pattern which is optimum with respect to property 1 reduces to the determination for each r_0, limited by the inequality (4), of a function $P(\rho)$ which satisfies the inequality (2) and the equality (3) and which maximizes the expression

$$\left| \int_0^{\rho_m} \rho P(\rho) d\rho \right|. \tag{5}$$

As shown in the Appendix a maximizing function $P_0(\rho)$ may be defined as follows:

$$\begin{aligned} P_0(\rho) &= -|\Psi(\rho)| \quad \text{when } 0 \leqq \rho \leqq \rho_1, \\ P_0(\rho) &= +|\Psi(\rho)| \quad \text{when } \rho_1 < \rho \leqq \rho_m, \end{aligned} \tag{6}$$

provided that the point of discontinuity ρ_1 is so chosen that the function $P_0(\rho)$ thus defined satisfies Eq. (3), i.e.,

$$\int_0^{\rho_1} \rho |\Psi(\rho)| J_0(2\pi r_0 \rho) d\rho = \int_{\rho_1}^{\rho_m} \rho |\Psi(\rho)| J_0(2\pi r_0 \rho) d\rho. \tag{7}$$

The coating function $c(\rho) = P_0(\rho)/\Psi(\rho)$ thus defined is equal to $-\exp\{-i\theta(\rho)\}$ when $0 \leqq \rho \leqq \rho_1$ and to $+\exp\{-i\theta(\rho)\}$ when $\rho_1 \leqq \rho \leqq \rho_m$, where $\theta(\rho)$ is determined so that $\Psi(\rho) = |\Psi(\rho)| \exp\{i\theta(\rho)\}$. The coating, therefore, introduces phase changes that are equal and opposite to those produced by the objective and described by the function $\Psi(\rho)$. In addition, the coating introduces a uniform phase retardation of one-half wave-length over the inner zone $0 \leqq \rho \leqq \rho_1$ of the exit pupil relative to the outer zone $\rho_1 < \rho \leqq \rho_m$. No alteration in the relative amplitude transmission of the two zones is introduced by the coating.

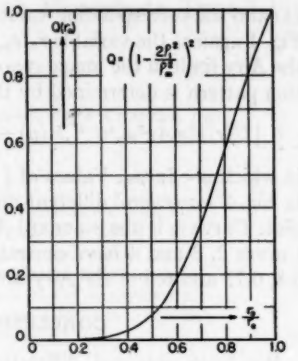

FIG. 1. The highest possible central maximum intensity for any diffraction pattern with central diameter $2r_0$.

THE A-TYPE OBJECTIVE

An A-type objective will be considered as an objective for which $|\Psi(\rho)|$ is a non-zero constant, which can be assumed to be one without loss of generality. Any objective can be regarded as an A-type objective if the aperture ρ_m is sufficiently small. For such objectives Eq. (7) determining ρ_1 reduces to

$$\int_0^{\rho_1} \rho J_0(2\pi r_0 \rho) d\rho = \int_{\rho_1}^{\rho_m} \rho J_0(2\pi r_0 \rho) d\rho. \tag{8}$$

Let $x = 2\pi r_0 \rho_1$, $y = 2\pi r_0 \rho_m$. Then Eq. (8) becomes

$$2xJ_1(x) = yJ_1(y). \tag{9}$$

The central maximum intensity is $|U(0)|^2 = \pi^2(\rho_m^2 - 2\rho_1^2)^2$, and this is the highest possible central maximum intensity attainable by any diffraction pattern whose central bright disk has radius r_0. In order to state this result in an invariant fashion, let Q be the ratio of $|U(0)|^2$ in the coated case to $|U(0)|^2$ in the uncoated case. Then the maximum value of Q is

$$Q(r_0) = (1 - 2\rho_1^2 \rho_m^{-2})^2 = (1 - 2x^2 y^{-2})^2. \tag{10}$$

Equation (9) has been solved numerically for x as a function of y on the interval $0 \leqq y < 3.8317$ equivalent to

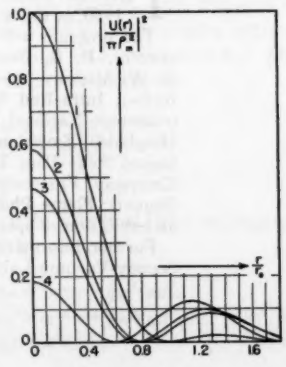

FIG. 2. Diffraction patterns vanishing at 0.6, 0.75, 0.8 of the Airy limit which have the highest possible central maximum intensity. Curve 1 is the classical Airy diffraction pattern.

(4) and the corresponding values of $Q(r_0)$ are plotted in Fig. 1 against the variable r_0/r_a, where $r_a=0.6098/\rho_m$ is the Airy limit in the image space. The optimum diffraction pattern is determined by the function

$$|U(r)|^2=4\pi^2\rho_m{}^4u^{-2}[J_1(u)-2xy^{-1}J_1(xy^{-1}u)]^2, \quad (11)$$

in which $u=2\pi r\rho_m$. Values of $|U(r)/\pi\rho_m{}^2|^2$ are plotted in Fig. 2 for several different radii of the central bright disk. Curve 1 is the standard Airy diffraction pattern. Curves 2, 3 and 4 have central bright disks with radii 0.8, 0.75 and 0.6 of the Airy limit.

CONCLUSION

We have obtained diffraction patterns which are optimum with respect to property 1. We have not proved that objectives coated as described above will necessarily produce the best possible resolution, although this may be true in some cases. It was made quite clear in a paper by Osterberg and Wissler[3] that the resolving power depends critically upon the particles observed. Instead what we have obtained is a sort of limiting barrier with respect to property 1 beyond which it is useless to attempt to explore. No matter what diffraction pattern is found, if it has a central bright disk with radius r_0, its central maximum intensity can never exceed the fraction $Q(r_0)$ of the value for the uncoated objective.

APPENDIX

The proof that the function $P_0(\rho)$ defined by Eqs. (6) maximizes the expression (5) in the class of all functions $P(\rho)$ satisfying the inequality (2) and the equality (3) follows. Let $P(\rho)$ be such a function which is real. Define $\eta(\rho)=P(\rho)-P_0(\rho)$. Then $\eta(\rho)\geqq 0$ when $0\leqq\rho\leqq\rho_1$, $\eta(\rho)\leqq 0$ when $\rho_1<\rho\leqq\rho_m$. Since $2\pi r_0\rho_m<3.8317$ when $r_0<r_a$, the function $J_0(2\pi r_0\rho)$ is a decreasing function of ρ. Hence

$$\int_0^{\rho_1}\rho\eta(\rho)J_0(2\pi r_0\rho)d\rho\geqq J_0(2\pi r_0\rho_1)\int_0^{\rho_1}\rho\eta(\rho)d\rho,$$

$$\int_{\rho_1}^{\rho_m}\rho\eta(\rho)J_0(2\pi r_0\rho)d\rho\geqq J_0(2\pi r_0\rho_1)\int_{\rho_1}^{\rho_m}\rho\eta(\rho)d\rho.$$

Adding these inequalities and remembering that both $P(\rho)$ and $P_0(\rho)$, and hence $\eta(\rho)$, satisfy Eq. (3), we find that

$$0\geqq J_0(2\pi r_0\rho_1)\int_0^{\rho_m}\rho\eta(\rho)d\rho,$$

$$J_0(2\pi r_0\rho_1)\int_0^{\rho_m}\rho P(\rho)d\rho\leqq J_0(2\pi r_0\rho_1)\int^{\rho_m}\rho P_0(\rho)d\rho. \quad (12)$$

By a similar consideration of the sum $\zeta(\rho)=P(\rho)+P_0(\rho)$,

$$0\leqq J_0(2\pi r_0\rho_1)\int_0^{\rho_m}\rho\zeta(\rho)d\rho,$$

$$-J_0(2\pi r_0\rho_1)\int_0^{\rho_m}\rho P(\rho)d\rho\leqq J_0(2\pi r_0\rho_1)\int_0^{\rho_m}\rho P_0(\rho)d\rho. \quad (13)$$

Combining the inequalities (12) and (13)

$$J_0(2\pi r_0\rho_1)\int_0^{\rho_m}\rho P_0(\rho)d\rho\geqq|J_0(2\pi r_0\rho_1)|\left|\int_0^{\rho_m}\rho P(\rho)d\rho\right|,$$

and so, provided that $J_0(2\pi r_0\rho_1)\neq 0$,

$$\left|\int_0^{\rho_m}\rho P_0(\rho)d\rho\right|\geqq\left|\int_0^{\rho_m}\rho P(\rho)d\rho\right|,$$

as was to be proved. If $J_0(2\pi r_0\rho_1)$ were zero, it would follow from the monotonicity of $J_0(2\pi r_0\rho)$ that

$$\int_0^{\rho_1}\rho|\Psi(\rho)|J_0(2\pi r_0\rho)d\rho\geqq 0\geqq\int_{\rho_1}^{\rho_m}\rho|\Psi(\rho)|J_0(2\pi r_0\rho)d\rho,$$

and so Eq. (7) could not be true unless $\Psi(\rho)$ were identically zero. Since this is not the case, it cannot happen that $J_0(2\pi r_0\rho_1)=0$.

The case when $P(\rho)=P_1(\rho)+iP_2(\rho)$ is not real can be reduced to the real case by multiplying $P(\rho)$ by a complex constant $a+ib$ of absolute value unity so chosen that

$$\int_0^{\rho_m}\rho[aP_2(\rho)+bP_1(\rho)]d\rho=0.$$

If $P^*(\rho)=aP_1(\rho)-bP_2(\rho)$ is the real part of the product $(a+ib)P(\rho)$, then $|P^*(\rho)|\leqq|P(\rho)|\leqq|\Psi(\rho)|$, the expression (5) is unaltered when $P(\rho)$ is replaced by $P^*(\rho)$ since $a+ib$ has absolute value unity, and $P^*(\rho)$ satisfies Eq. (3) because $P_1(\rho)$ and $P_2(\rho)$ must do so. Since $P^*(\rho)$ is real, the proof above shows that

$$\left|\int_0^{\rho_m}\rho P_0(\rho)d\rho\right|\geqq\left|\int_0^{\rho_m}\rho P^*(\rho)d\rho\right|=\left|\int_0^{\rho_m}\rho P(\rho)d\rho\right|.$$

[3] H. Osterberg and F. Wissler, J. Opt. Soc. Am. **39**, 558 (1949).

Society for Applied Spectroscopy

THE 5th Annual Meeting of the Society for Applied Spectroscopy will be held May 26 and 27, 1950, at the Socony Vacuum Training Center, 63 Park Row, New York City.

The program will include: a **Symposium on Spectroscopic Sources**—J. T. Agnew (Franklin Institute), B. R. Boyd (Applied Research Laboratories), J. H. Enns (University of Michigan), R. W. Murphy (Polytechnic Institute of Brooklyn), H. Bedell (National Spectrographic Laboratories); **Infra-Red Spectroscopy**—Committee on Punch Cards—Carroll Creitz; Recording Spectrometer—National Technical Laboratories; Cathode-Ray Infra-Red Spectrometer—Handel Powell (England); **Emission Spectroscopy**—Geiger Counter Detector—O. G. Koppius; Minerals and Biological Ash—Paul E. Lighty; **X-Ray Spectroscopy**—Determination of Sulfur—Atlantic Refining Company; Fluorescent Analysis of Steel—L. C. Chang; **Radiofrequency Mass Spectrometer**—W. H. Bennett; **Flame Photometry**—Frank M. Biffen; **Neutron Spectroscopy**—T. I. Taylor. There will be an exhibition of spectroscopic equipment during both days.

Further information concerning the meeting may be obtained from Dr. Harold K. Hughes, Socony-Vacuum Laboratories, 412 Greenpoint Avenue, Brooklyn 22, New York.

JOURNAL OF THE OPTICAL SOCIETY OF AMERICA VOLUME 40, NUMBER 4 APRIL, 1950

The Electro-Optic Effect in Uniaxial Crystals of the Dihydrogen Phosphate Type.*† III. Measurement of Coefficients

ROBERT O'B. CARPENTER

Physics Department, Harvard University, Cambridge, Massachusetts and Research Laboratory, Baird Associates, Inc., Cambridge, Massachusetts

(Received February 2, 1950)

The electro-optic coefficients of two crystals have been measured by both static and dynamic methods. For $NH_4H_2PO_4$, $r_{63}=2.54$, $r_{41}=6.25$; for KH_2PO_4, $r_{63}=3.15$, $r_{41}=2.58$ (units 10^{-7} c.g.s., 20°C λ5560). The variation of the electro-optic response with the frequency of the applied field is given and related to the piezoelectric vibrations of the crystal. A theoretical relation for the difference in the electro-optic constants measured at constant stress and at constant strain is derived, which provides a check on the consistency of the presently available electro-optic, photo-elastic, piezoelectric, and elastic coefficients for these crystals. The use of a.c. methods to obtain high precision in polarization measurements is discussed.

INTRODUCTION

IN two previous papers[1] of this series, hereinafter referred to as (I) and (II), Billings has discussed the theory and some applications of the electro-optic effect in crystals of tetragonal scalenohedral symmetry. In addition to the applications to high frequency light modulation, the electro-optic properties of $NH_4H_2PO_4$ and KH_2PO_4 are of considerable interest because of their relation to the anomalous piezoelectric and ferroelectric properties of these crystals.[2] Zwicker and Scherrer[3] investigated the optical behavior of KH_2PO_4 under fields parallel to the Z or optic axis to temperatures below the ferroelectric transition, utilizing the optical effects for a very graphic means of observing the spontaneous polarization, hysteresis, Barkhausen jumps, etc.

In this paper are presented methods and results of measurements of the electro-optic coefficients r_{63} and r_{41} of $NH_4H_2PO_4$ and KH_2PO_4 at room temperature. Some of these values have also been measured by H. Jaffe and W. L. Bond but not published. The method for the measurement of r_{41} is new. Under an electric field parallel to the x axis in these crystals the principal axes of the index ellipsoid are rotated. The method consists of a direct measurement of this rotation. Sensitivity and precision are obtained by the use of a.c. fields on the crystal and detection by means of a multiplier photo-cell and sharply tuned amplifier.

Since most of the previous measurements of electro-optic coefficients have utilized visual compensator methods, the chief contribution which this paper seeks to make is the discussion of the advantages of the a.c. method for precision in measuring very small changes in the polarization properties of a light beam. In addition, by measuring the variation of the electro-optic coefficient with frequency, the effect of the piezoelectric vibrations is observed and a new method is obtained for distinguishing the electro-optic coefficient at constant strain and at constant stress.

THEORY OF MEASUREMENTS

In (I) it was shown that the equation of the Fresnel index ellipsoid for crystals of tetragonal scalenohedral symmetry under arbitrary electric fields can be written

$$o^2(x^2+y^2)+e^2z^2+2r_{41}(E_zyz+E_yzx)+2r_{63}E_zxy=1, \quad (1)$$

where the coordinate axes xyz are taken as the standard crystallographic axes, o and e are the reciprocals of the ordinary and extraordinary refractive indices ω and ϵ of the crystal in the absence of an electric field and r_{41} and r_{63} are the two independent electro-optic coefficients describing the changes in the index ellipsoid when a field is applied. Thus, r_{63} describes the effect of a field parallel to the optic axis and r_{41} the effect of a field perpendicular to this axis. Under an electric field the crystal becomes biaxial and the three axes of the index ellipsoid no longer coincide with the standard crystallographic axes xyz. The determination of the new principal axes and indices is a purely algebraic problem of rotating the coordinate axes to coincide with the principal axes of the ellipsoid defined by Eq. (1). This was discussed at some length in (I), so that the results only will be repeated here.

For a field in the z direction ($E_x=E_y=0$), the axes of the ellipsoid will be called $x'y'z'$. z' coincides with z, while x' and y' are rotated by $-45°$ from x and y. The values of the three indices of refraction are

$$\begin{aligned} n_{x'}&=\omega+\tfrac{1}{2}\omega^3r_{63}E_z \\ n_{y'}&=\omega-\tfrac{1}{2}\omega^3r_{63}E_z, \\ n_{z'}&=\epsilon \end{aligned} \quad (2)$$

and the birefringence of plane waves of light propagated along these axes is given by

$$\begin{aligned} B_{x'}&=n_{y'}-n_{z'}=\omega-\epsilon-\tfrac{1}{2}\omega^3r_{63}E_z \\ B_{y'}&=n_{z'}-n_{x'}=\omega-\epsilon+\tfrac{1}{2}\omega^3r_{63}E_z \\ B_{z'}&=n_{x'}-n_{y'}=\omega^3r_{63}E_z. \end{aligned} \quad (3)$$

* This work was done as part of a thesis to be submitted in partial fulfillment of the requirements for the Ph.D. degree at Harvard University.

† This work was supported in part by the Air Force Cambridge Research Laboratories under Contract W19-122 ac-32.

[1] B. H. Billings, J. Opt. Soc. Am. **39**, 797 (1949); **39**, 802 (1949).

[2] W. P. Mason, Phys. Rev. **69**, 173 (1946).

[3] B. Zwicker and P. Scherrer, Helv. Phys. Acta **17**, 346 (1944).

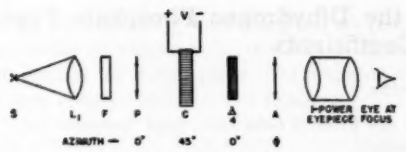

FIG. 1. Senarmont compensator method for static measurement of r_{63}; F—filter, P—polarizer, C—z cut crystal of retardation, $\Gamma=\omega^3 r_{63}V/\lambda$, A—2° split field analyzer. When analyzer is rotated to match intensities, $\phi=\pi\Gamma$.

The maximum induced birefringence is for light along the z axis and further, observation along this direction is not complicated by any natural birefringence.

For a field in the x direction ($E_y=E_z=0$) the principal axes of refraction will be denoted by $x''y''z''$. In this case x'' coincides with x, but $y''z''$ are rotated from yz by an angle α which depends on the field.

$$2\alpha\approx\tan 2\alpha=-\frac{2r_{41}E_x}{\epsilon^2-o^2}. \tag{4}$$

As shown in the measurements given below, α is only a few minutes of arc for the largest practical fields, so that $\tan\alpha\approx\alpha$. To the order of terms in the square of the field the principal indices become

$$\begin{aligned} n_{x''}&=\omega \\ n_{y''}&=\omega+\tfrac{1}{2}\frac{\omega^5\epsilon^2}{\omega^2-\epsilon^2}(r_{41}E_x)^2 \\ n_{z''}&=\epsilon-\tfrac{1}{2}\frac{\epsilon^5\omega^2}{\omega^2-\epsilon^2}(r_{41}E_x)^2. \end{aligned} \tag{5}$$

This situation is somewhat more complicated than the case of E_z. If light is propagated along $x(\equiv x'')$ the crystal forms a retardation plate with directions of vibration rotated by the field (angle α) while the change in indices is a very small quantity proportional to the square of the field. Observation along the direction y or z introduce no induced birefringence as is seen by inspection of Eq. (1) (for $E_y=E_z=0$). However, a first-order induced birefringence is obtained by propagating the light along the bisector of the direction y and z, i.e., normal to the plane

$$y-z=0. \tag{6}$$

The birefringence in this direction denoted B_{yz}, will be given by the major and minor axes of the elliptical intersection of the plane (6) and the ellipsoid (1). After making use of the approximations $r_{41}E_x\ll 1$ and $\omega\approx\epsilon$, the result can be written

$$B_{yz}=\tfrac{1}{2}(\omega-\epsilon)-(\omega^3/2)r_{41}E_x. \tag{7}$$

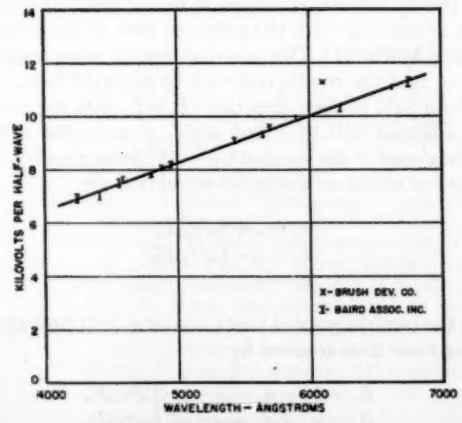

FIG. 2. Voltage required to produce ½-wave retardation in basal section of $NH_4H_2PO_4$ as function of wave-length.

MEASUREMENT OF r_{63}

For the static measurement of r_{63} there are a number of simple optical compensator methods[4] for the determination of the retardation through a basal section of crystal which is given by

$$\Gamma=\frac{B_{z'}d}{\lambda}=\frac{\omega^3 r_{63}V}{\lambda}, \tag{8}$$

where V is the voltage applied across the crystal. If the crystal is placed between parallel polarizers, the light is extinguished when the voltage is increased to give one-half wave retardation. This can be determined by a photo-cell or by visual observation. The precision is considerably increased by using split field half-shadow analyzer. By insertion of a Babinet compensator between crystal and analyzer a series of interference fringes are produced whose displacement on applying a field can be observed. A third method involves the observation of the angle between the two optic axes on a suitable goniometer. In air this angle is given by

$$\Omega=2\omega\left(\frac{2r_{63}E_z}{\epsilon^2-o^2}\right)^{\frac{1}{2}}.$$

The method which was finally selected as being most convenient and accurate was the use of the Senarmont compensator shown in Fig. 1. The electro-optic retardation plate and a fixed $\lambda/4$ plate are oriented at 45° and 0° to the initial polarizer and the split field analyzer is mounted on a calibrated circle with a vernier reading to 0.1°. The intensity transmitted by this system is

$$\frac{I}{I_0}=\cos^2(\pi\Gamma-\phi), \tag{9}$$

where Γ is the retardation of the unknown plate and ϕ is the aximuth angle of the analyzer. Therefore, the retardation for any voltage is read directly from the extinction angle.

Figure 2 shows the voltage required to produce one-

[4] H. G. Jerrard, J. Opt. Soc. Am. 38, 35 (1948).

half wave retardation as a function of wave-length for $NH_4H_2PO_4$. The wave-lengths were chosen by a series of Baird Associates, Inc. interference filters. Linearity of retardation with voltage as indicated by Eq. (8) was verified. Since the results show a linear relation between voltage and wave-length, no dispersion of the value of r_{63} was found in the range 4000–7000A within the precision of the measurements (about 2 percent). The crosses on the figure are data supplied by H. Jaffe of the Brush Development Company in which the wave-lengths were chosen by means of rather broad Corning glass filters, which perhaps explains the small discrepancy at λ6100. Reduced to c.g.s. units, the value of r_{63} obtained is $2.54\pm0.05\times10^{-7}$ cm/statvolt. A similar measurement of the coefficient for KH_2PO_4 resulted in the value $r_{63}=3.15\pm0.05\times10^{-7}$.

The value of r_{63} for $NH_4H_2PO_4$ was checked on a total of five crystals in which different methods of mounting and attaching electrodes were utilized. The technique of laminating the crystal between Nesa glass electrode plates was discussed in paper (II). An error in the measurement of r_{63} might conceivably be introduced by the mounting in two ways, by a loss of voltage across the laminating layer or by a mechanical stress introduced by the mount.

All crystals were approximately 2 in.×2 in.×$\frac{1}{8}$ in. One crystal was prepared with directly adherent evaporated chromium electrodes, two were laminated between 2-in. squares of Nesa glass and two were laminated between 1$\frac{1}{2}$-in. circles of Nesa. Identical results were observed on all crystals, indicating that the laminating techniques used do not introduce any loss in efficiency at low frequencies.

Many of the most interesting applications of the electro-optic plate involve the use of a.c. fields. Therefore, the variation of r_{63} with frequency was determined. This is done by placing the crystal in series with a fixed quarter-wave plate between crossed polarizers and applying alternating voltage $V_a \sin\omega t$ (Fig. 3). The transmitted intensity is given by

$$I/I_0=\sin^2\pi\Gamma=\tfrac{1}{2}(1-\cos2\pi\Gamma). \tag{10}$$

By Eq. (8), the combined retardation of crystal and λ/4 plate is

$$\Gamma=\tfrac{1}{4}+\frac{\omega^3 r_{63}V_a\sin\omega t}{\lambda}.$$

On using the trigonometric identity $\cos(\pi/2-\theta)=-\sin\theta$ and restricting the voltage V_a to small amplitudes where $\sin\theta\approx\theta$, the intensity can be written

$$\frac{I}{I_0}=\tfrac{1}{2}-\frac{\pi\omega^3 r_{63}V_a}{\lambda}\sin\omega t. \tag{11}$$

A voltage of approximately 500 volts and variable frequency was applied to the crystal and the horizontal plates of an oscilloscope. The amplified output of an

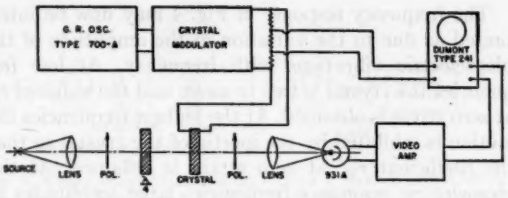

FIG. 3. Arrangement for measuring relative frequency response of electro-optic effect.

RCA 931 multiplier photo-cell was applied to the vertical deflection plates. The ratio of the light modulation to the crystal voltage then gives the relative variation of r_{63} or the electro-optic response with frequency. The results for a crystal of $NH_4H_2PO_4$ are shown in Fig. 4.

For an explanation of the frequency response one must consider the photo-elastic and piezoelectric behavior of the crystal. For a crystal of general symmetry the index ellipsoid is written

$$a_1x^2+a_2y^2+a_3z^2+2a_4yz+2a_5zx+2a_6xy=1. \tag{12}$$

The changes Δa_i in the coefficients of the index ellipsoid, due to both electro-optic and photo-elastic effects, can be expressed in terms of the electric field and either the stress or the strain in the crystal.

$$\Delta a_i=\sum_{j=1}^{3} r_{ij}E_j+\sum_{j=1}^{6}\pi_{ij}X_j \tag{13}$$

$$\Delta a_i=\sum_{j=1}^{3} r_{ij}'E_j+\sum_{k=1}^{6} p_{ik}x_k, \tag{14}$$

where X_j and x_j are the components of stress and strain, π_{ij} and p_{ik} the stress-optic and strain-optic coefficients. These relations are not independent because of the piezoelectric relations

$$x_k=-\sum_{j=1}^{6} s_{kj}X_j+\sum_{j=1}^{3} d_{jk}E_j, \tag{15}$$

where s_{kj} and d_{kj} are the elastic and piezoelectric constants. Substituting Eq. (15) in Eq. (14) we obtain

$$\Delta a_i=\sum_{j=1}^{3}\{r_{ij}'+\sum_{k=1}^{6} p_{ik}d_{jk}\}E_j+\sum_{j=1}^{6}\{\sum_{k=1}^{6} p_{ik}s_{rj}\}X_j.$$

On comparing with Eq. (13) it is evident that

$$\pi_{ij}=\sum_{k=1}^{6} p_{ik}s_{kj} \tag{16}$$

$$r_{ij}=r_{ij}'+\sum_{k=1}^{6} p_{ik}d_{jk}. \tag{17}$$

Therefore, the electro-optic coefficient r_{ij}, measured at zero stress (free crystal), differs from r_{ij}' measured at zero strain (clamped).

The frequency response of Fig. 4 may now be interpreted as due to the variation in the amplitude of the piezoelectric vibrations with frequency. At low frequencies the crystal is free to move and the value of r_{63} at zero stress is obtained. At the highest frequencies the motion is inhibited by the inertia of the crystal so that the coefficient r_{63}' at zero strain is obtained. At the piezoelectric resonance frequencies large amplitudes of vibration are set up which can be directly observed by this optical method. Tawil[5] and others have used the polarized light method for the qualitative study of vibration patterns in quartz.

Similar curves were obtained for several other crystals of $NH_4H_2PO_4$ in different styles of mounting. The resonant amplitudes are quite sensitive to the size and shape of the crystals and electrodes and the mechanical load introduced by the mount, but the same values of r_{63} and r_{63}' were obtained at low and high frequencies.

This method of comparing the electro-optic coefficient at zero stress and at zero strain can be compared with values obtained by two other methods. H. Jaffe (unpublished) determined the clamped effect by applying the field to very small electrodes while the remainder of the crystal was shorted by an additional pair of electrodes which served to clamp the center section. His value for r_{63}' was 58 percent of r_{63} as compared to 65 percent found here. This discrepancy is probably not outside the uncertainties of the two measurements. The second method is the direct determination of the photo-elastic and piezoelectric constants and the use of Eq. (17), which for the case considered reduces to

$$r_{63}=r_{63}'+p_{66}d_{36}. \tag{18}$$

Using Mason's[2] value of $d_{36}=146\times10^{-8}$ c.g.s. and West's[6] value of $p_{66}=0.111$, r_{63}' calculates to be 37 percent of r_{63}. The source of this discrepancy has not been determined. Mason's value for d_{36} has been checked in a number of laboratories. West's value for p_{66} was confirmed at the Crystal Section of the Naval Research Laboratory. However, G. W. Willard of the Bell Telephone Laboratories reports a measurement of $p_{66}=0.076$ which would make r_{63}' 57 percent of r_{63} in closer agreement with Eq. (18) and the other measurements.

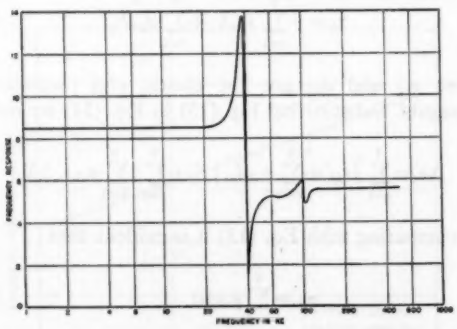

FIG. 4. High frequency response of electro-optic effect in $NH_4H_2PO_4$ crystal.

[5] E. P. Tawil, Comptes Rendus **183**, 1099 (1926); Rev. gén. de l'élec. **25**, 58 (1929); W. G. Cady, *Piezoelectricity* (McGraw-Hill Book Company, Inc., New York, 1946), p. 465.

[6] C. D. West and A. S. Makas, reported at April, 1949 meeting of Crystallographic Society of America.

MEASUREMENT OF r_{41}

With a 45° x cut crystal the induced birefringence indicated by Eq. (7) can be used to measure r_{41}. However, for a light path of $\frac{1}{4}$ inch at λ5500, the natural retardation will be about 275 waves and varying by one wave every 20A. With a monochromatic source, such as a mercury or sodium lamp, it is still possible to use a Babinet or Sernarmont compensator method. Dr. Jaffe made a rough determination of r_{41} in $NH_4H_2PO_4$ by the slightly different method of observing with a spectrograph the displacement of the chromatic interference fringes.

In order to obtain more precise values a new method was devised based on the direct measurement of the field induced rotation of the axes of the index ellipsoid. The optical arrangement is shown in Fig. 5. The crystal is an x cut plate prepared with transparent electrodes according to any of the methods described in paper (II). The light is propagated along the x direction in which case the crystal forms a plate of retardation Γ with the fast axis oriented at an angle α (Eq. (4)) to the initial polarizer. The intensity transmitted through the system is

$$I/I_0=\tfrac{1}{2}+\tfrac{1}{2}\sin^2\pi\Gamma\sin4\alpha,$$

since $\Gamma=(\omega-\epsilon)d/\lambda$ is a rapidly varying function of wave-length for a sufficiently thick crystal, by using a broad continuous source, $\sin^2\pi\Gamma$ may be integrated over wave-length and replaced by its mean value of $\frac{1}{2}$. Then substituting from Eq. (4) for $\alpha\approx\sin\alpha\approx\tan\alpha$ we obtain

$$\frac{I}{I_0}=\tfrac{1}{2}+\alpha=\tfrac{1}{2}-\frac{r_{41}E_x}{e^2-o^2}. \tag{19}$$

In order to detect this small modulation, 60 c.p.s. alternating voltage $V_s\sin\omega t$ was applied to the crystal and the resulting light intensity modulation $I_s\sin\omega t$ was detected by the multiplier photo-cell and a sharply tuned amplifier. Then r_{41} is given by

$$r_{41}=\frac{d(e^2-o^2)}{I_0}\frac{I_s}{V_s}. \tag{20}$$

I_0 is twice the observed d.c. current in the photo-cell.

The values obtained by this method for r_{41} in $NH_4H_2PO_4$ and KH_2PO_4 are tabulated in Table I. Three crystals of $NH_4H_2PO_4$ and two of KH_2PO_4 gave identical results within the reproducibility of the measurements.

TABLE I. Electro-optic coefficients of $NH_4H_2PO_4$ and KH_2PO_4 at 22°C, λ5560, in c.g.s. units (statvolts/cm)$^{-1}$.

	ϵ	ω	$r_{63}\times10^7$	$r_{41}\times10^7$
$NH_4H_2PO_4$	1.5254	1.4798	2.54±0.05	6.25±0.1
KH_2PO_4	1.5100	1.4684	3.15±0.07	2.58±0.05

SENSITIVITY OF THE A.C. METHOD

The ultimate sensitivity of a.c. methods in light polarization measurements can be made considerably greater than can be obtained with the best visual compensator methods. When sufficient light intensity is available, the limiting noise becomes the electron shot effect in the multiplier photo-cell.

$$(I_N)_{\text{r.m.s.}}=\left(\frac{GIe}{\tau}\right)^{\frac{1}{2}},$$

where G=gain of multiplier, e=electronic charge, τ=time constant of amplifier-detector. The modulated photo-current is of the form

$$I(1+\beta\sin\omega t)$$

so that the signal-to-noise ratio is

$$\frac{I_s}{I_N}=\beta\left(\frac{I\tau}{2Ge}\right)^{\frac{1}{2}}$$

and the smallest detectable β is

$$\beta_{\min}=\left(\frac{2Ge}{I\tau}\right)^{\frac{1}{2}}.$$

Since I/G is just the photo-cell cathode current, the ultimate sensitivity depends only on the time constant, the available light energy and the absolute energy sensitivity of the photo-surface.

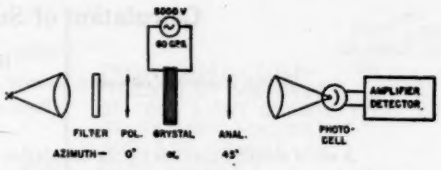

FIG. 5. Arrangement for measuring r_{41} by a.c. method; vibration direction of x cut crystal depends on the field: $(\alpha=r_{41}E_z/(\epsilon^2-\sigma^2))$.

Under the conditions of the r_{41} measurement $G=10^8$, $I=10^{-4}$, $\tau=3$ seconds, $\beta_{\min}=10^{-6}$. In this experiment the modulation factor β is twice the angular rotation α of the principal index axes. Thus, $\alpha_{\min}=5\times10^{-7}$ radian, $(r_{41})_{\min}=10^{-9}$ for the field $E_z=21$ statvolts/cm which was used. In measuring r_{63}, β is the phase retardation $(2\pi\Gamma)$ of the retardation plate. According to Jerrard[4] the ultimate detection limit of the best optical compensators is not better than 10 sec. of arc or 5×10^{-6} radian.

ACKNOWLEDGMENT

The author wishes to express his appreciation to Dr. W. P. Mason for his discussions of and interest in the problem and to Dr. H. Jaffe for advice, suggestions, and the furnishing of crystals. To both are due thanks for the results of unpublished measurements at their respective laboratories. The interest and cooperation of Dr. B. H. Billings and the entire research staff at Baird Associates, Inc. have contributed much to this work. Acknowledgement should also be made to the Air Force Cambridge Research Laboratories whose support helped make this work possible.

Physics Abstracts

For many years the dues of the American Physical Society have included a subscription to Physics Abstracts, published by the Institute of Electrical Engineers of London. There has been, however, no convenient method by which persons not members of the A.P.S. could receive this publication. The Optical Society of America has now instituted an arrangement under which any O.S.A. member can receive Physics Abstracts at an annual subscription price of $4.50. All correspondence in this connection should be addressed to the American Institute of Physics, 57 East 55th Street, New York 22, New York.

Calculation of Subtractive Color Mixtures*

H. R. DAVIDSON
Central Research Laboratory, General Aniline and Film Corporation, Easton, Pennsylvania
(Received December 1, 1949)

A set of simple equations for the calculation of tristimulus values of subtractive color mixtures in solution has been developed for the specialized case in which the ratios of transmittances of the component colorants are constant over all wave-lengths in the visible spectrum. The values calculated are shown to represent the maximum values for mixtures of components with ratios of transmittance which differ from the specialized case, and it may also be demonstrated that no points of inflection may exist in the plots of tristimulus values *vs.* concentration of components. In practical mixtures, departures from these theoretically derived relationships are due to interaction of the components. In use, the equations prove to be sufficiently accurate for calculation of tristimulus values of most mixtures in which the color gamut is small.

DURING the course of some work with dye solution mixtures, it appeared as though some very simple formula for approximating the tristimulus values of mixtures on the basis of the tristimulus values of the component solutions would be of use. In order to investigate this possibility, the following derivations were undertaken. A few of the results obtained may prove of general interest.

The basic equation for calculation of the X tristimulus value is

$$X=\int E\bar{x}Rd, \tag{1}$$

where the standard notation is used. Since equations for Y and Z are similar, derivations will be carried out only for X, it being understood that similar derivations apply for Y and Z.

Eq. (1) may be rewritten in the incremental form so that

$$\Delta X=E\bar{x}T\Delta\lambda \tag{2}$$

where R is replaced by T to indicate transmittance of solutions. Now if two components M and N having transmittances T_M and T_N are mixed together in the proportions m and $1-m$, the transmittance at a given wave-length will be

$$T=T_M{}^mT_N{}^{(1-m)} \tag{3}$$

provided that Beer's law holds and that there is no interaction of the dye molecules. The incremental tristimulus values of the resultant mixture must then be

$$\Delta X=E\bar{x}T_M{}^mT_N{}^{(1-m)}\Delta\lambda=\Delta X_M{}^m\Delta X_N{}^{1-m}. \tag{4}$$

The total tristimulus value of the mixture must be given by a summation of the incremental values over all wave-lengths, or

$$X=\Delta X_{M_1}{}^m\Delta X_{N_1}{}^{1-m}+\Delta X_{M_2}{}^m\Delta X_{N_2}{}^{(1-m)}+\cdots \tag{5}$$

where the subscript numbers refer to the different incremental wave-length bands.

Let

$$k_1\frac{\Delta X_{M_1}}{\Delta X_{N_1}}=k_2\frac{\Delta X_{M_2}}{\Delta X_{N_2}}=\cdots \tag{6}$$

and

$$K=k_1\Delta X_{M_1}+k_2\Delta X_{M_2}+\cdots; \tag{7}$$

then

$$X=X_N{}^{(1-m)}K^{(m-1)}(k_1{}^{1-m}\Delta X_{M_1}+k_2{}^{1-m}\Delta X_{M_2}+\cdots). \tag{8}$$

Eq. (8) gives the exact tristimulus value of the mixture in terms of the tristimulus value of one of the components, the incremental tristimulus values of the other, and a set of constants (k) related to the ratios of the incremental tristimulus values of the two components at specified wave-lengths. Since the incremental tristimulus values are proportional to the transmittance, the k's are proportional to the ratio of transmittances of the components at specified wave-lengths.

When partial derivatives of X with respect to each of the k's in turn are formed and set equal to zero, X is found to be maximum under the condition

$$k_1=k_2=\cdots. \tag{9}$$

If Eq. (9) is fulfilled, however, then Eq. (8) reduces to

$$X=X_M{}^mX_N{}^{1-m}. \tag{10}$$

Equation (10), therefore, represents the maximum tristimulus value of any mixture in the proportions m

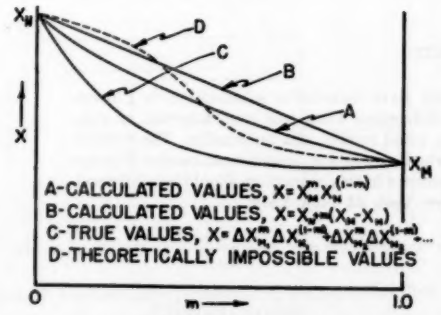

FIG. 1. Typical plots of X against m as calculated from the three Eqs. (5), (10), and (11).

* Presented at the Buffalo meeting of the Optical Society of America (October 1949).

and $1-m$ of any two components having tristimulus values of X_M and X_N. Furthermore, it represents the exact tristimulus value of any mixture of two components whose ratios of transmittances are constant over all wave-lengths in the visible spectrum.† Both statements, of course, assume the validity of Beer's law and the absence of chemical interaction.

Equation (10) may be further simplified by a binomial expansion to

$$X=X_N+m(X_M-X_N), \qquad (11)$$

providing that the difference between X_M and X_N is small in comparison with either one.

It will be noted that the second derivatives of X with respect to m are always zero or greater for all three equations. This means that the plots must be concave downward and that they must contain no points of inflection (see Fig. 1). A plot of the measured, or true, tristimulus values for any mixture, therefore, must be of the form shown by curve C, and any curve of the form shown by D is impossible unless there are deviations from Beer's law or interaction of the molecules in the mixture.

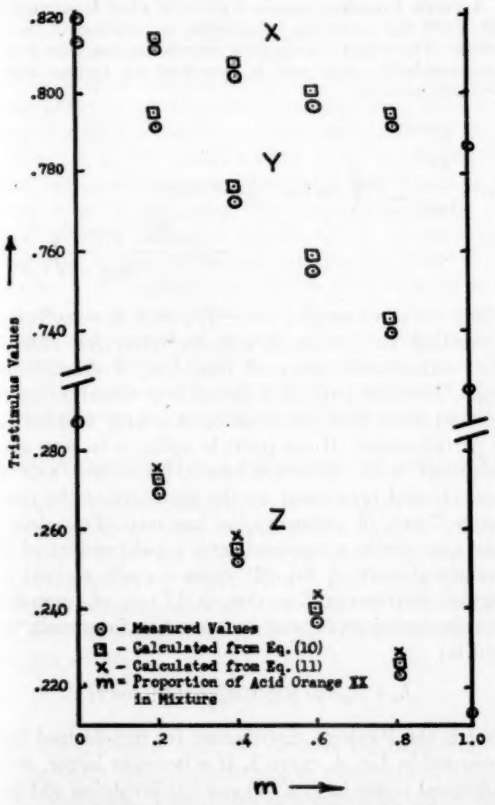

FIG. 2. Tristimulus values of mixtures of fast light orange GE-GA (conc.=0.0025 percent) and acid orange XX (conc. =0.0020 percent) in solution.

† The comparable equation for a three-component mixture is

$$X=X_M{}^mX_N{}^nX_L{}^{(1-m-n)}.$$

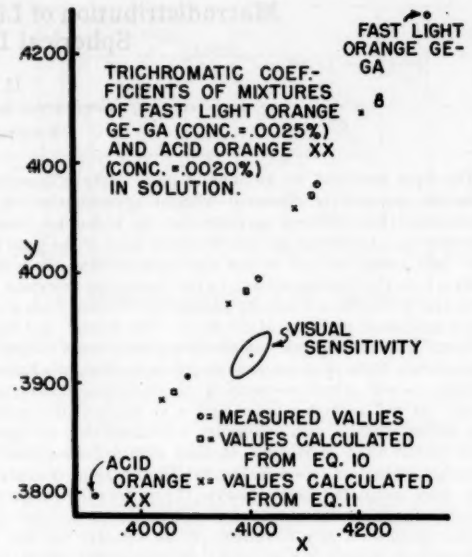

FIG. 3. Trichromatic coefficients of mixtures of fast light orange GE-GA (conc.=0.0025 percent) and acid orange XX (conc. =0.0020 percent) in solution.

In order to check the validity of the approximations given by Eqs. (10) and (11), sixteen pairs of acid dyes were examined. The two components in each pair were fairly close in color; that is, one pair consisted of two different red dyes, another of two different purple blue dyes and so forth. A typical plot of tristimulus values against m is given in Fig. 2, and a plot of the trichromatic coefficients is shown in Fig. 3. An ellipse showing the visual sensitivity[1] of the eye is drawn in Fig. 3 in order to show the magnitude of color change and the degree of approximation of the equations.

Equation (10) proved to be an excellent approximation for ten of the sixteen pairs of dyes examined. The differences between calculated and true trichromatic coefficients were no greater than the size of the visual sensitivity ellipse. In four cases it was a fair approximation and in two it was very poor. Equation (11) was an excellent approximation in seven cases, fair in five cases and poor in four cases. Inflections in the plots of tristimulus values *versus* m and tristimulus values greater than those predicted by Eq. (10) were found in several cases, indicating interaction of the molecules.

[1] D. L. MacAdam, J. Opt. Soc. Am. 32, 247 (1942).

Macrodistribution of Light Scattered by Dispersions of Spherical Dielectric Particles*

H. H. THEISSING
Signal Corps Engineering Laboratories, Fort Monmouth, New Jersey
(Received October 24, 1949)

The light scattered by an infinite plane layer of suspended dielectric particles is discussed without consideration of the interference from different particles. Let the first-order quantity function (q.f.) be defined as that fractional part of the total incident light energy subject to one scattering process, the second-order q.f. as the fraction subject to two scattering processes, etc. Then the first-order q.f. and its angular distribution from a very dilute medium is given by Mie's theory. The second- and higher order q.f. from a denser medium are derived in terms of elementary exponentials. Polar plots are presented showing that for a Rayleigh medium ($\alpha \to 0$, where α=particle circumference/wave-length) second- as well as higher order light is of substantially uniform distribution whereas such uniformity is attained only for light of order greater than eight for a medium with a pronounced Mie primary distribution ($\alpha=5$ in Fig. 6). The fractions of scattered light were calculated in two ways: (1) as forward progressive quantity functions for the several orders, to be multiplied by angular factors for any direction; (2) as separate forward and backward progressive half-space q.f. for the several orders, to be multiplied by angular factors taken in the corresponding half-spaces. Comparison of the ratio r of total backward to total forward light as obtained from both calculations, (1) and (2), gives similar results in most cases. r becomes smaller as both, α and the medium dilution increase ($r=1$ for $\alpha \to 0$, $r=\sim 1/1000$ for $\alpha=5$). For very dense dispersions (still neglecting interference) r approaches unity for all α according to method (1), while it decreases slightly from $r=1$ for $\alpha=0$ with increasing α according to the more detailed method (2). The latter method, however, proves to be the only one appropriate to trace the large backward reflection combined with the low forward transmission in some absorbing media.

Corrections are made for the q.f. of the several orders in terms of a slenderness factor where the medium is defined as a limited region of an infinite plane layer.

A specific numerical example is given for a low density medium for which this correction is negligible and method (1) is good enough. The weight of suspended material necessary for a barely photographable vapor trail is calculated for various sizes of dielectric particles.

A STUDY of the phenomena of light scattering by small particles involves the investigation of what happens when a light wave impinges on a single small particle (microdistribution) and determination of how the result of this investigation can be applied to an accumulation of dispersed particles (macrodistribution).

A. SCATTERING BY A SINGLE PARTICLE

This subject has been discussed in a number of publications;[1–3] Mie's theory[3] is best known and solves the problem exactly. A plane linear polarized wave hits a spherical particle of radius a and is disturbed by this inhomogeneity. The boundary conditions along the spherical surface of the particle require steadiness of the tangential components of the electric and magnetic field vector; to fulfill these conditions, two additional waves, one in the interior of the particle and one scattered in the outside space, have to be stated. Both intensities of the scattered wave in a distance r, $J_\perp$ perpendicular and $J_\parallel$ parallel to the vision plane, which is the plane formed by the primary beam axis and the observation direction, form Mie's essential equations:[4]

$$J_\perp=\frac{\lambda^2}{4\pi r^2}\left|\sum_{m=1}^{\infty} i^m\left(B_m'\frac{P_m(\cos\theta)}{\sin\theta}-B_m''P_m^{(1)\prime}(\cos\theta)\sin\theta\right)\right|^2, \quad (1)$$

$$J_\parallel=\frac{\lambda^2}{4\pi r^2}\left|\sum_{m=1}^{\infty} i^m\left(B_m'P_m^{(1)\prime}(\cos\theta)\sin\theta-B_m''\frac{P_m^{(1)}(\cos\theta)}{\sin\theta}\right)\right|^2, \quad (2)$$

where λ=wave-length, $i=(-1)^{\frac{1}{2}}$, $B(\alpha,\tilde{n})$=coefficients depending on $\alpha=2\pi a/\lambda$ and on refractive index $\tilde{n}$, $P_m^{(1)}$=associated spherical functions, θ=meridional† angle. Thus the particle is forced into vibration by the incident wave with the emission of a large number (m) of partial waves. If the particle radius a is very small compared with the wave-length [$\alpha=(2\pi a)/\lambda<0.1$], Eqs. (1) and (2) caused by the structure of the coefficients B' and B'' reduce to the first term. Equation (1) only then yields a constant term c independent of the meridional angle θ, Eq. (2) yields $c\cdot\cos^2\theta$, so that the angular distribution function (a.d.f.) q_θ of intensities into the directions θ about one steradian for unpolarized light is:

$$J_\perp+J_\parallel=q_\theta \text{ Rayleigh}=c(1+\cos^2\theta). \quad (3)$$

That is the Rayleigh distribution for unpolarized light presented in Fig. 4, curve 1. If α becomes larger, other additional terms in Eqs. (1) and (2) involving odd $\cos\theta$ powers contribute a positive amount in the propagation direction $\theta=0°(\cos 0°=+1)$ and a negative amount in the backward direction $\theta=180°(\cos 180°=-1)$.‡ Thus the well-known dissymmetry favoring the propagation direction of light is developed. This dissymmetry is

* Extract from Signal Corps Engineering Laboratories Technical Memorandum M-1149 (October 15, 1948).

[1] Lord Rayleigh, Phil. Mag. **47**, 375 (1899); **36**, 365 (1918).

[2] P. Debye, Ann. d. Physik **30**, 57 (1909); Math. Ann. **67**, 540 (1909).

[3] G. Mie. Ann. d. Physik **25**, 377 (1908); compare the presentation of Mie's theory in reference 4.

[4] M. Born, *Optik* (Verlag. Julius Springer, Berlin, 1933), Edwards Brothers reprint (1943), pp. 274–292.

† Within any plane containing the primary beam.

‡ This notation for the directions θ, contrary to Mie's notation in Eqs. (1) and (2), will be used henceforth.

usually referred to as "Mie effect." (Compare Figs. 5 and 6, curve 1.)

Equations (1) and (2) were laboriously solved for some values of the refractive index $\bar{n}$ including $\bar{n}=\infty$ and values of α between 0.1 to 8 by H. Blumer,[5] for 16 values of α for the refractive index $\bar{n}=1.333$ by H. Holl[6a, 7] and for 15 values of α for the refractive indices $\bar{n}=1.33$, 1.44, 1.55, and 2.0 by the National Bureau of Standards (see reference 7). The present paper considers only the results of Blumer for dielectric particles.

Besides giving the a.d.f. for the radius vector q_θ the theory reveals that the total amount of light

$$q=2\pi\int_0^\pi q_\theta \sin\theta d\theta \tag{4}$$

scattered all around by the particle increases at a high rate with increasing α. Putting

$$q=K(\alpha,\bar{n})\cdot a^2\pi, \tag{5}$$

$K(\alpha,\bar{n})$ denotes the deficiency (or excess) of the scattering effect below (or above) the geometric area $a^2\pi$. That is why q is usually quoted as "scattering cross section." K is very small for the small Rayleigh particles, increases then with about the sixth power of α, passes a maximum, and then approaches unity. K functions were presented by Jobst,[8] by Stratton and Houghton[9] and, in connection with the important work done by V. K. LaMer,[10] by D. Sinclair.[11] A very complete $K(\alpha)$ function for $n=1.333$, showing several maxima and minima up to large α values, was recently given by H. Holl.[6b] In Fig. 1 the dotted curve for $\bar{n}=1.25$ was fitted into Sinclair's curves for the numerical calculations following later on (Table II, column K).

B. SCATTERING BY A DISPERSION OF PARTICLES

In actual experiments there is no single particle, but dispersions of particles. Investigations have shown that the theory holds for dilute dispersions. The scattered light is obtained by multiplying q_θ (cm²) from Mie's or Blumer's work by n (cm^{-3}) = number of particles per ccm and the path d (cm) of the light in the medium, so that per sterad.:

$$S_\theta=q_\theta\cdot n\cdot d. \tag{6}$$

This dimensionless quantity denotes the percentage of incident unit light flux emerging in the direction θ about unit solid angle. This simple expression Eq. (6) suffices in many cases. Since higher densities may sometimes occur,[12, 13] an extension for denser dispersions is presented in the following discussion. For low densities, of course, the extension must reduce to Eq. (6) as will be shown in Eq. (33). Arrangement of particles in the medium is still assumed at random and at sufficient distance so that phase interaction and interference phenomena between the radiations of different particles are neglected. But the difference between the diluted condition when Eq. (6) is valid and the following discussion is that now light will be not only scattered once before leaving the medium as in Eq. (6) but that secondary, tertiary . . . scattering will be included.

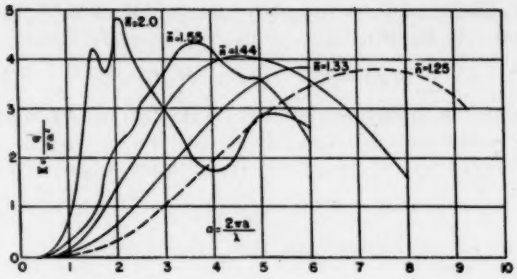

FIG. 1. Scattering coefficient K (see reference 11).

C. QUANTITY FUNCTIONS

The idea is that for a non-absorbing medium infinite in the yz directions (Fig. 2a) there will be present at any distance x within the medium from the plane $x=0$ where the unpolarized parallel light of unit intensity impinges, an amount $M_0(x)$ of the original parallel beam, plus an amount $M_1(x)$ of light scattered once all around, an amount $M_2(x)$ of light scattered twice all around and so on. Of course every quantity M_k has its own a.d.f. $q_k(\theta)$, beginning with Mie's microdistribution $q_1(\theta)$. The higher order a.d.f.'s will be considered later in paragraph

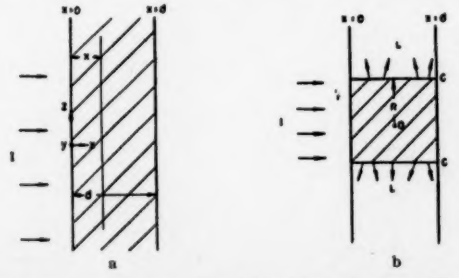

FIG. 2. Infinite plane layer (Fig. 2a) and limited volume (Fig. 2b) of scattering medium. I = incident light flux parallel to x axis. L = loss through the side cuts (C), assumed as centered about 90° around the axis of the incident beam I.

[5] (a) H. Blumer, Zeits. f. Physik **32**, 119 (1925); (b) **38**, 304 (1926); (c) **38**, 920 (1926).
[6] (a) H. Holl, Optik **2**, 213 (1947); (b) **4**, 173 (1948–1949).
[7] Nat. Bur. Stand. App. Math. Series 4 (January 25, 1949).
[8] G. Jobst, Ann. d. Physik **76**, 863 (1925).
[9] Stratton and Houghton, Phys. Rev. **38**, 159 (1931).
[10] LaMer and Barnes, J. Colloid Sci. **1**, 71 (1941); **1**, 79 (1946).
[11] D. Sinclair, J. Opt. Soc. Am. **37**, 476 (1947).

[12] Compare University of Michigan Engineering Research Institute, Ann Arbor, Michigan Progress Report No. 5 on Contract W 36-039 sc-32307 (Signal Corps), April 15, 1948.
[13] Compare University of Michigan Engineering Research Institute, Ann Arbor, Michigan Progress Report No. 6 (July 15, 1948) and Final Progress Report (February 15, 1949) on Contract W 36-039 sc-32307 (Signal Corps).

d. First consider the quantity functions M_k. For M_0, the primary incident beam yields $-dM_0=nqM_0dx$ and

$$M_0(x)=\exp(-qnx);\quad M_0(0)=1, \tag{7}$$

which is an exponential decrease through the medium. For the scattered light divide the whole space in a forward (v) and backward (h) half-space, where, when

$$f_k(\theta)=(q_\theta/q)_k, \tag{8}$$

and Eq. (4) is considered, then

$$v_k=2\pi\int_0^{\pi/2} f_k(\theta)\,\sin\theta d\theta$$

and

$$h_k=2\pi\int_{\pi/2}^{\pi} f_k(\theta)\,\sin\theta d\theta. \tag{9}$$

Both v_k and h_k depend on the shape of the a.d.f. According to definition:

$$v_k+h_k=1. \tag{10}$$

Now, denote the light flux entering the forward half-space by Q_k, and the light flux entering the backward half-space by P_k. Then

$$\sum M_k=\sum Q_k+\sum P_k. \tag{11}$$

The alteration of the primary scattered light within $+dx$ is proportional to the difference of the parallel light $M_0(x)$ minus the primary amount itself, since the latter has to be converted into secondary light (compare Eq. 23):

$$\left.\begin{aligned}&(1/qn)(dQ_1(x)/dx)+Q_1(x)=v_1M_0(x)\\ &\text{and the alteration of the primary scattered light within } -dx \text{ is:}\\ &(1/qn)(dP_1(x)/dx)-P_1(x)=-h_1M_0(x),\end{aligned}\right\} \tag{12}$$

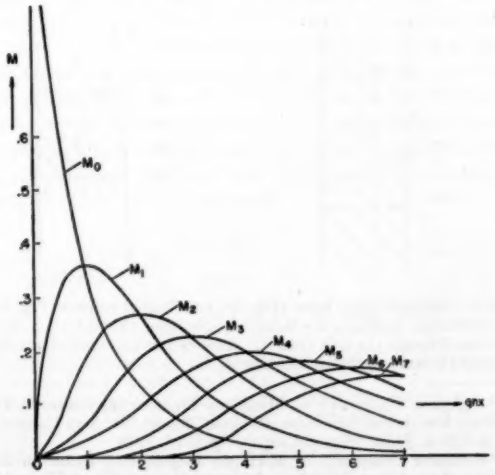

FIG. 3. Quantity function vs. density. $M0$ = parallel beam intensity $M1$, $M2\cdots$ = light intensity of higher scattering orders.

yielding

$$Q_1=v_1qnx\cdot\exp(-qnx)=v_1M_1, \tag{13}$$

if

$$M_1=qnx\cdot\exp(-qnx) \tag{14}$$

is put for abbreviation, and

$$P_1=(h_1/2)M_0-(h_1/2)\exp(-2qnd)\cdot\exp(qnx). \tag{15}$$

Therefore, if the medium has a thickness d and if the scattering density qnd is small enough so that only primary scattered light has to be considered

$$Q_1(d)=v_1qnde^{-qnd} \tag{16}$$

emerges at the border $x=d$ into the forward half-space and

$$P_1(0)=(h_1/2)(1-e^{-2qnd}) \tag{17}$$

emerges from the border $x=0$ into the backward half-space. For the 90 degree equator both half-spaces must yield the same value. Therefore, with $f_k(\theta=90°)$ from Eq. (8) the equatorial condition

$$\frac{Q_1(d)f_1(90)}{v_1}+\frac{Q_2(d)f_2(90)}{v_2}+\cdots=\frac{P_1(0)f_1(90)}{h_1}+\frac{P_2(0)f_2(90)}{h_2}+\cdots \tag{18}$$

yields for low densities

$$Q_1(d)h_1=P_1(0)v_1. \tag{19}$$

Inserting Eqs. (13) and (15) we get

$$qnde^{-qnd}=\sim\tfrac{1}{2}(1-e^{-2qnd}) \tag{20}$$

which is fulfilled indeed for low scattering densities qnd, as proved by expansion of the e-functions.

On the other hand, if only one flux $M_{1(x)}$ all around had been considered, but no double flux $Q_{1(x)}$ and $P_{1(x)}$ into both half-spaces there would emerge into the forward half-space:

$$F=M_1(d)\cdot v_1 \tag{21}$$

and into the backward half-space:

$$B=M_1(d)\cdot h_1, \tag{22}$$

Eq. (21) agrees with (13). Inserting Eq. (14) into (22) and comparing the result with Eq. (17) representing the backward radiation $P_{1(0)}$ one finds both sides are equal as already confirmed by Eq. (20). Thus, instead of considering two light flux Q and P forward and backward, it is sufficient for low densities to consider one flux M in the propagation direction of light (from Eqs. (13) and (14)) by temporarily using $v_1=1$ and $h_1=0$ and then multiplying $M(d)$ by the corresponding forward or backward angular quantities according to Eqs. (21) and (22).

For a dense medium, the two-flux and one-flux method will be compared in paragraph e.

TABLE I. Coefficient scheme for Blumers angular distribution function $n=1.25$ and $\alpha=5(k=1)$ and the correlated scattering functions of higher order $k=2, 4, 8, 16$ according to W. Hartel's formula Eqs. (36) and (37). m = term number in Eq. (34), k = order number in Eqs. (36).

	$m=$	1	2	3	4	5	6	7	8	9	10	11	12	13	14	15	16	17
Zonal harmonics	$P(\cos 0°)$	1	1	1	1	1	1	1	1	1	1							
	$P(\cos 10°)$	0.9848	0.9548	0.9106	0.8532	0.7840	0.7045	0.6164	0.5218	0.4228	0.3214							
	$P(\cos 20°)$	0.9397	0.8245	0.6649	0.4750	0.2715	0.0719	−0.1072	−0.2518	−0.3517	−0.4013							
	$P(\cos 45°)$	0.7071	0.2500	−0.1768	−0.4063	−0.3757	−0.1484	0.1271	0.2983	0.2855	0.1151							
	$P(\cos 90°)$	0	−0.5000	0	0.3750	0	−0.3125	0	0.2734	0	−0.2461							
	$P(\cos 180°)$	−1	+1	−1	+1	−1	+1	−1	+1	−1	+1							
Coefficients of Eq. (37)	$k=1(a_1, a_3\cdots)$	2.00	2.81	3.50	4.05	4.40	4.34	4.00	3.36	2.75	2.22	1.75	1.28	1.00	0.69	0.40	0.25	0.15
	$k=2\left(\frac{a_1^2}{3}, \frac{a_3^2}{5}\cdots\right)$	1.33	1.58	1.75	1.82	1.76	1.45	1.07	0.663	0.398	0.235	0.133	0.066	0.037				
	$k=4\left(\frac{a_1^4}{3^3}, \frac{a_3^4}{5^3}\cdots\right)$	0.593	0.501	0.438	0.386	0.282	0.162	0.076	0.036	0.008	0.003							
	$k=8\left(\frac{a_1^8}{3^7}, \frac{a_3^8}{5^7}\cdots\right)$	0.117	0.050	0.027	0.015	0.007												
	$k=16\left(\frac{a_1^{16}}{3^{15}}, \frac{a_3^{16}}{5^{15}}\cdots\right)$	0.004	0.0005															

For second-order scattering the statement would be similar to Eq. (12):

$$\begin{aligned}(1/qn)(dQ_2/dx)+Q_2&=v_2Q_1+h_2P_1\\(1/qn)(dP_2/dx)-P_2&=-h_2Q_1-v_2P_1,\end{aligned}\qquad(23)\S$$

with the solutions

$$\begin{aligned}Q_2=&\frac{h_1h_2}{2}M_1+v_1v_2M_2-\frac{h_1h_2}{4}e^{-2qnd}e^{qnx}\\&+\frac{h_1h_2}{4}e^{-2qnd}e^{-qnx},\\P_2=&\frac{v_1h_2+v_2h_1}{4}M_0+\frac{v_1h_2}{2}M_1+\frac{v_2h_1}{2}qnx\cdot e^{-2qnd}e^{qnx}\\&-\frac{v_1h_2+v_2h_1}{4}(2qnd+1)e^{-2qnd}e^{qnx},\end{aligned}\qquad(24)$$

where

$$M_2(x)=[(qnx)^2/2!]e^{-qnx}.\qquad(25)$$

For very high densities the third and fourth terms in both equations vanish. For $v_1=v_2=1$ and $h_1=h_2=0$, the one flux conception yields, independent of density:

$$Q_2=M_2=\frac{(qnx)^2}{2!}e^{-qnx};\quad P_2=0.$$

Then the backward scattered light can once more be determined approximately by multiplying $M_2(d)$ by the corresponding $f_2(\theta)=(q_\theta/q)_2$ in any direction in the backward half-space, again neglecting the fact that h was first made equal to 0 to reduce Eq. (24) to M_2 alone.

§ Note that h_2P_1 is a forward light flux, h_2Q_1 and v_2P_1 a backward flux.

In the same way a pair of equations like Eq. (23) set up for Q_3 and P_3 gives:

$$\left.\begin{aligned}Q_3=&\frac{v_1h_2h_3+v_2h_1h_3}{4}M_1\\&+\frac{v_3h_1h_2+v_1h_2h_3}{2}M_2+v_1v_2v_3M_3\\&+\text{three terms vanishing for large } qnd\\P_3=&\left(\frac{v_1v_2h_3}{8}+\frac{v_2v_3h_1}{8}+\frac{v_1v_2h_2}{4}+\frac{h_1h_2h_3}{8}\right)M_0\\&+\text{one term containing } M_1\\&+\text{one term containing } M_2\\&+\text{several terms vanishing for large } qnd\end{aligned}\right\}.\qquad(26)$$

If consideration is again limited to the one-flux method, the result is:

$$M_3(x)=[(qnx)^3/3!]e^{-qnx}.\qquad(27)$$

For order k:

$$M_k(x)=[(qnx)^k/k!]e^{-qnx}.\qquad(28)$$

These quantity functions M_k of various scattering orders k are plotted *vs.* density qnd in Fig. 3. It is seen that with increasing density the next higher order takes over from the preceding lower orders. For any qnd the sum of all orders is:

$$\begin{aligned}\textstyle\sum_k M_k=&M_0+M_1+M_2+\cdots=e^{-qnx}\\&+(qnx/1!)e^{-qnx}+[(qnx)^2/2!]e^{-qnx}+\cdots=1,\end{aligned}\qquad(29)$$

which is equal to unit incident energy. However, only a certain range of orders is actually operating for a specific value of qnd; all lower and all higher orders become so small that they make no practical contribution to the

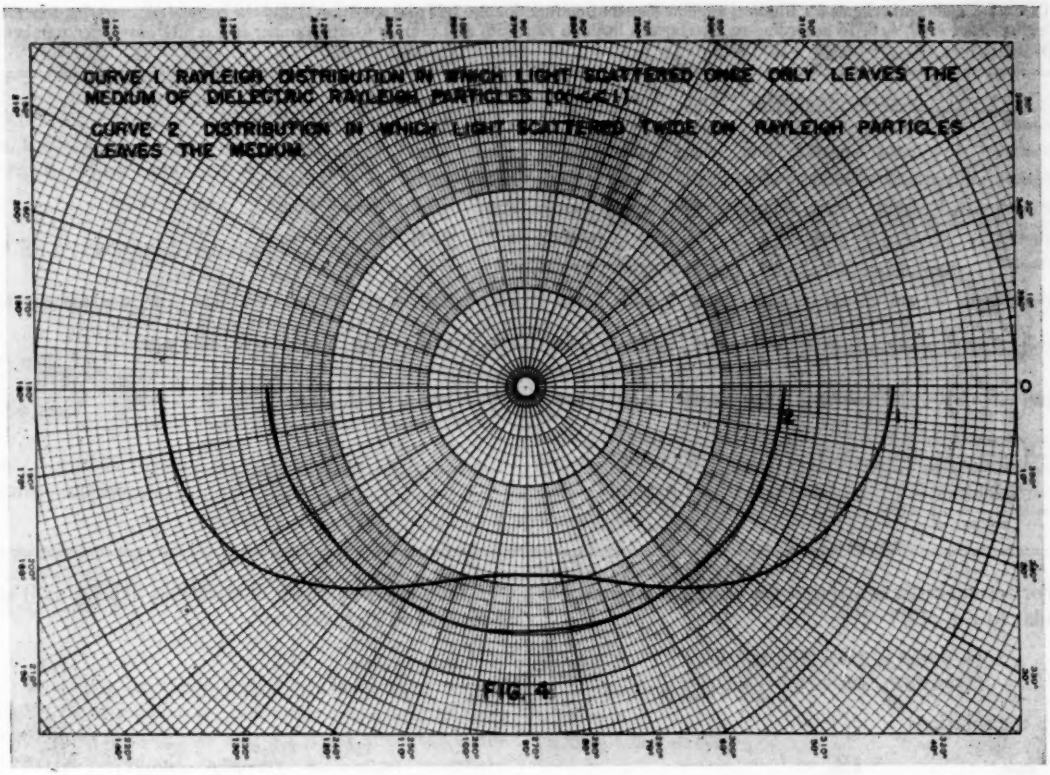
CURVE 1. RAYLEIGH DISTRIBUTION IN WHICH LIGHT SCATTERED ONCE ONLY LEAVES THE MEDIUM OF DIELECTRIC RAYLEIGH PARTICLES ($\bar{n}=\infty 1$).
CURVE 2. DISTRIBUTION IN WHICH LIGHT SCATTERED TWICE ON RAYLEIGH PARTICLES LEAVES THE MEDIUM.
FIG. 4.

FIG. 4.

sum. From Eqs. (11) and (29):

$$\sum M_k=\sum Q_k+\sum P_k=1. \tag{30}$$

D. ANGULAR FUNCTIONS

The a.d.f. $q_{\theta k}$ remains to be established for every order k that must be linked with the quantity function M_k of the same order. Apparently the angular factor $f_k(\theta)$ has to be normalized in such a way

$$2\pi\int_0^{\pi} f_k(\theta)\sin\theta d\theta=1 \tag{31}$$

that it influences only the angular distribution and not the quantity of light which is exclusively controlled by M_k. $f_k(\theta)$, stated in Eq. (8), satisfies this condition as Eq. (4) shows. If such factors $f_k(\theta)$ can be found, the total radiation emerging from all scattering orders into the direction θ, not counting the incident parallel flux M_0, would be:‖

$$S_\theta=M_1f_1(\theta)+M_2f_2(\theta)+\cdots. \tag{32}$$

‖ With the split-up quantity functions Eq. (32) would read $S_\theta=\sum Q_kf_k(\theta)$ for $-\pi/2<\theta<+\pi/2$ and $S_\theta=\sum P_kf_k(\theta)$ for $+\pi/2<\theta<(3\pi)/2$.

First, note that Eq. (6) is contained within Eq. (32). Low densities require only the first scattering order 1, hence: $S_\theta=qnd\cdot e^{-qnd}(q_\theta/q)$, which for very small qnd reduces to

$$qnd(q_\theta/q)_1=q_\theta\cdot n\cdot d, \tag{33}$$

as in Eq. (6).

Now, W. Hartel[14] found (Eq. (36)) that the angular factor $f_k(\theta)$ for order k can be expressed by $f_1(\theta)$ for order 1, provided that the latter is known in the form:

$$f_1(\theta)=(q_\theta/q)_1=1/(4\pi)[1+a_1P_1(\cos\theta)+a_2P_2(\cos\theta)+\cdots a_mP_m(\cos\theta)\cdots], \tag{34}$$

where $P_m(\cos\theta)$ denote the surface zonal harmonics. W. Hartel calculated $f_1(\theta)$ from a formula established by Rayleigh[2,15] that holds for $\bar{n}=\sim 1$ only. This limitation will be dropped here. Since $f_1(\theta)$ represents the sum of Eqs. (1) and (2) i.e., the micro a.d.f. for unpolarized light, $f_1(\theta)$ may always be expressed in terms of Eq. (34) no matter whether the a.d.f. is given by an analytic expression or by individual radii vectors $q_1(\theta)$ as in Blumer's[5] or Holl's[6] results. E.g., for the Rayleigh a.d.f.

[14] W. Hartel, Das Licht **10**, 141 (1940).
[15] Lord Rayleigh, Phil. Mag. **12**, 81 (1881).

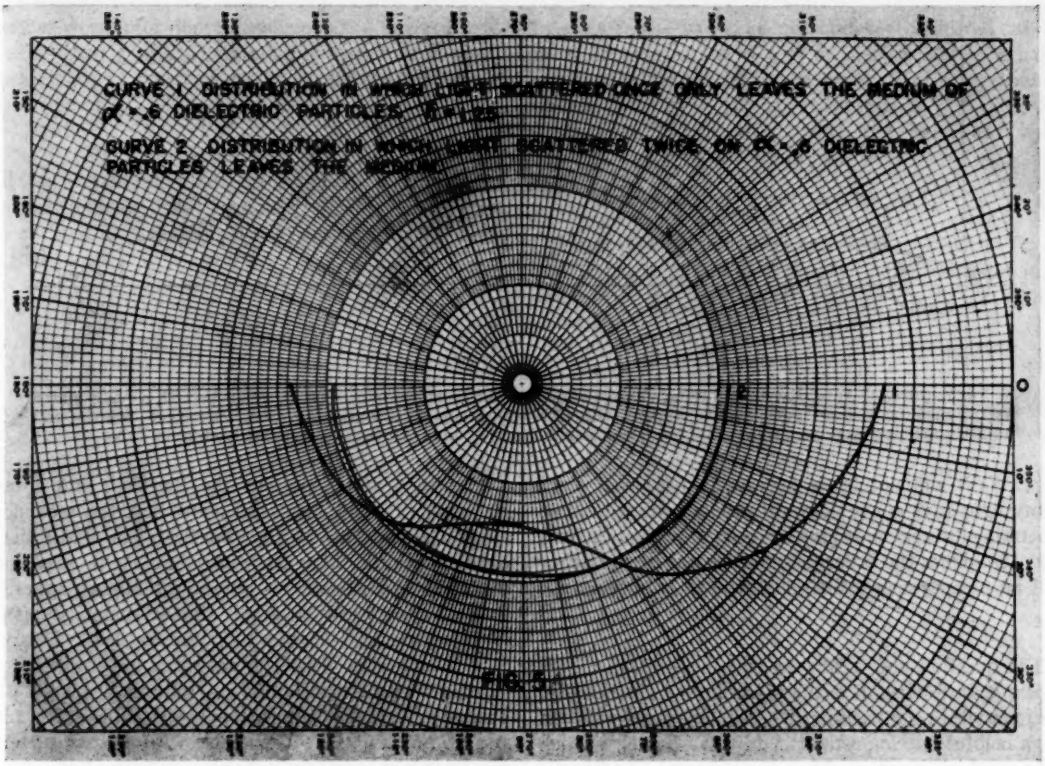
CURVE 1 DISTRIBUTION IN WHICH LIGHT SCATTERED ONCE ONLY LEAVES THE MEDIUM OF
CURVE 2 DISTRIBUTION IN WHICH LIGHT SCATTERED TWICE OR
PARTICLES LEAVES THE MEDIUM
FIG. 4.

FIG. 5.

Eq. (3) the condition Eq. (31) requires

$$f_1(\theta)=(q_\theta/q)_1=C(1+\cos^2\theta);$$

$$2\pi C\int_0^\pi (1+\cos^2\theta)\sin\theta d\theta=1$$

yielding

$$f_1(\theta)=3/16\pi(1+\cos^2\theta)$$
$$=1/4\pi[1+a_1P_1(\cos\theta)+a_2P_2(\cos\theta)+\cdots]$$

which, by comparison of coefficients, results in:

$$f_1(\theta)=1/(4\pi)[P_0(\cos\theta)+\tfrac{1}{2}P_2(\cos\theta)]$$
$$=1/4\pi(1+\tfrac{1}{2}P_2(\cos\theta)). \quad (35)$$

All coefficients except $a_2=\frac{1}{2}$ are zero.

For Mie shape a.d.f.'s, of course, a greater number of coefficients is needed, the greater, the narrower the Mie a.d.f. is. The coefficients can then be found from given a.d.f. data ($f_1(\theta)$ from Blumer's work) by setting up as many equations (34), each for a different θ, as coefficients will be needed. One of these equations, for $f_1(0°)$, contains the sum of all coefficients, another $f_1(180°)$, contains the difference of all even (including $P_0(\cos\theta)=1$) minus all odd coefficients, as may be seen from the zonal harmonics listed in Table I. The slimness of the a.d.f. depends on the higher order terms since the higher $P_m(\cos\theta)$ decrease rapidly even for small changes in θ (compare Table I).¶

It can be stated in advance that for the next following

¶ This way of finding the coefficients a_m which requires the solution of a system of linear equations is feasible only for small α, where only a few m need to be considered. This method has the advantage of furnishing the coefficients with their respective signs, which may alternate (+ and −) in this small η range to trace, e.g., the 90° constriction of the a.d.f. Figs. 4 and 5. For large α however, where a greater number of m has to be considered, all the small loops in narrow angular districts, as shown in Blumer's graphs, become more or less negligible details as compared with the most interesting phenomenon of the pronounced Mie shape. In this case, the coefficients become all positive. Their dependence on the order number m can be seen when plotting the coefficients a_m listed, e.g., in Table I, line $k=1$ *vs.* m. The best way to find the coefficients a_m for a given Mie a.d.f. is approximative: first, draw an optional graph a_m *vs.* m like the plot of Table I, $k=1$, mentioned above. The area of this plot (sum of all a_m) equals $4\pi f_1(\theta=0)$ (Eq. 34 for $\theta=0$). The difference (usually small) between the area of all even coefficients and the area of all odd ones equals $4\pi f_1(\theta=180°)$. Then Eq. (34) for $\theta=90°$ furnishes an additional relation between the various even coefficients alone. If the assumed graph were corrected to fit these three conditions, a check with a small angle, say $\theta=10°$, will show whether it fits the slimness of the given a.d.f. If $4\pi f_1(\theta=10°)$ is too large as compared with the original graph, the maximum of the graph must be shifted towards higher m while the total area is kept constant. Then repeat the check as described. That way the approximation may be accomplished to any desired degree.

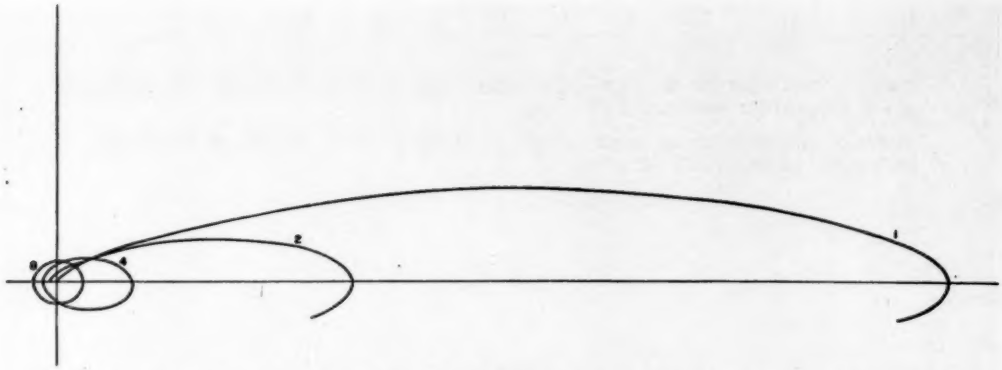

FIG. 6. Curve 1: Approximation to Blumer's angular distribution function for dielectric particles $\bar{n}=1.25$, $\alpha=5$ by means of the coefficients listed under $k=1$ in Table I. Other curves: Angular distribution functions for second-, fourth-, and eighth scattering order according to W. Hartel's formula Eqs. (36) and (37), coefficients listed likewise in Table I.

a.d.f., $f_2(\theta)$ will not be as narrow as $f_1(\theta)$ was, since many light rays going sideward produce other random scattering directions. It may be recognized qualitatively that the higher the order k is, the greater the tendency will be to approach a final spherical distribution with

$$f_\infty(\theta)=1/(4\pi).$$

The question now is how to find the a.d.f. of higher orders k. If, for instance, the coefficients a_m in Eq. (34) are found from comparison with Blumer's graphs we can use a helpful relation established by W. Hartel,[14] which links any higher order a.d.f. to the primary a.d.f. Hartel finds the a.d.f. of order k, $f_k(\theta)$ as follows:

$$f_k(\theta)=\frac{1}{4\pi}\sum_0^m \frac{{a_m}^k}{(2m+1)^{k-1}}P_m(\cos\theta) \qquad (36)$$

or more extensively written:

$$\left.\begin{aligned}
4\pi f_1(\theta)&=1+a_1P_1(\cos\theta)\\
&\quad +a_2P_2(\cos\theta)+a_3P_3(\cos\theta)+\cdots\\
4\pi f_2(\theta)&=1+\frac{{a_1}^2}{3}P_1(\cos\theta)\\
&\quad +\frac{{a_2}^2}{5}P_2(\cos\theta)+\frac{{a_3}^2}{7}P_3(\cos\theta)+\cdots\\
4\pi f_4(\theta)&=1+\frac{{a_1}^4}{3^3}P_1(\cos\theta)\\
&\quad +\frac{{a_2}^4}{5^3}P_2(\cos\theta)+\frac{{a_3}^4}{7^3}P_3(\cos\theta)+\cdots
\end{aligned}\right\}. \qquad (37)$$

In Table I, a scheme of such coefficients shows that the higher the order k the fewer the coefficients that need be considered in accordance with the above statement that the rounder shape of a.d.f. requires fewer coefficients.

Figures 4 and 5 present the Rayleigh and a near Rayleigh primary a.d.f. and show that the secondary a.d.f. is already practically spherical. For a Mie shape $\alpha=5$, however, Fig. 6 shows that eight scattering processes are needed to obtain an almost spherical shape. Figure 7 evaluates only the 90° quantity $f_k(90°)$ for dielectric particles ($\bar{n}=1.25$) and $\alpha=0$, 1.2, 2, 5, and 8. For first-order $k=1$ the ordinates are known from Blumer's graphs according to column $f_1(\alpha, 90°)$ in Table II. The other values are calculated from Eq. (36) and (37) with $\theta=90°$. The curves with the parameter α can be traced approximately by the expression

$$f_k(\alpha, 90°)=1/4\pi[1-\exp(-ck^2/\alpha+k)], \qquad (38)$$

where c is determined for each value $k=1$ by:

$$f_1(\alpha, 90°)=1/4\pi[1-\exp(-c/\alpha+1)] \qquad (39)$$

inserting $f_1(\alpha, 90°)$ from column f_1 in Table II. With the value c from Eq. (39) the $f_k(\alpha, 90°)$ in Eq. (38) can be obtained.

E. TWO-FLUX METHOD APPLIED FOR A VERY DENSE DISPERSION

As shown in paragraph C, the two-flux method (Q, P) reduces to the one-flux method (M) for very dilute media ($qnd\to 0$). The present paragraph will deal with very dense dispersions (qnd large). Denoting $Q_k(d)=Q_{k\infty}(d)$ for those large densities, it may be seen from Eqs. (13), (24), and (26) that the $Q_{k\infty}$ are composed of $M_1, M_2, \cdots M_k$. As mentioned for the M_k in connection with Eq. (29), only a certain range k of $Q_{k\infty}$ carries the whole light. For large qnd this range is centered about a high k for which $f_k\to 1/4\pi$ (compare Fig. 7) and $v_k\to h_k\to\frac{1}{2}$ (compare Fig. 8). Hence the equatorial condition Eq. (18) goes over into:

$$\frac{1}{2\pi}\sum Q_{k\infty}(d)=P_{1\infty}(0)\frac{f_1(90°)}{h_1}+P_{2\infty}(0)\frac{f_2(90°)}{h_2}+\cdots. \qquad (40)$$

In other words: for dense dispersions the forward scattered amount $\sum Q_{k\infty}(d)$ contains light scattered many times (k large), whereas the backward scattered light (right side of Eq. (40)) is composed of low order (1, 2, $\cdots$) light.

The $P_{k\infty}(0)$** can be obtained from Eqs. (15), (24), and (26) and correspondingly for higher k. Dropping the terms with $\exp(-2qnd)$, $qnd\cdot\exp(-2qnd)$, $\cdots$ for large qnd and recalling that $M_0(0)=1$, but $M_k(0)=0$ if $k\neq 0$, we find:

$$P_{1\infty}(0)=\frac{h_1}{2};\quad P_{2\infty}(0)=\frac{v_1h_2+v_2h_1}{4};$$
$$P_{3\infty}(0)=\frac{v_1v_2h_3}{8}+\frac{v_2v_3h_1}{8}+\frac{v_1v_3h_2}{4}+\frac{h_1h_2h_3}{8}. \tag{41a}$$

For simplification the three first terms in the latter equation for $P_{3\infty}(0)$ may be replaced by $v_2^2h_2/2$ and the fourth term by $h_2^3/8$ so that $P_{3\infty}(0)$ reduces to:

$$P_{3\infty}(0)=\sim\frac{v_2^2h_2}{2}+\frac{h_2^3}{8}. \tag{41b}$$

With the same approximation, for the next higher orders k:

$$P_{4\infty}(0)=\frac{v_3^3h_3}{2}+\frac{3v_3h_3^3}{8},$$
$$P_{5\infty}(0)=\frac{v_4^4h_4}{2}+\frac{3v_4^2h_4^3}{4}+\frac{h_4^5}{16},$$
$$P_{6\infty}(0)=\frac{v_5^5h_5}{2}+\frac{5v_5^3h_5^3}{4}+\frac{5v_5h_5^5}{16},$$
$$P_{7\infty}(0)=\frac{v_6^6h_6}{2}+\frac{15v_6^4h_6^3}{8}+\frac{15v_6^2h_6^5}{16}+\frac{5h_6^7}{128}, \tag{41c}$$
$$P_{8\infty}(0)=\frac{v_7^7h_7}{2}+\frac{21v_7^5h_7^3}{8}+\frac{35v_7^3h_7^5}{16}+\frac{35v_7h_7^7}{128},$$
$$P_{9\infty}(0)=\frac{v_8^8h_8}{2}+\frac{7v_8^6h_8^3}{2}+\frac{135v_8^4h_8^5}{32}+\frac{275v_8^2h_8^7}{256}+\frac{7h_8^9}{256}.$$

The sequence of the $P_{k\infty}(0)$ was plotted *vs.* k in Fig. 9 for the Rayleigh a.d.f. ($v_k=h_k=\text{const.}=\frac{1}{2}$) as well as for the Mie a.d.f. Fig. 6, from which v_k and h_k were plotted first according to Eq. (9) in Fig. 8. Curve $\alpha=0$ of Fig. 9 represents the sequence of orders for the light flux scattered into the backward half-space for a very dense Rayleigh dispersion. Curve $\alpha=5$, lower and beginning close to zero, shows this sequence for a very dense Mie dispersion. Both curves (and the same is true for intermediate α-values as indicated by the dotted curve) meet as soon as the v_k and h_k plotted in Fig. 8 have sufficiently approached each other. The area circumscribed by every $P_{k\infty}(0)$ curve represents $\sum P_{k\infty}(0)$, the total light flux scattered into the backward half-space.†† For $\alpha=5$ the area furnishes:

$$\sum P_{k\infty}(0)=0.36. \tag{42}$$

From the $P_{k\infty}(0)$ in Fig. 9, from the $f_k(90°)$ in Fig. 7 and from the h_k in Fig. 8, Eq. (40), expressing the high order $Q_{k\infty}$ by low order $P_{1\infty}(0)$, $P_{2\infty}(0)\cdots$ terms, furnishes:

$$\sum Q_{k\infty}(d)=0.58. \tag{43}$$

The sum of Eqs. (42) and (43) yields 0.94 instead of 1 which may be considered as a good result since the

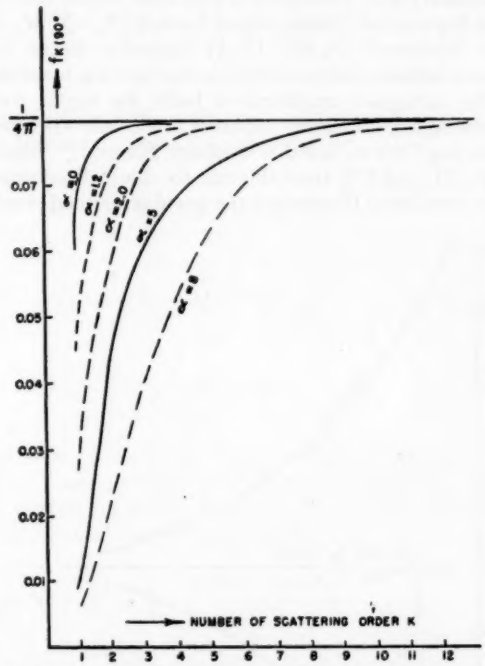

FIG. 7. Increase of 90° scattered intensity $fk(90°)$ with increasing scattering order k and with α as curve parameter for dielectric particles $n=1.25$. $f1(90°)$ evaluated from Blumer's graphs as listed in Table II. Curve $\alpha=5$ plotted from Table I and Fig. 6. Curve $\alpha=0$ plotted from Eqs. (35). Curves $\alpha=1.2$, 2, 8 approximated by Eqs. (38) and (39).

** Representing the backward half-space light flux at the boundary $x=0$ for order k.

†† For $\alpha=0$ with $h_k=\frac{1}{2}$ and $f_k(90°)=1/4\pi$ Eqs. (40) and (30) furnish $\sum Q_{k\infty}(d)=\sum P_{k\infty}(0)=0.5$ as expected (equal light intensity scattered backward and forward). The area for $\alpha=0$ in Fig. 9 is slightly larger than 0.5. However, since the area for $\alpha=5$ in Fig. 9 closely fits Eqs. (30) and (40) (compare Eqs. (42) and (43)), the lowest terms $P_{1\infty}(0)$, $P_{3\infty}(0)\cdots$ which contribute much more to $\alpha=0$ than to $\alpha=5$ seem to be slightly too high by Eq. (41), the higher $P_{k\infty}(0)$ being more and more exact. It has to be borne in mind that the quantity functions were split up into half-spaces and were linked with a.d.f. set up for the whole space (compare reference || of Eq. (32)) a procedure used, e.g. in Eq. (40). For this rather rigid model a better accuracy could not be expected.

approximation in Eq. (41) (shown at $P_{3\infty}(0)$) lowers the $P_{k\infty}(0)$ by a few percent.‡‡

More important than these figures is the qualitative dependency of the backward scattered intensity as expressed by the areas in Fig. 9 for small $\bar{n}$. The highest (Rayleigh) curve $\alpha=0$, starting from $h_1/2=\frac{1}{4}$, confines the area to 0.5 (equal intensity scattered backward and forward). The Mie curves, starting from their respective $h_1/2$, blend into the limiting curve the lower, the larger α becomes. From this it may be recognized that even the macrodistribution for the Mie dispersions shows a certain preference for the propagation direction of the illuminating beam, since the area representing the backward intensity becomes smaller than 0.5. This preference is very small when compared with the Mie microdistribution for the same α for which the forward scattering may exceed the backward by a hundred or a thousand times. Therefore even for dense dispersions the one-flux method, yielding equal forward ($F_\infty=\sum M_k\cdot\frac{1}{2}$) and backward ($B_\infty=\sum M_k\cdot\frac{1}{2}$) intensity, traces the actual behavior fairly well for α that are not too large.

An analogous consideration holds for media with overweighing backward radiation in the microdistribution (e.g., $\bar{n}=\infty$, $\alpha=0.1$, compare Blumer).[5a] Again, Eqs. (21) and (22) trace this case for dilute dispersions. For very dense dispersions the one-flux method would again level out the backward prevalence entirely ($F_\infty=B_\infty=\sum M_k\cdot\frac{1}{2}$), and the more exact two-flux method (yielding the $P_{k\infty}(0)$ curve in Fig. 9 this time above $\alpha=0$) would maintain the original micro a.d.f. type to a certain extent.

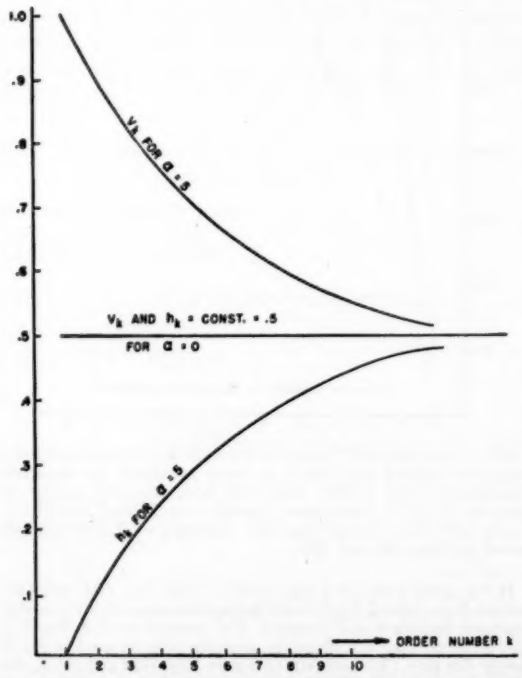

FIG. 8. $v_k=2\pi\int_0^{\pi/2} fk(\Theta)\sin\Theta d\Theta$ and $h_k=2\pi\int_{\pi/2}^{\pi} fk(\Theta)\sin\Theta d\Theta$ for the sequence k of angular distribution functions $\alpha=5$ shown in Fig. 6.

‡‡ But is correct for $\alpha=0$.

However, this tendency toward all-around uniformity in dense dispersions cannot explain the properties of a dense cloud that may scatter a considerable intensity backward but passes only a small intensity into the forward half-space. Here the transformation of light into other forms of energy must be considered by an absorption index μ in the exponentials of M, Q, and P (e.g., $M_0=\exp[-(qn+\mu)x]$, $M_1=qnx\cdot\exp[-(qn+\mu)x]$ etc.). In this case the one-flux method does not even describe the facts qualitatively. $F_\infty(d)=B_\infty(d)=\sum M_k(d)\cdot\frac{1}{2}$ would decrease equally with increasing absorption μ, thus lowering the backward intensity together with the forward intensity. In the two-flux method, however, the $P_{k\infty}(0)$, caused by the $M_0(0)$ term, remain uninfluenced by μ, but still depend on $\bar{n}$ and α as discussed in connection with Fig. 9. Thus the backward scattered light is still capable of changing for different media. The $Q_{k\infty}(d)$, however, containing $\exp[-(qn+\mu)d]$, decrease exponentially with μ, thus lowering the forward intensity. Thus the scattering into both half-spaces, forward and backward, corresponds to the behavior expected for an absorbing cloud. The final angular distribution is no longer traced by the present method, after the Q_k are removed from the play of light flux.[16]

F. TRANSITION FROM AN INFINITE HAZY LAYER TO A LIMITED CUT OUT VOLUME

Thus far, all relations for the quantity functions in Sections C and E were derived for a medium forming an infinite layer in the yz plane of a thickness d (Fig. 2a). The quantity functions M_k' remain to be checked for a limited piece of that layer of the dimension R (Fig. 2b).

With unchanged

$$M_0'(x)=M_0(x) \tag{44}$$

from Eq. (7), Eq. (12) now becomes:

$$(1/qn)(dM_1'(x)/dx)+M_1'(x)(1+\gamma_1) = M_0(x)=e^{-qnx} \tag{45}$$

yielding

$$M_1'=\frac{e^{qn\gamma_1 x}-1}{\gamma_1}\cdot e^{-qn(1+\gamma_1)x}, \tag{46}$$

where

$$\gamma_k=\Omega\cdot f_k(90°)\cdot e^{-qnR} \tag{47}$$

accounts for the loss of light L in Fig. 2b through the cuts in the kth order in an approximated geometry. If, for example, a cube were cut out, $R=d/2$ results for an average scattering particle assumed to be in the center 0 of the cube. The loss of energy all around in the equator 90° is obtained by multiplying $f_k(90°)$ which refers to 1

[16] Compare J. W. Ryde, Proc. Roy. Soc. London **131**, 451 (1931), likewise without angular distribution.

TABLE II. Weight of barely photographable clouds of dielectric particles for different particle sizes. Total sun radiation: 1.35×10^6 ergs/sec. cm², filter at $\lambda=0.63\mu$, transmission $s=0.11$, refractive index $n=1.25$, angle $\theta=90°$, dimension of cloud $d=1000$ cm, $p=\pi/4\times(D/f)^2f=0.42\times10^{-3}$ = photographic factor.

				$f_1(a,\theta=90°)=\frac{q_{90}}{2\pi\int_0^\pi q_\theta \sin\theta d\theta}$	Minimum data required for photographability (0.2 erg/cm² assumed) 90° away from the incident sunlight flux							
$a=2\pi a/\lambda$	Particle radius a (μ)	Scattering coefficient K	Scattering cross section $q=Ka^2\pi$ (cm²)	coefficient taken from Blumer's graphs	Required density qnd	Percentage of Secondary Contribution %	Tertiary %	Number of particles per cm³ $n=qnd/q\cdot d$	Number of particles in d^3 cloud element $N=n\cdot d^3$	Weight of particles in d^3 cloud element (spec. wt. =1) G (kg)	Total weight of 30,000 meter vapor trail, 10 meter width, =3000 elementary cubes G (kg)
0.1	0.010	6.0×10^{-6}	2.1×10^{-17}	0.060	0.058	small		2.76×10^{12}	2.76×10^{21}	11.7	35 100
0.6	0.060	8.3×10^{-3}	1.0×10^{-13}	0.059	0.058			5.80×10^{7}	5.80×10^{16}	0.058	174
1.2	0.120	0.14	0.63×10^{-10}	0.045	0.071	5.6		1.12×10^{6}	1.12×10^{15}	0.0070	21.0
2	0.200	0.5	6.3×10^{-10}	0.027	0.12	12.5		1.90×10^{5}	1.90×10^{14}	0.0075	22.5
5	0.500	2.8	2.2×10^{-8}	0.0088	0.27	76	10	1.23×10^{4}	1.23×10^{13}	0.0070	21.0
8	0.800	3.7	7.4×10^{-8}	0.0069	0.39	67	15	5.25×10^{3}	5.25×10^{12}	0.0112	34.0
	(5.000)	(1)	(7.85×10^{-7})	$\left(\frac{1}{4\pi}=0.0795\right)$	(0.0425)	small		(54)	(54 $\times10^{9}$)	(0.028)	(84)
	(20.000)	(1)	(1.25×10^{-5})	$\left(\frac{1}{4\pi}=0.0795\right)$	(0.0425)			(3.4)	(3.4 $\times10^{9}$)	(0.116)	(348)

sterad., by the solid angle $\Omega=4\pi-2\omega_0$ sterad., where ω_0 is the solid angle describing the square-shaped front or rear side of the cubic cloud, which encloses, at the center, the average particle. Since $\omega_0=2\pi(1-0.707)4/\pi=2.34$ sterad., $\Omega=4\pi-4.68=7.87$ sterad. Both, Ω and e^{-qnR} increase the more the cut-out volume approaches a narrow tube. For the latter and Rayleigh scattering one finds: $\gamma_{\max}=\text{const.}=4\pi\cdot1/4\pi\cdot1=1$. But this is too great a departure from the initial assumption of an infinite layer. For a cube $R=d/2$ and Rayleigh scattering, we find:

$$\gamma_1=7.87\cdot0.0595\cdot e^{-(qnd)/2}=0.466\cdot e^{-(qnd)/2}$$

in the first order and (47a)

$$\gamma_k=7.87\cdot0.0795\cdot e^{-(qnd)/2}=0.626\cdot e^{-(qnd)/2}$$

for practically all higher orders. γ then depends on qnd only, ranging from 0.466 for $qnd=0$ to, e.g., 0.019 for $qnd=7$.

It is easy to see from Eq. (46) that for

$$\lim\gamma\to0,\quad M_1'\to M_1=qnx\cdot e^{-qnz} \tag{48}$$

(compare Eq. 14) as it must be. For the second-order M_2' one finds from an equation set up corresponding to Eq. (45) that

$$M_2'=\frac{e^{qn\gamma_2 z}-1-qn\gamma_2 x}{\gamma_2^2}\cdot e^{-qn(1+\gamma_2)x} \tag{49}$$

which, for $\lim\gamma_2\to0$, likewise turns back to

$$M_2=[(qnx)^2/2!]e^{-qnz}$$

(compare Eq. (25)). The same is true for

$$M_3'=\frac{1}{\gamma_3^3}\left(e^{qn\gamma_3 z}-1-qn\gamma_3 x-\frac{(qn\gamma_3 x)^2}{2}\right)\cdot e^{-qn(1+\gamma_3)x}. \tag{50}$$

From Eqs. (46), (49), and (50) the following approximative recursion formulas may be derived:

$$\begin{aligned} M_1'&\sim\frac{1}{\gamma_1}(M_0'-M_0e^{-qn\gamma_1 z})=M_0\frac{1-e^{-qn\gamma_1 z}}{\gamma_1}\\ M_2'&\sim\frac{1}{\gamma_2}(M_1'-M_1e^{-qn\gamma_2 x})\\ M_3'&\sim\frac{1}{\gamma_3}(M_2'-M_2\cdot e^{-qn\gamma_3 x}) \end{aligned} \tag{51}$$

and so on, which for $\gamma_k=\text{const.}=\gamma$ as in Rayleigh scattering (compare $f_k(90°)$ in Fig. 7) become exact. The M_k denote always the functions of Eq. (28) or Fig. 3. Equation (51) furnishes for small γ:

$$\begin{aligned} M_1'(d)&\sim M_1(d)\left(1-\frac{qnd\gamma_1}{2}+\frac{(qnd\gamma_1)^2}{6}-+\cdots\right)\\ M_2'(d)&\sim M_2(d)\left(1-\frac{2qnd\gamma_2}{3}+\frac{(qnd\gamma_2)^2}{4}-\cdots\right)\\ M_3'(d)&\sim M_3(d)\left(1-\frac{3qnd\gamma_3}{4}+\frac{3(qnd\gamma_3)^2}{10}-\cdots\right) \end{aligned} \tag{52}$$

and so on. For $\gamma\to0$ every M_k' necessarily turns back to the former M_k. Considering that the first negative term in Eq. (52) increases as $\frac{1}{2}$, $\frac{2}{3}$, $\frac{3}{4}\cdots$, and that for Mie a.d.f. γ_k increases with k because of $f_k(90°)$, it follows that every higher order M_k' becomes smaller compared with the coordinated M_k from Eq. (28). Considering Eq. (47a) the losses through the cuts as shown by the second and third terms in the parentheses of Eq. (52)

have the general form for $R=d/t$($R=d/2$ for a cube):

1. order: $c_1 \cdot M_1(qnd/t) - c_1' M_1^2(qnd/t)$
2. order: $c_2 \cdot M_1(qnd/t) - c_2' M_1^2(qnd/t)$

and so on, with increasing c_k and c_k' for kth order. Since $M_1(x)$ reaches its maximum for $x=1$ (comp. Eq. (14) and Fig. 3), the losses for all orders are maximum for $qnd=t$($qnd=2$ for a cube). This is shown in Table III. The maximum loss through the cut occurs for $qnd=t=2$ in all orders. The first order loss 0.153 for $qnd=2$ means that 15.3 percent of M_1 emerges laterally into the surroundings of the equatorial circumference about 90°, namely into 7.87 sterad. as mentioned above, yielding $15.3/7.87=2$ percent of M_1 per sterad. On the other hand, M_1 radiates into 90° (Rayleigh): $0.0595 M_1=6$ percent per sterad. For the surroundings of 90° the emerging light therefore constitutes a larger percent increase (2:6=33 percent) then the loss for the total all-around M_1 which is only 15.3 percent.

Hence, the cut-off volume actually turns out of a modified angular distribution, modified with respect to Section D in the sense that the equatorial surroundings increase at the expense of the all around intensity.

Table III shows that for a volume of nearly equal dimensions (for example, cube) the modification by

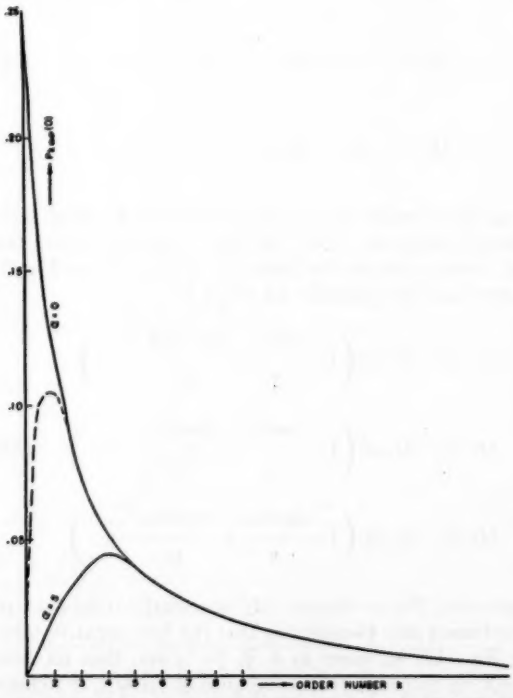

FIG. 9. Light scattered into the backward half-space $P_{k\pi}(0)$ in various orders k for very dense dispersions. Curve parameter=α. Areas show how total backward radiation decreases for narrower Mie dispersions ($\alpha>0$) starting from maximum amount=$\frac{1}{2}$ for Rayleigh dispersion ($\alpha=0$).

$\gamma \gtrless 0$ is small if the density is enough below $qnd=2$. The medium can then be treated as an infinite layer.

G. APPLICATION—PHOTOGRAPHABILITY OF A VAPOR TRAIL

It was shown in Section E that the quantity functions from Eq. (28) suffice to describe the macrodistribution of light around a scattering medium and in Section F that a limited volume ($\gamma \gtrless 0$) may be replaced by an infinite layer ($\gamma=0$) for dilute dispersions.

Both simplifications are used in the following example, which deals with the 90° scattered light from a dilute suspension of dielectric smoke or fog particles ($\bar{n}=1.25$ assumed) irradiated by the sun. A knowledge of the weight of material for a vapor trail is required for various particle sizes on the assumption that the trail is barely photographable from a certain distance.[17] If the trail is considered as composed of a large number of elementary cubes, the "cut-off" light from Section F will add to the 90° light calculated herein, thus forming a security factor.

The following data were assumed: I_0=incident sunlight flux=1.35×10^{-6} erg/cm² sec., d=dimension of the cubic cloud element=1000 cm. This dimension was assumed to insure sufficient resolution on a photographic film. If the cloud element of the vapor trail is photographed at a distance of 6×10^4 meters by a 24-in. focal length lens, an image of 0.102 mm on a side is formed on the film. This image will be resolvable by the photographic system. p=photographic exposure factor using a $D=f/5$ objective and an exposure time of $t=1/75$ sec.

$$p=\pi/4(D/f)^2 \cdot t=0.42 \cdot 10^{-3} \text{ sec.}$$

In order to improve contrast against the sky a red filter is desirable. The transmission band centered about 0.63μ might have a transmission of $s=0.11$ of the radiation of the sun.

$E_{90°}$ (erg/cm²) denotes the energy reaching the photographic emulsion. Spectral sensitometric work[18] showed that for blackening a panchromatic emulsion at 0.63 micron by $\sigma=\log_{10} 1/T=0.5$ over the film fog (T is transmission of the exposed film) $E=0.2$ erg/cm² is required. Hence $E_{90°}=I_0 \cdot s \cdot p \cdot S_{90}=0.2$; $I_0 \cdot s \cdot p=61.8$

$$S_{90}=0.00324. \tag{53}$$

The problem is to determine from Eq. (32) for what density qnd for each chosen α Eq. (53) is fulfilled. Taking the first-order

$$S_{90}=qnd \cdot e^{-qnd} \cdot f_{1(90°)}=0.00324$$

and inserting $f_{1(90°)}$, taken from Blumer's graphs for the various α as listed in Table II we find for $\alpha=0.1$, with

[17] For the general problem, compare Evans Signal Laboratory Technical Memorandum No. M 1195, entitled "Structure of the wind," (Signal Corps), May 9, 1949.

[18] Theissing and Goebert, Zeits. tech. Physik 23, 139 (1942); Zeits. f. angew. Phot. 5, 11 (1942).

$f_{1(90°)}=0.060$

$$M_1=qnd\cdot e^{-qnd}=(0.00324/0.060)=0.0547.$$

Figure 3 shows that this value corresponds to such a small $qnd=0.058$ that the secondary scattering is negligible.

About the same results apply for $\alpha=0.6$.

For $\alpha=1.2$ the second order begins to contribute. With $f_{1(90°)}=0.045$ from Table II and $f_{2(90°)}=0.071$ from Fig. 7:

$$0.045qnd\cdot e^{-qnd}+0.071[(qnd)^2/2]e^{-qnd}=0.00324$$

yields $qnd=0.071$, giving for the ratio of secondary:primary scattering

$$M_2f_2(90):M_1f_1(90)=\sim 5.6 \text{ percent.}$$

Similarly

$\alpha=2$ yields $qnd=0.12$ with 12.5 percent secondary:primary contribution.

$\alpha=5$ yields $qnd=0.27$ with 76 percent secondary:primary and 10 percent tertiary:primary contribution.

$\alpha=8$ yields $qnd=0.39$ with 67 percent secondary:primary and 15 percent tertiary:primary contribution.

From the calculated qnd for each α, from the known dimension d of the cloud and from $q=Ka^2\pi$, all listed in Table II, the number of particles n per ccm can be obtained. From this the weight per cloud element and the total weight of a 30,000 meter vapor trail was obtained assuming a specific weight = unity.

Table II shows a considerably increasing efficiency (light per weight) with increasing α at the transition from Rayleigh to Mie range. The efficiency then remains relatively unaltered for a large α range. So the question arises what will happen with very large particles of for instance $2a=40\mu$ diameter ($q=a^2\pi=1.25\times10^{-5}$ cm) and $\lambda=0.63\mu$ as before. Assuming, for a rough estimation, a spherical a.d.f.—the theory not covering this range—we find $f_{1(90°)}=1/(4\pi)$ and $I_0\cdot s\cdot p\cdot qnd\cdot\exp(-qnd)1/(4\pi)=0.2$ erg/cm² and $qnd=0.0425$. This yields with $q=1.25\times10^{-5}$ cm² and $d=1000$ cm $n=3.4$ particles per ccm. This number is in agreement with the order of magnitude 1 to 10 particles per ccm as listed in the progress report of the University of Michigan (reference 12, p. 19) and confirms the photographability of such clouds even when considering the small photographic factor p and filter factor s as used herein. Of course such particles do not yield optimum efficiency as may be seen from Table II where these values for large particles are attached in parentheses. Thus, calculation shows an increase of required vapor trail weight for both very small and very large particles. For the Rayleigh range the efficiency with respect to weight becomes very poor because of the enormous decrease in the actual scattering cross section. In the case of very large droplets beyond the Mie range, however, the weight embodied within large spheres increases faster than the scattering cross section. Thus, an optimal diameter of about 0.2 to 1.0μ for $\bar{n}=1.25$ dielectric particles gives highest efficiency in the 90° direction with respect to weight for 0.63μ light wave-length.

TABLE III. Lateral losses (L in Fig. 2b) of Rayleigh scattered light by cutting a cubic volume $R=d/2$ out of the infinite hazy layer.

qnd	1. order	2. order	3. order
0.1	0.0219	0.0389	0.0436
0.5	0.0859	0.148	0.165
2.0	0.153	0.254	0.281
7.0	0.0507	0.084	0.0945

ACKNOWLEDGMENT

The author wishes to thank H. J. Merrill for his continuous interest in the present work, C. M. Sliepcevich and R. O. Gumprecht of the University of Michigan for discussions on their scattering experiments with dense dispersions, and Lt. Colonel W. E. Lotz for his encouragement in writing this paper.

Optical Refraction and Fermat's Principle at a Point*

RICHARD SCHLEGEL
Department of Physics, Michigan State College, East Lansing, Michigan
(Received February 3, 1950)

The law of refraction of light rays is derived from Fermat's principle by means of the Weierstrass-Erdmann corner condition of the calculus of variations. In such a derivation the optical path need only be considered at the point of refraction, and the refraction principle follows from a differential equation rather than from an integral equation or geometric construction for a finite length of path. Likewise, the corner condition taken with Fermat's principle is a differential equation which requires that an optical path be straight at all points where the velocity is unchanged.

THE derivation of Snell's law from Fermat's principle is usually made by determining the stationary value of an expression for the time of traversal of a light ray over a path, and then showing that the condition that the actual path give the stationary value is equivalent to Snell's Law. In this paper we wish to show that Fermat's principle and a theorem of the calculus of variations, known as the Weierstrass-Erdmann corner condition, require the optical laws of refraction, without consideration of any region of the optical path beyond that of a single point; by the same considerations, an optical path is a straight line at points where the light velocity is unchanged.

The Weierstrass-Erdmann corner condition[1] gives a condition which must be met by a minimizing or maximizing function on an arc at a corner of the arc. By a "corner" is meant a point at which the first derivative of the arc does not exist, although the arc itself is continuous at the corner. Thus, a sharp turn, as at a point of refraction or reflection of an otherwise straight light ray, constitutes a corner. Suppose a function $f(x, y, y')$, where y' is dy/dx, is to have a maximum or minimum value on the arc. The Weierstrass-Erdmann condition then demands that at a corner of the arc,

$$\partial f^+/\partial y' = \partial f^-/\partial y', \tag{1}$$

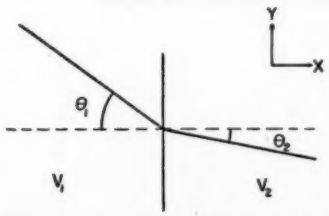

FIG. 1. The vertical line indicates the interface between two media; the solid lines extending to the left and right represent light rays in the two media of light velocities v_1 and v_2, respectively.

where the plus and minus signs indicate the left- and right-hand derivatives at the corner point.†

For a light ray, Fermat's principle states that the optical path length divided by the light velocity takes an extremal value. The function $f(x, y, y')$, for a light ray, is therefore $(1+y'^2)^{\frac{1}{2}}/v$, where v is the light velocity and $(1+y'^2)^{\frac{1}{2}}$ the usual calculus element for length; the integral $\int f \cdot dx$ over the path length would be the total time for passage.

Suppose light to have different velocities v_1 and v_2 in two different media (Fig. 1) such that refraction occurs at the interface between the media. At the point of refraction we apply the corner condition (1), and find

$$y_1'/v_1(1+y_1'^2)^{\frac{1}{2}} = y_2'/v_2(1+y_2'^2)^{\frac{1}{2}}, \tag{2}$$

where y_1' and y_2' are y' in the media 1 and 2, respectively. Since y' is $\tan\theta$, Eq. (2) is equivalent to

$$\tan\theta_1/v_1(1+\tan^2\theta_1)^{\frac{1}{2}} = \tan\theta_2/v_2(1+\tan^2\theta_2)^{\frac{1}{2}},$$

or, using $1+\tan^2\theta = \sec^2\theta$,

$$\sin\theta_1/\sin\theta_2 = v_1/v_2,$$

which is Snell's Law.

The corner condition also requires that the incident and refracted rays lie in a plane. In three dimensions, such that f is a function of (x, y, z, y', z'), the equations of the condition are:

$$\partial f^+/\partial y' = \partial f^-/\partial y' \tag{3}$$

and

$$\partial f^+/\partial z' = \partial f^-/\partial z'. \tag{3}$$

For the case of refraction the function to be given an extremal value is now $f=(1+y'^2+z'^2)^{\frac{1}{2}}/v$. From (3) we

† The Weierstrass-Erdmann corner condition is derived as an immediate consequence of the Euler-Lagrange condition for an extremal between two points x_1 and x_2. The equation of that condition is:

$$\partial f/\partial y' = \int_{x_1}^{x} (\partial f/\partial y)dx + C.$$

The corner condition follows because the integral, $\int_{x_1}^{x} (\partial f/\partial y)dx$, is continuous at a corner, even though $\partial f/\partial y$ is not continuous, provided that $\partial f/\partial y$ is bounded across the corner—i.e., provided that $\partial f/\partial y$ does not go to infinity. Subject to this restriction, the condition could be applied at any corner in an optical path.

* Presented in part at the Buffalo Meeting of the Optical Society of America, October, 1949.

[1] G. A. Bliss, *Lectures on the Calculus of Variations* (University of Chicago Press, Chicago, 1946), p. 12; G. A. Bliss, *Calculus of Variations* (Open Court Publishing Company, LaSalle, Illinois, 1925), p. 143.

then have,

$$y_1'/v_1(1+y_1'^2+z_1'^2)^{\frac{1}{2}}=y_2'/v_2(1+y_2'^2+z_2'^2)^{\frac{1}{2}}, \quad (4a)$$

and

$$z_1'/v_1(1+y_1'^2+z_1'^2)^{\frac{1}{2}}=z_2'/v_2(1+y_2'^2+z_2'^2)^{\frac{1}{2}}, \quad (4b)$$

where subscripts 1 and 2, as before, refer to the media with light velocities v_1 and v_2. Division of (4b) by (4a) gives

$$z_1'/y_1'=z_2'/y_2',$$

or

$$(dz_1/dx_1)/(dy_1/dx_1)=(dz_2/dx_2)/(dy_2/dx_2).$$

Elimination of the differentials dx_1 and dx_2 gives

$$dz_1/dy_1=dz_2/dy_2. \quad (5)$$

Referring to Fig. 2, in which the Y–Z plane is the interface between the two media (or is a plane tangent to the interface at the point of refraction) we see that (5) is equivalent to

$$\tan\phi_1=\tan\phi_2,$$

where ϕ is the angle between the Y axis and the normal projection of the ray on the Y-Z plane. The condition that both incident and refracted rays lie in the same plane is just that ϕ_1 and ϕ_2 be equal angles.

If $v_1=v_2$, Eq. (2) becomes a stipulation that the arc be a straight line at the point in question. In this manner the corner condition requires that the optical path be a straight line through points where the velocity is unchanged.

The law of regular optical reflection follows from the requirement that a straight line is the stationary time path between two points, in a medium of constant velocity. For reflection, however, a further physical condition must be stated, in addition to Fermat's principle, in order to take account of the change of direction at the reflecting surface. That is, Fermat's principle alone does not distinguish between a reflected ray and a continuation of the incident ray beyond the reflection point, or *vice versa*. Customarily, the straight line path in reflection is taken to be the reflected ray extended back to a virtual source which is itself a reflection of the actual source across the plane tangent to the reflecting surface at the point where the incident ray strikes the surface. The corner condition would then require that the path be straight at the reflection point, as at any other point, because of the constant velocity. The equality of incidence and reflection angles then follows as in the usual derivations.

The use of Fermat's principle in optics has sometimes been cited as an example of teleology in natural processes; the argument is that all parts of the light path must in some manner affect the light during its process of traversal, the influences being such as to insure that the actual path will give an extremal value for the time of passage. It is interesting to note that the derivation of the law of refraction from the Weierstrass-Erdmann condition is, however, a counter example to that argument, for in this derivation a condition at a single point on the path suffices to describe the refraction, without reference to any finite extent of path length. Likewise for unchanged velocity the corner condition requires a straight line optical path (assuming Euclidian geometry) at any point, without consideration of other points. These results show an equivalence of differential equations—i.e., the corner condition—and integral equations in two of the fundamental laws of optics. A comment on the role of equivalences between differential and integral equations and the problem of purpose in nature has recently been given by H. Margenau.[2]

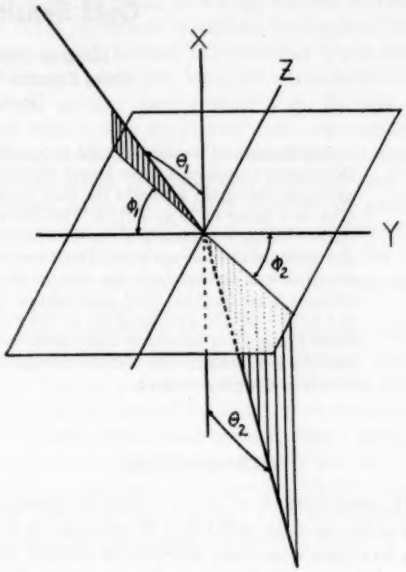

FIG. 2. The medium of light velocity v_1 is above the $Y-Z$ plane; that of velocity v_2 is below it. The lines making angles θ_1 and θ_2 with the X axis represent the light rays in the two media, and ϕ_1 and ϕ_2 are the angles in the $Y-Z$ plane between the Y axis and the normal projections of the light rays on the plane.

The topic of this paper was first suggested to me in lectures on the calculus of variations given by Professor S. B. Myers of the University of Michigan, and I wish to express my gratitude to Professor Myers for his guidance on several aspects of the paper.

[2] H. Margenau, American Scientist **38**, 141 (1950).

Gold Sensitization of X-Ray Films*

HERMAN HOERLIN AND F. W. H. MUELLER
Ansco Research Laboratories, Binghamton, New York
(Received February 20, 1950)

Sensitization of non-screen type x-ray emulsions with aqueous solutions of ammonium or alkali aurous thiocyanates leads to a wave-length dependent increase of their x-ray and gamma-ray sensitivities. For a particular fine-grain emulsion the gain in photographic speed is shown to increase from a factor of 1.5 at 1.3A to a factor of 10 at 0.011A. This wave-length dependence of the sensitizing effect is governed by the range—energy relationship of electrons, by the shape of the energy loss curve of electrons, and the threshold sensitivity of the average grain. The sensitivity of the average grain in an unsensitized and a gold-sensitized emulsion was derived from the number of quanta required to produce the same photographic effects at different wave-lengths. Gold sensitization caused an increase in threshold sensitivity from $(6\ \text{kev})^{-1}$ to $(1.2\ \text{kev})^{-1}$ for the average grain of the emulsion under investigation. A comparison of the quantities of latent image silver formed by light exposure on one hand, and by electrons on the other, indicates that gold sensitization increases the effective radius of action of the sensitivity centers and also the number of active centers at the grain surface.

INTRODUCTION

THE sensitization of silver halide in photographic emulsions with solutions of complex gold compounds has been described recently in several publications and patent disclosures.[1] It was learned that a pronounced increase in photographic sensitivity to visible and ultraviolet radiation can be obtained by the addition of aqueous solutions of ammonium or alkali aurous thiocyanates to silver halide emulsions either during the second digestion, or shortly before coating. Gold salt solutions are also effective in hypersensitization or latensification treatments of many photographic films which have not received prior gold treatment during the manufacturing process. Most of the published data were related to the effect on light sensitivity.

Little is generally known about sensitizing processes for x-ray emulsions; the reviewer of photographic literature will gain the impression that the sensitivity to x-rays is hardly affected by chemical sensitization. Successful activation experiments were, however, carried out by Mueller,[2] using very small quantities of heavy metal compounds, in particular those of lead and thallium. The sensitizing effect by means of lead salts is particularly interesting; in this case a decrease of the light sensitivity takes place concurrent with the increase in x-ray response. The mechanism of both effects is at present the object of renewed investigations.

More recently Mueller observed in the course of bathing treatments with gold salt solutions a positive effect on the response of a non-screen type x-ray emulsion to 65-kv radiation, in addition to increased light sensitivity. In general, photographic manufacturers are holding the light sensitivity of non-screen x-ray products on the low side in order to facilitate processing in bright red light. It was, however, noticed by Hoerlin that of two basically similar x-ray emulsions, the one having higher light sensitivity frequently also shows a better response to high energy x-ray and gamma-ray radiation. Following this lead the authors conducted an investigation of the sensitizing effect of gold salts for exposures to x-rays and gamma-rays in the 1.3A to 0.01A range. In recent years these studies have led to a substantial improvement of the speed of certain non-screen type x-ray films, which is particularly noticeable in exposures to high energy x-rays and gamma-rays.

PROCEDURE

Two experimental fine-grain silver bromo-iodide emulsions were prepared under identical conditions except that one emulsion was gold-sensitized by addition of ammonium aurous thiocyanate solution during the second digestion.† Each emulsion was coated to a thickness of 20 microns on both sides of a 200-micron cellulose acetate base. The silver bromide concentration was 56 percent by weight; the average grain size of the roughly spherical grains 0.4 micron.

Both films were exposed to seven strongly filtered bands of x-rays and gamma-rays yielding effective wavelengths in the range between 1.3A and 0.011A. The films were developed for 4 minutes in Ansco Liquadol x-ray developer, their characteristic curves plotted, and for each wave-length band the relative speeds of the untreated and gold-treated films were determined at the density level of 1.5 above fog.

Furthermore, the incident energy, the number of quanta absorbed in the film, and the truly absorbed energy (i.e., the kinetic energy of electrons spent in the formation of the latent image to yield a photographic density of 1.5 above fog) were measured and calculated. The techniques employed in the course of our work were similar to those described in greater detail

* Presented at the New York Meeting of the Optical Society of America, March, 1950.

[1] For review, see F. W. H. Mueller, J. Opt. Soc. Am. 39, 494 (1949).

[2] R. Koslowsky and F. W. H. Mueller, Agfa Film Plant, Wolfen, Germany (1936). Bibliography of Scientific and Industrial Reports (U. S. Department of Commerce, Washington), Vol. 8, p. 873, PB 70053, fr. 831–50.

† The quantities added are so small that the increase in x-ray mass absorption can be neglected.

by Hoerlin.[3] Evaluation of the experiments led to the determination of the threshold sensitivity of the gold-sensitized and unsensitized average grain of our particular emulsion for exposures to electrons and to visible light. Subsequently the bearing of these investigations on the possible mechanism of the gold sensitization was examined.

WAVE-LENGTH DEPENDENCE OF SPEED INCREASE

The relative speed values for gold-treated and unsensitized emulsions are plotted in Fig. 1 for three emulsion series as a function of the effective wave-length. Their averages are shown in Table I which also contains a closer identification of the radiation employed.

It is evident that the gold sensitization results in considerably higher speeds throughout the spectrum. The effect is, however, wave-length dependent; whereas the speed gain is rather moderate for exposures to the softer x-rays, it increases from a factor of about 1.5 at 1.3A to a fivefold sensitizing effect at 1.07A and a factor of 10 for gamma-radiation. The increase for light exposures is also quite strong and was found to be eleven-fold for the average of the three emulsions.

The wave length dependence of the effect is remarkable. In order to understand the cause of it one must recall that the photographic action of x-rays is due to the dissipation of the energy of their photo- or recoil electrons in the silver halide. The energy loss of electrons per unit path length increases with decreasing kinetic energy. Therefore, grains exposed by short range electrons or at the end of a longer track receive large amounts of energy. Even if their sensitivity is low the energy transmitted is usually sufficient to induce developability. Hence, sensitization for soft radiation, ejecting only short range electrons, is hardly needed and the gold sensitizing effects are barely evident. With decreasing wave-length both the energy and especially the range of the photo-electrons increase and increasing numbers of grains are hit by a single photo-electron. The energy transmitted to a grain by a very energetic electron is relatively small throughout the greater portion of its path, and increases sharply only toward the end of its track. Evidently the gold sensitization has raised the threshold of developability sufficiently to permit effective exposure for a large number of grains in that part of the electron path where the energy dissipation is small. These observations deserve the following quantitative investigation.

QUANTUM EFFICIENCY AND THRESHOLD SENSITIVITY

There are two ways to gain knowledge of the number of grains which are made developable by photo-electrons of different energies. One method consists of the application of techniques used in nuclear track work, i.e., to count the grains in a large number of individual tracks. This procedure would be inadequate for x-ray emulsions which deviate from nuclear track emulsions by their larger grain size, lower silver concentration, and somewhat greater background fog. In the second method which was employed here, one obtains for several wave-lengths the number of quanta needed to produce a given photographic density, and derives from these data the relative number of successfully exposed grains. The absolute numbers are then obtained by quantitative determination of the number of grains made developable per absorbed quantum for one properly chosen wave-length only.

The values obtained by this procedure, which also has been described previously in greater detail,[3] are shown in Table I and plotted in Fig. 2. The number of grains which are needed to build up an optical density of 1.5 has been determined by analyzing a series of thin coatings and was found to be slightly less than 30×10^7 per cm² for exposure to 1.3A photons. On the other hand, 27×10^7 quanta of wave-length 1.3A must be absorbed to produce the same optical density; hence it happens

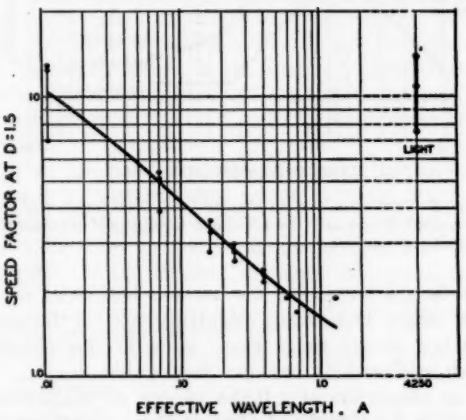

FIG. 1. Response of gold-sensitized emulsion relative to unsensitized emulsion as function of wave-length.

that approximately 1 grain becomes effectively exposed per 1.3A photon. We may interpret these data now as follows:

In the gold-sensitized emulsion 27×10^7 quanta of 1.3A produce the same photographic effect as 2×10^7 quanta of 0.07A. Since, as we have just seen, one 1.3A photon makes 1 grain developable, the average photo-electron ejected by the 0.07A photon will expose effectively close to 14 grains. We may wish now to determine the energy loss of the photo-electron in the fourteenth grain from the end of its path. But, for reasons which will become evident later, these fourteen grains will not appear as an uninterrupted chain of developed particles and the sensitivity of the fourteenth grain, though significant in several respects, would not be representative of the threshold sensitivity of the

[3] H. Hoerlin, J. Opt. Soc. Am. 39, 891 (1949).

average grain. The latter value can be obtained, however, by a different approach.

If one calculates for each wave-length the range of the average electron in the emulsion, expresses it as the number of grains hit and multiplies this figure by the total number of quanta absorbed, one arrives at the total number of grains hit in the emulsion layer. These values are plotted for both emulsions in the lower part of Fig. 2. While their shapes are roughly similar one will notice that a significant inflection exists at 0.35A in the curve for the gold-sensitized emulsion. The long

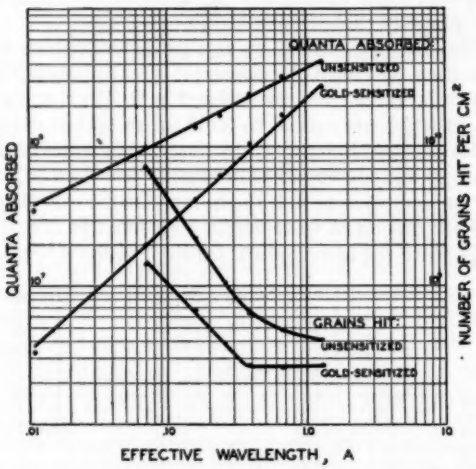

FIG. 2. Number of quanta absorbed and total number of grains hit per cm² to produce $D=1.5$ above fog for gold-sensitized and unsensitized emulsion.

wave-length portion of the curve is horizontal over a wide range. This means essentially that in the corresponding energy range every grain in this emulsion which receives a hit becomes developable.

The absorption of a 0.35A photon occurs predominantly in the K-shells of silver and bromine; the resulting photo-electrons have energies of 10 kev and 21 kev respectively; they will hit and amply expose from one to three grains. An appreciable portion, approximately 20 percent, of the primary radiation is absorbed in the L-shells of the silver and bromine atoms, and photo-electrons of 31-kev and 33-kev energies covering ranges from 5 to 6 grains are produced. It is quite certain that, on the whole, all these grains become developable. Taking now Bethe's[4] energy loss data for air, and assuming a constant stopping power of 3500 for silver bromide relative to air, one obtains an energy loss of 3 kev/micron or 1.2 kev/grain for the 33-kev electron at the beginning of its path. It is obvious that $(1.2\text{ kev})^{-1}$ is the threshold sensitivity of the average grain of the gold-sensitized emulsion.

In the unsensitized emulsion about $\frac{1}{3}$ of the grains exposed to filtered 10-kev radiation (1.3A) do not respond to development. Because the energies of the corresponding photo-electrons are 6 kev and 8 kev (L-shells of Ag and Br), the threshold sensitivity cannot be very far from the reciprocals of these two values. But such a low sensitivity does not seem to agree with the fact that close to 3 grains are made developable by the 0.07A photon in the unsensitized emulsion: The second and third grain from the end of the path of a 160-kev electron (average energy of photo-electron ejected by 0.07A photon) will receive from 2 to 3 kev, which is considerably less than the value derived from 1.3A exposures. This discrepancy can be reconciled if one considers that the potential range of a 160-kev electron is of the order of 70 grains. It seems conceivable that along this long path, it is not always the grains close to the end of the track which become developable, but rather the most sensitive ones and those which receive the highest amount of energy (long path length within the grain, path also close to the grain surface). The grains which are "picked" for developability in the unsensitized emulsion are therefore less representative of the average grain; one deals here with the exception rather than the rule. On the other hand the requirement of 6 kev to 8 kev indicated by the 1.3A exposure is probably on the high side, because some of the resulting photo-electrons may escape from the grain surface into the gelatin before they have lost all of their kinetic energy. Hence the requirement for developability of the average grain in the unsensitized emulsion can only be estimated and the value of 6 kev has been chosen.

LATENT IMAGE SILVER

Having gained information on the energies involved in the formation of the latent image in individual grains by electrons, we now consider the actual quantities of latent image silver which are produced in the silver halide crystal. We are also including in our considerations corresponding data for light exposures. Although interesting modifications of the Mott and Gurney[5] theory of latent image formation have been proposed recently by Mitchell,[6] we will continue to express the quantities of latent image in units of silver atoms, assuming that ultimately one atom of silver is produced for every absorbed photon of visible and ultraviolet radiation, or for every ion pair formed by a charged particle.

When comparing the effects of light and x-ray exposures one must bear in mind that due to differences in the space and intensity distribution of absorption in the emulsion layer, equal developed densities must not necessarily represent the same group of exposed grains, particularly not in coarse grain emulsions. In the case of our fine grain gold-sensitized emulsion it is however safe to say that the 14 grains which, on the average,

[4] H. A. Bethe, *Handbuch der Physik* **24**, No. 1, 522 (1933).

[5] N. F. Mott and R. W. Gurney, *Electronic Processes in Ionic Crystals* (Oxford University Press, New York, 1940), p. 227.

[6] J. W. Mitchell, Phil. Mag. (a) **40**, 249 (1949); (b) **40**, 667 (1949).

become effectively exposed by each 0.07A photon represent a fair cross section of the available grains. While a certain selection may still occur, preference being given to the more sensitive grains of the group, these conditions are very similar to those which occur with exposures to light particularly if we confine our studies to the medium density levels. Here also, the more sensitive grains reach the state of developability first, and while the size and sensitivity distribution of the affected grains may not be exactly the same in both cases, it should nevertheless be sufficiently similar to permit a fair comparison on an equal density basis. This view is supported by the great similarity between the shapes of the characteristic curves of our emulsions for exposures to light and 250-kv filtered x-rays.

In order to obtain quantitative data on the amount of silver formed in exposures with 0.07A x-rays, one must first calculate the truly absorbed energy, that is, the kinetic energy of the electrons spent in the process of latent image formation to yield our density of 1.5 above fog. This was found to amount to 1.9 ergs/cm² for the gold-sensitized emulsion. Since 7.6 ev are required to produce one ion pair in AgBr, which will lead to the formation of one atom of latent image silver, one arrives at the figure of 16×10^{10} silver atoms per cm².

The quantity of visible radiation of wave-length 4250A which must be absorbed to produce the same photographic effect was determined in a double prism monochromator, exposing the film from both sides. It was found to amount to 6×10^{10} photons per cm², which in turn form the same number of latent image silver atoms. Hence, the ratio of latent image silver formed by x-rays *versus* light is 16/6. Assuming now that the same ratio holds for the average grain, one can calculate the silver atoms required per grain for visible light. Having learned that a threshold exposure of 1.2 kev with x-rays forms $1200/7.6=160$ Ag atoms, it follows that the corresponding value for light exposures will be 160 times $6/16=60$ Ag atoms per average grain. These and the corresponding data for the unsensitized emulsion are shown in Table II. It is an interesting fact that in the unsensitized emulsion, roughly equal quantities of silver are formed by either exposures. The gold-sensitized grain requires not only much smaller total amounts, but there is also a distinct difference between the x-ray and the light exposures. These findings will serve as basis for the following discussion of the mechanism of sensitization by gold treatment.

SENSITIZING MECHANISM

The existence of a surface and an internal latent image has been well established; under ordinary circumstances, only that fraction of the latent image silver which is formed at the grain surface can be effective in inducing developability. Very little is known about the geometrical distribution of the latent image over the surface area. Photo-micrographs of partially developed grains, and electron micrographs of slightly "printed out" grains, point to the likelihood that the formation of the surface latent image occurs at certain discrete places, but one supposes that the sensitivity specks are distributed over the total surface area more or less at random.

If we are now permitted to assume that the same amount of surface latent image is needed to induce developability regardless of the type of exposure, then the differences in the total amounts should be accounted for by different amounts of internal latent

TABLE I. Speed factor of gold sensitization and number of absorbed quanta to produce $D=1.5$ above fog for gold-sensitized and unsensitized emulsions; number of grains hit per average photo-electron.

Tube voltage kv	Filtration	Effective wave-length A	Speed factor: gold-sensitized emulsion / unsensitized emulsion	Quanta absorbed $\times10^{-7}$ per cm² Gold-sensitized emulsion	Quanta absorbed $\times10^{-7}$ per cm² Unsensitized emulsion	Number of grains hit per electron
10	3 mm air 1 mm paper	1.3	1.5	27	41	1
30	2 mm glass 5 mm Bakelite	0.79	1.7	—	—	—
25	3 mm air 2 mm Al	0.67	1.9	17	32	1.5
65	5 mm Al	0.39	2.3	10.5	24	2.6
65	19 mm Al	0.24	2.7	6.2	17	6.3
150	21 mm Al	0.16	3.3	4.2	14	16
250	0.5 mm Pb 4 mm Cu 5 mm Fe	0.07	5	2.0	10	72
Radium gamma-rays	20 mm Pb	0.011	10.5	0.33	3.5	—
Light		4250	11	6000	66000	—

image. Considering that the absorption of visible radiation in a particular grain is nearly uniform throughout its volume and that, in the x-ray case, the dissipation of the energy of the photo-electron occurs along a linear path, we may calculate the one thickness of the photographically active spherical shell for which equal numbers of ionization acts occur for light on one hand and for an electron on the other. Having this thickness the actual number of the ionization acts in the shell can then be calculated. These calculations were carried out for the 0.4 micron gold-sensitized grain with the result that in the case of light, 16 out of a total of 60,‡ and in the case of electrons 16 out of 160 absorption events take place in a surface shell of 0.02 micron thickness. Neglecting for the moment differences in the initial local distribution of conduction electrons as produced by the two kinds of exposures in the shell, it would seem that the surface latent image is formed by the addition of not more than 16 silver atoms to the sensitivity centers. In the developable unsensitized grain the thickness of the shells in which 16 ion pairs are formed by electrons and photons is only a few thousandths of a micron. Even if we consider that in the latter case the sensitivity centers are possibly smaller to begin with and that more silver atoms may be needed to build up their size, it is quite obvious that the gold-sensitized centers are capable of collecting the latent image components (conduction electrons and interstitial silver ions or vacant lattice sites) over a wider radius of action. In order to account for the actual differences in the initial local distribution of conduction electrons we must assume that gold sensitization increases also the number of active sensitivity centers.

The above-described "shell" model is perhaps oversimplified; however, the scheme should be useful since it is in qualitative agreement with a number of observations and effects which will be described briefly.

The photographic action of gamma-rays is due to ionization by recoil electrons. The range of the majority of these electrons (mean energy is of the order of 400 kev) exceeds the emulsion thickness; the number of grains exposed at the end of a track is small in relation to the total receiving hits. Calculation shows that almost all developable grains must have received an average of two hits which produce between 50 and 100 ion pairs each. These in turn will yield 10 to 20 silver atoms in the 0.02-micron surface shell of the sensitized grain, a figure which is in agreement with those for x-rays and light.

The breakdown of the reciprocity law at high intensities of illumination is attributable to the inability of the sensitivity specks to attract and hold at one time more than a few conduction electrons and to the ensuing formation of internal silver. It has been found that the high intensity reciprocity law failure of gold-treated emulsions is greatly decreased; apparently the formation of internal latent image is reduced by the strong field forces of the sensitive surface in the gold-treated emulsion. Greater resistance of gold-treated emulsions to latent image-destroying Herschel-exposures should also be expected and was observed indeed by James, Vanselow, and Quirk.[7] The gold nuclei appear to prevent ejection of photo-electrons by the infra-red radiation or cause their recapture.

Of considerable significance is the observation that the speed increase obtainable with gold sensitization depends on the grain size; the sensitizing effect is the greater the finer the grain. This applies to x-ray as well as to light exposures. Quantitative experiments were carried out with unsensitized and gold-sensitized emulsions having twice the grain size of the emulsions used in our main experiments. Whereas in the fine-grain emulsion (0.4 micron) gold sensitization resulted in speed factors of 11 for light and 5 for 0.07A x-rays, the corresponding factors for the coarser emulsion (0.8 micron) were found to be only 3 for light and 2.5 for 0.07A x-rays. The lower efficiency of gold sensitization in the coarse-grain emulsion is due primarily to the decreased ratio of the surface shell volume to total volume. For light exposures, however, this change in the volume ratios accounts for only one-half the observed change of the speed factor. The other half appears to depend on the ratio of the surface area to the volume of the grains which, in turn, may mean that the gold treatment brings additional surface sensitivity centers into play, besides increasing the effective radius of action of the existing centers. The fact that the change of the speed-factor with grain size differs quantitatively for light and for x-ray exposures can be explained by the different nature of the two absorption mechanisms. Extension of the quantitative studies of the effectiveness of the gold sensitization over a wider range of grain sizes should prove very fruitful.

TABLE II. Truly absorbed energy, threshold sensitivity, and latent image silver data for gold-sensitized and unsensitized emulsion.

	Gold-sensitized emulsion	Unsensitized emulsion
Energy truly absorbed to produce $D=1.5$, 0.07A	1.9 ergs/cm²	9.5 ergs/cm²
Latent image silver atoms/cm², 0.07A	16×10^{10}	80×10^{10}
Latent image silver atoms/cm², 4250A	6×10^{10}	66×10^{10}
Threshold sensitivity, x-rays	$(1.2\text{ kev})^{-1}$	$(6\text{ kev})^{-1}$
Silver atoms per grain, x-rays	160	780
Silver atoms per grain, 4250A	60	660*

* The value of 660 Ag atoms per grain is calculated from the ratio of light sensitivities (sensitized *versus* unsensitized emulsion) taking 60 silver-atoms as the reference value. A value of 640 atoms is obtained if we apply a different procedure and base the calculation for the unsensitized grain on the x-ray threshold sensitivity of $(6\text{ kev})^{-1}$ (780 Ag atoms) which must be multiplied by the ratio of total number of silver atoms/cm² for 4250A to the total number of silver atoms/cm² for 0.07A.

‡ This corresponds to a utilization factor of 0.27. J. H. Webb [J. Opt. Soc. Am. 38, 312 (1948)] determined the utilization factor for the average grain of a positive emulsion through an entirely different approach. It is uncertain whether or not there is significance in the fact that he found, for a different emulsion, a utilization factor of similar magnitude (0.24).

[7] James, Vanselow, and Quirk, PSA Journal 14, 349 (1948).

Further experimentation is also required to fit the gold sensitization effect more closely into present theories of latent image formation.[4,6,8] The questions arise, among others, whether "gold-plated" centers have a greater trap depth than "ordinary" centers and to what extent the number of active centers actually increases. Quantitative investigations on a variety of emulsions together with studies of photo-conductance and ionic conductance on better defined models, that is, on large gold treated silver halide crystals, may throw more light on the exact nature of this interesting sensitizing process.

ACKNOWLEDGMENT

Thanks are due to Dr. Robert Clark for preparing the test emulsion, to Dr. Frank Hamm of the Central Research Laboratory of General Aniline and Film Corporation for grain size determinations and to Mr. Donald Jones for his active help in experimental work

[8] O. Stasiw and J. Teltow, Ann. d. Physik (a) [5] 40, 181 (1941); (b) [6] 1, 261 (1947).

Research and Development in Applied Optics and Optical Glass at the National Bureau of Standards

A Review and Bibliography by IRVINE C. GARDNER AND CLARENCE H. HAHNER. Miscellaneous Publication 194, National Bureau of Standards. Obtainable from Superintendent of Documents, U. S. Government Printing Office, Washington 25, D. C. Price 15 cents.

The National Bureau of Standards has within its own organization facilities to perform all the work required in the development and production of prototype optical instruments. Included are facilities for production of optical glass, for the determination of its optical and chemical properties, for the optical and mechanical design and construction of an optical instrument, and finally the analysis of the instrument performance. Although all of these facilities are available, they are in general utilized only for research work, production of prototype instruments or of optical glass for special purposes being undertaken only when such work, for economic or for other reasons, is not attractive to our domestic manufacturers. Although technological studies of optical instruments and of optical glass date almost from the establishment of the Bureau, such work received a general stimulus and was greatly augmented during World Wars I and II.

To optical glass technology the Bureau has contributed a process for producing the clay melting pots by casting to replace the earlier tedious hand-forming method; a substantial group of publications dealing with the effects of change of chemical composition upon the optical properties of glass; a detailed study of the annealing of glass including measurements of the change in the final index of a melt of glass resulting from a change of annealing temperature and a method for eliminating variations in the index of refraction of large pieces of glass resulting from temperature gradients in the annealing furnace; methods for the chemical analysis of glass; and for measuring the chemical analysis of glass; and for measuring the chemical durability of glass. The first large disk of glass (the 70-in. disk for the observatory of the Ohio Wesleyan University) made in this country for the construction of a large astronomical telescope was made at the National Bureau of Standards. The refractometry work at the Bureau includes measurement of the index of refraction of the Bureau's optical glass for control purposes, the testing and calibration of refractometers, and the determination of the accepted values of the index of refraction for a large number of liquids and crystals. A notable contribution is a most precise determination of the index of refraction of water over a broad range of temperatures and wave-lengths. Work on optical instruments includes the design of an $f/6.3$ airplane camera lens of 50-in. focal length with definition sufficiently good to show individuals on the streets of a city photographed from an altitude of nearly two miles (10,000 ft.), a telephoto lens of 20-ft. focal length for photographing the solar corona, and many smaller optical systems for special purposes. In the field of optical instrument testing, the Bureau has developed precise methods and instruments for testing airplane camera lenses and is responsible for the certification of airplane camera lenses to be used on government mapping contracts. A special testing laboratory has been constructed for the testing of range finders. Facilities are available for testing optical instruments over the temperature range 0 to 100°F and when exposed to radiation simulating that from the sun in the tropics thus enabling different climatic conditions to be reproduced.

Miscellaneous Publication 194 recounts these and other achievements of the National Bureau of Standards during the past 35 years and also contains a Bibliography of 195 Bureau publications dealing with optical glass and optical instruments.

Book Reviews

La Théorie de la Relativité Restreinte

O. COSTA DE BEAUREGARD. Masson and Cie, Paris, 1949. Pp. 173, with a preface of Louis de Broglie. Price, about $3.50.

The book gives an excellent mathematical description of the ideas of special relativity. Starting with a historical introduction of the relativity principle from Newton to Einstein, the author develops the general tensor calculus and the theory of integral invariants based upon the methods developed by E. Cartan for the pseudo Euclidian-Minkowski space. The second chapter deals with the relativistic kinematics of the solid body and a short introduction to the kinematics of fluids. The third chapter deals with the electrodynamics in Minkowski space considering several different tensors which can be connected with such an electromagnetic relativistic field.

The chapter on relativistic dynamics starts with Einstein's equation connecting matter and energy. The dynamics of liquids with or without spin are developed and the deviations of the results from the classical theory for high velocities exemplified. The author announces three general theorems concerning the interaction of two mass points and gives a critical survey of the limitation of the theory developed. This is followed by a study of relativistic thermodynamics. In this chapter the author gives a definition of temperature which is invariant against the Lorentz transformation and formulas for heat conduction. The fifth chapter treats hypotheses of Synge, Lichnerowicz, and Eisenhart which attempt a foundation of a relativistic theory of vortices and gives the generalization of the Jacobi-Hamilton theory in Minkowski space. A short survey of the theory of wave mechanics by de Broglie forms the end of the interesting book and the appended index contains 168 references to important books and papers in special relativity theory.

The book is very beautifully printed, the exposition is lucid and mathematically rigorous. The physical and philosophical assumptions of special relativity theory are clearly enunciated. The preface of de Broglie draws the attention of the reader to the elegance of the mathematical representation and to the similarity of some of the conclusions of the author to the recent work of Schwinger with respect to the quantum theory of electromagnetic fields.

MAX HERZBERGER
Kodak Research Laboratories
Eastman Kodak Company
Rochester, New York

Optics (Volume III of Principles of Physics Series).

FRANCIS W. SEARS. Addison-Wesley Press, Cambridge, 1949. Third edition. Pp. 526. Price $6.00.

The third edition of this text does not differ markedly from the second edition. The principle differences are a splitting of the original fourth chapter on "Lenses and Lens Aberration" into expanded separate chapters on these two subjects, and a slight rearrangement of the order of presentation of these chapters has been made. There is a marked improvement in the typography and most of the figures have been redrawn or shaded so as to improve the appearance and also the ease of comprehension.

The number of problems at the end of chapters has been nearly doubled. As in the earlier editions, the mathematical approach to the subject has been elementary and a facility in calculus is not required for the handling of the course material.

WALLACE R. BRODE
National Bureau of Standards
Washington, D. C.

Infrared Determination of Organic Structures

H. M. RANDALL, R. G. FOWLER, NELSON FUSON, AND J. R. DANGL. D. Van Nostrand Company, Inc., New York, 1949. Pp. 239+v. Price $10.00.

Because it is limited severely in its scope, this book is not the reference book for which infrared workers have long felt a great need. The authors recognize this fact, however, and state in the preface that "no claim is made to a complete treatment of the present status of infrared spectroscopy, even in its application to molecular structure."

For anyone interested in the possibilities of infrared as a tool applicable to the determination of organic structures, this book offers a clear and readable presentation of the methods and techniques employed by the University of Michigan group. Although it will not serve as a manual nor as a textbook covering the subject, it will be useful, together with other publications, to supply general information and many valuable suggestions. It is largely limited as far as the results shown, to aliphatic or phenyl-substituted aliphatic compounds; the examples chosen having been taken from the authors' work in connection with the search for the structure of penicillin.

Following the first chapter which is of general and historical interest is a chapter dealing with the interpretation of infrared spectra in terms of specific structure groups. This chapter is well written and it is unfortunate that it is not more complete. The next two chapters are interesting in that they present, respectively, in tabular form the empirical assignments in the double bond region arranged according to wave-length, and the assignments which have been published in the literature on theoretically analyzed molecules.

Chapter V should serve excellently to show the reader just how an infrared spectrum may be interpreted in terms of the possible structure of the sample.

Chapter VI contains a description of the particular recording spectrographs used at Michigan, together with certain helpful suggestions regarding experimental techniques. Here again the limited scope of the book is noted.

Chapter VII which comprises sixty percent of the book, presents the actual recorder tracings obtained on a Firestone amplifier for 354 samples. These spectra are of considerable value, and it is therefore all the more unfortunate that they are not available in a form more readily usable by the average infrared worker who does not have this type of equipment.

In spite of the somewhat restricted point of view adopted throughout by the authors, this book will be of considerable value to those interested in the application of infrared to structure problems.

R. BOWLING BARNES
Research Laboratory
American Optical Company
Stamford, Connecticut

Letter to the Editor

On the Shape of the Sensitive Cathode Area of Electron Multiplier Photo-Tubes

E. W. PETERSON AND DAN H. HOLLAND*
The Dow Chemical Company, Midland, Michigan
January 30, 1950

IF one is measuring the intensity of a narrow beam of light with an electron multiplier photo-tube such as the RCA 931A, how precisely must he position his light beam to get accurate measurements? This problem has been treated in at least four publications, which show considerable disagreement. Hasler *et al.*[1] gave no data, but stated that the sensitive area appeared to be, "a broad plateau which usually extends one-eighth of an inch." Dieke[2] shows sensitivity curves which are very non-uniform and with a half-width of about 4 mm. Marshall *et al.*[3] mentioned half-widths of about 5 mm. In the publication from this laboratory,[4] a width of 1 or 2 mm was suggested and one curve was given which showed a half-width of less than 1 mm.

This problem was recently reopened by J. H. Jurmain[5] of the Baird Associates, Inc., who made measurements on some tubes with a technique similar to that described later. Jurmain's results indicated a sensitive region appreciably wider than that reported in reference 4, and at his request we measured a few of his tubes and confirmed his results.

On repeating our experiments, with some of the same tubes as reported in reference 4, we found that we had been incorrect in stating that the voltage between the cathode and the first dynode was set at 100 volts per stage—the same as other stages—for the curves which were published. We have since discovered that the size and shape of the sensitive cathode area is strongly influenced by this voltage, which we had been adjusting as a gain control.

The experimental arrangement for obtaining all data presented here was essentially the same as was used before.[4] A small tungsten lamp was placed 75 cm from a 0.2-mm slit about 1 cm long. The photo-tube was placed about 10 cm behind the slit, with the grid wires of the tube normal to the line joining the slit and the lamp. The vertical axis of the tube was set approximately parallel to the slit. The slit was moved by means of a screw to scan the cathode.

Figure 1 is a set of curves obtained from one tube. The voltage between the cathode and the first dynode was set at the values shown on each curve, all other stages operating at 100 volts per stage. To prevent overlapping, each successive curve was displaced upward one unit from the previous curve. The left and right extremities of each curve correspond to zero sensitivity. It is suggested that the maximum occurring between 4 and 5 mm on the abscissa scale might be due to photo-electrons which by-pass dynode 1 and go directly to dynode 2. The small sensitivity maxima at each side are due to reflections from the grid wire supports. Although the width of the sensitive area increases rapidly with the voltage on the first stage at the lower voltages, the broadening increases more slowly at higher voltages so that little advantage results from operation of the tube with a first stage voltage higher than that on the other stages. Of five tubes measured with varying voltages on the first stage, all showed an essentially similar behavior.

TABLE I. Result of measurements made of the width of the sensitive cathode area on 35 multiplier photo-tubes. No correction is made for angle of incidence or width of light probe.

	Largest	Smallest	Average
95 percent width	1.7 mm	0.5 mm	1.1 mm
50 percent width	4.0 mm	2.1 mm	3.3 mm

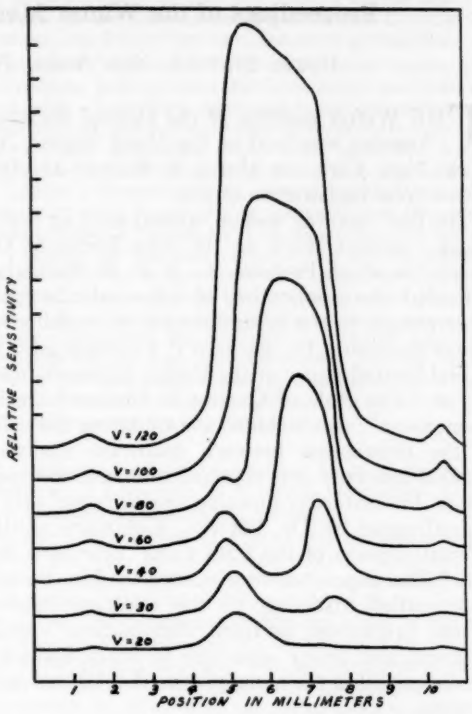

FIG. 1. Variation in the sensitivity of a multiplier photo-tube with position of illumination on the cathode, for various values of voltage between the cathode and first dynode.

There is considerable variation among tubes as to the size and shape of the sensitive cathode area. Table I is from data taken on 35 tubes with the experimental arrangement described. The widths reported are actual distances which the slit moved, with no allowance being made for the width of the light beam or angle of incidence on the cathode. All tubes were operated at 100 volts per stage on all stages. By "95 percent width" is meant the distance the slit was moved to increase the tube output (dark current subtracted) from 95 percent of its maximum value to 100 percent and back to 95 percent. A similar meaning applies to "50 percent width." Table I gives the largest and smallest values of these widths found among all the tubes tested as well as the average value for all 35 tubes. The tubes measured included Types 931, 931A, 1P21, 1P22, and 1P28. No significant correlation was found between the shape of the sensitive area and the tube type.

Measurements were also made with many of the same tubes operated at reduced voltage, down to 50 volts per stage on all stages. In most cases the 95 percent width became slightly smaller at lower voltages but in one case it became larger. The effect is small and in many cases could not be detected.

As given in Table I, a beam of light centered on the sensitivity maximum can be moved on the average about ± 0.55 mm for a five percent change in photo-current. It should be pointed out, however, that for a light beam centered elsewhere, the change in photo-current with position is greater than that given above by at least a factor of two and in most cases by a much larger factor.

* Now at Cornell University, Ithaca, New York.
[1] Hasler, Lindhurst, and Kemp, J. Opt. Soc. Am. **38**, 789 (1948).
[2] Dieke, War Production Board Report W-193.
[3] Marshall, Coltman, and Bennett, Rev. Sci. Inst. **19**, 744 (1948).
[4] Saunderson, Caldecourt, and Peterson, J. Opt. Soc. Am. **35**, 681 (1945).
[5] Private communication.

Proceedings of the Winter Meeting of the Optical Society of America

HOTEL STATLER, NEW YORK, NEW YORK, MARCH 9, 10, AND 11, 1950

THE Winter meeting of the Optical Society of America was held at the Hotel Statler, New York, New York, on March 9, 10, and 11, 1950, with a total registration of 455.

The first morning session opened with an invited paper, "Recent Work on the Two Forms of Diamond," in which Professor G. B. B. M. Sutherland indicated the application of infra-red absorption spectroscopy to the determination of crystal structure of diamonds. Dr. Richard P. Feynman gave the second invited paper at the Friday afternoon meeting on "The Role of Quanta in Ordinary Optical Phenomena"; this included a stimulating discussion of the connection between quantum electrodynamical concepts and classical interference experiments. The Saturday morning session began with an invited paper by Dr. Peter C. Goldmark entitled "Visual Aspects of the CBS Color Television System." The paper, which was read by Mr. Bernard Erde, called attention to the relations between picture brightness, ambient illumination, viewing distance, and image structure in black-and-white television and in the three proposed color television systems.

The twelve sessions for contributed papers were not classified under descriptive headings. Among the topics which received considerable attention were infra-red instrumentation, lens design, ruling engines, ultraviolet emission spectroscopy, and interference filters.

On Thursday evening many members and guests of the Society visited the Selective Sequence Electronic Calculator of the International Business Machines Corporation. The elements of this digital computer include more than twelve thousand vacuum tubes and over twenty thousand multicontact relays.

The dinner on Friday evening was attended by 241 members and guests. The main speaker was Dr. Newbern Smith, Chief of the Central Radio Propagation Laboratory of the National Bureau of Standards. He discussed recent developments in the television field, and gave particular attention to the conflict between the band-width requirements of high fidelity transmission and the limitations of the radio-frequency spectrum.

The 1950 Annual Meeting of the Inter-Society Color Council was held just prior to the Optical Society meeting on March 8 and was attended by many members of the Optical Society. A meeting of the U. S. National Committee of the International Commission on Optics was held on March 9 under the chairmanship of Dr. Stanley S. Ballard who serves as Vice President of the International Commission.

A breakfast meeting of Local Section Officers of the Optical Society of America was held on March 10 and enabled these officers to meet with Society officers to discuss future programs.

A meeting of the Board of Editors was held on the afternoon of March 10 to discuss the publication policies of *The Journal of the Optical Society* and to provide the new editor, Dr. Wallace R. Brode, with information and advice on the publication and editorial form of *The Journal of the Optical Society*.

MEETING OF THE BOARD OF DIRECTORS

A meeting of the Board of Directors was held on Wednesday, March 8. The minutes of this meeting and the reports of the officers will appear in a later issue of *The Journal of the Optical Society*.

CONTRIBUTED PAPERS

The abstracts of the contributed papers presented are appended.

The program committee included H. R. J. Grosch, *Chairman*, W. F. C. Ferguson, R. Clark Jones, J. Rud Nielsen, Daniel Smith, and John E. Tyler. The chairman wishes to express his particular appreciation to John E. Tyler, who was in charge of the local arrangements.

H. R. J. GROSCH, *Chairman*
Program Committee

Program of Sessions

Titles and Abstracts of Papers

1. Invited paper, entitled "Recent Work on the Two Forms of Diamond," BY PROFESSOR G. B. B. M. SUTHERLAND, *University of Michigan.*

2. Recent Far Infra-Red Investigations. T. KING MCCUBBIN, JR. AND WILLIAM M. SINTON, *The Johns Hopkins University.*

A far infra-red spectrograph has been constructed using a 66⅔ lines per inch echelette grating, Professor Wood's crystal quartz focal isolation lenses* as telescope and collimator, and a Golay cell detector. Spectra of an H-3 high pressure quartz mercury arc in the region of 100 to 350 microns obtained with this instrument for various atmospheric transmission paths up to 8 meters indicate decreasing absorption at longer wavelengths. Using the focal isolation apparatus with a quartz plate interferometer, as described in *Physical Optics*, inter-

ference "fringes" were obtained to measure the wave-lengths of the radiation transmitted by various thicknesses of rock salt. Fourier analysis of these "fringes" showed that a spectrum of wave-lengths from 300 to 2000μ was transmitted by the rock salt. The transmission of rock salt and its extinction coefficient were computed from the spectra. Values of the extinction coefficient were somewhat larger than those values which are summarized in Czerny's† article on the optical constants of rocksalt. This work was supported by ONR Contract N5ori-166, T. O. V.

* R. W. Wood, *Physical Optics*, 3rd Edition, p. 535.
† Czerny, Zeits. f. Physik 65, 600.

3. Iron Arc Spectrum between 1.2 and 2.0 Microns.* RUSSELL A. FISHER, WILLIAM C. KNOPF and MASON E. CLARK, *Northwestern University.*

Wave-length measurements have been made on 85 iron lines in the interval between 1.2 and 2.0 microns using the Northwestern recording grating spectrograph[1] with lead sulfide detector cell. Sources used were a stabilized iron arc and a hollow cathode type discharge tube. Accuracy in measurement is of the order of 0.1 angstrom units. The new measurements are in approximate agreement with 25 lines in this region observed in 1919 by Randall and Barker,[2] although some of Randall and Barker's lines are now resolved into multiplets. Twenty of the infra-red lines have been identified as arising from already known terms of FeI. At this time progress is reported in the classification of a considerable number of the remaining lines by means of hitherto unobserved but relatively low lying states of the FeI atom.

* Investigation supported in part by a grant from the Research Corporation.
[1] Described by R. C. Nelson, J. Opt. Soc. Am. 39, 68 (1949).
[2] Randall and Barker, Astrophys. J. 49, 42 (1919).

4. The Infra-Red Spectrum of CH_2ClF. EARLE K. PLYLER AND MARY A. LAMB, *National Bureau of Standards.*

The infra-red spectrum of CH_2ClF has been measured in the gaseous state from 2 to 30μ. The longest wave-length band was observed at 26μ. Twenty-five bands have been observed with cells of 5, 60, and 100 cm in length and with gas pressures up to 60 cm of mercury. Nine of the observed bands have been classified as fundamentals, and the remaining bands are attributed to harmonics and combinations. Several bands in the region from 1.5 to 2.5μ were measured on a high resolution grating instrument, and it was possible to resolve seven bands in a series of lines in this region. These bands are located at 1.657, 1.686, 1.699, 1.755, 2.229, 2.285, and 2.430μ. From these results some of the constants of the molecule have been determined.

5. Extensions to the Infra-Red Emission Spectrum of Mercury. CURTIS J. HUMPHREYS, *National Bureau of Standards.*

The spectrum of neutral mercury has been observed in the region between 1 and 2.5μ, using several different sources in conjunction with a high resolution grating spectrometer employing a lead sulfide detector. About 20 lines in addition to those reported by McAlister* in the same region have been found. A noteworthy feature of the new observations is the essentially complete resolution of the *D-F* multiplets involving both first and second members of *F* series. Such resolution was achieved only with a low pressure source. Nearly all new lines have been classified. A few changes in existing classifications and minor revisions in term values are suggested.

* E. D. McAlister, Phys. Rev. 34, 1142 (1929).

6. Raman Spectra of *Cis-* and *Trans-*2-Butene and 1,3-Butadiene in the Gaseous and Liquid States. CHARLES M. RICHARDS AND J. RUD NIELSEN, *University of Oklahoma.*

The Raman Spectra of *cis*-2-butene, *trans*-2-butene and 1,3-butadiene in the gaseous and liquid states have been obtained with a Lane-Wells spectrograph and internally-water-cooled mercury lamps. Polarization measurements have been made on these compounds in the liquid state. The Raman frequencies in the 3000-cm^{-1} region are generally about 10 cm^{-1} higher in the gaseous state, those between 1200 and 1700 cm^{-1} are from 3 to 10 cm^{-1} higher, while the lower frequencies are about equal in the two states of aggregation. For each of the 2-butenes the observed spectrum has been interpreted in detail, several new fundamentals have been determined, and a couple of changes made in previous assignments. The spectrum of 1,3-butadiene has been interpreted on the assumption that the molecule has the symmetry C_{2h} ("*trans-*" form), two new fundamentals have been determined and one change made in previous assignments. The fact that seven faint bands could not be interpreted indicates that a small fraction of the molecules have a "*cis-*" configuration.

7. Apparatus for Low Temperature Study of the Raman Effect.* R. C. LORD AND E. NIELSEN, *Spectroscopy Laboratory, Massachusetts Institute of Technology.*

A simple modification of a conventional excitation unit[1] enables the study of the Raman effect in liquids at any temperature down to about −160°C. The chief feature of the arrangement consists of a Dewar-jacketed sleeve that fits around the Raman tube and enables the cooling of the tube by a flow of cold nitrogen gas. By adjustment of the temperature of the gas and its rate of flow, easy and precise control of the temperature of the Raman tube can be obtained. It is also possible to use elevated temperatures (up to 150°C) by heating the nitrogen. The advantages of the system are its simplicity, ease of operation, quick change from low temperatures to normal operation and vice versa, and the same intensity of illumination as that afforded by room-temperature operation. The set-up has most recently been used to obtain Raman spectra of liquid diborane and heavy diborane, including qualitative depolarization factors, at a temperature near −120°C.

* This research was supported by the ONR under Contract N5ori-07810.
[1] Harrison, Lord, and Loofbourow, "Practical spectroscopy," pp. 511–513.

8. Method of Tracing Skew Rays. DONALD P. FEDER, *National Bureau of Standards.*

A vector method is given for tracing skew rays through a system of spherical refracting surfaces.[1] The surfaces need not be centered. These equations have been in use for some years and are believed to be quite simple. Useful check formulas are given which need be applied only to the initial and final data of the ray.

[1] Ludwil Silberstein, *Simplified Method of Tracing Rays Through Any Optical System* (Longmans, Green and Company, New York).

9. Calculation of Third-Order Aberrations with the Aid of IBM Machines. L. IVAN EPSTEIN, *Bausch & Lomb Optical Company.*

The IBM automatic calculating punch, type 602, can perform all the fundamental arithmetical operations, including sign control, in any prescribed order, provided that excessively complicated computing programs are avoided. Hence, the third-order aberrations of optical systems can be calculated. Each refracting or reflecting surface and the space following it is represented by one card. The end of an optical system is marked by a trailer card bearing a control signal. Thus, a number of optical systems totaling a few hundred surfaces may be analyzed at the same time. To facilitate lens

bending, a surface of cementation is represented as two surfaces separated by an infinitely thin airspace. After paraxial rays have been traced, the "airspace" is removed by sorting, before surface contributions to the aberrations are calculated.

10. On the Design of Wide Angle Schmidt Optical Systems.* ERIC M. WORMSER, *Servo Corporation of America.*

A method of balancing the optical aberrations over a wide angular field of a Schmidt optical system will be described. This design method will be demonstrated for a Schmidt optical system of focal ratio F:0.7 and covering an angular field of 40°. The reduction in off-axis secondary aberrations over those present in a classical Schmidt system is obtained by computing a "wide angle" aspheric corrector plate through the use of "Lucy's Approximate Method"[1-5] instead of using the conventional "exact equations." The choice of the location of the neutral zone of the corrector plate is found not to be critical in the particular Schmidt optical system under consideration.

* The work described in this abstract was carried out in part in connection with development contracts of the Bureau of Aeronautics of the Navy Department.
[1] F. A. Lucy, J. Opt. Soc. Am. **30**, 251–254 (1940).
[2] V. B. Strömgren, Vierteljahres. d. Astronom. Ges. **70**, 65–86 (1935).
[3] F. B. Wright, Pub. A.S.P. **47**, 300–304 (1935).
[4] E. H. Linfoot and E. Wolf, J. Opt. Soc. Am. **39**, 752–756 (1949).
[5] E. H. Linfoot, M.N.R.A.S. **109**, 280–297 (1949).

11. High Speed Spectrograph Objectives. D. H. RANK, *Pennsylvania State College.*

Design characteristics of an $f/2$ spectrograph objective suitable for the middle of the visible region of the spectrum will be discussed. This objective is of simple design, has a flat field for tangential images, and gives extremely sharp definition. The corrections achieved in the design are good enough so that at a focal length of 12 inches the definition is considerably better than Type I plates are capable of recording. Aberration characteristics will be given for a medium fast "spectroaplanat" type of objective of very simple design. The definition of this lens is extremely sharp. However, the field is somewhat inclined due to imperfect achromatization and no correction for curvature of field is possible. Lenses of the types mentioned above have been in use for several years on spectrographs used for the study of the Raman effect and Rayleigh scattering.

12. Lens for Institute of Optics' High Speed Camera. ROBERT E. HOPKINS AND LOUISE RIVOLI, *University of Rochester.*

The image dissection principle used in the Institute of Optics' high speed camera places stringent requirements on the taking lens. The lens forms images of two slits 90 mm long by 0.025 mm wide. Each image is 32 mm high, 0.008 mm wide, and separated by 50 mm. It was considered necessary to have the lens work at an aperture ratio of $f/1.5$ and form blur circles approximately 0.010 in diameter with no appreciable vignetting. Since no known available lenses approached the required image quality, a special lens was designed and made. This lens will be described, and some of the optical design problems encountered will be discussed. The authors will point out that some of the most difficult problems encountered in this type of a lens design are solved by third-order analysis.

13. Measurements of the Thermal Conductivity of Optical Crystals.* KATHRYN A. MCCARTHY AND STANLEY S. BALLARD, *Tufts College.*

There is a need for better values of the thermal conductivity of the optical crystals used in infra-red instrumentation, both because new materials have recently been introduced, and because most available literature values are for natural crystals rather than the synthetics that are now in more common use. An apparatus has been developed for making measurements on small crystal samples, whose thermal conductivity is compared with that of a standard material. Reproducibility data given by check runs, as well as comparisons with certain literature values, indicate an accuracy of about five percent within the temperature range of 15°C to 90°C that is available with the present apparatus. Typical results obtained include: silver chloride, thermal conductivities of 27.1 and 25.6 c.g.s. units at average temperatures of 52° and 64°C, respectively; KRS-5 (thallium bromide-iodide), thermal conductivities of 21.3 and 18.4 c.g.s. units at average temperatures of 54° and 64°C respectively. The conductivities measured for air-grown lithium fluoride (249 at 36°C) and for vacuum-grown lithium fluoride (280 at 34°C) indicate a difference in physical properties of this crystal resulting from the conditions of growth, which is consistent with data on certain elastic constants reported by Combes and Ballard.[1]

* This work has been assisted by a grant from the Rumford Fund of the American Academy of Arts and Sciences.
[1] L. S. Combes and S. S. Ballard, J. Opt. Soc. Am. **38**, 1101A (1948).

14. Studies of the Inelastic Behavior of Optical Crystals.* LEWIS S. COMBES AND STANLEY S. BALLARD, *Tufts College.*

Since the previous report[1] on this general subject, a thermostatically controlled enclosure has been constructed which makes it possible to keep the sample under test at a temperature which is constant within 0.2°C. Additional measurements of cold flow in flexure have been made at controlled temperatures on KRS-5 (thallium bromide-iodide) and Plexiglas 1A. Similar measurements have been made on KRS-6 (thallium bromide-chloride), potassium chloride, air-grown lithium fluoride, and vacuum-grown lithium fluoride. The KRS-6 and Plexiglas showed typical "two-stage" deformation *vs.* time curves, while all KRS-5 curves had a third stage in which the rate of deformation was increasing. The air-grown lithium fluoride gave a typical "two-stage" cold flow curve, while the vacuum-grown lithium fluoride showed practically no cold flow at stresses twice as great as those applied to the air-grown crystals. Another difference between these two samples was shown in tests made on strain hardening, which was very pronounced with the vacuum-grown crystals but practically zero for the air-grown crystals. The air-grown crystals apparently showed the Bauschinger effect while the vacuum-grown did not; yet the polariscope showed practically identical strain patterns in the two crystals.

* This work has received support from the Permanent Science Fund of the American Academy of Arts and Sciences.
[1] Combes, Travis, and Ballard, J. Opt. Soc. Am. **39**, 635A (1949).

15. Comatic Aberration in Infra-Red Spectrometer Design. F. P. ELBY, *The Johns Hopkins University.*

Comatic images formed by off-axis rays reflected from a good ellipsoidal mirror were studied experimentally. Horizontal and vertical knife edges were used to chop slices of these images, and the alternating current output of a photo-multiplier tube, proportional to the chopped radiation, was used to indicate the intensity distributions in the comatic images. Calculations[1] of intensity distributions in comatic images were made, and the experimental observations were predicted from them satisfactorily. Infra-red detector sensitivity is inversely proportional to the square root of the detector area. Accordingly, the intensity distribution in the comatic image may be used to calculate optimum dimensions for both the exit slit and the detector in an infra-red spectrometer.

[1] J. R. Nielsen, J. Opt. Soc. Am. **39**, 59 (1949) has also made calculations of coma.

16. The Resolving Power of Infra-Red Prism Spectrometers. ROBERT J. MELTZER, *The Johns Hopkins University.*

The equation for the resolving power of a spectrometer under conditions of fixed wave number band pass, in instances where available source brightness or available detector sensitivity, and not diffraction, sets the limitation, has been given by Strong.[1] The energy-limited and diffraction-limited resolving powers have been computed for four prism materials, LiF, NaCl, KBr, and KRS5, as a function of apex angle under two conditions: (1) The aperture is limited by the size of the prisms which may be cut from crystals presently available. (2) The aperture of the spectrometer is limited by the opacity of the prism material at the base of the prism. In the first instance the resolving power is a maximum for some apex angle: LiF, 60°; NaCl, 52°; KBr, 47°; KRS5, 32°. In the second instance the apex angle should be as large as is consistent with the critical angle of the material. These computations lead to a comparison of double dispersion with zero dispersion systems, such as the recent system proposed by Shurcliff.[2] The former provide at least twice the detector response at constant wave number band pass, when absorption losses are negligible, and even higher response when such absorption losses cannot be ignored. A design of a multiple-prism polarizing spectrometer will be mentioned.

[1] John Strong, J. Opt. Soc. Am. **39**, 320 (1949).
[2] W. A. Shurcliff, J. Opt. Soc. Am. **39**, 1048 (1949).

17. A Rapid Scanning Spectrometer for Oscillographic Presentation in the Near-Infra-Red.* B. W. BULLOCK AND S. SILVERMAN, *Applied Physics Laboratory, The Johns Hopkins University.*

A rapid scanning spectrometer[1-5] for oscillographic presentation has been built for use in the "photo-conductive" infra-red region. It is designed to produce spectra from 0.36mμ to better than 5mμ using a PbTe cell. The CO_2 doublet at 4.2mμ is resolved with a scanning rate of 120 cycles per second and a scanned interval of better than 1.5mμ with fluorite optics. A wave-length calibrating device has been incorporated into the instrument; this presents a fiduciary scale, synchronized with the spectrum, on the second beam of the twin-beam C.R.O. Adequate solutions have been found for the problems of synchronizing oscilloscope sweep and scanning drive, and for the problems of amplifier design for the sensitive cells.

* This work was supported by ONR and Navy Bureau of Ordnance under Contract NORD 7836.
[1] Feldt and Berkley, National Electronics Conference (Chicago, 1946).
[2] F. F. Daly and G. B. B. M. Sutherland, Proc. Phys. Soc. (London) **59**, 77 (1946).
[3] Deal, Bradshaw, and Matsen, J. Chem. Phys. **38**, 209 (1948).
[4] S. Silverman, J. Opt. Soc. Am. **38**, 664A (1948).
[5] B. W. Bullock and S. Silverman, J. Opt. Soc. Am. **39**, 200 (1949).

18. A System of Static Multislit Spectrometer. MARCEL J. E. GOLAY, *Signal Corps Engineering Laboratory.*

If the uniformly illuminated entrance field of a spectrometer is subdivided into a fine-grained pattern of open and closed apertures, and if one-half of this pattern is exactly imaged, for a given wave-length, on an identical (positive) pattern at the exit field while the other half is imaged on a reversed (negative) exit pattern, the difference between the radiation leaving the two exit patterns will be a measure of the radiation of the given wave-length. If the entrance apertures are determined at random, and if their number is not large, this subtraction process will be imperfect owing to random fluctuations. On the other hand, there are groups of entrance and exit slit patterns which give exact cancellation. A discussion is given of these groups.

19. Lens Testing Bench.*† BERNARD MARCUS, *Signal Corps Engineering Laboratories* AND BURTON W. WHEELER, JR., *Laboratories of David W. Mann.*

A lens testing bench has been constructed for the especial purpose of testing photographic objectives. The construction is of such accuracy that all measured defects of imagery are due solely to the objective lens under test. The bench was the cooperative effort of Mr. Edward K. Kaprelian of the Signal Corps Engineering Laboratories and Mr. David W. Mann who have elaborated on the design of Professor Rudolph Kingslake, the latter having described a bench of this type before the Optical Society at the Rochester Meeting in 1930. The bench is of the nodal slide type and is provided with flat field bars. It accommodates lenses of all focal lengths up to 1220 mm and diameters from 0.5 inch to 7 inches. It includes provisions for centering and revolving the lens under test and the microscope is capable of being moved in three mutually perpendicular planes through calibrated micrometer screws. The microscope is capable of rotation about its object point through an angle of 100° to permit testing of telephoto lenses and lenses having extreme distortion.

* R. Kingslake, J. Opt. Soc. Am. **22**, 207 (1932).
† J. L. Houghton and E. W. H. Selwyn, J. Sci. Inst. **15**, 367 (1938).

20. A New Resolving Power Test Chart. IRVINE C. GARDNER, *National Bureau of Standards.*

This is essentially a progress report on a method of measuring resolving power being developed at the National Bureau of Standards. A new test chart consisting of a series of parallel lines assumed normal to the x axis has been designed. The widths of the lines and spaces progressively decrease in such a manner that the "instantaneous" value of the number of lines per millimeter is a linear function of x. The densities of the lines and spaces along the y axis vary in such a manner that the contrast is a linear function of y and the density of the chart (averaged over an area embracing several pairs of lines) is uniform for the entire pattern. A test negative, made to measure resolving power shows an area unresolved and of uniform density, and a resolved area. A boundary between these two areas is a curve showing the resolving power as a function of contrast. Assessment of the chart may be made visually on the test negative or by scanning with a microdensitometer. Ordinarily these charts will be used in pairs, oriented for measuring the resolving powers for tangential and radial lines. Preliminary charts, not sufficiently good for making accurate determinations, have been made and the visual method of assessment has been tested. The results are distinctly encouraging. A photographic double exposure method promises to produce charts of satisfactory quality.

21. Lens Tester. FRANK G. BACK, *Research and Development Laboratory, New York City.*

This lens tester is an optical instrument which allows the testing of lenses, specially photographic lenses, in a simple, fast, and accurate manner. It is basically a modified autocollimator in conjunction with an assembly consisting of an adjustable microscreen and a lens holder. This assembly can be rotated around an axis perpendicular to the optical axis of the system. Built-in color filters allow the testing for different wave-lengths. Contrary to the lens bench method, it does not require the determination of the nodal points and the focal length for extra-axial aberrations, and the results can be read off immediately without further computations. The following tests can be made easily and with great precision: 1. Determination of the back focal length. 2. Shift of axial focus for different lens apertures. 3. Longitudinal chromatic aberration. 4. Tangential and sagittal focus for any angular distance from the axis and for any aperture.

22. Criteria for Detection and Recognition of Photographic Detail.* DUNCAN E. MACDONALD, *Boston University Optical Research Laboratory.*

Test objects have been photographed under various scale, resolution, and contrast conditions. The negatives have been viewed through binocular microscopes. Forced discrimination has been employed to arrive at data giving percent detection and percent recognition as a function of angular resolution expressed in terms of object dimension. Contrast on the film is given as a function of the angular resolution required for various reliabilities of detection and recognition.

* This work was sponsored by the Photographic Laboratory of the Air Materiel Command. The work was performed under Contract W33-038-ac-14075 between the United States Air Force and Boston University.

23. A Workshop Method of Figuring Concave Mirrors by Quantitative Foucault Tests.* CLAUS M. ASCHENBRENNER, *Boston University Optical Research Laboratory.*

A method is described to obtain quantitative data from conventional Foucault zonal tests along the axis of concave mirrors. By graphical integration, the deviations of the actual optical surface from the desired shape are found in every stage of the figuring. This enables the optician to conduct his step-by-step figuring most efficiently and to take the action of his figuring tool into account. The method was developed in the Boston University Optical Research Laboratory. It was successfully employed for the construction of two 30-inch $f/5$ parabolic mirrors for schlieren equipment. Routine procedure, experiences, and results are discussed.

* This work was sponsored by the Photographic Laboratory of the Air Materiel Command. The work was performed under Contract W33-038-ac-14075 between the United States Air Force and Boston University.

24. Optical Quality in Large Glass Blanks. JOHN T. WATSON, *Boston University Optical Research Laboratory,* AND VINCENT YOUNG, *Bausch & Lomb Optical Company.*

The quality of several large lens blanks has been tested. The blanks up to 38 inches in diameter and 3½ inches in thickness include some made by Jenaer Glaswerk Schott and Genossen and others made by the Bausch & Lomb Optical Company. The tests, mainly concerned with striae, strain, and homogeneity of index show that large pieces of excellent quality can now be obtained by proper techniques. Maximum variation of index within these blanks of less than five parts in the fifth decimal place is reported. Methods used for the testing are described.

25. Deterioration of Image Quality by Photographic Windows.* JOHN T. WATSON AND WILLIAM C. BRITTON, *Boston University Optical Research Laboratory.*

Tests to determine the effect of plate glass photographic quality windows on the resolution of long focal length cameras are described. The deterioration of image quality by these windows is given in terms of a standard system which resolves 20 lines/mm. The results of tests made with pressure on the windows and tests made with the camera axis oblique to the window are also shown. A 50-inch $f/6.3$ autocollimating camera was employed for the tests.

* This work was sponsored by the Photographic Laboratory of the Air Materiel Command. The work was performed under Contract No. W33-038-ac-14075 between the United States Air Force and Boston University.

26. The Precise Topography of Optical Surfaces. JAMES B. SAUNDERS, *National Bureau of Standards.*

A method of applying the interference of light to determine the deviation of optical surfaces from a standard has been used for ultra high precision work. The methods previously applied use the wave-length of a monochromatic source of light as the unit and enable one to produce a contour map of the surface under test with a contour interval of one-half wave-length. The method used here also uses the wave-length of light as a standard but the separation of the interference fringes represent much smaller fractions of the unit. In practice fringes representing contour intervals of approximately one-twentieth wave-length have been photographed and it appears that the interval can be further reduced without introducing serious difficulties of technique. This method obviously requires the use of narrow line fringes produced by multiple reflection from the two surfaces being compared; consequently, the surfaces must be made highly reflecting, but not opaque, in order to resolve the contour lines. With the interpolated fringes at small intervals characteristic of this new method it is possible, by reducing the air wedge between the surfaces, to enhance the curvature of the contours indicative of local irregularities and, at the same time, the lines are so closely spaced that the entire surface is adequately represented.

27. New Johns Hopkins Ruling Engine.* JOHN STRONG, *The Johns Hopkins University.*

Professor Rowland's design for an engine to rule diffraction gratings, which has been widely copied with minor alterations, is not suited for producing large gratings. A ruling engine built by Johns Hopkins for 6-in. gratings has been recently finished. I have introduced many new features in this engine which are based on experience here and elsewhere. I believe the new design will be equally functional in much larger size. The cardinal feature of the new design is the use of two precision lead screws and the practice of reciprocating the grating blank. This contrasts with the use of a single lead screw and the practice of reciprocating the diamond ruling point, as in Rowland's design. The first grating showed that the new features to make the engine immune to friction, oil films, flexures, and temperature expansion were successful. The first 6-in. grating was ruled without any preliminary cross rulings. Periodic errors of construction gave a Rowland ghost intensity less than 1/400 in the first order and the grating resolved the 546 line of mercury into four components. No certain lead error of the screws or curvature of lines was indicated by parallel and perpendicular knife-edge tests of the focal distances in the second orders. The inherent stability of the engine design is attested by the results of these tests in spite of the fact that the driving belt failed in the middle of this first ruling—one whole day repairing the machine was necessary before ruling was resumed. Furthermore, the temperature varied by about ¼° during the ruling period. A motion picture of the engine and of its components will be shown. We will show spectra taken with gratings ruled on the new engine.

* The new engine was made possible by the confidence of ONR from whom we received support to develop and prove its components under Contract N6onr-243, T. O. II.

28. The Baird Associates Ruling Engine. WILLIAM G. LANGTON, *Baird Associates, Inc.*

In the course of the past eight years two ruling engines have been built at Baird Associates, Inc. for the production of diffraction gratings. One of these has been in operation for five years. Both have been designed to rule a maximum of 15,000 lines per inch over a maximum length of six inches, or 90,000 lines in all. Provision was made on the older engine for ruling sub-multiples of 15,000 lines per inch, i.e., 7500, 3650, etc. The two engines are essentially identical, both having been patterned fairly closely after those in use at the Johns Hopkins University. A unique feature of the Baird engines is the use of a continuous advance of the table carrying the plate being ruled, rather than a stepwise advance produced by the more conventional rachet and pawl mechanism. The continuous advance is accomplished by means of a worm gear coupled to the main drive shaft through elliptical gears

which produce a 9 to 1 variation in the rotational speed of the worm for each cycle of operation. The phasing of the elliptical gears is such that the worm, and hence the grating table, is moving very slowly during the ruling stroke and much more rapidly during the return stroke. The bulk of the gratings that have been produced on the older engine were ruled on aluminized spherical mirrors four inches in diameter and of three meter radius of curvature. Gratings have been ruled showing resolution approaching the theoretical limit and Rowland ghost intensities less than 0.1 percent of the intensity in the main line at the first-order mercury green line. A description of the construction and housing of the engine will be given, together with a discussion of the results achieved.

29. Improved Diffraction Gratings and Echelles.[1] DAVID RICHARDSON, R. S. WILEY, AND G. J. SHELDON, *Bausch & Lomb Optical Company.*

The efficiency of both gratings and echelles depends upon the flatness and angle of the active groove face. A microscope interferometer equipped with oil immersion objectives is used for observing test rulings and controlling the setting of the grating ruling diamond. A similar instrument with 32-mm objectives is suitable for the work with echelles. Extreme equality of spacing is required for an approach to theoretical resolving power. This property of a ruling can be observed through the use of a refinement of the Gale[2] interferometer test method. A plano-interferometer equipped with an Hg 198 lamp permits observation of random or periodic spacing errors that reduce resolving power and produce Rowland ghosts. Some examples of the relation between interferometer tests and the actual performance of experimental plane gratings and echelles will be given.

[1] G. R. Harrison, J. Opt. Soc. Am. **39**, 522 (1949).
[2] H. G. Gale, Astrophys. J. **86**, 437 (1937).

30. Rapid Interferometric Calibration of Precision Screws. GEORGE R. HARRISON AND JAMES E. ARCHER, *Massachusetts Institute of Technology.*

The difficulty of correcting screws having as much as twenty inches of thread, to within a fraction of a millionth of an inch, has set serious limitations on the production of large diffraction gratings. Calibration of a large screw by photographing or visually counting interference fringes is likely to take longer than the period during which the initial measurements remain valid. A new device called a "commensurator" has been developed, which automatically plots the error curve of a screw in a few hours. Moving fringes from a Michelson interferometer mounted on the ruling engine are detected photoelectrically, producing a varying voltage of frequency equal to that of the fringes passing across a slit. The commensurator is operated in close synchronism with the turning of the screw to be calibrated, and produces an electrical comparison signal whose frequency can be adjusted mechanically to that of the fringes to within 1 part in 10^8. Departures from constancy of pitch in the screw cause phase discrepancies between fringe and commensurator signals, and the shifting of phase needed to maintain synchronism is plotted continuously on a paper chart by means of a phase-sensitive motor. The speed of screw calibration is limited only by increasing amplitude of vibration with speed. Compensation for varying barometric pressure, and screw and air temperature, can be made during calibration. Advantages of the device, in addition to speed which makes possible many tests not previously feasible, are insensitivity to transient mechanical disturbances, ease of adjustment of the comparison mirror to reset fringes in proper phase, and direct production of a cam to correct for periodic and cumulative errors. Successive curves are found to reproduce details of displacement to within 0.2 millionths of an inch.

31. Simultaneous Recording of Two Wave-Length Ranges with the Littrow Spectrograph. ROBERT W. MURPHY AND HAROLD K. HUGHES, *Socony-Vacuum Laboratories, Brooklyn, New York.*

This paper reports another phase of the program being followed by Socony-Vacuum laboratories, Technical Service Department, designed to reduce the size of sample and improve the efficiency of spectroscopic analyses.[1] Two wavelength ranges are recorded from a single exposure by the use of an auxiliary mirror system in a Littrow-type prism spectrograph. Radiation passing into the spectrograph is divided into two parts. The portion incident on the upper-half of the prism-lens aperture receives the dispersion and collimation to produce the normal ultraviolet spectrum on the photographic plate. A system of two mirrors, interposed before the lower-half aperture, provides an additional angular deviation and increase in path length to produce a visible spectrum adjacent to the ultraviolet spectrum. The instrument described was designed for use with the Bausch & Lomb large Littrow spectrograph. Its purpose is to record, in one exposure, a spectral range sufficient for the detection and estimation of all the elements, except boron, which can be excited in the arc. Through the use of the auxiliary unit, the ranges 2530–3500A and 3540–10,000A are covered, including, for example, the phosphorus lines and the potassium lines at 7665 and 7699A. The elimination of an extra exposure results in substantial reductions in analytical time and in sample requirements.

[1] H. K. Hughes and R. W. Murphy, "Emulsion calibration scale for quantitative spectroscopic analysis," J. Opt. Soc. Am. **39**, 501 (1949).

32. A Recording Grating Monochromator for the Range 180 to 4000 Millimicrons. WALTER S. BAIRD, *Baird Associates, Inc.*

A grating monochromator has been built for use over a spectral range extending from the ultraviolet through the lead sulphide cell region to four microns. A flat grating is used with a spherical mirror four inches in diameter and of one meter focal length, serving as both collimator and telescope. Two gratings are provided; one of 15,000 lines per inch to cover the range from 180 to 2000 millimicrons with a first-order theoretical resolving power of 60,000 and a second of 7500 lines per inch to cover the range from 180 to 4000 millimicrons with a first-order theoretical resolving power of 30,000. Provision has been made for automatic recording of a spectrum on a scale linear in wave-length with the aid of either a photocell or a sulphide cell and a Leeds and Northrup Speedomax recorder. Sample curves will be shown illustrating the application of the instrument to the recording of narrow band filter characteristics and absorption spectra in the ultraviolet, visible, and near infra-red regions.

33. The Theory of the Refractometer. J. ERNEST WILKINS, JR., *American Optical Company.*

In a paper appearing in the 1943 volume of Zeitschrift für Instrumentenkunde, H. Schulz has shown how to design a refractometer consisting of two prisms, the usual measuring prism and an auxiliary prism, in such a manner that the angle which the critical ray makes with the normal to the last surface of the auxiliary prism is an approximately linear function of the index of the sample to be measured. We shall describe in this paper a different method of design based on the use of a power series expansion which has enables us to obtain a function approximately twice as linear as that of Schulz.

34. Phase Contrast Microscopy for Opaque Specimens. JAMES R. BENFORD AND RICHARD L. SEIDENBERG, *Bausch & Lomb Optical Company.*

Phase contrast microscopy is by now a familiar subject in the field of transmitted light microscopy. Its application

in reflected light is more recent.[1,2] Early systems for reflected light phase contrast[3-5] either located the phase annulus directly in the objective focal plane, or else compromised on this desired location and placed it beyond the vertical illuminator, somewhere between aperture and field planes in the microscope. This paper describes a different approach to the problem, resulting in an instrument design which obviates the elaborate equipments required by the above mentioned systems, requires only one phase annulus and one illuminating annulus for all objectives, and in which the phase annulus is located in the ideal aperture plane of the microscope.

[1] Jupnik, Osterberg, and Pride, abstract, J. Opt. Soc. Am. **36**, 710 (1946).
[2] Cuckow, "Phase contrast in the photomicrography of metals," Nature 639 (May 10, 1947).
[3] Jupnik, Osterberg, and Pride, "Phase microscopy with vertical illumination," J. Opt. Soc. Am. **38**, 338 (1948).
[4] Cuckow, "The phase contrast incident light microscope," Iron and Steel Inst. Papers (April, 1949).
[5] Taylor, "The phase contrast microscope with particular reference to vertical illumination," J. Roy. Microscop. Soc. 49 (May, 1949).

35. Luminescence and Trapping in Zinc-Sulfide-Type Phosphors. RICHARD H. BUBE, *Radio Corporation of America, RCA Laboratories Division, and Princeton University.*

Measurements of luminescence emission during excitation, thermo-stimulated phosphorescence emission, and decay of phosphorescence emission were obtained for temperatures between −196° and 200°C for samples of cubic and hexagonal ZnS:Cu(0.0–0.3), [NaCl(2)], specially prepared from pure ZnS with no spectroscopically detectable impurities, and for other samples of ZnS-type phosphors. A series of discrete trap depths was indicated, the maximum depth being 1.00 ev. The energy difference between trap depths generally decreases with decreasing depth. Cu causes the traps of the six deepest depths found in ZnS:Cu phosphors, the depths being independent of crystal structure. Traps of all other depths, however, are found with the same depth in all ZnS-type phosphors, regardless of activator, presence or absence of NaCl in the preparation, or the crystal form. Only substitutional sites in ZnS have the required invariance to account for the experimental results. It is concluded that traps are located at substitutional sites, principally omission defects, in ZnS-type phosphors. When many of the deeper traps were empty at the start of a glow curve, a large proportion of the electrons freed from shallower traps were retrapped. An hypothesis concerning the correlation between trap depth and type of omission defect is advanced on the basis of all the experimental results.

BIBLIOGRAPHY:
J. T. Randall and M. H. F. Wilkins, Proc. Roy. Soc. **184**, 366, 390 (1945).

36. Temperature Dependence of the Emission of an Improved Manganese-Activated Magnesium Germanate Phosphor. LUKE THORINGTON, *Westinghouse Lamp Division–Research Department, Bloomfield, New Jersey.*

A number of recent researches[1-4] have been concerned with magnesium germanate phosphors. An improved such phosphor is reported here having over twice the brightness of the previous compositions as prepared in this laboratory, and which shows peak luminescence efficiency at temperatures near 350°C. Temperature dependence of luminescence studies on the improved composition and the others showed little difference between them in this respect though the data are in striking contrast with those reported by others. A partial explanation of the pronounced temperature effect (for temperatures <350°C) is presented and is based upon the broadening of the excitation spectrum at elevated temperatures in such a way as to increase absorption of the exciting radiation (3650A). Data are presented showing differences in the temperature dependence relation effected by wave-length of excitation and method of measurement; in addition, curves are included showing the variation of phosphorescence ($t=1/120$ sec.) with temperature as well as curves showing excitation and emission characteristics of the phosphor. Finally a practical application of this high temperature luminescence is demonstrated in the color corrected high pressure mercury lamps the emission characteristics of which are briefly discussed.

[1] F. E. Williams, J. Opt. Soc. Am. **39**, 702 (1949).
[2] F. E. Williams, J. Opt. Soc. Am. **37**, 302 (1947).
[3] F. E. Williams, U. S. Patent No. 2,447,448 (1948).
[4] H. W. Leverenz, U. S. Patent No. 2,066,044 (1936).

37. An Improved Image Dissector for Very High Speed Motion Photography. BRIAN O'BRIEN, GORDON G. MILNE, AND WILLIAM COVELL, *Institute of Optics, University of Rochester.*

In the image dissector for very high speed photography previously described* the absolute aperture of each unit of the multi-objectives is limited by the length of each slit element forming the picture. This in turn, together with the magnification, limits the effective relative aperture of the camera, so that large relative aperture is achieved only by reducing the size of the negative and thus picture quality. This conflict can be avoided by simultaneously increasing both field and relative aperture of the multi-objectives, but this involves serious technical difficulties. As alternative the multi-objectives can be doubled in linear aperture, but arranged in two rows, and their images reassembled by means of a pair of toothed rhombs. In this way no increase in field is required to double the relative aperture of the camera or the linear dimension of the negative. Placing the multi-objectives in two rows also permits very effective regrouping of the entrance pupils of the 24 elements into a 53-mm circular aperture. This permits low power photomicrography of small very fast events at magnifications, referred to the final 16-mm motion picture print, of unity or greater. The new image dissector will be exhibited and its performance discussed.

* O'Brien and Milne (J. Soc. Mot. Pict. Eng. **52**, 30–40 (January, 1949).

38. A Fast Closure Slit Shutter with Low Inertia. BRIAN O'BRIEN, GORDON G. MILNE, AND WILLIAM COVELL, *Institute of Optics, University of Rochester.*

When two or more slits are used in an image dissector for photographing fast events of duration greater than the film run of the camera, a rapid capping shutter is required to terminate the run and prevent overlapping exposure. When the start of the event is unpredictable the capping shutter must have low enough inertia to permit tripping from standstill by the event. A Kerr cell is substantially inertialess but is too wasteful of light for many applications. Since all the light in an image dissector passes through two or three long slits very close together, the capping is accomplished by two parallel aluminum wires 0.6-mm diameter spaced 2 mm apart and mounted under tension very close to the slit plate. Electrically insulated, they may be driven together or apart by their interacting magnetic fields when carrying heavy currents in the same or in opposite directions respectively. Current is supplied from a 2-kv condenser firing through a connectron tube triggered by the event. At 5000 amperes per wire acceleration is approximately 10^6 g, and complete closure requires less than 20 microseconds. To absorb the kinetic energy and prevent recoil, the wire system is oil immersed in a sealed chamber with optical quality windows. The shutter will be exhibited and its performance discussed.

39. Unique Method of Obtaining a Uniformly Bright Area. RICHARD N. NIERENBERG, *U. S. Air Forces, Photographic Laboratory, Wright Field.*

A very simple and unique method of obtaining an efficient uniformly bright area as a source of illumination which re-

mains cool with a minimum of depth of the unit has been developed by the U. S. Air Forces. This invention probably will be used by the Air Forces in a new portable illuminator for viewing positive and negative transparencies. It may be used also as the source of illumination in scientific apparatus, x-ray viewers, etc. The basic elements of the illuminator are two wedge-shaped pieces of clear transparent plastic which has all the surfaces highly polished except the inclined planes which are uniformly roughened by a fine sand blast. The two wedges are placed with the roughened surfaces in contact to form a solid rectangular block of plastic. A light source is placed at the base of each wedge. The thickness of the base of the wedge is the aperture stop of the system and is determined by the diameter of the light source. Two models will be exhibited. One model which has a 10 in. × 20 in. illuminated area is 1¾ inches thick and uses two 20-w. photo-color fluorescent lamps.

40. Trapping of Light in Fluorescent Bodies. R. CLARK JONES, *Polaroid Corporation.*

When fluorescent light is produced within transparent bodies having certain geometrical shapes and having an index of refraction greater than that of the environment, a fraction (trapping fraction) of the light is trapped within the body by repeated total internal reflection. In a fluorescent glass sphere in air, for example, a light ray proceeding tangentially from a point of origin near the surface will be totally internally reflected at every successive reflection, with the result that the light ray will never emerge from the sphere. The trapping fraction has been calculated previously[1] for the sphere, plane-parallel plate, and the rectangular parallelepiped. Results will be given for the right circular cylinder, the right triangular prism, and for infinitely long cylinders whose cross sections are respectively circular, triangular, and rectangular. These results may have some significance in connection with the construction of scintillation counters.

[1] W. A. Shurcliff and R. Clark Jones, J. Opt. Soc. Am. 39, 912 (1949).

41. Invited paper, entitled, "The Role of Quanta in Ordinary Optical Phenomena," BY DR. RICHARD P. FEYNMAN, *Cornell University.*

42. Electrical Computer for Calculating the Optical Properties of Multilayer Interference Films. S. M. MACNEILLE AND E. O. DIXON, *Eastman Kodak Company.*

This computer is an "analog" device in which the amplitude and phase of a light wave are represented by the amplitude and phase of an a.c. voltage. Each layer in the film is simulated by a four terminal network containing adjustable attenuators and an adjustable phase-shifter. The network obeys the same difference equation[1] as that which relates the reflectivity of $n+1$ interference layers to the separate reflectivities of the first n layers and the $n+1th$ layer. With these networks connected in sequence, reflectance or transmittance can be read on a meter when the circuit parameters are adjusted to correspond to the optical constants of the various layers of the film. For each layer the adjustments are made with three calibrated dials. One indicates reflectivity at the interface between layers, the second, phase retardation with passage through the layer, and the third, attenuation with passage through the layer. Thus the instrument can treat problems involving oblique incidence, polarization and absorption. A six-layer computer has been built and results with this instrument will be shown.

[1] Lord Rayleigh, Proc. Roy. Soc. 93, 565 (1917); P. Rouard, Ann. de physique Ser. 11 7, 291 (1937); W. Pfister and O. H. Roth, Hoch.: Tech. u. Elek.: akus. 51, 156 (1938); S. M. MacNeille, U. S. Patent No. 2,403,731; A. Vasicek, J. Opt. Soc. Am. 37, 145 (1947); D. Caballero, J. Opt. Soc. Am. 37, 176 (1947).

43. Phase Shifts in Interference Filters. F. D. SMITH, *University of Rochester,* AND A. F. TURNER, *Bausch & Lomb Optical Company.*

A simple transmission interference filter of the type metal-spacer-metal produces accelerated changes of phase in the neighborhood of its pass band both in transmitted and reflected light. The phase change curves have been followed with a Michelson interferometer for a number of typical filters. For example, a Ag-MgF_2-Ag uncemented filter having a second-order pass band of 50 percent peak transmittance at 498 millimicrons and a half-width of 14 millimicrons showed the following phase shift behavior: In transmission there was a rapid increase of 125° in retardation toward shorter wavelengths over a region 30 millimicrons wide surrounding the pass band. In reflection, the phase retardation was approximately that of a silver mirror except close to the reflectance minimum. Here there was a symmetrical kink in the curve, the retardation being increased by 50° on the long wavelength side and decreased by 50° on the short. This total 100° excursion took place within 5 millimicrons. The doublet pass bands found[1] in a multiplex interference filter have their origin in these phase changes.

[1] A. F. Turner and O. A. Ullrich, J. Opt. Soc. Am. 38, 662A (1948); Chas. Dufour, J. de phys. et rad. (in print).

44. Optical Constants of Metallic Films. HOWARD S. COLEMAN AND RALPH G. ALLEN, *The Optical Research Laboratory, The University of Texas.*

A rigorous method of determining the optical constants of semitransparent metallic films has been developed. The method includes a graphical solution of Maxwell's equations and makes allowances for the fact that the films are not continuous metallic sheets. The degree of continuity is determined by means of an electron microscope. The optical constants may be calculated from either reflectance or transmittance measurements at normal incidence. The measurements are made photoelectrically by means of a precision reflectometer and transmissometer. The preliminary results, obtained in the case of silver films of different average thickness, show the optical constants to be practically independent of film thickness for ranges in thickness over which the optical constants are found to vary by as much as a factor of ten when determined by classical polarization methods.

45. Position of the Bands of Fabry Perot Type Filters as a Function of Angle of Incidence. GRACE E. GRIFFITH, *Baird Associates, Inc.*

The positions of the bands of a number of transmission interference filters of the type described by Hadley and Dennison[1] were measured as a function of the angle of incidence. When these filters are tilted, the peaks shift to shorter wave-lengths and split due to a phase shift at reflection. The two bands are polarized with the electric vector parallel and perpendicular to the plane of incidence. The position of the bands is a function of the thickness and index of refraction of the dielectric layer, the position of the band at normal incidence, the angle of incidence, and ∂y, the difference between the values of the phase angle for the two polarizations. For the filters measured, ∂y was found to be independent of wavelength and dependent only on angle and order. It is therefore possible to determine where the bands occur as a function of angle for a given filter. A comparison was made between experimental and theoretical results.

[1] L. N. Hadley and D. M. Dennison, "Reflection and transmission interference filters," J. Opt. Soc. Am. 37, 451 (1947); 38, 483 (1948).

46. A One-Angstrom Pass-Band Polarization Interference Filter.* B. H. BILLINGS, S. SAGE, AND W. DRAISIN, *Baird Associates, Inc.*

One of the main difficulties in the construction of a narrow band Lyot-Öhman[1] type polarization interference filter is the procurement of large slabs of transparent birefringent material. Previous filters have been built mainly of quartz. The narrower the band width, the thicker the required birefringent slabs. A 1A band width would need a quartz thickness of approximately 8.6 inches. Optical quartz of this thickness is essentially unavailable in quantity. A filter has been constructed using ammonium dihydrogen phosphate as the birefringent material. Although this crystal is easily available it is extremely difficult to work because of its softness and because it is water soluble. Furthermore, it has to be held to finer tolerances than the quartz slabs because of its higher birefringence. The filter which will be shown has mechanical tuning which enables it to be adjusted over a range of about 3A. It is planned in future work to tune[2] these filters both electrically and mechanically over a wide spectral region.

* This work has been supported by the Air Force, Cambridge Research Laboratories and the U. S. Navy, Bureau of Aeronautics, Bureau of Ordnance, Bureau of Ships, and ONR.
[1] B. Lyot, Comptes Rendus 197, 1593 (1933); Y. Öhman, Nature 141, 291 (1938).
[2] B. H. Billings, J. Opt. Soc. Am. 37, 738–746 (1947).

47. The Effect of Antireflection Films on Color in Optical Instruments. ALLEN E. MURRAY, *Bausch & Lomb Optical Company.*

While highly colored in reflection, antireflection films exert slight effect on the color of the transmitted light per surface. The cumulative effect of a substantial number of surfaces can be large enough to give a distinct color to the image, which in some instances may be objectionable. Conversely, filming can be used to control the residual color arising from glass absorption. Using an unpublished schema of Dr. A. F. Turner's, the spectrophotometric curves have been computed for several glasses, film thicknesses, and numbers of surfaces. The colorimetric data have been assembled for this preliminary report, and some useful rules are indicated. The dominant wave-length of the transmitted light with respect to illuminant "*C*" is independent of the glass and the number of surfaces, but is a function of film thickness. The film of minimum purity in all cases has a reflection minimum at about 505 millimicrons. Purity is a function of index and number of surfaces.

48. Absorption and Emission Spectra of Promethium. W. F. MEGGERS, B. F. SCRIBNER, AND W. R. BOZMAN, *National Bureau of Standards.*

A 5-mg sample of 61 Promethium, prepared by the Oak Ridge National Laboratory, was loaned for spectroscopic research. This sample was put in solution and its absorption spectrum between 3000A and 9000A was plotted with the aid of a Beckman spectrophotometer. These results are practically identical with those reported by Parker and Lantz.[1] The strongest absorption bands have wave-lengths 494.5, 548.5, 568.0, 685.5, 702.5, and 735.5 mμ (±0.5 mμ). Small portions of the solution were dried on copper electrodes employed in photographing a.c. arc and spark spectra with a concave grating of 22 feet radius. Wave-lengths and relative intensities were determined for more than 1000 lines between 2200A and 6900A. Excepting 62 Samarium no other rare earths could be detected in this 61-Promethium sample but common impurities from chemical ware and reagents were troublesome. Most of the 59 lines reported by Timma[2] have been confirmed. The strongest lines appear to be 3892.17 and 3998.97A (±0.02A). Hyperfine structure is suspected in many lines, e.g., 5868.79, 5875.32, 5927.17, and 5946.49A, indicating that the nuclei of $^{147}_{61}$Pm atoms possess mechanical and magnetic moments.

[1] G. W. Parker and P. M. Lantz, J. Am. Chem. Soc. (in press).
[2] D. L. Timma, J. Opt. Soc. Am. 39, 898 (1949).

49. Spectrographic Determination of High Hafnium in Hafnium-Zirconium Dioxide. ALFRED B. CHANDLER, *Foote Mineral Company, Paoli, Pennsylvania.*

A method is presented for the direct determination of hafnium in the concentration ranges of 2–50 percent Hf in $(Hf-Zr)O_2$. It is based on the use of intensity ratios of a pair of weaker lines of these elements,[1] Hf 2638.710A and Zr 2640.151A. These lines were selected to give a log ratio of 1.0 at 10 percent Hf. Hafnium analyses above 50 percent have been made using a 1:1 dilution with Hf-free ZrO_2. Standards were prepared from Hf-free ZrO_2 obtained by a double fractionation of 3 $ZrCl_4-2$ $POCl_3$ complex.[2] HfO_2 was obtained from Phillips Eindhoven, Holland.

[1] J. H. Coullette, Anal. Chem. 15 (1943).
[2] D. M. Gruen and J. J. Katz, AEC U-498 (U.A.C.-123) (June, 1949).

50. The Ultraviolet Dissociation Spectra of Nylons.* GLADYS A. ANSLOW AND RUTH C. SHEA, *Smith College.*

The ultraviolet absorption spectra of Nylon films, formed of polyhexamthylene adipamide and of polyhexamethylene sebacamide and of Nylon 6B** in a 10^{-5}M 85/15 ethyl alcohol/water solution, are compared with the spectra of adipamide, malonamide, and pelargonamide in crystalline form or in water or alcohol solutions. The amide solutions had been heat-treated to impose the two types of association of amides through hydrogen bridges which result from fast or slow cooling and exhibit distinctive absorption spectra.[1] The short wave-length continuum which appears in the spectra of these molecules has been attributed to the dissociation of the hydrogen-bridged bonds following electronic excitation.[2] The spectra of the Nylon films resemble those of slowly cooled amides, and that of the Nylon 6B solution the spectra of rapidly cooled amides, the former being long linear polymers, the latter dimers or polymers with only a few members, in which the hydrogen bridges between units are ruptured by the absorption.

* This work was supported by the ONR.
** The Nylons were kindly furnished by the du Pont de Nemours Experimental Station.
[1] G. A. Anslow and R. C. Shea, Phys. Rev. 75, 1318 (1949).
[2] Anslow, Hsieh, and Shea, J. Chem. Phys. 17, 426 (1949).

51. Hyperfine Structure of U^{235}. G. L. STUKENBROEKER AND J. R. MCNALLY, JR., *Oak Ridge National Laboratory.*

Preliminary spectroscopic studies on enhanced U^{235} point to a nuclear spin of 5/2 and give strong evidence for the existence of a nuclear electric quadrupole moment, arising from asymmetry of the nuclear charge distribution.

52. Interferometric Investigation of Ca and Hg. PAUL M. GRIFFIN AND J. RAND MCNALLY, JR., *Oak Ridge National Laboratory.*

Some results on the interferometric investigations of mercury and calcium isotopes are presented together with discussion of equipment and techniques used. Comparison interferograms of normal Hg and Hg^{202} for a wide range of interferometer spacings are shown. Hyperfine studies on the only natural occurring odd mass isotope of calcium, Ca^{43}, are also discussed.

53. Spectrochemical Methods of Brass Analysis. M. F. HASLER AND C. E. HARVEY, *Applied Research Laboratories.*

Two analytical techniques are discussed: a point-to-plane procedure suitable for the rapid routine analysis of metal specimens, and a solution method that permits the validation

of standards. The latter also offers an alternative method for control analysis under some circumstances. Certain fundamental problems are discussed from the standpoint of the above procedures: the interrelation of metallurgical variables and discharge conditions; other related variables; the synthesis of standards; quantitative calculations in varying two and three major constituent systems; comparison of photographic and quantometric recording.

54. Invited paper entitled, "Visual Aspects of the CBS Color Television System," BY DR. PETER C. GOLDMARK, *Director of Engineering Research, Columbia Broadcasting System.*

Contributed Papers

55. Video Techniques in Aerial Reconnaissance.* DUNCAN E. MACDONALD AND GRANT D. ROSS, *Boston University,* AND WILLIAM W. TUNNICLIFFE, *Optical Research Laboratory.*

This paper describes both laboratory and aerial tests. These tests have explored the possibilities of increasing the scope of aerial reconnaissance by the use of primary photosensitive receivers other than the photographic emulsion. The work is not concerned with the transmission of signals but only with the definition and sensitivity that may be achieved through the employment of video devices. Aerial slit scan television has been achieved and is presented. Tests with a laboratory line scan system are reported. The employment of line scan in conjunction with cylindrical lenses and with image segmentation is discussed. The use of an ADP light modulator is proposed.

* This work was sponsored by the Photographic Laboratory of the Air Materiel Command. The work was performed under Contract W33-038-ac-14075 between the United States Air Force and Boston University.

56. The Colors of Distant Objects.* W. E. KNOWLES MIDDLETON, *National Research Council of Canada.*

A general expression is developed for the apparent color of an object of any intrinsic color, seen through a given thickness of an atmosphere of any specified optical properties. In deriving this expression, the author has made use of modern theories of the alteration of contrast by the atmosphere. Some examples of this theory are given, and in conclusion it is shown that the visual range of colored objects differs little from that of achromatic objects of the same luminance factor.

* W. E. K. Middleton, "On the colours of distant objects, and the visual range of coloured objects," Trans. Roy. Soc. Canada, Section III **29**, 127–154 (1935).

57. The Effect of Wave-Length on the Attenuation of Brightness Contrast by the Atmosphere.* HOWARD S. COLEMAN AND HAROLD E. ROSENBERGER, *Optical Research Laboratory, University of Texas.*

A study has been made of the influence of wave-length on atmospheric attenuation of brightness contrast along a horizontal path for the lower atmosphere in the visible region of the spectrum. The results of the study have been expressed in terms of the variation of meteorological range with wavelength for various degrees of transparency of the atmosphere. Attenuation measurements were made for objects that were darker and objects that were brighter than their backgrounds, using photoelectric telephotometry. The wave-lengths at which the measurements were made were selected by the use of filters in the telephotometer. These filters effectively transmitted wave-lengths ranging from 4200 to 6720A. The results indicate that the meteorological range is a linear function of wave-length for meteorological ranges from 7000 to 200,000 yd. This linear function was found to hold for objects that were brighter and that were darker than the background against which they were viewed.

* The work described in this paper was performed, in part, under terms of Task IX of Contract N6onr-266 between the ONR of the Navy Department and The University of Texas.

58. Application of Bouguer's Law to Non-Uniform Films. FRANCIS P. CALLAHAN, JR., *Interchemical Corporation.*

When Bouguer's law holds, the transmittance curve of a non-uniform film is uniquely determined by the thickness distribution function of the film and by the absorption coefficient as a function of wave-length. This transmittance curve can be obtained by means of a Laplace transform. Conversely, when the absorption coefficient function and the transmittance curve are known, the thickness distribution is uniquely determined. Even when Bouguer's law does not hold exactly, this is often of qualitative value. An estimate can be made of the size and shape of the locus in color space which contains the points corresponding to all possible non-uniform films of a material of which the absorption coefficients are known. Experimental errors resulting directly from non-uniformity of film thickness in absorption coefficient determinations can be estimated.

BIBLIOGRAPHY:
R. Courant and D. Hilbert, *Methoden der Mathematischen Physik.*
Arthur C. Hardy, *Handbook of Colorimetry.*

59. A Curve Computer. W. E. KNOWLES MIDDLETON, *National Research Council of Canada.*

An instrument has been designed and constructed for the purpose of multiplying, dividing, adding, or subtracting the ordinates of two Cartesian curves, and plotting the result. The principle is that of the Wheatstone net, balanced automatically by means of a servo system. Certain logarithmic operations can also be performed, and a planimeter attachment integrates the area under the curve representing the product, etc. The over-all accuracy is about 0.3 percent. The curve computer has many applications in photometry and colorimetry, such as the conversion of filters from one thickness to another, and the computation of tristimulus values.

60. New Automatic Colorimeter for Cotton. DOROTHY NICKERSON, *U. S. Department of Agriculture,* AND RICHARD S. HUNTER AND MARSHALL G. POWELL, *H. A. Gardner Laboratory, Inc.*

This instrument is based on a satisfactory application of the Hunter color and color-difference meter[1] to problems of raw cotton measurement. For cotton colors Hunter's coordinates "R_d" and "b" provide, without conversion, a picture close to that of measurements in terms of Munsell value and chroma. Therefore an instrument was designed to be fully automatic and self-standardizing, and graphically to show on a two-dimensional scale simultaneous values for reflectance and yellowness. Further, the instrument is self-contained in a movable cabinet about table height, with a minimum of exposed parts, and working parts in the horizontal plane of the table. Electrical measurements of photo-cell currents are converted to color as in the color-difference meter, except that Brown Electronik amplifiers replace the galvanometer, and reversible motors responding to the signals from these amplifiers replace the human operator, both in standardizing the instrument and in turning dials to obtain color settings. While this particular instrument is limited to the range of cotton colors, the principles upon which it is designed are adaptable to other limited ranges of color, in either two or three dimensions.

[1] R. S. Hunter, "Photoelectric color-difference meter," J. Opt. Soc. Am. **38**, 661(A) (1948).

61. Determination of Flame Temperature from the OH Emission in the Ultraviolet. J. A. CURCIO, H. S. STEWART AND C. C. PETTY, *Naval Research Laboratory.*

A new method for flame temperature measurement has been developed involving measurement of radiations, emitted by flames, in a narrow wave-length interval within the ultraviolet emission band of the OH radical. The mean value of flame emissivity within the wave-length interval is evaluated by measurement of mean flame transmission for a continuous-spectrum source. The method requires that the wave-length interval studied be so narrow that the emission of the source used for transmission measurement and that of a blackbody at flame temperature both be approximately constant over the interval. The method has been tested on steady flames over temperature ranges from 2000°K to 3000°K and excellent agreement obtained with sodium line reversal measurements. Temperatures of pulsed flames have been determined from photographic traces obtained with a monochromator-photomultiplier-oscilloscope-camera combination. Two high speed light choppers were used, one to interrupt the radiations entering the monochromator and the other to interrupt, at a different frequency, the radiations, from a hydrogen discharge lamp, transmitted by the flame to the monochromator. The time resolution was 0.10 msec. and the accuracy in temperature measurement about 40°K in the range 2000°K to 3000°K.

62. A Monochromator for the Vacuum Ultraviolet. R. TOUSEY AND F. S. JOHNSON, *Naval Research Laboratory,* AND JOHN RICHARDSON AND NESTOR TORAN, *Baird Associates, Inc.*

For the purpose of simplifying research in the vacuum ultraviolet a vacuum grating monochromator with motorized wave-length control and externally changeable slit widths was constructed. The design emphasized flexibility, convenience, and speed of operation. A 15,000 line per inch one meter grating is used near normal incidence and the wave-length range covered is from 4000A to the central image. The grating is pivoted about the center of the Rowland circle and is moved by a synchronous motor. This permits changing the wave-length and at the same time maintaining the focus. Speeds of 600 and 120A per minute are available and the wave-length setting is reproducible to one angstrom. The entrance and exit slits are carried on separate assemblies. In order to make it possible to change slit widths without disturbing the vacuum or the wave-length calibration or focus three entrance and three exit slits of different widths are provided and are carried on turrets similar to large stopcocks. The exit slit assembly can be removed and replaced by a camera. The exit slit housing and any equipment attached to it can be shut off from the monochromator by means of a vacuum valve.

63. Thermocouple Measurements of Spectral Intensities in the Vacuum Ultraviolet. D. M. PACKER AND C. LOCK, *Naval Research Laboratory.*

The spectral energy distribution of the radiation from a high intensity hydrogen arc, after dispersal by the vacuum monochromator described by Tousey *et al.*,[1] was measured with a thermocouple. The receiver was located just beyond the exit slit in an enclosure pressure-connected to the main vacuum chamber, thus obviating the use of a window over the thermocouple. The thermocouple, made by Eppley of Bi-Ag, was compensated. The voltages generated by the thermocouple (up to 0.1 microvolt) were sufficiently large that a Perkin-Elmer amplifier and a Brown recorder afforded adequate sensitivity. The spectrum was recorded down to 900A, near the end of the many lined spectrum of hydrogen. The entrance and exit slits used were 1 mm wide, and the dispersion was 17A per mm. Estimates of energies encountered in the various spectral regions will be given.

[1] Paper presented at this meeting.

64. Ultraviolet Spectral Sensitivity Characteristics of Photo-Multipliers Having Quartz and Glass Envelopes. LAWRENCE DUNKELMAN AND CHARLES LOCK, *Naval Research Laboratory.*

The ultraviolet response characteristics of the conventional 1P28 and of several special 1P28 photo-multipliers in quartz envelopes were investigated. Characteristics of conventional photo-multipliers including spectral response in the near ultraviolet have been described in detail by Engstrom.[1] The spectral response of the 1P28 and the quartz 1P28 tubes was measured on the vacuum monochromator described by Tousey *et al.*[2] using data obtained with a thermocouple by Packer.[3] The quartz photo-multiplier was found to respond to the spectrum of the hydrogen arc to 1530A and the 1P28 to 1850A. It was also found that the 1P28 and 1P21 tubes responded to a small extent at wave-lengths below the envelope cut-offs due to fluorescence of the envelopes. The quartz multipliers were manufactured by RCA at the request of the Naval Research Laboratory. The quartz envelopes with graded seals were supplied by Hanovia.

[1] R. W. Engstrom, J. Opt. Soc. Am. 37, 420 (1947).
[2] Paper presented at this meeting.
[3] Paper presented at this meeting.

65. Fluorescence Sensitized Photo-Multipliers for the Measurement of Vacuum Ultraviolet Radiation. F. S. JOHNSON AND R. TOUSEY, *Naval Research Laboratory.*

The use of fluorescent coatings with photo-multipliers to extend their response range into the vacuum ultraviolet was investigated with the vacuum monochromator described by Tousey *et al.*[1] The light source used was a hydrogen arc with an open slit. With a 1P21 photo-multiplier with a coating of pump oil on the envelope strong responses were obtained down to 900A, the end of the many lined spectrum of hydrogen. The relative sensitivities of different multipliers and fluorescent coatings and their relative susceptibilities to stray light will be discussed.

[1] Paper presented at this meeting.

66. The Application of Projective Geometry to the Theory of Color Mixture. F. J. BINGLEY, *Philco Corporation.*

It has been known for some time that the laws of color mixture could be expressed geometrically using an analog between the light sources and appropriate corresponding weights supposed located at the points on the chromaticity diagram corresponding to the colors being mixed. It is the purpose of this paper to develop some general theoretical considerations of a geometric nature, which are believed to represent a new analytical technique. By use of the method it is possible to uncover general properties of color mixture which might not otherwise be apparent. Additionally, useful geometric constructions for the solution of color mixture problems, without laborious arithmetical computation, are presented. Applications to problems in the field of color reproduction are discussed. The possibilities of this method of geometric analysis are pointed out, not only with regard to its use for purely theoretical analysis with a simple direct and pictorial approach, but also as the basis for a range of graphical design methods which should be capable of wide application.

67. Loci of Constant Hue Determined with Various Surrounding Colors. D. L. MACADAM, *Kodak Research Laboratory.*

It is well known that a series of colors, all of which evoke the same hue, is in general represented by a curve in the chro-

maticity diagram. A certain yellow constant hue series has a very nearly straight locus, as has also a series having the same hue as the extreme violet end of the spectrum. The fact that the two series having straight loci are not exactly complementary has been definitely established. The loci of constant hue found in other regions of the chromaticity diagram appear to rule out the possibility of other constant hue series having straight loci. The various loci tend to converge on a point which represents an acceptable white under the conditions of adaptation produced by the surrounding color.

68. Two Methods of Determining a Recognizable Relationship between Areas of Color, Related to Both Munsell and Ostwald. W. E. CARSWELL, *School of Architecture, University of Toronto.*

For area balance in relation to power factor, Ostwald's full colors were matched against Munsell colors and plotted on a Munsell power factor grid. As Ostwald's full colors are arranged as if constant in chroma, differences in power factor had to be made up in value. When black, white, and full color of an Ostwald hue triangle occupied their correct position as to power factor, all other colors occupied approximately correct positions. Area balance in relation to contrast[1] originally described for Munsell's charts was converted to Ostwald's hue triangles in a similar manner. In each case, transparent graphs were developed indicating area relations without computation. Demonstrations indicate that precision is not a requisite of recognizable area balance.

[1] Moon and Spencer, J. Opt. Soc. Am. **34** (February, 1944).

69. Color Harmony Manual: Colorimetric Analysis of Third Edition. WALTER C. GRANVILLE, *Container Corporation of America, Chicago, Illinois,* CARL E. FOSS, *Princeton, New Jersey,* AND I. H. GODLOVE, *General Aniline & Film Corporation, Easton, Pennsylvania.*

The third edition[1] (1948) of the *Color Harmony Manual* represents a complete revision of the earlier editions[2] and includes 263 colors in addition to the 680 in the regular abridgment of the Ostwald system of color organization. The new edition will be shown and the basis for the revision discussed. Spectrophotometric measurements have been made for both the matte and glossy sides of all chips on a G.E. recording spectrophotometer. Tristimulus specifications for ICI illuminant *C* were obtained at the same time from an automatic, continuous tristimulus integrator[3] attached to the spectrophotometer. Representative portions of these data will be presented, and a comparison made with the corresponding data[4] of the earlier edition of chips.

[1] Jacobson, Granville, and Foss, *Color Harmony Manual* (Container Corporation of America, Chicago, 1948).
[2] Egbert Jacobson, *Color Harmony Manual* (Container Corporation of America, Chicago, 1942 and 1946).
[3] H. R. Davidson and L. W. Imm, J. Opt. Soc. Am. **39**, 633 (1949).
[4] W. C. Granville and E. Jacobson, J. Opt. Soc. Am. **34**, No. 7 (1944).

70. Application of the Hunter Color-Difference Meter to a Tomato Color Measurement Problem. S. G. YOUNKIN, *Campbell Soup Company.*

In the present study, a Hunter color-difference meter was used to obtain color specifications of tomato purees, and for the first time it has been possible in our laboratories to make rapid, repeatable, small color-difference measurements. A porcelain-enamel reference standard having color specifications similar to tomato purees was used to obtain values of Hunter's L, a_L, and b_L by viewing 130 ml of each puree through the base of a specially constructed glass cell. Values of a_L and b_L were plotted on a chromaticity diagram with L values designated numerically for each plotted point. Munsell renotation loci for hue and chroma were placed on these diagrams for orientation purposes. Visual examinations were made of purees contained in square glass bottles. Samples were viewed by daylight and scored on the basis of appearance. Altogether there were several thousand purees prepared from fruits grown at widely separated points, under different environmental conditions, and harvested at different degrees of maturity. Essentially a perfect correlation was obtained between color-difference meter specifications and visual scores regardless of the magnitude of color differences.

71. Measurement of 60° Specular Gloss. HARRY K. HAMMOND III AND ISADORE NIMEROFF, *National Bureau of Standards.*

A critical part of the definition of gloss is the amount the reflected beam may depart from strict mirror reflection and still be counted as contributing to gloss. For measuring the 60° specular gloss of paint finishes, the ASTM method[1] based on research done ten years ago,[2] prescribed the illuminator and receiver apertures to be used, but gave no tolerances. To determine permissible tolerances for a given uncertainty in gloss measurement, data have been obtained on the variation of gloss reading with change in source and receiver apertures. A problem directly related to gloss measurement is the evaluation of the diffuse corrections to be applied to glossmeter readings to obtain true specular gloss values. The values derived on the basis of simple theory do not agree with the measured values for this correction, but further investigation showed that agreement could be obtained by taking into account polarization of the light source and departure of specimen reflectance from that of a perfect diffusor. The technician's problem of checking glossmeter adjustment and conformance to aperture specification may be solved by using standards having different angular distributions of reflected light flux. Such standards may be obtained from the National Bureau of Standards.

[1] "ASTM tentative method of test for 60° specular gloss of paint finishes," ASTM designation D523, ASTM Book of Standards. Part II (1949).
[2] R. S. Hunter and D. B. Judd, ASTM Bull., No. 97, 11 (March, 1939).

72. A New Goniophotometer. RICHARD S. HUNTER, *Henry A. Gardner Laboratory, Inc.*

Glossiness, transparency, haziness, and turbidity are properties of materials attributable to the geometric manners in which they reflect and transmit light much as color is an appearance property attributable to the spectral distribution of light. A new goniophotometer has been designed to measure the manners in which materials reflect and transmit light with changing directions of illumination and view. It consists of (1) a stationary photo-cell which receives light (through a colored filter if desired), (2) a specimen table which may be rotated to place the specimen in any desired attitude with respect to the photo-cell, and (3) an illuminating arm with light source for directing a beam of light onto the specimen from any desired direction. On the illuminating arm, there is a comparison photo-cell constantly lighted by the source to provide a reference current for measurement of the output of the first photo-cell. Directions of illumination and view may be adjusted to within 5° of grazing. Amount of light reflected or transmitted under specified geometric conditions is expressed either as (1) fraction of that incident on the specimen, or (2) as fraction of that which would be given off under the same conditions by an imaginary, perfect diffusor. The first scale properly measures fraction of incident-beam flux in a beam leaving the specimen (specular reflectance, etc.). The second scale properly measures light that is wholly or partially diffused as it leaves the specimen (directional reflectance, etc.).

73. Photosensitive Glass.* S. D. STOOKEY, *Corning Glass Works.*

Photosensitive glass, a new photographic medium recently developed to a commercial stage, is glass in which permanent

photographic images may be printed. Two basic types exist, distinguished from one another by the nature of their photographic images. The "color transparency" image contains submicroscopic particles of gold, silver, or copper and is essentially grainless. The "photosensitive opal" image contains microscopic non-metallic crystals capable of diffusing light. The photographic process consists of two steps: exposing the clear, optically homogeneous glass to ultraviolet or ionizing radiation through suitable negatives or stencils, and development by heating. A description is given of optical phenomena in the photographic process, and optical properties of some of the finished products. Examples of various applications are shown including the louver-glass "Fota-Lite" used in lighting fixtures.

* S. D. Stookey, "Photosensitive glass—A new photographic medium," Ind. Eng. Chem. 41, 856 (April, 1949).

74. Low Intensity Reciprocity-Law Failure in Photographic Exposure. II. Multiplet-Quantum Hits in Critical Time Period τ and Effect of Variable τ-Period among Grains. J. H. WEBB, *Kodak Research Laboratories.*

The low intensity reciprocity-law failure in photographic exposure is due to thermal instability of the latent image when it starts to form and while it is still small. Experimental evidence indicates that the latent image can start to form only if the grain receives a burst of quanta s ($=2, 3, 4$) within a small critical time τ. In a previous paper[1] this problem was treated by probability methods and it was shown that if a multiplet of quanta of size s is required by a grain in a definite critical time τ for establishment of the stable subspeck, then the slope of the reciprocity curve must approach at low intensities the value $-(s-1)$. In this previous paper, the critical time τ was assumed to be a constant, fixed value, the same for every grain in the emulsion. The present paper is an extension of the previous paper to the case of variable τ-period among the grains of the emulsion. While a variable τ-period has some effect on the shape of the H and D curves at low intensity, it is found that the simple conclusions about the slope of the reciprocity failure curve for a constant τ-period also hold true for a variable τ-period among the grains.

[1] J. H. Webb, J. Opt. Soc. Am. 40, 3 (1950).

75. On the Equation of the Characteristic Curve of Photographic Emulsions. MILTON GREEN, *Signal Corps Engineering Laboratories, Fort Monmouth.*

At the last meeting of the Optical Society of America the author presented the following simple empirical equation, derived from a study of the preliminary curve, as a good approximation for emulsion calibration curves of SAI, SAII, and 103F film as processed in this laboratory. $\ln(Ds/D) = (Io/I)^n$ where the symbols stand for the following: D density; Ds saturation density; I intensity; Io and n constants. Further examination of a fairly good sampling of calibration curves taken for the three types of film shows that the equation is a very good fit in most cases. In the few cases where the fit is not too good Ds and n are not constant over all values of intensity but change rapidly over a short interval of intensities from one set of values, constant below the "transition interval," to another set of values, constant above the "transition interval."

76. Gold Sensitization of X-Ray Films. HERMAN HOERLIN AND F. W. H. MUELLER, *Ansco Research Laboratories.*

Sensitization of non-screen type x-ray emulsions with aqueous solutions of ammonium or alkali aurous thiocyanates leads to a wave-length dependent increase of their x-ray and gamma-ray sensitivities. For a particular fine-grain emulsion the gain in photographic speed is shown to increase from a factor of 1.5 at 1.3A to a factor of 10 at 0.011A. This wavelength dependence of the sensitizing effect is governed by the range-energy relationship of electrons, by the shape of the energy loss curve of electrons, and the threshold sensitivity of the average grain. The sensitivity of the average grain in an unsensitized and a gold-sensitized emulsion was derived from the number of quanta required to produce the same photographic effects at different wave-lengths. Gold sensitization caused an increase in threshold sensitivity from $(6\text{ kev})^{-1}$ to $(1.2\text{ kev})^{-1}$ for the average grain of the emulsion under investigation. On the basis of a comparison of the quantities of latent image silver formed by light exposure on one hand, and by electrons on the other hand, the effective radius of attraction of a gold-treated sensitivity center was calculated for this specific case.

77. Measurement of Verdet and Cotton-Mouton Constants Using Transient Magnetic Fields and a Photo-Multiplier Type Compensator.* M. J. WALKER† AND R. C. RAYMOND, *The Pennsylvania State College.*

The Faraday rotation for transient magnetic fields is measured using a Polaroid spinning at 10,000 r.p.m. as analyzer. The transmitted light is incident on a photo-multiplier tube which indicates on an oscilloscope. The sweep is synchronized with the spinning analyzer. The beam chopper serves also to keep the photo-multiplier dark during the cycle except when the polarizer and analyzer are nearly crossed. Faraday rotation indicates as a shift of the minimum on the oscilloscope pattern, and is independent of random changes in light intensity. The apparatus was used to determine the dispersion curve of the Verdet constant in the visible for methacrylate polymer, styrene monomer, allyl diglycol carbonate monomer, and toluene. The Cotton-Mouton elliptization is determined with the same apparatus by introducing between sample and spinning analyzer a quarter wave plate with its axis parallel to the plane of vibration of the original incident polarized light which lies at 45 degrees to the direction of the magnetic field. The elliptization is thus reconverted to plane polarization, and the angular position of this plane polarized light is a function of the elliptization produced by the magnetic field acting on the sample. The method was tested successfully by determining the Cotton-Mouton elliptization of nitrobenzene.

* This work was part of a doctorate thesis presented to the Pennsylvania State College.
† Now at the University of Connecticut.

78. Refractive Indices of Rutile and Sphalerite. J. R. DEVORE, *Research Division, Technical Department, The New Jersey Zinc Company (of Pennsylvania), Palmerton.*

Prisms were made from single crystals of rutile and sphalerite and used in measuring the refractive indices of these materials. The method described by Pfund[1] was used to measure the indices at various wave-lengths. The measurements were extended to 1.5 microns in the infra-red by the use of an infra-red sensitive screen as described by Paul.[2] The dispersion curves and the equations for the curves are presented. These results demonstrate the high dispersion in the visible spectrum and the large birefringence of rutile. The experimental results also demonstrate the strong absorption of rutile in the violet end of the visible spectrum which accounts for the slight yellow color of rutile.

[1] A. H. Pfund, J. Opt. Soc. Am. 29, 291 (1939).
[2] F. W. Paul, J. Opt. Soc. Am. 36, 175 (1946).

79. Color Centers in Fused and Crystalline Quartz. ALEXANDER SMAKULA, *Engineer Research and Development Laboratories, Fort Belvoir, Virginia.*

Fused quartz exposed to hard x-rays (200 kv) shows two characteristic absorption bands, at 540 mu and 305 mu. The

strong increase of absorption toward the shorter wave-lengths indicates at least one more band below 205 mu. Similarly crystalline quartz, after coloration by x-rays exhibits two bands, one below 205 mμ and the second between 400 and 435 mμ depending on the crystal orientation. The half-width of the absorption bands is about 1 ev; it decreases with the shifting of the bands toward the longer wave-lengths. The intensity of the bands at shorter wave-lengths is two times higher than the intensity of the bands at longer wave-lengths. This intensity ratio is the same for fused and crystalline quartz and independent of the degree of coloration. Both bands can be bleached by heat, but only the band at shorter wave-lengths can be bleached by light corresponding to its absorption maximum. It is assumed that the absorption bands are caused by the electrons which are freed by x-rays and subsequently trapped in lattice defects. Since the intensity and stability against light of the two bands are different they must correspond to two different traps.

Author Index of Papers

Allen, Ralph G.—see Coleman, Howard S.
Anslow, Gladys A. and Ruth C. Shea—No. 50
Archer, James E.—see Harrison, George R.
Aschenbrenner, Claus M.—No. 23
Back, Frank G.—No. 21
Baird, Walter S.—No. 32
Ballard, Stanley S.—see McCarthy, Kathryn A.
——see Combes, Lewis S.
Benford, James R. and Richard L. Seidenberg—No. 34
Billings, B. H., S. Sage, and W. Draisin—No. 46
Bingley, F. J.—No. 66
Bozman, W. R.—see Meggers, W. F. and B. F. Scribner
Britton, William C.—see Watson, John T.
Bube, Richard H.—No. 35
Bullock, B. W. and S. Silverman—No. 17
Callahan, Francis P., Jr.—No. 58
Carswell, W. E.—No. 68
Chandler, Alfred B.—No. 49
Clark, Mason E.—see Fisher, Russell A. and William C. Knopf
Coleman, Howard S. and Ralph G. Allen—No. 44
—— **and Harold E. Rosenberger**—No. 57
Combes, Lewis S. and Stanley S. Ballard—No. 14
Covell, William—see O'Brien, Brian and Gordon G. Milne
Curcio, J. A., H. S. Stewart, and C. C. Petty—No. 61
DeVore, J. R.—No. 78
Dixon, E. O.—see MacNeille, S. M.
Draisin, W.—see Billings, B. H. and S. Sage
Dunkelman, Lawrence and Charles Lock—No. 64
Elby, F. P.—No. 15
Epstein, L. Ivan—No. 9
Feder, Donald P.—No. 8
Feynman, Richard P.—No. 41
Fisher, Russell A., William C. Knopf, and Mason E. Clark—No. 3
Foss, Carl E.—see Granville, Walter C. and I. H. Godlove
Gardner, Irvine C.—No. 20
Godlove, I. H.—see Granville, Walter C. and Carl E. Foss
Golay, Marcel J. E.—No. 18
Goldmark, Peter C.—No. 54
Granville, Walter C., Carl E. Foss, and I. H. Godlove—No. 69
Green, Milton—No. 75
Griffin, Paul M. and J. Rand McNally, Jr.—No. 52
Griffith, Grace E.—No. 45
Hammond, Harry K., III and Isadore Nimeroff—No. 71
Harrison, George R. and James E. Archer—No. 30
Harvey, C. E.—see Hasler, M. F.
Hasler, M. F. and C. E. Harvey—No. 53
Hoerlin, Herman and F. W. H. Mueller—No. 76
Hopkins, Robert and Louise Rivoli—No. 12
Hughes, Harold K.—see Murphy, Robert W.
Humphreys, Curtis J.—No. 5
Hunter, Richard S.—No. 72
——see Nickerson, Dorothy and Marshall G. Powell
Johnson, F. S. and R. Tousey—No. 65
——see Tousey, R., John Richardson, and Nestor Toran
Jones, R. Clark—No. 40
Knopf, William C.—see Fisher, Russell A. and Mason E. Clark
Lamb, Mary A.—see Plyler, Earle K.
Langton, William G.—No. 28
Lock, Charles—see Dunkelman, Lawrence
——see Packer, D. M.
Lord, R. C. and E. Nielsen—No. 7
MacAdam, David L.—No. 67
Macdonald, Duncan E.—No. 22
—— **Grant D. Ross, and William W. Tunnicliffe**—No. 55
MacNeille, S. M. and E. O. Dixon—No. 42
Marcus, Bernard and Burton W. Wheeler, Jr.—No. 19
McCarthy, Kathryn A. and Stanley S. Ballard—No. 13
McCubbin, T. King, Jr. and William M. Sinton—No. 2
McNally, J. Rand, Jr.—see Stukenbroeker, G. L.
——see Griffin, Paul M.
Meggers, W. F., B. F. Scribner, and W. R. Bozman—No. 48
Meltzer, Robert J.—No. 16
Middleton, W. E. Knowles—Nos. 56 and 59
Milne, Gordon G.—see O'Brien, Brian and William Covell
Mueller, F. W. H.—see Hoerlin, Herman
Murphy, Robert W. and Harold K. Hughes—No. 31
Murray, Allen E.—No. 47
Nickerson, Dorothy, Richard S. Hunter, and Marshall G. Powell—No. 60
Nielsen, E.—see Lord, R. C.
Nielsen, J. Rud—see Richards, Charles M.
Nierenberg, Richard N.—No. 39
Nimeroff, Isadore—see Hammond, Harry K., III
O'Brien, Brian, Gordon G. Milne, and William Covell—Nos. 37 and 38
Packer, D. M. and Charles Lock—No. 63
Petty, C. C.—see Curcio, J. A. and H. S. Stewart
Plyler, Earle K. and Mary A. Lamb—No. 4
Powell, Marshall G.—see Nickerson, Dorothy and Richard S. Hunter
Rank, D. H.—No. 11
Raymond, R. C.—see Walker, M. J.
Richards, Charles M. and J. Rud Nielsen—No. 6
Richardson, David, R. S. Wiley, and G. J. Sheldon—No. 29
Richardson, John—see Tousey, R., F. S. Johnson, and Nestor Toran
Rivoli, Louise—see Hopkins, Robert
Rosenberger, Harold E.—see Coleman, Howard S.
Ross, Grant D.—see Macdonald, Duncan E. and William W. Tunnicliffe
Sage, S.—see Billings, B. H. and W. Draisin
Saunders, James B.—No. 26

Scribner, B. F.—see Meggers, W. F. and W. R. Bozman
Seidenberg, Richard L.—see Benford, James R.
Shea, Ruch C.—see Anslow, Gladys A.
Sheldon, G. J.—see Richardson, David and R. S. Wiley
Silverman, S.—see Bullock, B. W.
Sinton, William M.—see McCubbin, T. King, Jr.
Smakula, Alexander—No. 79
Smith, F. D. and A. F. Turner—No. 43
Stewart, H. S.—see Curcio, J. A. and C. C. Petty
Stookey, S. D.—No. 73
Strong, John—No. 27
Stukenbroeker, G. L. and J. Rand McNally, Jr.—No. 51
Sutherland, G. B. B. M.—No. 1
Thorington, Luke—No. 36
Toran, Nestor—see Tousey, R., F. S. Johnson, and John Richardson
Tousey, R., F. S. Johnson, John Richardson, and Nestor Toran—No. 62
——see Johnson, F. S.
Tunnicliffe, William W.—see Macdonald, Duncan E. and Grant D. Ross
Turner, A. F.—see Smith, F. D.
Walker, M. J. and R. C. Raymond—No. 77
Watson, John T. and William C. Britton—No. 25
—— **and Vincent Young**—No. 24
Webb, J. H.—No. 74
Wheeler, Burton W., Jr.—see Marcus, Bernard
Wiley, R. S.—see Richardson, David and G. J. Sheldon
Wilkins, J. Ernest, Jr.—No. 33
Wormser, Eric M.—No. 10
Young, Vincent—see Watson, John T.
Younkin, S. G.—No. 70